ENGINEERING AMINOTRANSFERASES FOR THE BIOCATALYTIC PRODUCTION OF AROMATIC D-AMINO ACIDS.

CURTIS JAMES WILLIAM WALTON

Thesis submitted to the University of Ottawa
in partial fulfillment of the requirements for the
Doctorate in Philosophy Chemistry

Department of Chemistry and Biomolecular Sciences
Ottawa-Carleton Chemistry Institute
Faculty of Science
University of Ottawa

Abstract:

Optically pure aromatic D-amino acids, such as D-phenylalanine (D-Phe) and its derivatives, are high-value building blocks for the pharmaceutical industry. These compounds can be prepared using biocatalytic methods relying on various enzymes, including aminotransferases (ATs). ATs, also called transaminases (EC 2.6.1.X), are a subclass of pyridoxal 5′-phosphate-dependent enzymes that catalyze the transfer of the amino group from a donor substrate to a ketone acceptor. Synthesis of optically-pure amino acids using whole-cell biocatalytic cascades based on ATs possess several advantages compared to traditional chemical methods, including excellent enantioselectivity and increased process and step efficiency, which is achieved through the catalysis of multiple steps in one-pot reactions without requirement for intermediate work-ups, cofactor recycling, or toxic metals. However, enzyme biocatalysts typically need to be engineered to alter their substrate specificity or to increase their catalytic efficiency, which has limited their industrial application. Therefore, to facilitate the engineering process of ATs broadly and to produce aromatic D-amino acids, we developed a high-throughput assay for the testing of a broad range of ATs against libraries of potential substrates, and developed a biocatalytic cascade to produce optically pure aromatic D-amino acids.

Acknowledgements:

I would like to thank my PhD supervisor, Dr. Roberto Chica, for providing the opportunity to pursue my academic and professional interests. The opportunities I was afforded, including earning a graduate diploma in scientific management and leadership at the Telfer School of Management and the numerous conferences I presented at, have made a lasting impact on my development as a scientist and entrepreneur. Roberto always supported and encouraged me to embrace all the opportunities graduate school offers aspiring scientists and for that I am deeply grateful.

Secondly, I would like to thank the Chica group for their support and feedback in preparing for presentations and trouble-shooting experiments. I'd also like to thank Phillip Pelletier, who was always available for a cup of coffee and showed me how to use pernickety equipment. The Department of Biomolecular Sciences and Chemistry and the larger University of Ottawa research community was a valuable resource throughout my training. The professors always taught with vigor and passion in their classes which led to many excellent discussions between graduate students.

Finally, I would like to thank Dr. Samuel Oteng-Pabi and Dr. James Davey for their kinship throughout graduate school. Our discussions on scientific, political, and intellectual topics are some of my best memories from graduate school.

Dedication:

This is dedicated to my father, who supported me and gave so much.

Thank you Dad.

Table of Contents

List of Figures

List of Tables

List of Abbreviations

% v/v	percent volume/volume
% w/v	percent weight/volume
% conversion	Percent conversion
Å	angstrom
α-kg	α-ketoglutarate
aq.	Aqueous
AT	Aminotransferase
BCAT	branched-chain amino acid aminotransferase
Cα	Alpha carbon
CHES	N-Cyclohexyl-2-aminoethanesulfonic acid
conc.	Concentration
D-AAs	D-amino acids
DAAT	D-amino acid aminotransferase
DDO	D-aspartate oxidase
DH	Dehydrogenase
DKR	Dynamic kinetic resolution
DMSO	dimethyl sulfoxide
DNA	deoxyribose nucleic acid
DPAT	D-phenylglycine aminotransferase
E.C.	Enzyme commission
E. coli	*Escherichia coli*

ee	enantiomeric excess
equiv.	equivalents
FAD	flavin adenine dinucleotide
GDH	L-glutamate dehydrogenase
GSAM	glutamate-1-semialdehyde-2,1-aminomutase from *Synechococcus elongates*
h	hour
H-bond	hydrogen bond
HPLC	high performance liquid chromatography
HRP	horseradish peroxidase
IPTG	isopropyl β-D-1-thiogalactopyranoside
L	Liter
L-AAO	L-amino acid oxidase
LAAD	L-amino acid deaminase
MeOH	methanol
MesAT	β-phenylalanine aminotransferase from *Mesorhizobium sp. LUK*
mg	milligrams
min	minute
mM	millimolar
NAD^+	β-nicotinamide adenine dinucleotide, oxidized form
NADH	β-nicotinamide adenine dinucleotide, reduced form

$NADP^+$	β-nicotinamide adenine dinucleotide 2′-phosphate, oxidized form
NADPH	β-nicotinamide adenine dinucleotide 2′-phosphate, reduced form
Ni-NTA	nickel-nitrilotriacetic acid
nm	nanometer
NMR	nuclear magnetic resonance
NRPS	Non-ribosomal peptide synthetases
PC	Peptidoglycan component
PCR	polymerase chain reaction
PDB ID	Protein data bank identification
PLP	Pyridoxal 5′-phosphate
rpm	revolutions per minute
RMSD	Root-mean-square deviation
s.d.	standard deviation
SDS-PAGE	Sodium dodecyl sulfate polyacrylamide gel electrophoresis
SI	Stereo-inversion
UV	Ultraviolet
VPAT	β-AT from *Variovorax paradoxus*

Epigraph:

"There is a single light of science,

and to brighten it anywhere is to brighten it everywhere."

- Isaac Asimov

Chapter 1.
Introduction to D-Amino Acids & Aminotransferases

1.1. Amino acids

In biology, deoxyribonucleic acid (DNA) is the originator of all genetic information; however, the translated product is the true driving force enabling the development of life. Proteins are responsible for a wide variety of functionality and their diversity is what makes life so complex. The monomeric unit of these intricate polymers are known as amino acids; comprised of a carboxyl group (-COOH), amine ($-NH_2$), and a variable side-chain (R-group) that provides the structural and functional diversity (Figure 1.1A). A condensation reaction between the carboxyl group of an amino acid and the amine of a second amino acid produces an amide linkage forming a peptide bond (Figure 1.1B). The carboxyl group of the second monomer can undergo a condensation reaction to extend the polymer or polypeptide strand. The cellular machinery for protein synthesis selectively controls the extension of the polypeptide strand with specific amino acid sequences giving rise to the diverse functionality attained by proteins.

A. **B.**

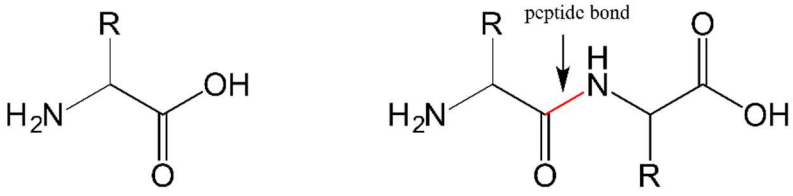

Figure 1.1 A. Generic amino acid involved in protein synthesis. B. Peptide bond between two generic amino acid monomers.

Amino acids are categorized based on the attachment position of the amine group. The carbon atom directly attached to carboxyl functional group is denoted as the alpha carbon (Cα). Primary amines bonded to the Cα are called α-amino acids. When the amine is attached to a position on the carbon backbone other than Cα, the name is based upon the attachment position such as beta (β-) or gamma (γ-) amino acids (Figure 1.2).

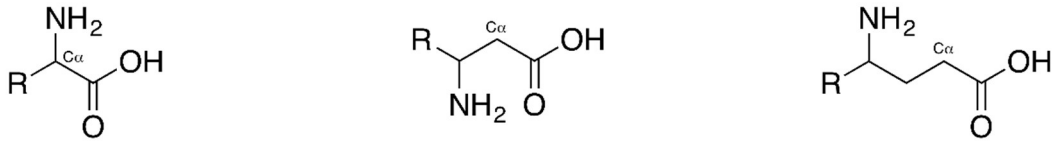

α-amino acid β-amino acid γ-amino acid

Figure 1.2 Generic α-, β-, and γ-amino acids with a R-group side-chain.

1.1.1. Stereochemistry of amino acids

Amino acids are commonly referred to using the D/L convention developed by Hermann Emil Fischer. The notation is based on the stereogenic centre of glyceraldehyde. The dextrorotatory (+) enantiomer of glyceraldehyde, which rotates polarized light clockwise, was assigned the D-glyceraldehyde configuration (Figure 1.3). The levorotatory enantiomer, which rotates polarized light counter-clockwise, was designated the L-configuration. In the Fischer projection, the vertical bonds extend below the plane of the page, while the horizontal bonds extend above the plane of the page. In Figure 1.3, the L- and D-enantiomers of the amino acid alanine are shown.

The Cahn-Ingold-Prelog (CIP) system for absolute configuration denotes amino acids having the stereoisomer form *sinister* (*S*) or *rectus* (*R*) which are derived from Latin meaning "left" and "right", respectively.[1,2] In Figure 1.4, the two enantiomers of alanine are shown based on the CIP system.

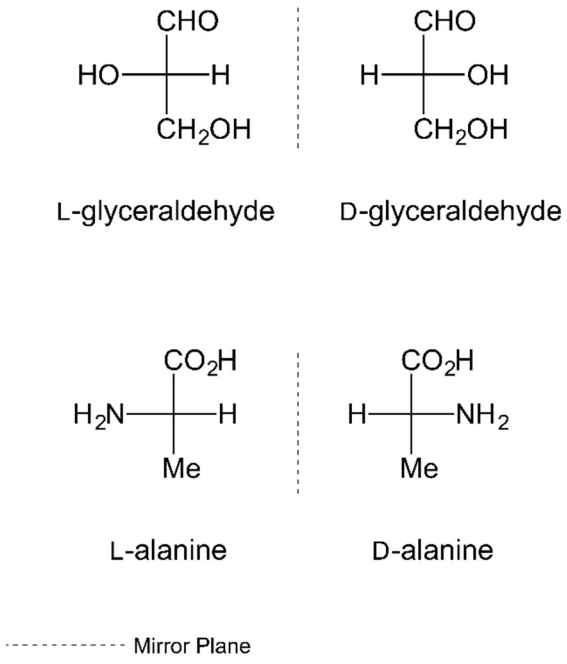

Figure 1.3 Fischer projections of the L and D enantiomers of glyceraldehyde and alanine.

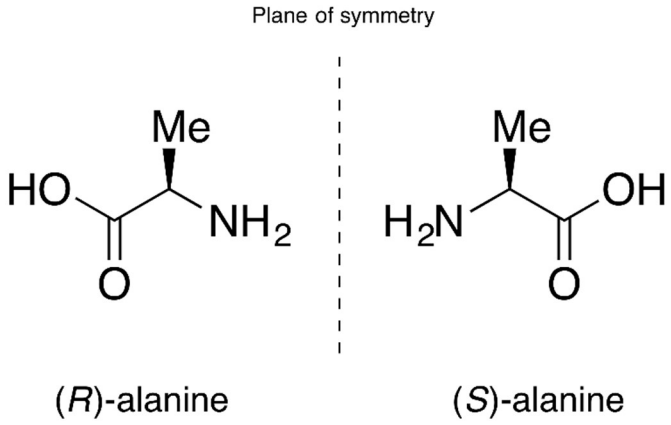

Figure 1.4 Stereoisomers of the amino acid alanine based on the Cahn-Ingold-Prelog system.

1.1.2. Proteinogenic amino acids

The proteinogenic amino acids are α-amino acids that are incorporated into proteins and encoded by the universal genetic code (Figure 1.5).[3,4] The proteinogenic amino acids are designated L-amino acids or L-α-amino acids, but the nomenclature without the α-designation is more commonly used as β- and γ-amino acids are not naturally incorporated into proteins. The CIP system classifies proteinogenic amino acids as having the stereoisomer form *sinister* (*S*). The notable exceptions are the achiral amino acid glycine and (*R*)-cysteine. Although the CIP system is commonly used in organic chemistry, the older D/L nomenclature has persisted for discussing amino acids.

The proteinogenic amino acids (Figure 1.5), also called canonical L-amino acids, were assigned single and three-letter notations to facilitate a concise and universal method to discuss the common amino acids and to minimize electronic storage space in the early days of bioinformatics.[5] The notation can be extended to clarify the enantiomer under discussion by placing the L/D notation in front of the abbreviated amino acid. For example, the proteinogenic amino acid alanine is represented by the three-letter code Ala or L-Ala, while the D-enantiomer can be represented as D-Ala.

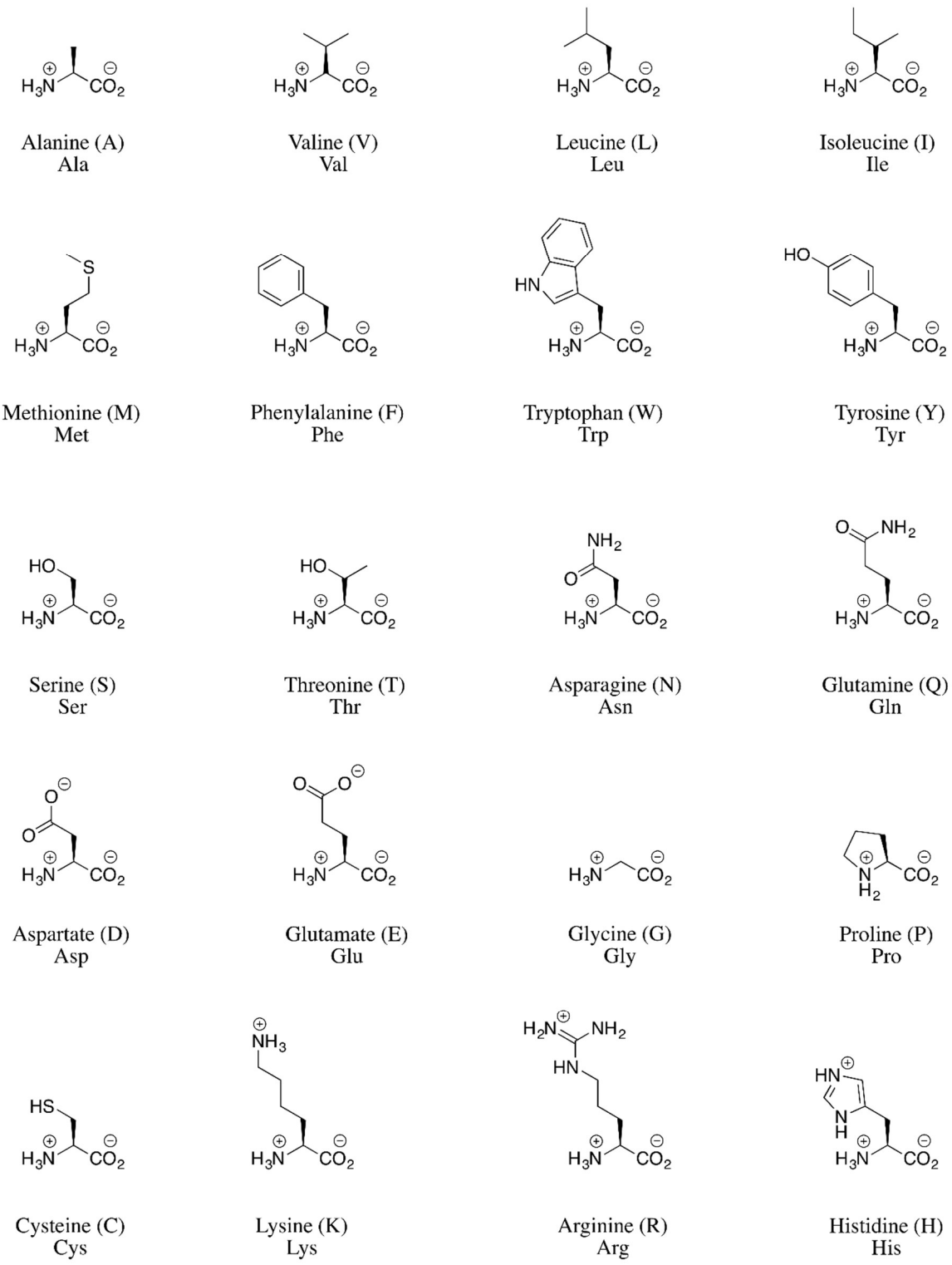

Figure 1.5 The proteinogenic amino acids structures with one and three-letter abbreviations.

1.2. D-amino acids in the environment

D-amino acids (D-AAs), although originally believed to be absent from life, are found in prokaryotic and eukaryotic organisms but are less abundant than their L-enantiomer counterparts.[6] However, D-AAs are not naturally incorporated into the polypeptide chain of proteins.[7,8] This exclusion of specific enantiomers from biomacromolecules is termed the homochirality of biomolecules.[9] The exclusion of a single enantiomer was previously believed to occur by chance, however newer theories propose a deterministic route to the homochirality observed in life.[10] Nonetheless, D-AAs are present in environment and metabolized by microorganisms and multicellular organisms.

1.2.1. Microorganisms

In 1943, Snell *et al.* noted that *Streptococcus lactis* could overcome a vitamin B_6 deficiency by the addition of D,L-alanine to the growth media.[11] This lead to the discovery of the most recognized role for D-AAs—the incorporation of D-Ala into the peptidoglycan component (PC) of the cell wall of gram-positive bacteria.[12,13] It is now recognized that all canonical D-AAs have been detected in microorganisms. The main roles of D-AAs are to modify and/or regulate the PC of the cell wall or as a building block of non-ribosomal peptides.[14] For example, in the bacterium *Enterococcus faecium,* D-Aspartate (D-Asp) forms the interpeptide bridge in the PC[15] and in *Vibrio cholerae* various D-AAs modulate the PC composition by incorporating into the PC or by regulating enzymes responsible for the synthesis of the PC.[16] The non-ribosomal peptide synthetases (NRPS) use D-AAs to synthesize peptides with broad structural diversity and biological activity. For example, D-phenylalanine (D-Phe) is found in the antimicrobial peptides Gramicidin[17], Tyrocidine[18], and Bacitracin[19] which are synthesized *in vivo* by NRPS.

1.2.2. Plants and animals

The pervasiveness of microorganisms in the environment and their ability to produce canonical D-AAs led researchers to investigate the effect D-AAs have on higher organisms. The canonical D-AAs have been identified in many plants,[20] including pea seedlings (*Pisum sativum*) where D-Asp, D-Ala, and D-glutamate (D-Glu) were identified in free and conjugated forms.[21,22] Plants are able to absorb free D-AAs in the soil through their roots.[23] However, an inhibitory effect on growth was observed in *Arabidopsis thaliana* with concentrations of ranging from <0.1 mM to 10 mM.[24]

In animals, D-AAs have been detected in proteins, peptides, and free in cellular lysates.[25] In the case of proteins, it's important to note the samples were from aged tissues such as teeth[26] and beta-amyloid proteins[27,28] where L-aspartate (L-Asp) or L-serine (L-Ser) underwent a racemization process generating the D-AAs. The D-AAs were not incorporated into the protein using the cell's translation machinery. However, some species have been found to incorporate D-AAs into peptides. For example, an opioid peptide containing D-Ala was isolated from a frog (*Phyllomedusa sauvagii*) which is more potent than morphine.[29] The neuropeptides isolated from snails (*Achatina fulica*)[30] and spiders (*Agelenopsis aperta*)[31] contain D-Phe and D-Serine (D-Ser), respectively. The peptide isolated from the snail, Achatin-I, demonstrated excitatory activity increasing the cardiac activity of the snail, while the peptide from the spider functions as a calcium channel blocker. The inclusion of the D-enantiomer was found to be essential for the biological activity as peptides containing the L-enantiomer displayed no biological activity.[31,32]

1.2.3. Foodstuff and metabolism of D-amino acids

The treatment of foodstuff with heat or alkaline pH can cause the racemization of amino acids. D-AAs have been detected in grain products, fruits and vegetables, dairy products, meats, and meat products.[33] However, most D-AAs found in the biosphere are not created by heat or chemical racemization but from enzymes involved in the metabolism of D-AAs. These enzymes span all six enzyme commission (E.C.) numbers (Table 1.1).[34]

Table 1.1 Several enzymes acting on D-amino acid metabolism.

Metabolic pathways are based on KEGG pathway database (http://www.genome.jp/kegg/pathway.html). 1: Alanine and aspartate metabolism (ec00252); 2: glycine, serine, and threonine metabolism (ec00260); 3: penicillin and cephalosporin biosynthesis (ec00311); 4: arginine and proline metabolism (ec00330); 5: D-arginine and D-ornithine metabolism (ec00472); 6: metabolic pathways (ec01100); 7: D-glutamine and D-glutamate metabolism (ec00471); 8: phenylalanine metabolism (ec00360); 9: nitrogen metabolism (ec00910); 10: one-carbon pool by folate (ec00670); 11: lysine degradation (ec00310); 12: D-alanine metabolism (ec00473); 13: peptidoglycan biosynthesis (ec00550); 14: vitamin B6 metabolism (ec00750); 15: cysteine metabolism. (Reproduced with permission from Martínez-Rodríguez, S. *et.al*., Chem. Biodivers. 2010. Copyright © 2010 Verlag Helvetica Chimica Acta AG, Zürich.)[35]

Enzymes	E.C. Number	Pathway
D-Aspartate oxidase	1.4.3.1	1
D-Amino acid oxidase	1.4.3.3	2-6
D-Glutamate oxidase	1.4.3.7	7
D-Glutamate (D-aspartate) oxidase	1.4.3.15	1,7
D-Amino acid dehydrogenase	1.4.99.1	8,9
D-Proline reductase (dithiol)	1.21.4.1	4
D-Alanine 2-hydroxymethyltransferase	2.1.2.7	6,10
D-Glutamyltransferase	2.3.2.1	7
D-Alanine g-glutamyltransferase	2.3.2.14	-
D-Tryptophan *N*-acetyltransferase	2.3.1.34	-
D-Amino acid *N*-acetyltransferase	2.3.1.36	8
D-Tryptophan *N*-malonyltransferase	2.3.1.112	-
D-Alanine transaminase	2.6.1.21	4-6,8,11-13
D-Methionine transaminase	2.6.1.41	12
Pyridoxamine phosphate transaminase	2.6.1.54	14
Cephalosporin C transaminase	2.6.1.74	3
D-Ala-D-Ala dipeptidase	3.4.13.22	-
Muramoylpentapeptide carboxypeptidase	3.4.17.8	13
D-Glutaminase	3.5.1.35	7
***N*-Acyl-D-glutamate deacylase**	3.5.1.82	-
***N*-Acyl-D-aspartate deacylase**	3.5.1.83	-
D-Arginase	3.5.3.10	5,6
D-Threonine aldolase	4.1.2.42	-
D-Glutamate cyclase	4.2.1.48	7
D-Serine dehydratase	4.3.1.18	2
D-Cysteine lyase	4.4.1.15	15
Amino acid racemases	5.1.1.x	
Alanine racemase	5.1.1.1	1,12,6
Methionine racemase	5.1.1.2	-
Glutamate racemase	5.1.1.3	6,7,16
Proline racemase	5.1.1.4	4
Lysine racemase	5.1.1.5	-
Threonine racemase	5.1.1.6	-
Arginine racemase	5.1.1.9	5-7,11
Amino acid racemase	5.1.1.10	2,5-7,15
Phenylalanine racemase	5.1.1.11	8
Ornithine racemase	5.1.1.12	5
Aspartate racemase	5.1.1.13	1
Serine racemase	5.1.1.18	2
D-Lysine 5,6-aminomutase	5.4.3.4	11
D-Ornithine 4,5-aminomutase	5.4.3.5	5
D-Alanine-poly(phosphoribitol) ligase	6.1.1.13	12
D-Aspartate ligase	6.3.1.12	-
D-Alanine-D-alanine ligase	6.3.2.4	12,12
UDP-*N*-Acetylmuramoylalanine-D-glutamate ligase	6.3.2.9	6,7,13
D-Alanine-alanyl-poly(glycerolphosphate) ligase	6.3.2.16	-

1.3. Industrial applications of D-amino acids

D-AAs are industrially relevant compounds used in high-value commercial and commodity products. The food industry developed compounds such as Alitame, which are dipeptides containing D-Ala. Alitame is significantly more potent than sucrose and more stable in acidic beverages than aspartame.[36,37] The cosmetic industry has patented the use of D-AAs for the treatment of wrinkle formation, protection against UV damage, and for use in deodorants (D-cycloserine).[38,39] However, the biggest market for D-AAs is the pharmaceutical industry, where they are incorporated into medications to treat an assortment of ailments. The inclusion of D-AAs has been shown to increase peptide drug resistance to proteolysis.[40]

1.3.1. Pharmaceuticals

The search for natural products with antimicrobial activity culminated in the identification of many compounds that contain D-AAs.[35,41–47] The most recognizable examples are the β-lactam antibiotics which contain penicillin and cephalosporin cores. The penicillin core contains D-valine and both cores can be functionalized with aromatic D-amino acids. For example, the antibiotics Ampicillin[48] and Cephalexin[49] both contain D-phenylglycine (D-Phg) (Figure 1.6).

The canonical aromatic D-AAs (D-Phe, D-tyrosine (D-Tyr), D-tryptophan (D-Trp)) and their derivatives are of particular importance as they have been incorporated into several pharmaceuticals. For example, D-Phe is a building block of nateglinide,[50] fungisporin,[51] PPACK,[52] octreotide,[53] and cetrorelix[54] and several other medications (Table 1.2, Figure 1.6).

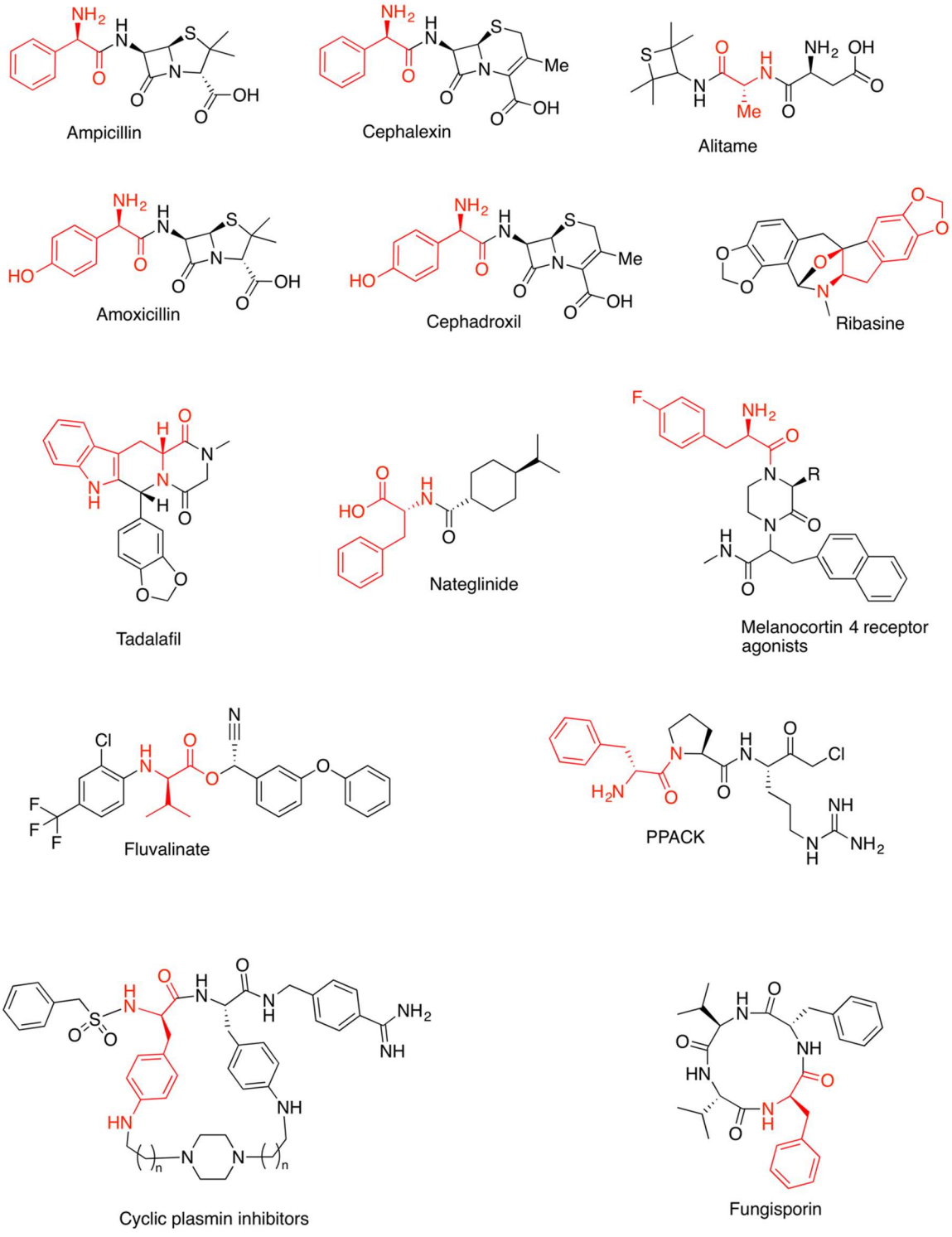

Figure 1.6 Industrially relevant bioactive compounds containing D-amino acids (highlighted in red). (Figure adapted from [35,55])

Table 1.2 Applications of aromatic D-amino acids.

D-Nal: D-3-(2-naphthyl)alanine, D-Pal: 3-(pyridine-3-yl)-D-alanine, D-Aph: 4-amino-D-phenylalanine, D-Cpa: 4-chloro-D-phenylalanine, D-Pyr:3-(3-pyridyl)- D-alanine, D-pHPhg: D-para-hydroxyphenylglycine, D-Phg: D-phenylglycine, D-dHPhg: D-2-(2,5-Dihydro)phenylglycine. (Adapted with permission from Martínez-Rodríguez, S. *et.al*., Chem. Biodivers. 2010. Copyright © 2010 Verlag Helvetica Chimica Acta AG, Zürich.)[35]

Compound	Amino Acid	Application	Ref.
D-Phe		Analgesic in warm blooded animals, antidepressant, treatment of *Parkinson's* disease	56
D-*O*-^{18}F-Fluoromethyltyrosine	D-Tyr	Screening of cancers using positron emission tomography (PET) imaging	57,58
Ac-rfwink-NH2(opioid peptide)	D-Phe, D-Trp	Analgesic activity	59
Nateglinide	D-Phe	Antidiabetic	50
Fungisporin, Gramicidin S, Tyrocidines A, B	D-Phe	Antibiotic	47,51
PPACK	D-Phe	Anticoagulant	52
Melanocortin 4 receptor agonists	4-F-D-Phe	Antiobesity	60
Tadalafil	D-Trp, 2-alkyl-D-Trp	phosphodiesterase type 5 inhibitor, hypertension	61,62
Thymodepressin	D-Trp	Atopic dermatitis	63
Cefatrizine, Cefatrizine, Cefprozil, Cefoperazone, Cefpiramide [SM-1652], Amoxicillin	D-pHPhg	Antibiotic	64–69
Cephalexin, Cefaloglycin, Cefaclor, Loracarbef, Ampicillin and derivatives	D-Phg	Antibiotic	64–66,69–74
Cefradine, Cefroxadine (CPG9000), Epicillin	D-dHPhg	Antibiotic	64,65,70,75
Somatostatin Analogs		Somatostatin Analogs are used to treat cancers, cardiovascular diseases, proliferative retinopathies, and rheumatoid arthritis.	
Octreotide (sandostatin)	D-Phe, D-Trp		53
Seglitide (MK 678)	D-Trp		53
Vapretide (RC-160)	D-Phe, D-Trp		53
KE108	D-Trp		53
Hexarelin	2-methy-D-Trp, D-Phe		76
Lanreotide	D-Trp, D-Nal		53
Gonadotropin- releasing hormone (GnRH) analogs		In general, GnRH analogs are used in the treatment of some hormone-dependent cancers (such as prostate cancers) and diseases and conditions which result from inappropriate sex hormones. GnRH Antagonists have applications in reproductive technologies	

Table 1.2 (cont.)

Compound	Amino Acid	Application	Ref.
Abarelix	D-Cpa*, D-Nal		77
Antarelix	D-Nal, D-Cpa*, D-Pal		77
Ganirelix	D-Nal, D-Cpa*, D-Pal		77
Iturelix (antide)	D-Nal, D-Cpa, D-Pal		77
Cetrorelix	D-Nal, D-Cpa, D-Pyr		54
AzalineB	D-Nal, D-Cpa, D-Pal		78
Degarelix	D-Nal, D-Cpa, D-Pal, D-Aph,		78
Synarel (naferelin)	D-Nal		78
Decapeptyl (triptorelin)	D-Trp		78

*Shown as D-Phe in reference.

1.4. Biocatalytic strategies for producing D-amino acids

In this section, we will describe the biocatalytic processes and highlight examples of each method for producing D-AAs. The strategies have been categorized as either deracemizations or asymmetric synthesis.

1.4.1. Deracemizations methods

The chemical synthesis of racemic α-amino acids is well-established chemistry achieved using methods such as the Strecker reaction.[79–81] Traditionally, the desired enantiomer was isolated using direct preferential crystallization, crystallization of diastereomeric salts, or kinetic resolutions.[82] However, these methods have a theoretical yield of 50% and the undesired enantiomer is considered a waste product.[83] To improve the chemical yield, biocatalytic deracemization strategies take racemic α-amino acids or precursors molecules and produce enantiopure D-amino acids. The broad definition of a deracemization proposed by Kurt Faber follows:

"*… any process during which a racemate is converted into a non-racemic product in 100% theoretical yield without intermediate separation of materials.*"[84]

Based on this definition, two common strategies have been employed to increase the chemical yield and obtain high enantiopurity: dynamic kinetic resolution (DKR) and stereo-inversion (SI).[85]

1.4.1.1. Dynamic kinetic resolution

DKR improves upon kinetic resolution (Figure 1.7A) by coupling an *in situ* racemization of the starting material. This is exemplified as follows (Figure 1.7B): the desired enantiomer (R_S) undergoes an enantioselective transformation to the desired product (R_P), while the undesired substrate (S_S) undergoes racemization which regenerates the equilibrium between R_S and S_S. This process converts the chiral pool of S_s to R_s, while R_s is transformed to R_P. This process results in a maximum theoretical yield of 100% as all S_s is converted to R_P. The success of this strategy relies on the racemization being performed under mild conditions to prevent loss of material by side reactions or racemization of the final product.[85]

A. Kinetic Resolution

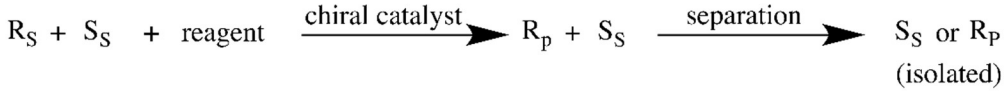

B. Deracemization by Dynamic Kinetic Resolution

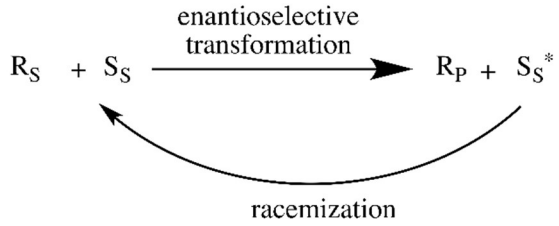

C. Deracemization by Stereo-Inverstion

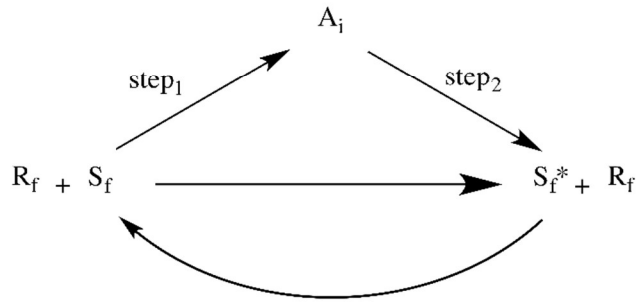

Legend

$R_S = R_{substrate}$

$S_S = S_{substrate}$

$R_P = R_{product}$

$R_f = R_{form}$

$S_f = S_{form}$

$A_i = A_{intermediate}$ (usually non-chiral)

$step_1$ = enantioselective step

$step_2$ = enatioselective or non-selective step

* lower relative abundance

D. Asymmetric Synthesis

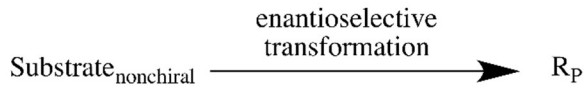

Figure 1.7 Strategies to produce optically pure D-amino acids. (Figure redrawn and adapted from [83,85])

An example of DKR to produce D-amino acids is the D-hydantoinase (E.C. 3.5.2.2) and D-carbamoylase (E.C. 3.5.1.77) process (Figure 1.8). The synthesis of racemic hydantoins can be achieved using the Bucherer-Berg synthesis,[86,87] the hydantoin/carbamoylase process is used to produce a variety of amino acids including D-histidine (D-His), D-Phg, and D-Phe.[88,89] The hydrogen in the 5-position of the hydantoin ring is more acidic than the corresponding free amino acid and undergoes racemization above pH 8. The enantioselective D-hydantoinase hydrolyzes the hydantoin to the D-carbamoyl amino acid. The D-carbamoylase hydrolyzes the D-carbamoyl amino acid to the free D-AA. The L-hydantoin undergoes racemization producing additional D-substrate for the hydantoinase.

This production method has a few limitations including: the substrate scope of hydantoinases are limited, hydantoins have low solubility, the specific activities of hydantoinases for non-proteinogenic amino acid side-chains are low, and the half-life for racemization can very from minutes to days depending on the hydantoin.[90,91] Other DKR processes for producing D-AAs include using Lipases[92] and Acylases[93,94] (Figure 1.9).

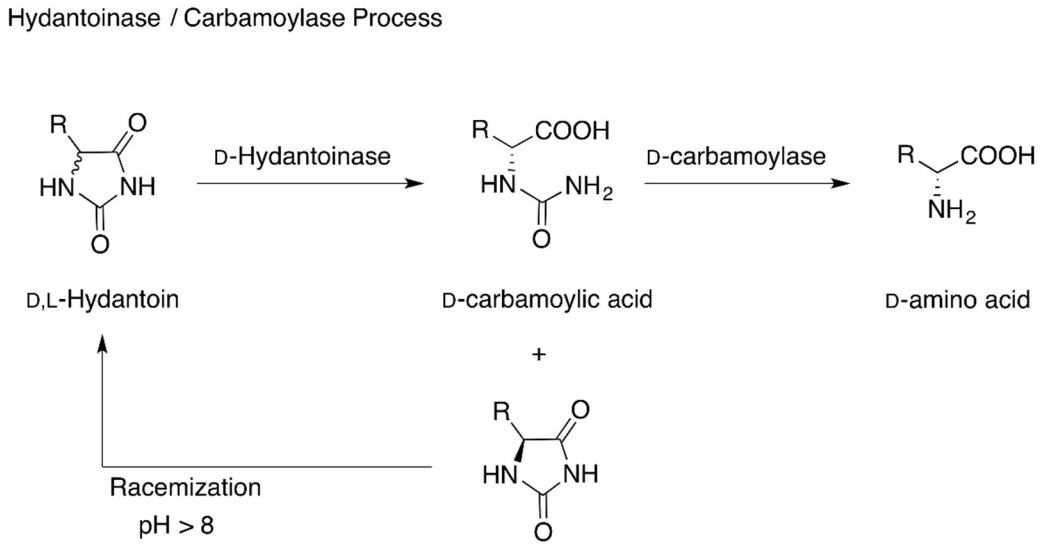

Figure 1.8 The D-hydantoinase / D-carbamoylase process for producing D-amino acids.

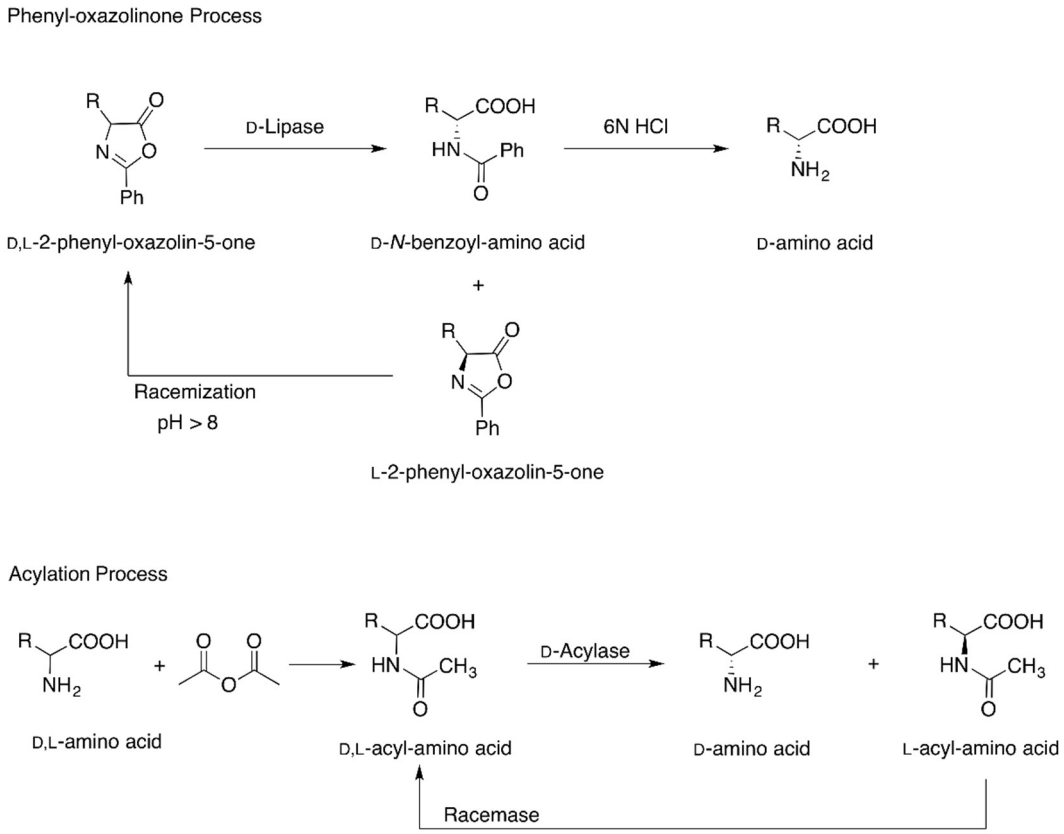

Figure 1.9 The phenyl-oxazolinone and acylation processes for producing D-amino acids. (Figure redrawn and adapted from [92] and [93,94])

1.4.1.2. Stereo-inversion

The SI method transforms the undesired enantiomer into an intermediate that is converted to the desired product. This is exemplified as follows (Figure 1.7C): Starting from a racemate of S_f and R_f, the undesired enantiomer (S_f) undergoes an enantioselective step that results in an intermediate (A_i) which is usually non-chiral. A_i then undergoes either a convergent transformation producing R_f or a nonconvergent synthesis producing a racemate of R_f and S_f. In the nonconvergent synthesis, multiple iterations through the cycle results in the accumulation of the desired enantiomer (R_f).

One example is the production of D-amino acids using the chemo-enzymatic deracemization with L-amino acid deaminase and amine-borane (Figure 1.10). The L-amino acid oxidase performs stereo-selective oxidization of the L-amino acid to produce the imine. In the presence of a reducing agent such as amine-borane it produces the L- or D-enantiomer. Multiple iterations through the cycle results in accumulation of the D-enantiomer.[95]

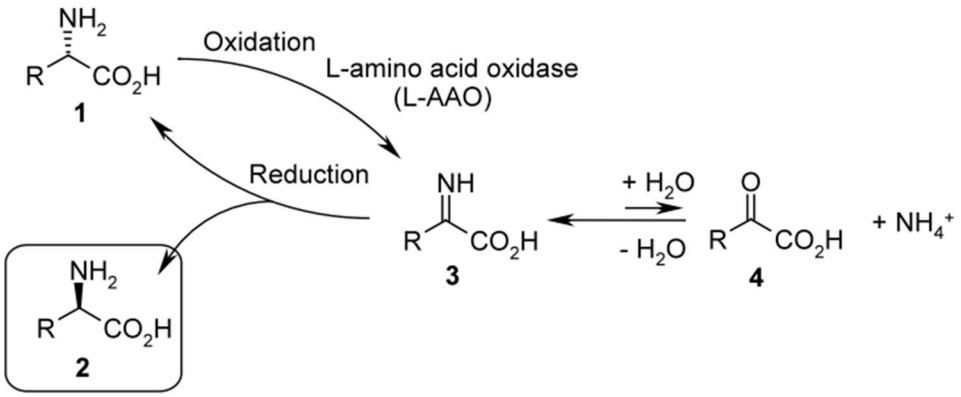

Figure 1.10 The chemo-enzymatic deracemization of racemic amino acids with L-AAO and chemical reduction. (Reproduced with permission from **Alexandre, F. R. *et. al., Tetrahedron Lett.* 2002, *43* (4), 707–710. Copyright © 2018 Elsevier Science Ltd. All rights reserved.)**[95]

1.4.2. Asymmetric synthesis

The synthesis of an enantiopure amino acid from prochiral starting materials is called an asymmetric synthesis, which allows for a theoretical yield of 100% but requires a stereo-selective catalyst. The genomic era has provided fast access to large sets of genes from numerous organisms. These gene sets coupled with high-throughput screening technologies enable the identification and engineering of enzymes that can perform the desired stereoselective transformation.

Enzymes that can perform the stereoselective synthesis of D-AAs include aminotransferases (AT) and dehydrogenases (DH) (Figure 1.11).[96,97] Starting from prochiral keto acids, a DH or AT performs a stereoselective reductive amination or transamination to produce the desired amino acid, respectively. For example, the production of D-cyclohexylalanine can be achieved using the D-amino acid dehydrogenase BC621 (Figure 1.12).[97] The cyclohexylpyruvate undergoes a reductive amination by D-amino acid DH by oxidizing the nicotinamide adenine dinucleotide phosphate cofactor ($NADP^+$) from the reduced state (NADPH). To drive the reaction to completion and perform cofactor recycling, the reaction is coupled with a second DH. Glucose dehydrogenase is commonly used to oxidize glucose to gluconolactone and produce NADPH from $NADP^+$.

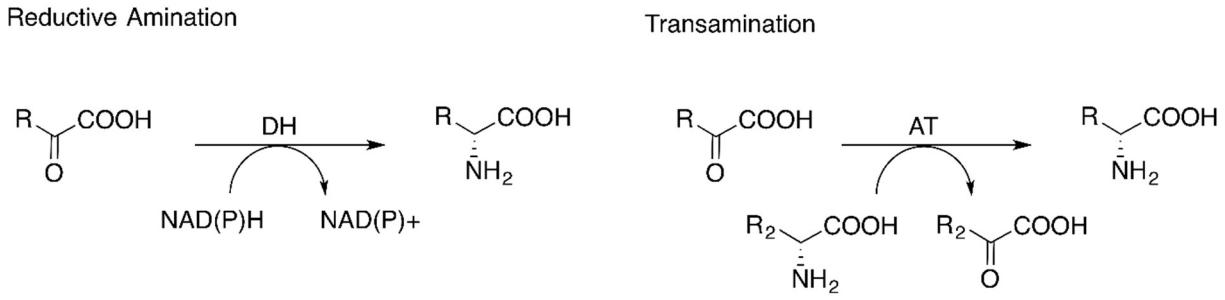

Figure 1.11 Methods for producing enantiopure D-amino acids using prochiral starting material.

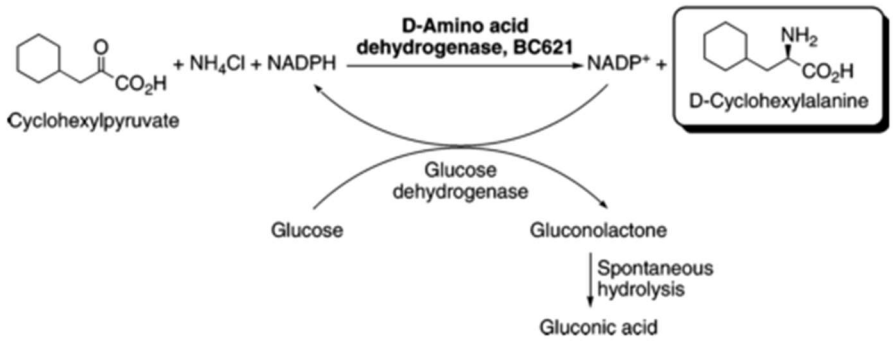

Figure 1.12 Asymmetric synthesis of D-cyclohexylalanine using two dehydrogenases. (Reprinted with permission from Vedha-peters, K. *et al.*, *J. Am. Chem. Soc.* 2006, *128* (5), 10923–10929. Copyright 2018. American Chemical Society.)[97]

The production of optically pure D-AAs from prochiral substrates with chiral catalysts is advantageous but the use of expensive NADPH or NADH is a major detractor on an industrial scale. The use of an AT to produce D-amino acids would enable production of D-AAs with a low-cost coenzyme. ATs are a subclass of pyridoxal 5′-phosphate (PLP) enzymes that are a diverse enzyme super family. Below, we will discuss the discovery and versatility of the coenzyme, the diversity and classification of this enzyme family, and the mechanism of ATs.

1.5. Pyridoxal 5′-Phosphate Enzymes

Pyridoxal 5′-phosphate (PLP) enzymes catalyze multifarious reaction types—racemizations,[98] decarboxylations,[99] side-chain eliminations,[100] β- or γ-elimination and/or replacements,[101–104] and transamination reactions (Figure 1.13).[105,106] This manifold of chemistry is achieved using the pyridoxal 5′-phosphate coenzyme which is part of the vitamin B6 group. These PLP-dependent enzymes are involved in the metabolism of many amino acids which situates them as potential biocatalysts to produce D-AAs. We will discuss below how this versatile coenzyme was identified, how it achieves its catalytic diversity, and take a more in depth at a promising subclass of PLP-dependent enzymes that hold biocatalytic potential for producing D-amino acids.

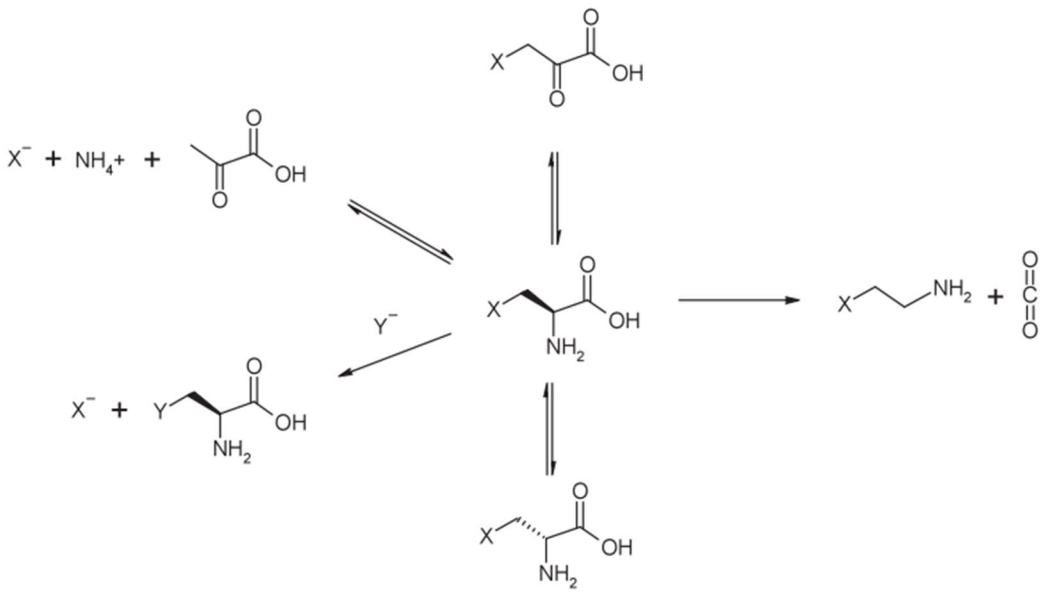

Figure 1.13 Multifarious reactions catalyzed by PLP-dependent enzymes. (Figure reproduced with permission from Phillips, R. S. *Biochim. Biophys. Acta - Proteins Proteomics* 2015, *1854* (9), 1167–1174. Copyright © 2018 Elsevier B.V. All rights reserved.)[106]

1.5.1. The identification of the vitamin B6 group

The beginning of 20th century marked a new paradigm for understanding human health and disease states. The earlier studies of scurvy,[107] beriberi,[108] and rickets,[109] established a dietary link to disease states but failed to construct the concept of nutrient deficiency. Instead, the foodstuff which cured the disease was believed to contain a "factor" that killed the responsible bacterium. Ultimately, this hypothesis was proven incorrect when Dr. Funk coined the "vitamine theory" in 1912 after isolating the vital amine required to treat beriberi disease.[110] This landmark paper established that certain nutrients are essential for the proper health of living beings.

Vitamines, later renamed to vitamins as not all essential nutrients contained amines, were characterized into two distinct factors by Elmer McCollum at the University of Wisconsin in 1916—fat-soluble vitamine A and water-soluble vitamine B.[111] In 1934, P. György studied a factor known to alleviate rat pellagra—a dermatitis of the skin with swelling of the paws and ears—and named it vitamin B_6.[112] In 1938, P. György and 3 other groups reported successfully isolating vitamin B_6 in crystalline form from rice bran and yeast. The chemical structure was determined to be 3-hydroxy-4,5-bis-(hydroxymethyl)-2-methylpyridine in 1939 and given the common name of pyridoxine (Figure 1.14, I).[113]

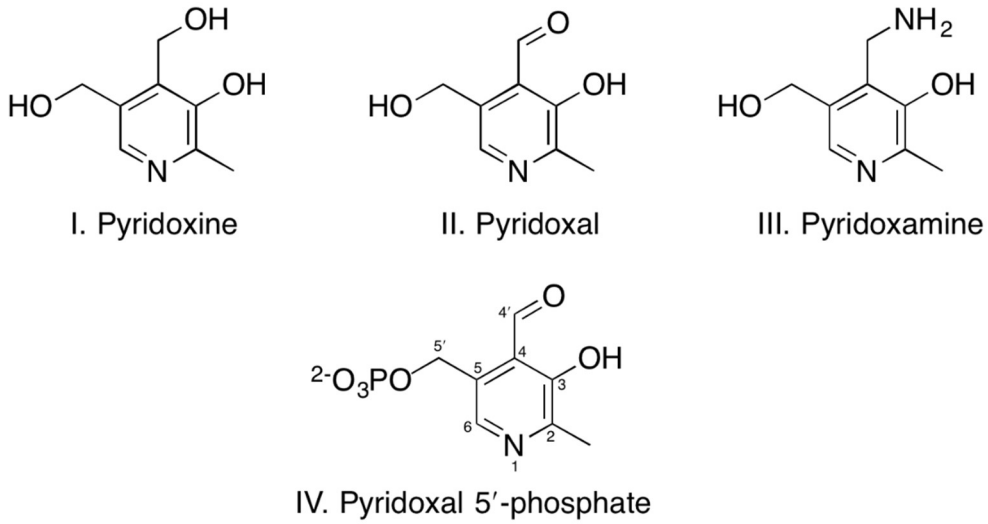

Figure 1.14 Chemical structures of pyridoxine and its metabolites.

In 1942, Dr. Snell *et al.* established that "pseudopyridoxine ", a material metabolically derived from pyridoxine in animals, induced higher growth rates in lactic acid bacteria.[114] Following this initial report, Dr. Snell elucidated two highly active pyridoxine derivatives that were obtained by oxidizing the hydroxymethyl group at C4 to an aldehyde (pyridoxal) or amine (pyridoxamine) which are represented in Figure 1.14, structures II & III, respectively.[115] Biological chemists endeavored to identify and elucidate the structure-function relationship of the vitamin B_6 group. Their works are extensively summarized by Dr. Snell in 1958 and culminated in the understanding that vitamin B_6 is comprised of 6 bioactive compounds that are interconvertible with the predominant form being pyridoxal 5′-phosphate (PLP, Figure 1.14, IV).[116,117]

1.5.2. The multifarious reactions of PLP

The PLP coenzyme is uniquely versatile at catalyzing multiple reaction types (Figure 1.15). The formation of the external aldimine between an amino acid and PLP leads to many

potential reactions pathways. Most PLP reactions can be categorized into 3 reaction types that occur following formation of the external aldimine: net reaction at the α, β, or γ position. Reactions that occur at the α position include racemization, transamination, decarboxylation, and α-elimination and replacement. At the β position, the β-elimination or β-substitution reactions occurs with enzymes such as serine dehydratase or tryptophan synthase, respectively. Reactions at the γ position include γ-elimination or γ-elimination and γ-addition with enzymes such as cystathionine γ-lyase and cystathionine γ-synthase, respectively.[118,119]

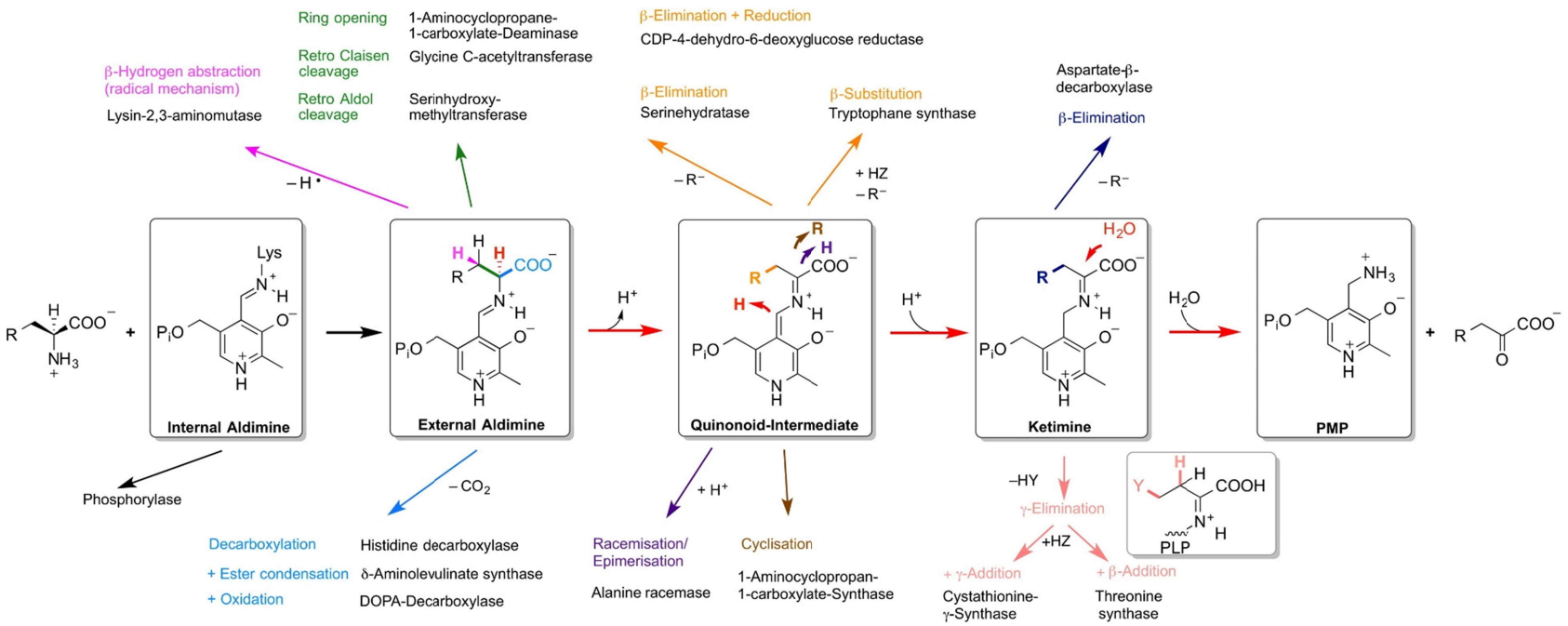

Figure 1.15 PLP-dependent enzymes catalyse a variety of chemical reactions by stabilising carbanionic intermediates, after the substrate formed a covalent aldimine intermediate with PLP. In many, but not all reactions, a quinonoid intermediate is formed during the reaction. In the centre of the figure, the most important intermediates observed during a transaminase reaction are shown. At each intermediate, there is a range of many possible reactions, as different bonds can be broken or formed, leading to distinct enzymatic activities. Possible bonds to be broken are shown in different colours, bonds to be formed with differently coloured electron arrows. One enzyme activity is given as an example for each reaction, but in nature a much larger collection of activities exist. Reproduced with permission from Steffen-Munsberg *et.al.*, Biotechnology Advances 2015. Copyright © 2018 Elsevier.)[118]

1.5.3. The Dunathan Stereoelectronic Hypothesis

In 1966, while investigating the determinants of reaction type specificity, Dunathan postulated the orientation of substituents on the Cα of an amino acid relative to the pyridine ring of PLP would determine which bond is cleaved on the Cα upon formation of the imine.[120] Specifically, alignment of a sigma bond perpendicular to the plane of the pyridine ring and parallel to the orbitals of the π electrons activates the sigma bond. The carbanion formed is stabilized by extending conjugation into the π system of PLP (Figure 1.16).[119] Thus, depending on the orientation of the amino acid—deprotonation, decarboxylation, or side-chain elimination will occur (Figure 1.17).

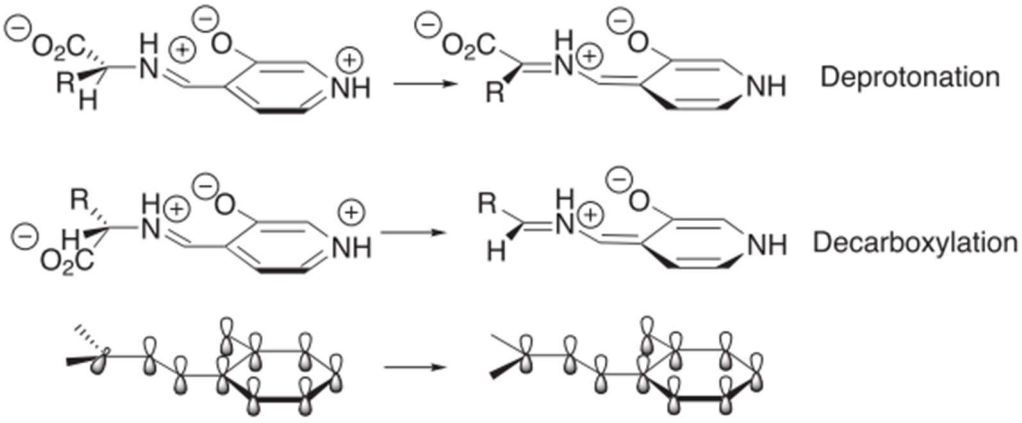

Figure 1.16 The Dunathan stereoelectronic hypothesis for deprotonation and decarboyxlation. The bond on the Cα of the substrate to be broken is perpendicular to the plane of the pyridine ring and aligned with pi orbitals. Figure reproduced with permission from Eliot, A. C.; Kirsch, J. F. *Annu. Rev. Biochem.* 2004, *73* (1), 383–415. Copyright © 2004, Annual Reviews.[119]

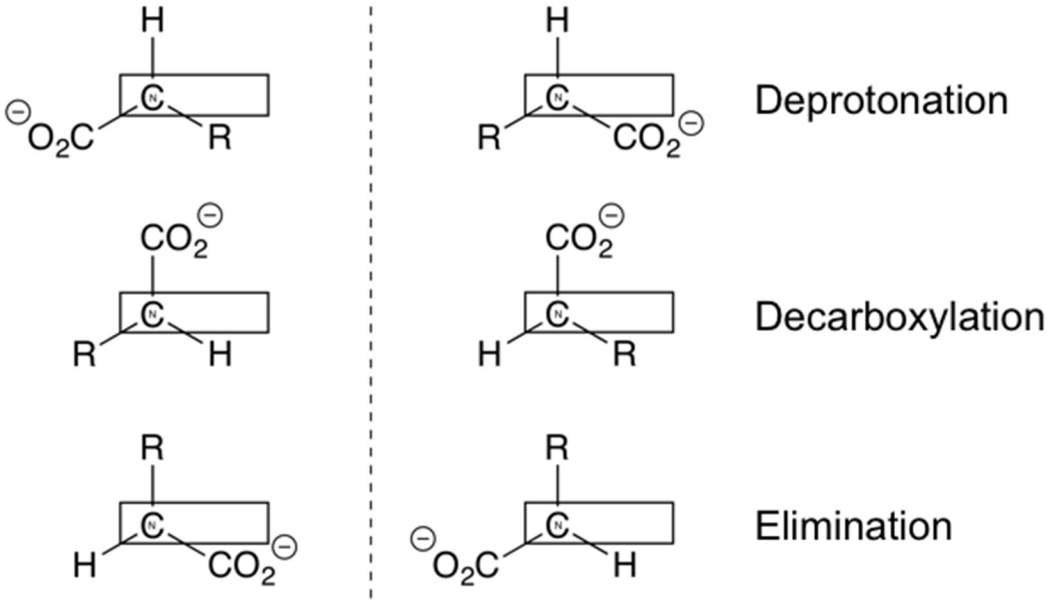

Figure 1.17 Conformations of L- and D- amino acids bound to PLP viewed down the Cα to nitrogen bond. The pyridine ring of PLP is represented by the box. The substituent perpendicular to the ring is in the activated position resulting in deprotonation, decarboxylation, or elimination. Figure adapted from Dunathan, H. C. *J. Cell. Biochem.* 1966, *49* (19), 712–716.[120]

1.5.4. The structural diversity of PLP-dependent enzymes

There are currently 7 distinct fold-types for PLP-dependent enzymes in the B6 database (Table 1.3).[121] These distinct fold-types share no homology and are believed to be examples of convergent evolution.[106] The prototype sequence for which a fold-type is named, e.g. the aspartate aminotransferase family, does not dictate reaction type. In fact, a fold-type can contain many reaction types and span several E.C. numbers. For example, fold-type I–the aspartate aminotransferase family–contains glycine dehydrogenase (E.C. 1.4.4.2),[122] histidinol-phosphate aminotransferase (E.C. 2.6.1.9),[123] kynureninase (E.C. 3.7.1.3),[124] tyrosine decarboxylase (E.C. 4.1.1.25),[125] and alanine racemase (E.C. 5.1.1.1)[98] which span 5 of the 6 E.C. numbers.

Table 1.3. Fold-types of the PLP-dependent superfamily.

Fold-type[a]	Fold Name	Prototype structure (PDB ID)	Main Fold	Primary Citation
I	Aspartate Aminotransferase Family	1AAT	3-layered α/β/α sandwich.	126
II	Tryptophan Synthase Family	1BKS	Two domains with mixed α/β structure.	127
III	Alanine Racemase Family	1SFT	PLP-binding barrel.	128
IV	D-Amino Acid Aminotransferase Family	1DAA	A small 2-layered sandwich domain and a large domain consisting of an α/β barrel.	105
V	Glycogen Phosphorylase Family	1PYG	Rossman fold.	129
VI	D-Lysine 5,6-Aminomutase Family	1XRS	TIM-barrel with the PLP imine linkage formed to the coenzyme B_{12} binding Rossmann domain.	130
VII	Lysine 2,3-Aminomutase family	2A5H	A $(\beta/\alpha)_6$-crescent that is reminiscent of a TIM Barrel $(\beta/\alpha)_8$.	131

[a] Based on the B6 database by Percudani and Peracchi.[121]

Since the enzyme fold-type does not determine reaction specificity, the enzyme scaffold is largely responsible for directing the catalytic route taken by the coenzyme. Following the formation of the external aldimine, the reaction type catalyzed by PLP is determined based on stereoelectronic effects, the protonation state of PLP, and active site interactions.[132] The scaffold dictates an active site topology forcing the substrate into a conformation in which the Cα bond to be broken is perpendicular to the pyridine ring of the coenzyme upon formation of the external aldimine (Dunathan Stereoelectronic Hypothesis). The subsequent carbanionic intermediate that forms will interact with active site residues to control the reaction outcome. In the context of this discussion, enzymes that perform reactions at the α-position and lead to transamination reactions are relevant as they can asymmetrically synthesize D-AAs.

1.6. Aminotransferases

Aminotransferases or ATs (E.C. 2.6.1.X) are PLP-dependent enzymes that are ubiquitous and essential for the nitrogen metabolism of cells. They have several characteristics which make them desirable biocatalysts to produce D-AAs including: high enantioselectivity, regioselectivity, stability, and activity. ATs are a subclass of PLP-dependent enzymes, therefore we will discuss how they are classified, the mechanism of transamination, and important nomenclature for describing the active site.

1.6.1. Classification of ATs

Although seven fold-types of PLP-dependent enzymes exist, ATs have only been identified in fold-types I and IV. Aminotransferases of fold-type I can be subdivided into 5 classes based on sequence similarity and structural features.[133] A representative example of each class is listed in Table 1.4. The "DAAT-like" fold-type IV ATs are also called class IV ATs. Below we will discuss the main structural features of fold-type I and IV enzymes and highlight key differences between the aminotransferases classes.

Table 1.4 Representative examples of aminotransferase classes I–VI. (Table adapted from [134]).

AT classes[a]	B_6 Fold-type	Enzyme[b]	E.C. Number	PDB ID	Main Substrates	
					Amino donor	Amino acceptor[c]
I	I	AspAT	2.6.1.2	1ASN	L-Asp	α-kg
II	I	HisPAT	2.6.1.9	1FG3	L-Histidinol	α-kg
III	I	OrnAT	2.6.1.13	2OAT	L-Ornithine	α-kg
IV	IV	DAAT	2.6.1.21	3DAA	D-Alanine	α-kg
V	I	PserAT	2.6.1.52	1BT4	3-phospho-L-serine	α-kg
VI	I	ArnB	2.6.1.87	1MDO	L-Glu	UDP-2-acetamido-4-keto-2,6-

[a] Pfam classification (http://pfam.xfam.org/), class VI is also called the DegT/DnrJ/EryC1/StrS family.
[b] AspAT: Aspartate Aminotransferase; HisPAT: Histidinolphosphate Aminotransferase; OrnAT: Ornithine Aminotransferase; DAAT: D-amino acid AT; PserAT: Phosphoserine Aminotransferase; ArnB: UDP-2-acetamido-4-amino-2,4,6-trideoxyglucose Aminotransferase.
[c] α-kg: α-ketoglutarate.

1.6.2. Fold-type I ATs

The aspartate aminotransferase fold-type or fold-type I family, is the largest PLP-dependent family with activities that range from E.C. classes 1–5 and is the most widely studied aminotransferase.[119,135] This fold-type is subdivided into 5 AT classes (I, II, III, V, VI) which is based on sequence similarity and the N-terminal portion of the polypeptide chain that folds similarly within each class. The only residue that is conserved between all 5 classes is the aspartic acid residue that is responsible for pronating the pyridine nitrogen of PLP.

1.6.2.1. Class I ATs

We will use the *E. coli* Aspartate Aminotransferase (Asp-AT) crystal structures (PDB ID: 1ASN and 1ASL) that was solved and analyzed by Jansonius and coworkers to describe this fold.[136] The Asp-AT fold-type forms an obligate homodimer with one active site per subunit (Fig 1.18). The backbones from both subunits contribute essential residues to each active site with some members of the fold-type assembling into larger complexes.[119] The subunit is composed of a large and small domain (Fig. 1.19). The small domain is composed of residues from the N- and C-terminal ends of the polypeptide chain (residues 5–45 and 330–409, respectively).

The large domain or "PLP-binding domain", shown in dark green, is a 3-layered α/β/α-sandwich of which the mixed β-sheet is composed of 7 β-strands (shown in dark green, residues 46-329). The β-strands are arranged in the following order: β2, 8, 7, 6, 5, 3, and 4 with β8 being the sole antiparallel strand. On the face of the β-sheet that forms the dimer interface are α-helices α5, α6, and α10. The α-helices on the opposite face are α8, α9, α3,

and α4. There are three α-helices (α2, α11, and α12) situated above α3 and the β-sheets. The α12 is bent and transitions from the large domain to the C-terminal portion of the small domain. The α7 is located between strands β3 and 4.

The C-terminal lobe of the small domain folds into a 3-stranded β-sheet (β9, 10, and 11) with α-helices α14 and α15 on one side. The short α13 links α12 and β9. The N-terminal lobe, does not have a common fold between classes but commonly contributes to the small domain, is extended over the second subunit which then turns forming α1 and loops around to form β1 which interacts with the β-strands of the C-terminal lobe.

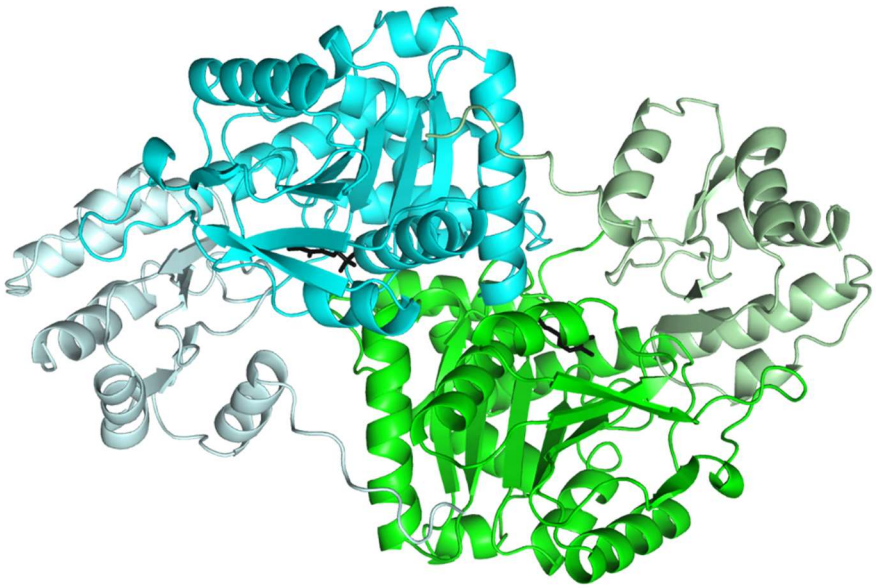

Figure 1.18: The overall structure of aspartate aminotransferase dimer. The two subunits are shown in green and cyan. The small and large domain of each subunit is show in light and dark colours, respectively. PLP is bound in each active site, shown in black. (PDB ID: 1ASN)

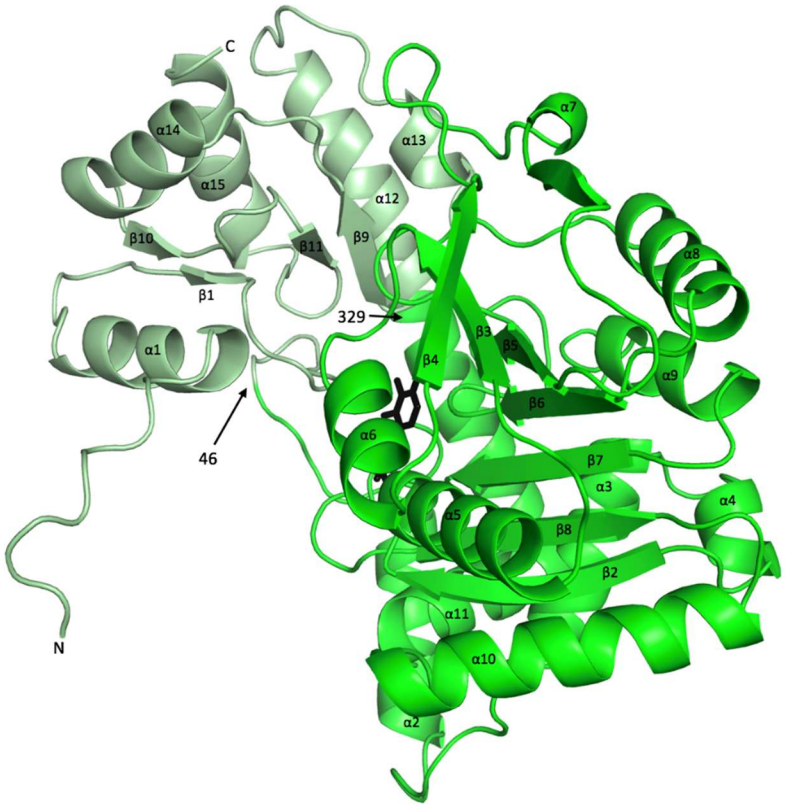

Figure 1.19: The subunit of Aspartate AT. The large and small domains are coloured dark and light green, respectively. PLP is bound in the active site, shown in black. The arrows indicate the small to large and large to small transition. (PDB ID: 1ASN)

The PLP coenzyme is bound in the cleft between the large and small domains with the *si*-face of PLP facing the protein (see section 1.6.5) and covalently attached to the enzyme via the ε-amino group of a K258 located on an α-helix between two anti-parallel β-strands of the large domain. The phosphate group is bound by polar contacts on α5, β7, R266, S256, Y70*, and S269* of the large domains (* indicates residue from second subunit). Upon substrate binding, the small domain undergoes a conformational rearrangement with the small domain rotating approximately 6° towards the large domain.[136] In Figure 1.20, the 2-methylasparate analog of L-aspartate is bound to the active site with the α-carboxylate

forming a salt bridge with R386 and the side chain carboxylate forming a salt bridge with R292*. D222 is found below the pyridine ring and W140 forms a π-stacking interaction with *re*-face of the PLP. The catalytic K258 residue is shown on the *si*-face of PLP.

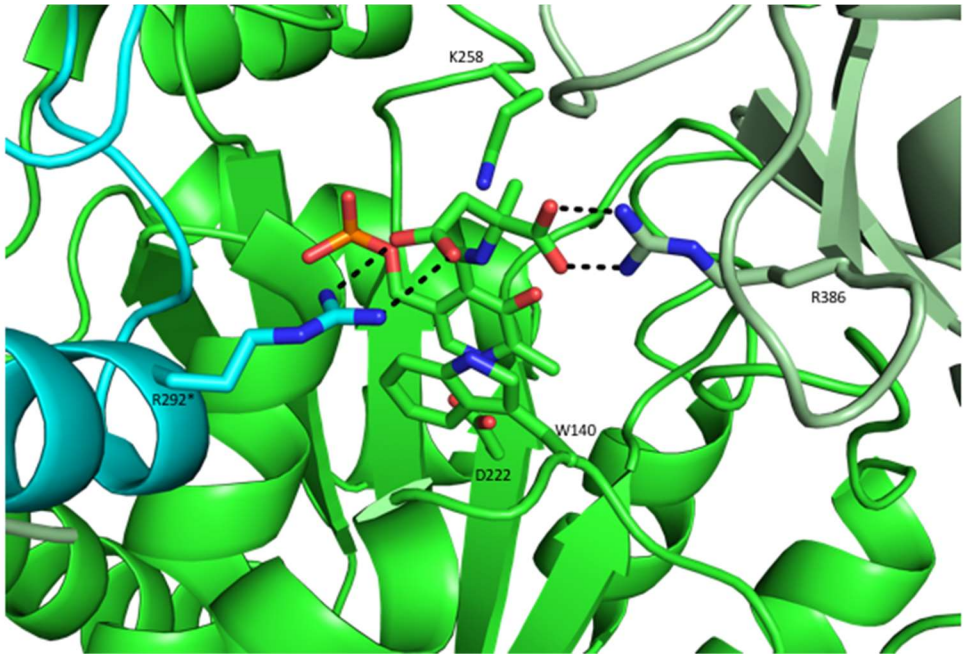

Figure 1.20: Active site of Aspartate AT with 2-methylaspartate bound to PLP. The large and small domains are shown in green and light green, respectively. The large domain of the second subunit is shown in cyan.

1.6.2.2. Other AT classes

The other fold-type I AT classes exhibit the same overall fold-type but have minor differences between the classes that can be observed. These structural modifications include twists of the β-sheet of the large domain, loops involved in substrate binding, loops involved in the dimer interface, and the size and fold of the N-terminal lobe.[137] In Figure 1.21, the N-terminal lobes of the five classes are shown up to the first β-strand of the large domain to highlight the differences between each class. In Class I, the N-terminus is outstretched over the second subunit which leads into the first α-helix of the subunit. In

Class II, the N-terminus is outstretched over the second subunit but the first α-helix is located over the second subunit. In Class III, there is no outstretched N-terminus over the second subunit. However, there is a 3-stranded antiparallel β-sheet that is believed to contribute to the reduced small domain movement that is observed in this class when substrates bind the active site.[118] The Class V and VI ATs do not have an N-terminal lobe but they display different conformations of the loop prior to the α-helices of the large domain.

There are other differences between the classes. For example, Class III ATs have an aromatic residue that forms a perpendicular π-stacking interaction with the pyridine ring of PLP whereas the corresponding residue in Class I ATs forms a parallel interaction.[137]

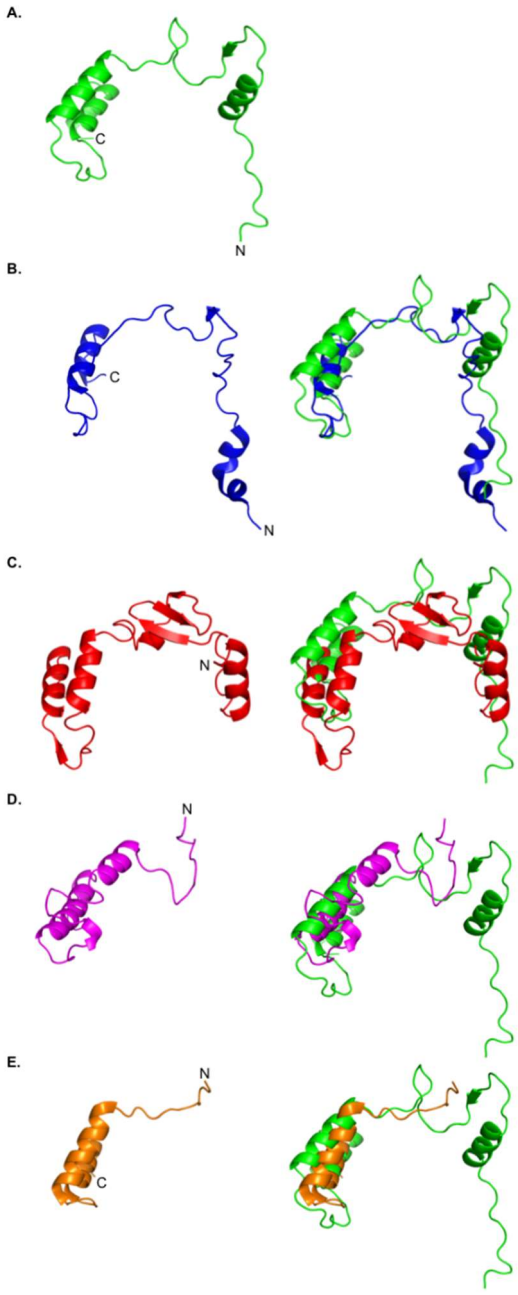

Figure 1.21 The N-terminal lobes of Class I, II, III, V, VI ATs up to the first β-strand of the large domain. The identical perspective is used for all six classes with class I overlaid on the other classes. A. Class I AT using Aspartate Aminotransferase shown in green (PDB ID: 1ASN; residues 5-99). B. Class II AT using Histidinolphosphate Aminotransferase shown in blue (PDB ID: 1FG3; residues 3-78). C. Class III AT using Ornithine Aminotransferase in red (PDB ID: 2OAT, residues 36-136). D. Class V AT using Phosphoserine Aminotransferase shown in magenta (PDB ID: 1BT4; residues 2-68).; Class VI AT using ArnB shown in orange: UDP-2-acetamido-4-amino-2,4,6-trideoxyglucose Aminotransferase (PDB ID: 1MDO; residues 9-56). The C-terminal label is hidden by an α-helix in C. and D.

1.6.3. Fold-type IV ATs

The fold-type IV was first confirmed by Sugio and coworkers when the crystal structure of D-amino acid aminotransferase was solved (PDB ID: 1DAA).[105] The enzyme forms an obligate homodimer with one active site per subunit (Fig. 1.22). The backbones of both subunits contribute essential residues to each active site of the AT and some other enzymes in this fold type assemble into larger complexes similar to what has been observed for fold-type I enzymes.[119,138]

The subunit is composed of a small and large domain which is shown in light and dark colours, respectively (Figure 1.23). The small domain is a 4-stranded anti-parallel β-sheet that forms a Greek key motif with β1, β4, β3, and β2, respectively. The first α-helix (α1) is short (< 2 turns) which interacts with the N-terminal domain of the second subunit. The α2 and 3 connecting β2 and 3, covers one face of the β-sheet. The loops between β1–2 and β2–3 form the N-terminal dimer interface with the loop between β2–3 contributing residues to the active site of the second subunit.

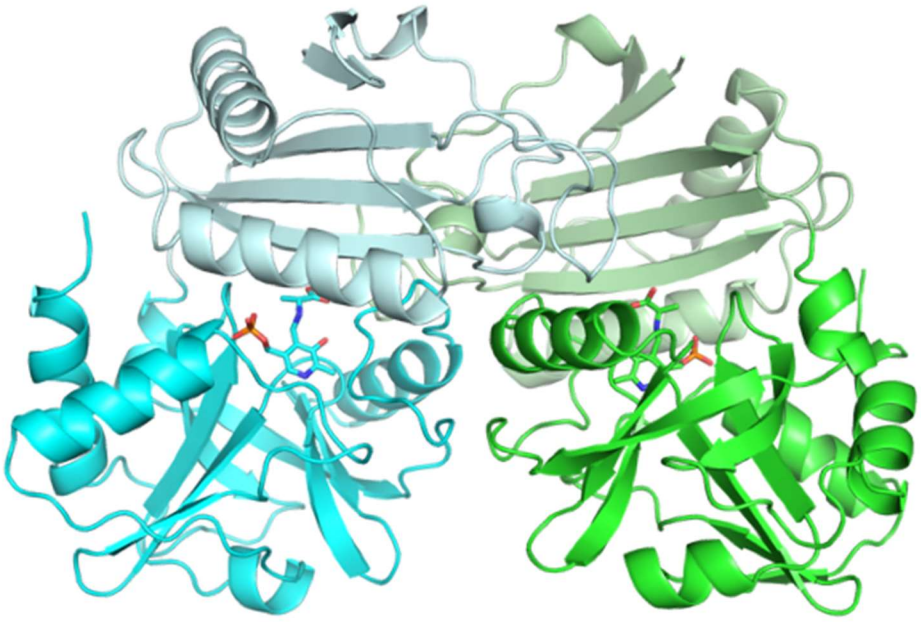

Figure 1.22 The overall structure of the D-amino acid aminotransferase (DAAT) dimer. The two subunits are shown in green and cyan. The small and large domain of each subunit is show in light and dark colours, respectively. (PDB ID: 3DAA).

The large domain is composed of two mixed β-sheets. The first mixed β-sheet is a β-α-β motif that is composed of a 3-stranded β-sheet with β5, 6, and 7. The β7 is antiparallel relative to β5 and 6. There is an interdomain loop and small α-helix (α4) between β4–5. Following β5, there is a loop and α5, which contribute resides to the dimer interface of the second subunit leading into β6. The second mixed β-sheet of the large domain is a 4-stranded antiparallel β-sheet composed of β8, 9, 11, and 12. The β10 is aligned parallel to β9 of this mixed β-sheet and forms the second β-α-β motif with α6. The α7 is located between β10-11 and the final α-helix (α8) is located at the C-terminal between α4 and 6 on one side of the mixed β-sheet.

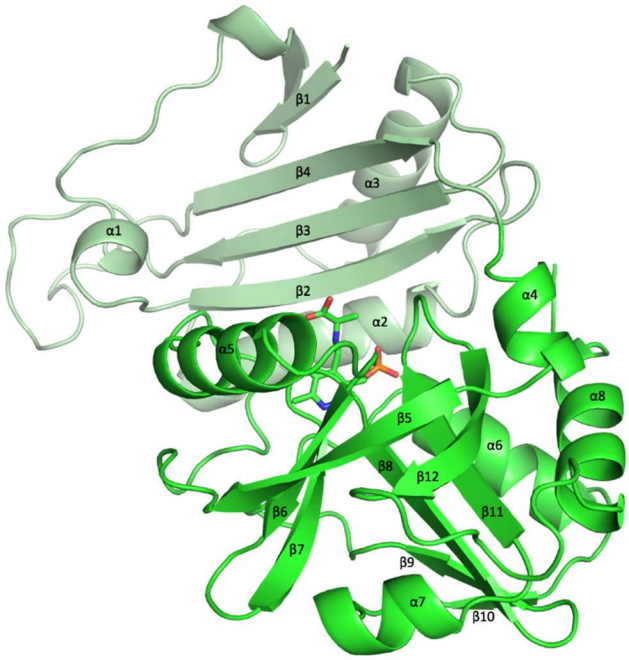

Figure 1.23 A subunit of DAAT (PDB ID: 3DAA). The small and large domain of each subunit is show in light and dark colours, respectively. The β-strands are numbered β1–11 and the α-helices are numbers α1–8.

The PLP coenzyme is bound in the cleft between the small and large domains with residues from both domains and subunits contributing to the active site (Figure 1.24). The phosphate group is bound by residues from α2 and 6 and the loop between β11 and 12. Unlike fold-type I ATs, there is no π-stacking interaction between the pyridine ring of PLP and an aromatic residue in the active site. The side-chain binding pocket is composed of V33, S240, and T242. The carboxylate binding pocket is formed from residues Y31 and R98* (* indicates residue from the second subunit).

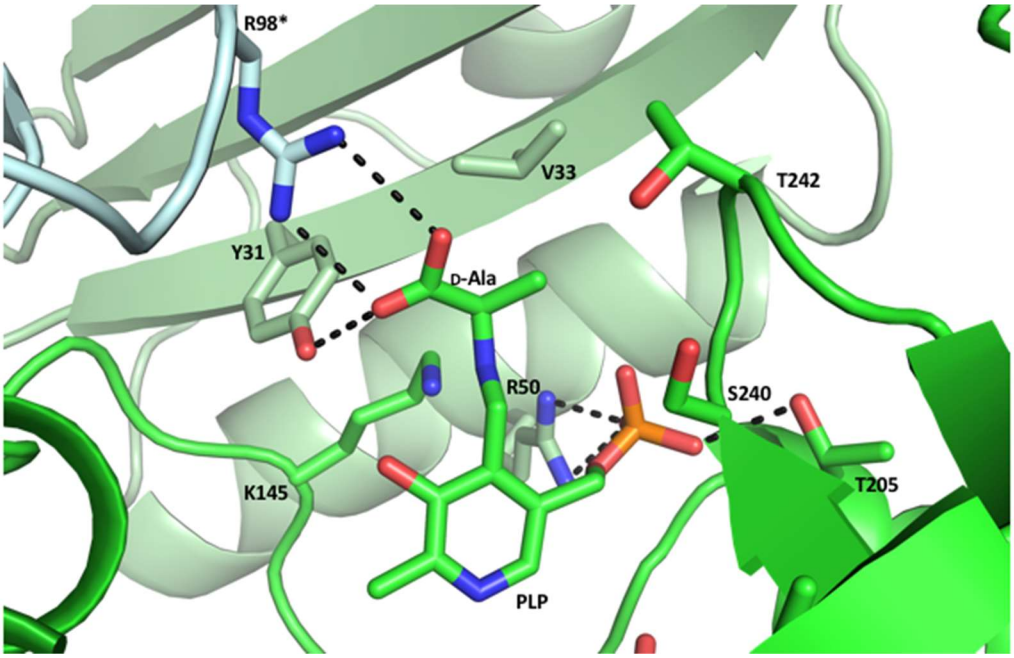

Figure 1.24 The active site of one subunit (shown in green) of DAAT (PDB ID: 3DAA) with D-alanine bound to PLP. The PLP is bound in the cleft between the small and large domain. The carboxylate binding pocket is composed of residues from both subunits with Y31 from the small domain of subunit 1 and R98* from the second subunit (shown in light blue). R50 of the small domain and T205 of the large domain contribute to binding the phosphate group of PLP. H-bond interactions are shown with black dotted lines.

1.6.4. The general mechanism of transamination

The general mechanism of transamination reported by Soda *et al.* follows: the PLP coenzyme forms a Schiff base with the ε-amino group of the catalytic lysine residue (Fig. 1.25A). This forms the internal aldimine between the coenzyme and enzyme scaffold. Next, the amino acid binds to the active site causing a transaldimination reaction which forms the external aldimine (external Schiff base, Fig. 1.25B). At this point, the reaction type is dictated by the orientation of the Cα substituents (Dunathan Stereoelectronic hypothesis). In this case, the Cα hydrogen is oriented perpendicular to the pi electrons of the pyridine ring. The Cα hydrogen is abstracted by the catalytic lysine or general base, forming an anion on the Cα that subsequently forms the quinonoid intermediate (Fig. 1.25C). The abstracted hydrogen is transferred to the C4′ of the coenzyme forming the ketimine (Fig. 1.25D). The keto acid is released by hydrolysis of the ketimine by a water molecule forming the pyridoxamine-5′-phosphate (PMP, Fig. 1.25E). With the first half of the transamination reaction complete, the second half can occur in the reverse order starting from PMP to form a new amino acid.

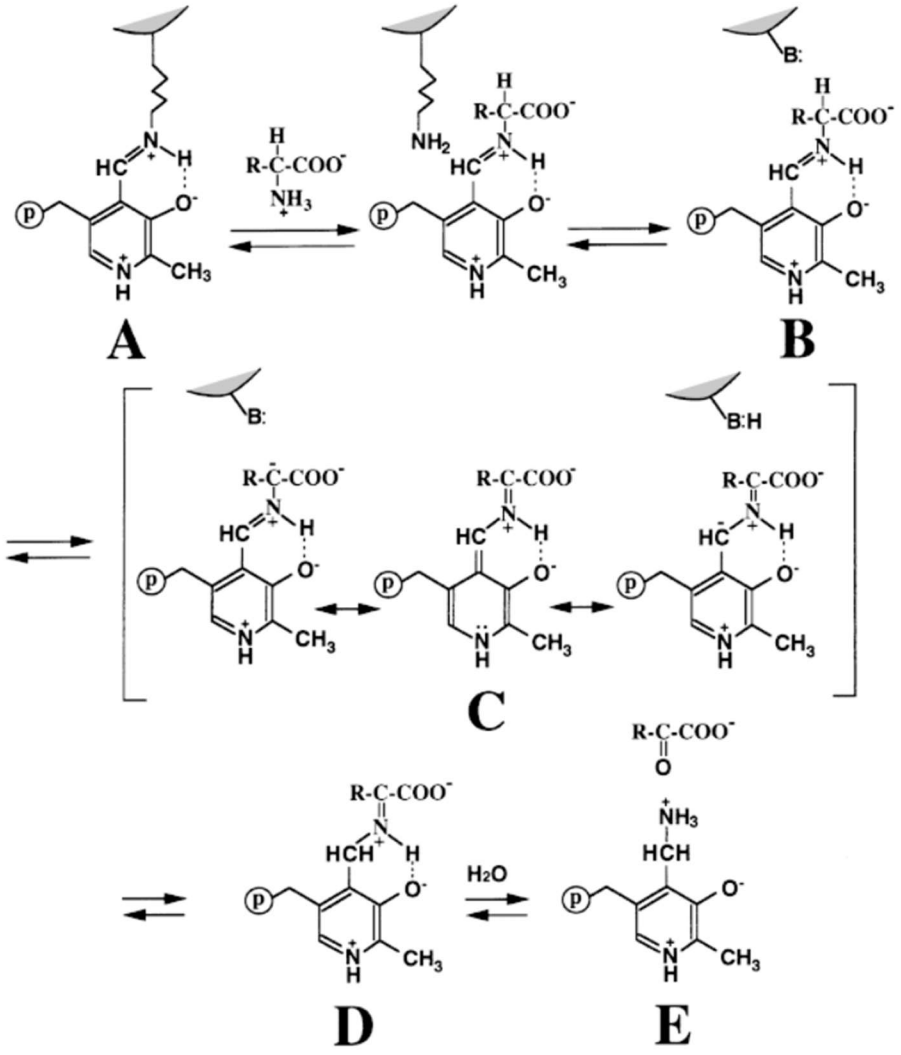

Figure 1.25 Reaction mechanism of aminotransferases. A. Internal aldimine prior to attack on the C4′ of PLP by the amino group of the substrate. B. External aldimine positioned with the Cα-H bond positioned for deprotonation with a general base catalyst, which can be the catalytic lysine residue or another residue. C. The carbanionic intermediate following deprotonation with three resonance structures. The middle structure is commonly called the quinonoid intermediate. D. The ketimine intermediate with the C4′ protonated. E. The addition of water to Cα results in the formation of PMP and release of the keto acid. (Reproduced with permission from Soda, K. *et.al*., The Chemical Record 2001. Copyright © 2001 John Wiley & Sons, Inc. and The Japan Chemical Journal Forum)[139]

1.6.5. Active site topology of ATs

To discuss the active site topology of ATs, several groups have developed terminology based on the relative position of the coenzyme. We will adopt these descriptors to facilitate our discussion on ATs. First, the hydrogen transfer that occurs at C4′ of PLP during transamination may occur on either face of the coenzyme. The *re* and *si*-face of the coenzyme refers to the face in which the pro-*R* or pro-*S* hydrogen is abstracted from C4′, respectively (Figure 1.26).[139]

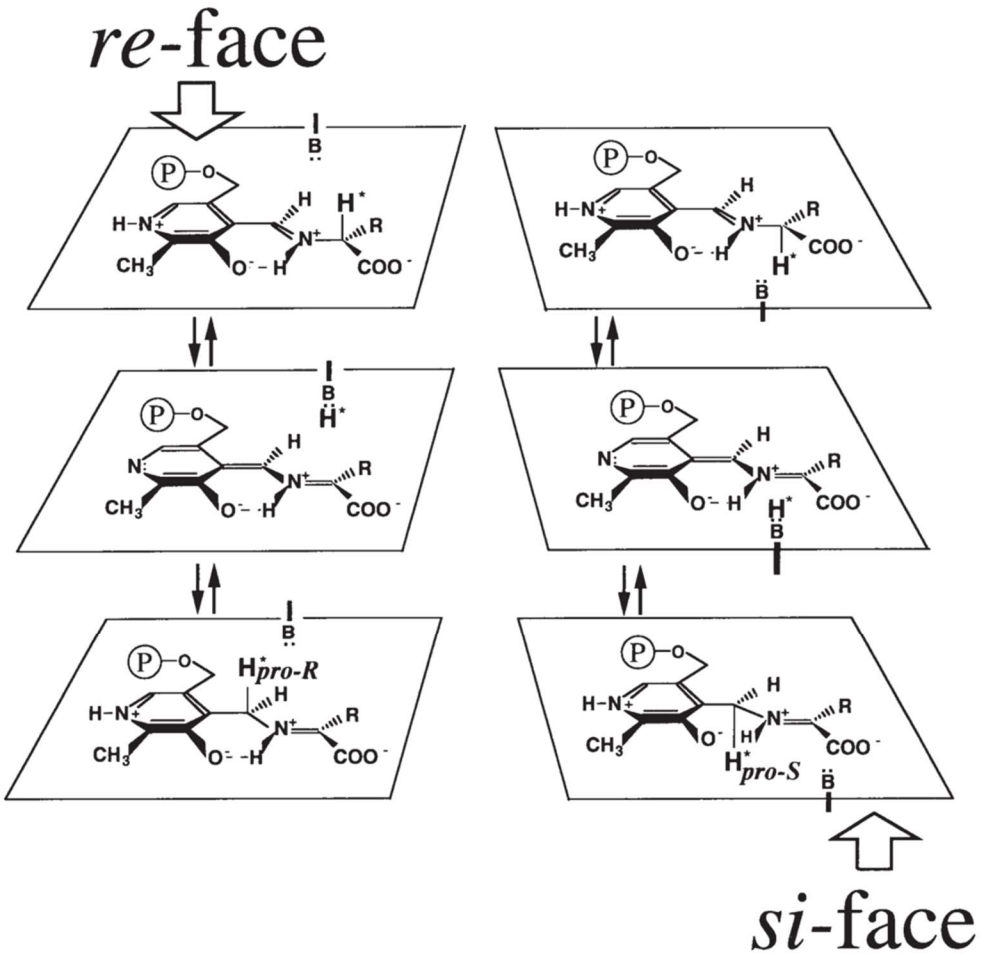

Figure 1.26 Stereospecificity for the hydrogen transfer. (Reproduced with permission from Soda, K. *et.al*., The Chemical Record 2001. Copyright © 2001 John Wiley & Sons, Inc. and The Japan Chemical Journal Forum)[139]

Additionally, the active site of ATs is comprised of two pockets that are responsible for binding the α-carboxylate and side-chain. To indicate the orientation of the carboxylate and side chain in the active site relative to the cofactor the P- and O-pocket nomenclature was developed by Wybenga *et al*..[140] The pocket located over the phosphate group is called the P-pocket and the pocket located over the O3′ atom of PLP is called the O-pocket. This is highlighted in Figure 1.27A, where the P-pocket is coloured yellow and the O-pocket is coloured orange. Figure 1.27B shows the catalytic lysine residue of *Vibrio fluvialis* AT on the *si*-face of the active site.

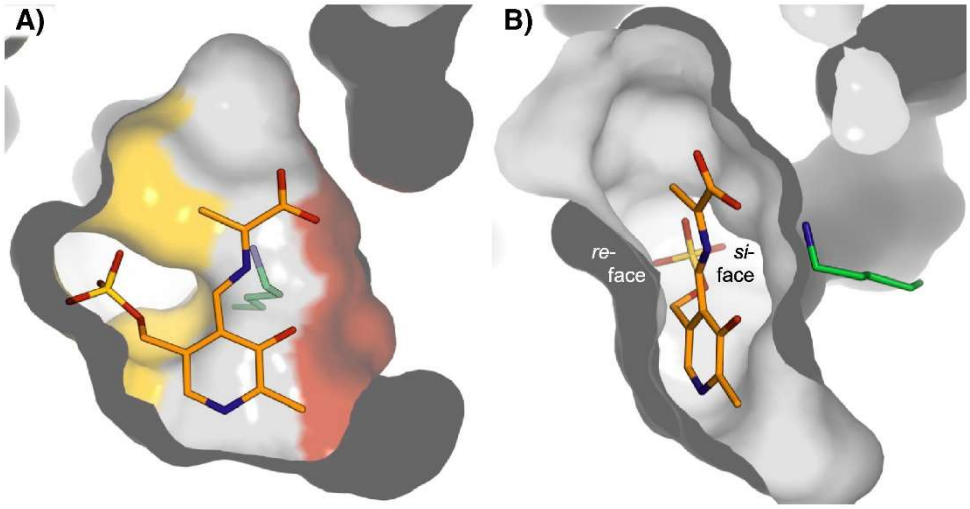

Figure 1.27 Model of the PLP quinonoid intermediate of alanine bound to the *Vibrio fluvialis* AT (PDB ID: 4E3Q) to exemplify the active site nomenclature. A) The P-Pocket is coloured yellow and the O-pocket is coloured orange. B) The protonation of the quinonoid intermediate is the chirality-introducing step in transamination. The (*S*)-enantiomer of alanine will be formed through protonation by the catalytic lysine, which is located at the *si*-face of the cofactor (relative to its C4′). (Reproduced with permission from Steffen-Munsberg, F., *et.al*., Biotechnology Advances 2015. Copyright © 2018 Elsevier)[118]

The proton abstraction occurs on the *si*-face of PLP as shown above for all AT classes except class IV. In the case of class IV, the proton abstraction occurs on the *re*-face of

PLP. In Figure 1.28, the lysine residue of D-amino acid AT from *Bacillus* sp. YM-1, a class IV AT, is positioned on the *re*-side of the coenzyme.

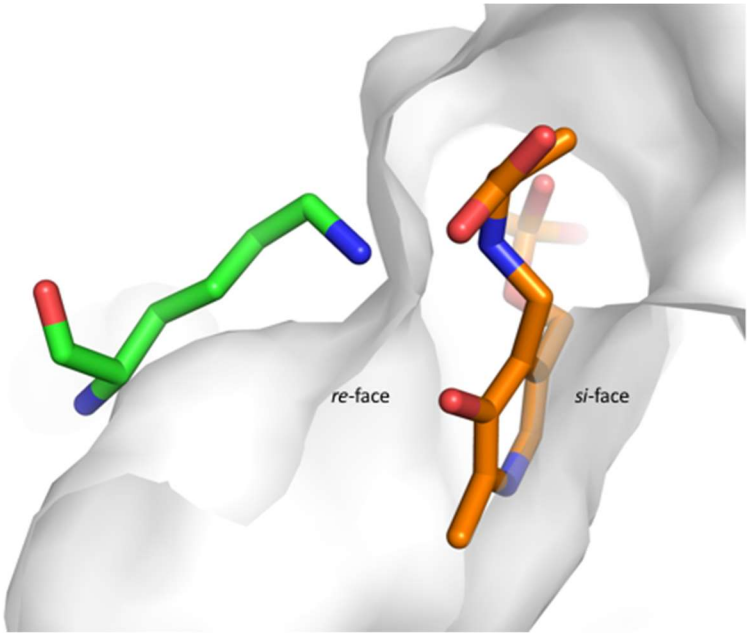

Figure 1.28 Crystal structure of D-amino acid aminotransferase from *Bacillus sp*. YM-1 active site with the catalytic lysine residue located on the *re*-face of PLP (PDB ID: 3DAA).[141]

1.7. Objectives of this thesis

In Chapter 1, we discussed the presence of D-amino acids in the environment, their synthesis, and physiological roles in microorganisms. It was highlighted that higher organisms such as plants and animals metabolize D-AAs and occasionally enlist them in specialized functions. Moreover, the pharmaceutical industry has employed D-AAs in the synthesis of many beneficial medications that improve human health.

The chemical synthesis of D-AAs by racemate production is well established and many strategies have been developed to simplify the deracemization procedure. However, there

are technical and regulatory challenges which limit the application of those strategies broadly (*e.g.* limited substrate scope of the biocatalyst). The regulatory and economic pressures to perform less hazardous synthesis, reduce waste, and improve efficiencies makes new routes desirable. Therefore, to expand the biocatalytic toolbox available to biological chemists to synthesis D-AAs, we set out to achieve the following goals: 1) Develop a generally applicable method to screen aminotransferases in a high-throughput manner to identify ATs with a desired substrate specificity. 2) Engineer an AT with high catalytic activity for aromatic D-AAs with pharmaceutical relevance and incorporate the AT into a biocatalytic cascade to synthesize D-AAs. 3) Investigate a stereo-inverting AT with potential as a D-AA biocatalyst. The goals outlined above will be addressed in the following chapters:

Chapter 2: A high-throughput assay for screening L- or D-amino acid specific aminotransferase mutant libraries.

Chapter 3: Engineered aminotransferase for the production of D-phenylalanine derivatives using biocatalytic cascades.

Chapter 4: Structural and kinetic analysis of the stereoinverting D-phenylglycine aminotransferase from *Pseudomonas stutzeri*.

Chapter 5: Conclusions and perspectives.

1.8. References

(1) Cahn, R. S.; Ingold, C. K.; Prelog, V. *Cell. Mol. Life Sci.* **1956**, *12* (3), 81–94.
(2) Gold, V.; Loening, K. L.; McNaught, A. D.; Shemi, P. *Blackwell Sci. Oxford* **1997**, 2197.
(3) Hinegardner, R. T.; Engelberg, J. *Science (80-.).* **1963**, *142* (3595), 1083–1085.
(4) Woese, C. R.; Hinegardner, R. T.; Engelberg, J. *Science (80-.).* **1964**, *144* (3621), 1030–1031.
(5) Dixon, H. B. F.; Moss, G. P. *Int. Union Pure Appl. Chem.* **1984**, *56* (5), 595–624.
(6) Corrigan, J. J. *Science (80-.).* **1969**, *164* (3876), 142–149.
(7) Fujii, N.; Saito, T. *Chem. Rec.* **2004**, *4* (5), 267–278.
(8) Mitchell, J. B. O.; Smith, J. *Proteins Struct. Funct. Bioinforma.* **2003**, *50* (4), 563–571.
(9) Keszthelyi, L. *Q. Rev. Biophys.* **1995**, *28* (4), 473.
(10) Blackmond, D. G. *Cold Spring Harb. Perspect. Biol.* **2010**, *2* (5), a002147–a002147.
(11) Snell, E. E.; Guirard, B. M. *Proc. Natl. Acad. Sci.* **1943**, *29* (2), 66–73.
(12) Barreteau, H.; Kovač, A.; Boniface, A.; Sova, M.; Gobec, S.; Blanot, D. *FEMS Microbiol. Rev.* **2008**, *32* (2), 168–207.
(13) Strominger, J. L.; Izaki, K.; Matsuhashi, M.; Tipper, D. J. In *Federation proceedings*; 1967; Vol. 26, pp 9–22.
(14) Radkov, A. D.; Moe, L. A. *Appl. Microbiol. Biotechnol.* **2014**, *98* (12), 5363–5374.
(15) Bellais, S.; Arthur, M.; Dubost, L.; Hugonnet, J.-E.; Gutmann, L.; van Heijenoort, J.; Legrand, R.; Brouard, J.-P.; Rice, L.; Mainardi, J.-L. *J. Biol. Chem.* **2006**, *281* (17), 11586–11594.
(16) Lam, H.; Oh, D.; Cava, F.; Takacs, C. N.; Clardy, J.; de Pedro, M. A.; Waldor, M. K. *Science (80-.).* **2009**, *325* (5947), 1552–1555.
(17) Stein, T.; Kluge, B.; Vater, J.; Franke, P.; Otto, A.; Wittmann-Liebold, B. *Biochemistry* **1995**, *34*, 4633–4642.
(18) Marahiel, M. A.; Krause, M.; Skarpeid, H.-J. *Mol Gen Genet* **1985**, *201*, 231–236.
(19) Konz, D.; Klens, A.; Schörgendorfer, K.; Marahiel, M. A. *Chem. Biol.* **1997**, *4* (12), 927–937.
(20) Brückner, H.; Westhauser, T. *Amino Acids* **2003**, *24*, 43–55.
(21) Ogawa, T.; Kimoto, M.; Sasaoka, K. *Agric. Biol. Chem.* **1977**, *41* (9), 1811–1812.
(22) Ogawa, T.; Kawasaki, Y.; Sasaoka, K. *Phytochemistry* **1978**, *17* (8), 1275–1276.
(23) Vranova, V.; Zahradnickova, H.; Janous, D.; Skene, K. R.; Matharu, A. S.; Rejsek, K.; Formanek, P. *Plant Soil* **2012**, *354* (1–2), 21–39.
(24) Gördes, D.; Kolukisaoglu, Ü.; Thurow, K. *Amino Acids* **2011**, *40* (2), 553–563.
(25) Fujii, N. *Orig. Life Evol. Biosph.* **2002**, *32* (2), 103–127.
(26) Masters, P. M. *Calcif. Tissue Int.* **1983**, *35* (1), 43–47.
(27) Kaneko, I.; Yamada, N.; Sakuraba, Y.; Kamenosono, M.; Tutumi, S. *J. Neurochem.* **2002**, *65* (6), 2585–2593.
(28) Roher, A. E.; Lowenson, J. D.; Clarke, S.; Wolkow, C.; Wang, R.; Cotter, R. J.; Reardon, I. M.; Zürcher-Neely, H. A.; Heinrikson, R. L.; Ball, M. J. *J. Biol. Chem.* **1993**, *268* (5), 3072–3083.

(29) Montecucci, P. C.; Castiglione, R.; Piani, S.; Gozzini, L.; Erspamer, V. *Chem. Biol. Drug Des.* **1981**, *17* (3), 275–283.
(30) Kamatani, Y.; Minakata, H.; Kenny, P. T. M.; Iwashita, T.; Watanabe, K.; Funase, K.; Xia Ping, S.; Yongsiri, A.; Kim, K. H.; Novales-Li, P.; Novales, E. T.; Kanapi, C. G.; Takeuchi, H.; Nomoto, K. *Biochem. Biophys. Res. Commun.* **1989**, *160* (3), 1015–1020.
(31) Kuwada, M.; Teramoto, T.; Kumagaye, K. Y.; Nakajima, K.; Watanabe, T.; Kawai, T.; Kawakami, Y.; Niidome, T.; Sawada, K.; Nishizawa, Y. *Mol. Pharmacol.* **1994**, *46* (4), 587–593.
(32) Fujimoto, K.; Kubota, I.; Yasuda-Kamatani, Y.; Minakata, H.; Nomoto, K.; Yoshida, M.; Harada, A.; Muneoka, Y.; Kobayashi, M. *Biochem. Biophys. Res. Commun.* **1991**, *177* (2), 847–853.
(33) Friedman, M. *J. Agric. Food Chem.* **1999**, *47* (9), 3457–3479.
(34) Webb, E. C. *Enzyme nomenclature 1992. Recommendations of the Nomenclature Committee of the International Union of Biochemistry and Molecular Biology on the Nomenclature and Classification of Enzymes.*; Academic Press, 1992.
(35) Martínez-Rodríguez, S.; Martínez-Gómez, A. I.; Rodríguez-Vico, F.; Clemente-Jiménez, J. M.; Las Heras-Vázquez, F. J. *Chem. Biodivers.* **2010**, *7* (6), 1531–1548.
(36) Sweeny, J. G.; D'Angelo, L. L.; Ricks, E. A.; Iacobucci, G. A. *J. Agric. Food Chem.* **1995**, *43* (8), 1969–1976.
(37) Brennan, T. M.; Hendrick, M. E. Branched amides of L-aspartyl-D-amino acid dipeptides. US 4411925 A, 1980.
(38) Omura, T.; Furukawara, T. Oil-in-water type emulsion skin cosmetic. US8697750 B2, 2014.
(39) Hayden, P. J.; Goldman, V. S. Deodorant composition containing D-amino acid. US6060043 A, 2000.
(40) Hamamoto, K.; Kida, Y.; Zhang, Y.; Shimizu, T.; Kuwano, K. *Microbiol. Immunol.* **2002**, *46* (11), 741–749.
(41) Simmaco, M.; Kreil, G.; Barra, D. *Biochim. Biophys. Acta - Biomembr.* **2009**, *1788* (8), 1551–1555.
(42) Kobel, H.; Traber, R. *Appl. Microbiol. Biotechnol.* **1982**, *14* (4), 237–240.
(43) Kuehl Jr, F. A.; Wolf, F. J.; Trenner, N. R.; Peck, R. L.; Buhs, R. P.; Howe, E.; Putter, I.; Hunnewell, B. D.; Ormond, R.; Downing, G.; others. *J. Am. Chem. Soc.* **1955**, *77* (8), 2344–2345.
(44) Chopra, C.; Hook, D. J.; Vining, L. C.; Das, B. C.; Shimizu, S.; Taylor, A.; Wright, J. L. C. *J. Antibiot. (Tokyo).* **1979**, *32* (4), 392–401.
(45) Bevan, K.; Davies, J. S.; Hall, M. J.; Hassall, C. H.; Morton, R. B.; Phillips, D. A. S.; Ogihara, Y.; Thomas, W. A. *Cell. Mol. Life Sci.* **1970**, *26* (2), 122–123.
(46) Burkhart, B. M.; Gassman, R. M.; Langs, D. A.; Pangborn, W. A.; Duax, W. L.; Pletnev, V. *Pept. Sci.* **1999**, *51* (2), 129–144.
(47) Katz, E.; Demain, A. L. *Bacteriol. Rev.* **1977**, *41* (2), 449.
(48) Petrauskas, A. A.; Švedas, V. K. *J. Chromatogr. A* **1991**, *585* (1), 3–34.
(49) Actor, P.; Uri, J. V; Phillips, L.; Sachs, C. S.; Guarini, J. R.; Zajac, I.; Berges, D. A.; Dunn, G. L.; Hoover, J. R. E.; Weisbach, J. A. *J. Antibiot. (Tokyo).* **1975**, *28* (8), 594–601.

(50) Tentolouris, N.; Voulgari, C.; Katsilambros, N. *Vasc. Health Risk Manag.* **2007**, *3* (6), 797–807.
(51) Miyao, K. *Bull. Agric. Chem. Soc. Japan* **1960**, *24* (1), 23–30.
(52) Berry, C.; Ferrari, P. Use of a direct-acting thrombin inhibitor for the manufacture of a medicinal product having thrombolytic activity. US5583113A, 1996.
(53) Dasgupta, P. *Pharmacol. Ther.* **2004**, *102* (1), 61–85.
(54) Kovacs, M. *Proc. Natl. Acad. Sci.* **2001**, *98* (4), 1829–1834.
(55) Parmeggiani, F.; Ahmed, S. T.; Thompson, M. P.; Weise, N. J.; Galman, J. L.; Gahloth, D.; Dunstan, M. S.; Leys, D.; Turner, N. J. *Adv. Synth. Catal.* **2016**, *358* (20), 3298–3306.
(56) Heller, B. D-phenylalanine treatment. US4355044 A, 1982.
(57) Murayama, C.; Harada, N.; Kakiuchi, T.; Fukumoto, D.; Kamijo, A.; Kawaguchi, A. T.; Tsukada, H. *J. Nucl. Med.* **2009**, *50* (2), 290–295.
(58) Urakami, T.; Sakai, K.; Asai, T.; Fukumoto, D.; Tsukada, H.; Oku, N. *Nucl. Med. Biol.* **2009**, *36* (3), 295–303.
(59) Dooley, C.; Chung, N.; Wilkes, B.; Schiller, P.; Bidlack, J.; Pasternak, G.; Houghten, R. *Science (80-.).* **1994**, *266* (5193), 2019–2022.
(60) Tian, X.; Switzer, A. G.; Derose, S. A.; Mishra, R. K.; Solinsky, M. G.; Mumin, R. N.; Ebetino, F. H.; Jayasinghe, L. R.; Webster, M. E.; Colson, A.-O.; others. *J. Med. Chem.* **2008**, *51* (19), 6055–6066.
(61) Coward, R.; Carson, C. *Ther. Clin. Risk Manag.* **2008**, *4* (6), 1315–1330.
(62) Argiolas, A.; Deghenghi, R. Peptides for treatment of erectile dysfunction. US6211156B1, 2001.
(63) Sapuntsova, S. G.; Mel'nikova, N. P.; Deigin, V. I.; Kozulin, E. A.; Timoshin, S. S. *Bull. Exp. Biol. Med.* **2002**, *133* (5), 488–490.
(64) Lode, H.; Stahlmann, R.; Koeppe, P. *Antimicrob. Agents Chemother.* **1979**, *16* (1), 1–6.
(65) Garcia-Rodriguez, J. A.; Bellido, J. L. M.; Sánchez, J. E. G. *Int. J. Antimicrob. Agents* **1995**, *5* (4), 231–243.
(66) Actor, P.; URI, J. V; PHILLIPS, L.; SACHS, C. S.; GUARINI, J. R.; ZAJAC, I.; BERGES, D. A.; DUNN, G. L.; HOOVER, J. R. E.; WEISBACH, J. A. *J. Antibiot. (Tokyo).* **1975**, *28* (8), 594–601.
(67) Fukasawa, M.; Noguchi, H.; Okuda, T.; Komatsu, T.; Yano, K. *Antimicrob. Agents Chemother.* **1983**, *23* (2), 195–200.
(68) Hinkle, A. M.; LeBlanc, B. M.; Bodey, G. P. *Antimicrob. Agents Chemother.* **1980**, *17* (3), 423–427.
(69) Petrauskas, A. A.; Švedas, V. K. *J. Chromatogr. A* **1991**, *585* (1), 3–34.
(70) Barbhaiya, R. H.; Turner, P. *Br. J. Clin. Pharmacol.* **1977**, *4* (4), 427–431.
(71) Clayton, J. P.; Cole, M.; Elson, S. W.; Ferres, H. *Antimicrob. Agents Chemother.* **1974**, *5* (6), 670.
(72) Fu, K. P.; Neu, H. C. *Antimicrob. Agents Chemother.* **1978**, *13* (3), 358–367.
(73) Bodin, N.-O.; Ekström, B.; Forsgren, U.; Jalar, L.-P.; Magni, L.; Ramsay, C.-H.; Sjöberg, B. *Antimicrob. Agents Chemother.* **1975**, *8* (5), 518–525.
(74) Ishida, M.; Kobayashi, K.; Awata, N.; Sakamoto, F. *J. Chromatogr. B Biomed. Sci. Appl.* **1999**, *727* (1), 245–248.
(75) Basch, H.; Erickson, R.; Gadebusch, H. *Infect. Immun.* **1971**, *4* (1), 44–49.

(76) Melis, M. R.; Succu, S.; Spano, M. S.; Locatelli, V.; Torsello, A.; Muller, E. E.; Deghenghi, R.; Argiolas, A. *Eur. J. Pharmacol.* **2000**, *404* (1), 137–143.
(77) Huirne, J. A. F.; Lambalk, C. B. *Lancet* **2001**, *358* (9295), 1793–1803.
(78) Coccia, M. E.; Comparetto, C.; Bracco, G. L.; Scarselli, G. *Eur. J. Obstet. Gynecol. Reprod. Biol.* **2004**, *115*, S44–S56.
(79) Strecker, A. *European J. Org. Chem.* **1850**, *75* (1), 27–45.
(80) Yet, L. *Angew. Chemie Int. Ed.* **2001**, *40* (5), 875–877.
(81) Wang, J.; Liu, X.; Feng, X. *Chem. Rev.* **2011**, *111* (11), 6947–6983.
(82) Sheldon, R. A. *J. Chem. Technol. Biotechnol.* **1996**, *67* (1), 1–14.
(83) Keith, J. M.; Larrow, J. F.; Jacobsen, E. N. *Adv. Synth. Catal.* **2001**, *343* (1), 5–26.
(84) Faber, K. *Chem. - A Eur. J.* **2001**, *7* (23), 5004–5010.
(85) Servi, S.; Tessaro, D.; Pedrocchi-Fantoni, G. *Coord. Chem. Rev.* **2008**, *252* (5–7), 715–726.
(86) Monteiro, J. L.; Pieber, B.; Corrêa, A. G.; Kappe, C. O. *Synlett* **2016**, *27* (1), 83–87.
(87) *Bucherer-Bergs reaction*; Springer Berlin Heidelberg: Berlin, Heidelberg, 2006.
(88) Bommarius, A. S.; Schwarm, M.; Drauz, K. *J. Mol. Catal. B Enzym.* **1998**, *5* (1–4), 1–11.
(89) Bommarius, A. S.; Schwarm, M.; Drauz, K. *Chim. Int. J. Chem.* **2001**, *55* (1–2), 50–59.
(90) Bommarius, A. S.; Kottenhahn, M.; Klenk, H.; Drauz, K. In *Microbial Reagents in Organic Synthesis*; Servi, S., Ed.; Springer Netherlands: Dordrecht, 1992; pp 161–174.
(91) Gao, X.; Ma, Q.; Zhu, H. *Appl. Microbiol. Biotechnol.* **2015**, *99* (8), 3341–3349.
(92) Gu, R.-L.; Lee, I.-S.; Sih, C. J. *Tetrahedron Lett.* **1992**, *33* (15), 1953–1956.
(93) Chibata, I. *Pure Appl. Chem.* **1978**, *50*, 667–675.
(94) Leuchtenberger, W.; Huthmacher, K.; Drauz, K. *Appl. Microbiol. Biotechnol.* **2005**, *69* (1), 1–8.
(95) Alexandre, F.-R.; Pantaleone, D. P.; Taylor, P. P.; Fotheringham, I. G.; Ager, D. J.; Turner, N. J. *Tetrahedron Lett.* **2002**, *43* (4), 707–710.
(96) Tanizawa, K.; Masus, Y.; Asano, S.; Tanaka, H.; Sodas, K. *J. Biol. Chem.* **1989**, *264* (5), 2445–2449.
(97) Vedha-Peters, K.; Gunawardana, M.; Rozzell, J. D.; Novick, S. J. *J. Am. Chem. Soc.* **2006**, *128* (33), 10923–10929.
(98) di Salvo, M. L.; Florio, R.; Paiardini, A.; Vivoli, M.; D'Aguanno, S.; Contestabile, R. *Arch. Biochem. Biophys.* **2013**, *529* (2), 55–65.
(99) Sutton, C. R.; King, H. K. *Arch. Biochem. Biophys.* **1962**, *96* (2), 360–370.
(100) Jiang, W.; Xia, B.; Liu, Z. *Microbiol. Res.* **2013**, *168* (8), 477–484.
(101) Shen, H.; Yang, Y.; Wang, F.; Zhang, Y.; Ye, N.; Xu, S.; Wang, H. *Acta Biochim. Biophys. Sin. (Shanghai).* **2009**, *41* (5), 379–388.
(102) Yamada, T.; Komoto, J.; Takata, Y.; Ogawa, H.; Pitot, H. C.; Takusagawa, F. *Biochemistry* **2003**, *42* (44), 12854–12865.
(103) Steegborn, C.; Messerschmidt, A.; Laber, B.; Streber, W.; Huber, R.; Clausen, T. *J. Mol. Biol.* **1999**, *290* (5), 983–996.
(104) Messerschmidt, A.; Worbs, M.; Steegborn, C.; Wahl, M. C.; Huber, R.; Laber, B.; Clausen, T. *Biol. Chem.* **2003**, *384* (3), 373–386.

(105) Sugio, S.; Petsko, G. a.; Manning, J. M.; Soda, K.; Ringe, D. *Biochemistry* **1995**, *34* (30), 9661–9669.
(106) Phillips, R. S. *Biochim. Biophys. Acta - Proteins Proteomics* **2015**, *1854* (9), 1167–1174.
(107) Griffith, J. P. C.; Jennings, C. G.; Morse, J. L. *Bost. Med. Surg. J.* **1898**, *138* (26), 605–609.
(108) Sugiyama, Y.; Seita, A. *J. R. Soc. Med.* **2013**, *106* (8), 332–334.
(109) Guy, R. A. *Am. J. Dis. Child.* **1923**, *26* (2), 112–116.
(110) Funk, C. *J. State Med.* **1912**, *20* (6), 341–366.
(111) McCollum, E. V.; Simmonds, N.; Pitz, W. *J. Biol. Chem.* **1916**, *27* (1), 33–43.
(112) György, P. *Nature* **1934**, *133* (3361), 498–499.
(113) Robinson, F. A. *The vitamin B complex*; John Wiley & Sons Inc, 1951.
(114) Snell, E. E.; Guirard, B. M.; Williams, R. J. *J. Biol. Chem.* **1942**, *143* (2), 519–530.
(115) Snell, E. E. *J. Biol. Chem.* **1944**, *154*, 313–314.
(116) Snell, E. E. *Vitam. Horm.* **1958**, *16*, 77–125.
(117) Heyl, D.; Luz, E.; Harris, S. A.; Folkers, K. *J. Am. Chem. Soc.* **1951**, *73* (7), 3430–3433.
(118) Steffen-Munsberg, F.; Vickers, C.; Kohls, H.; Land, H.; Mallin, H.; Nobili, A.; Skalden, L.; van den Bergh, T.; Joosten, H.-J.; Berglund, P.; Höhne, M.; Bornscheuer, U. T. *Biotechnol. Adv.* **2015**, *33* (5), 566–604.
(119) Eliot, A. C.; Kirsch, J. F. *Annu. Rev. Biochem.* **2004**, *73* (1), 383–415.
(120) Dunathan, H. C. *J. Cell. Biochem.* **1966**, *49* (19), 712–716.
(121) Percudani, R.; Peracchi, A. *BMC Bioinformatics* **2009**, *10* (1), 273.
(122) Nakai, T.; Nakagawa, N.; Maoka, N.; Masui, R.; Kuramitsu, S.; Kamiya, N. *EMBO J.* **2005**, *24* (8), 1523–1536.
(123) Marienhagen, J.; Sandalova, T.; Sahm, H.; Eggeling, L.; Schneider, G. *Acta Crystallogr. Sect. D Biol. Crystallogr.* **2008**, *64* (6), 675–685.
(124) Koushik, S. V; Sundararaju, B.; McGraw, R. A.; Phillips, R. S. *Arch. Biochem. Biophys.* **1997**, *344* (2), 301–308.
(125) KEZMARSKY, N.; XU, H.; GRAHAM, D.; WHITE, R. *Biochim. Biophys. Acta - Gen. Subj.* **2005**, *1722* (2), 175–182.
(126) Ford, G. C.; Eichele, G.; Jansonius, J. N. *Proc. Natl. Acad. Sci.* **1980**, *77* (5), 2559–2563.
(127) Hyde, C. C.; Ahmed, S. A.; Padlan, E. A.; Miles, E. W.; Davies, D. R. *J. Biol. Chem.* **1988**, *263* (33), 17857–17871.
(128) Shaw, J. P.; Petsko, G. A.; Ringe, D. *Biochemistry* **1997**, *36* (6), 1329–1342.
(129) Withers, S. G.; Goldsmith, E. J.; Fletterick, R. J.; Madsen, N. B.; others. *Science (80-.).* **1991**, *254* (5036), 1367–1371.
(130) Berkovitch, F.; Behshad, E.; Tang, K.-H.; Enns, E. A.; Frey, P. A.; Drennan, C. L. *Proc. Natl. Acad. Sci.* **2004**, *101* (45), 15870–15875.
(131) Lepore, B. W.; Ruzicka, F. J.; Frey, P. A.; Ringe, D. *Proc. Natl. Acad. Sci.* **2005**, *102* (39), 13819–13824.
(132) Toney, M. D. *Biochim. Biophys. Acta (BBA)-Proteins Proteomics* **2011**, *1814* (11), 1407–1418.
(133) Grishin, N. V; Phillips, M. A.; Goldsmith, E. J. *Protein Sci.* **1995**, *4* (7), 1291–1304.

(134) Hwang, B.-Y.; Cho, B.-K.; Yun, H.; Koteshwar, K.; Kim, B.-G. *J. Mol. Catal. B Enzym.* **2005**, *37* (1–6), 47–55.
(135) Jäger, J.; Markus, M.; Ursula, S.; Johan, J. N. *J. Mol. Biol.* 1994, pp 285–305.
(136) Jäger, J.; Moser, M.; Sauder, U.; Jansonius, J. N. *Journal of Molecular Biology*. 1994, pp 285–305.
(137) Käck, H.; Sandmark, J.; Gibson, K.; Schneider, G.; Lindqvist, Y. *J. Mol. Biol.* **1999**, *291* (4), 857–876.
(138) Okada, K.; Hirotsu, K.; Hayashi, H.; Kagamiyama, H. *Biochemistry* **2001**, *40* (25), 7453–7463.
(139) Soda, K.; Yoshimura, T.; Esaki, N. *Chem. Rec.* **2001**, *1* (5), 373–384.
(140) Wybenga, G. G.; Crismaru, C. G.; Janssen, D. B.; Dijkstra, B. W. *J. Biol. Chem.* **2012**, *287* (34), 28495–28502.
(141) Peisach, D.; Chipman, D. M.; Van Ophem, P. W.; Manning, J. M.; Ringe, D. *Biochemistry* **1998**, *37* (14), 4958–4967.

Chapter 2.
A high-throughput assay for screening L- or D-amino acid specific aminotransferase mutant libraries.

The contents of this chapter were published in:
Walton, C.J.W. and Chica R.A., A high-throughput assay for screening L- or D-amino acid specific aminotransferase mutant libraries. *Analytical Biochemistry,* **2013**, 441, 190-198.

2.1. Preface

In this chapter, we developed a high-throughput assay for screening α-kg-dependent aminotransferase mutant libraries using glutamate dehydrogenase. The assay enables screening of either L- or D-amino acid specific aminotransferase in a continuous fashion from clarified cell lysates. The assay enabled us to identify mutants from *Bacillus* sp. YM-1 D-amino acid aminotransferase and *Escherichia coli* branched-chain amino acid aminotransferase displaying modified catalytic efficiency and substrate specificity. The results demonstrate the potential of our assay as altered substrate specificity is an important goal of enzyme engineering and biocatalyst development.

2.2. Contribution Statement

The contributions of all authors are outlined below:

Conception:

The initial concept of this article was conceived by my supervisor Dr. Roberto A. Chica. Curtis J.W. Walton and Dr. Roberto A. Chica collaborated on the project direction, experimental design, and analysis of key results.

Writing:

The manuscript for this article was co-written by Curtis J.W. Walton and Dr. Roberto A. Chica.

Experimental:

The experimental results presented in this article were performed by Curtis J.W. Walton.

2.3. Introduction

Aminotransferases (E.C. 2.6.1.X), also called transaminases, are pyridoxal-phosphate-dependent enzymes that catalyze the transfer of the amino group from a donor substrate to a ketone acceptor. *In vivo*, these enzymes are primarily involved in the biosynthesis of amino acids and amino-acid-derived metabolites,[1] making their donor and acceptor substrates amino and keto acids, respectively. Many aminotransferases (ATs) displaying different donor substrate specificities have been studied over the years. For example, ATs that are specific for L-aliphatic,[2] L-aromatic,[3] L-acidic,[4] or D-amino acids[5] have been reported. Recently, ATs that synthesize β-[6,7] or ω-amino acids[8] have also been discovered. Although these ATs display markedly different donor substrate specificities, many have in common the use of the α-kg acceptor substrate, which is a key intermediate in the Krebs cycle and in amino acid metabolism.

The potential of ATs for the biocatalytic production of enantiopure natural and unnatural amino acids is increasingly recognized.[9,10] Because of this, there is a growing interest in engineering ATs to alter their substrate specificity and to increase their catalytic activity. To facilitate the enzyme engineering process, a high-throughput screening assay is required. This assay needs to reliably reflect the activity level of the mutant ATs and should allow screening of various amino acid substrates, since increased activity and altered substrate specificity are desirable characteristics of engineered biocatalysts. Assays that have been used to screen aminotransferase mutant libraries are generally low-throughput methods requiring separation of products by liquid chromatography followed by their detection in a discontinuous fashion.[11–13] In contrast, genetic selection methods have also

been developed to screen large aminotransferase mutant libraries, thereby increasing throughput.[14–16] However, genetic selection has the disadvantage of requiring auxotrophic bacterial strains, special growth media, and genetic engineering, increasing the complexity of the experimental setup. In addition, a requirement for genetic selection is that the amino acid produced by the mutant aminotransferase be essential for cell growth, limiting the use of this methodology in the development of biocatalysts that synthesize unnatural amino acids.

Over the years, numerous continuous coupled enzyme assays have been developed to study the kinetic properties of various ATs.[17–21] These coupled assays allow for the detection of one of the products of the aminotransferase catalyzed reaction, either the amino or the keto acid, through the catalytic action of a coupling enzyme. Typically, in aminotransferase coupled assays, the coupling enzyme transforms the aminotransferase product using oxidation/reduction of the NADH (β-nicotinamide adenine dinucleotide, reduced form)/NAD^+ (β-nicotinamide adenine dinucleotide, oxidized form) coenzyme, which can be followed spectrophotometrically. Coupling enzymes such as L-glutamate,[22] lactate,[17] D-2-hydroxyisocaproate,[23] leucine,[18] malate,[17] and (R)-2-hydroxyglutarate[24] dehydrogenases have all been used successfully to follow the catalytic activity of ATs in a continuous fashion. Recently, amino acid oxidase reactions have also been coupled to aminotransferase reactions, for the detection of the amino acid product.[19,25] In addition to requiring an amino acid oxidase, this type of assay requires a third enzyme which is typically a peroxidase that utilizes the hydrogen peroxide produced by the oxidase to oxidize a colorless compound into one that absorbs visible light.

In this study, we report the development of a high-throughput screening assay for any α-ketoglutarate-dependent aminotransferase. To achieve this, we exploited the reliable L-glutamate dehydrogenase (GDH) coupled assay that has previously been shown to allow for aminotransferase activity to be monitored *in vitro*.[22,26] We adapted this assay to allow screening of mutant libraries of either L- or D-amino acid specific ATs, in a continuous fashion. This assay requiring clarified cell lysates is reproducible, rapid, and sensitive, because it allowed for the identification of a catalytically active aminotransferase mutant displaying a decrease in k_{cat}/K_M of more than two orders of magnitude. In addition, this assay allowed us to discover a branched-chain amino acid aminotransferase mutant, F36W, with altered donor substrate specificity.

2.4. Results and Discussion

2.4.1. Screening assay development

Our goal was to develop a continuous high-throughput assay for screening aminotransferase mutant libraries. To make this screening method most useful, our requirements were for an assay that (i) could be used to screen many different ATs, (ii) would be sensitive enough for screening clarified cell lysates in 96-well plates, and (iii) that could be readily adapted for the screening of different amino acid substrates of either L or D configuration. To achieve our objectives, we selected GDH from bovine liver as the coupling enzyme to be used in our screening assay due to its successful application in numerous continuous coupled assays developed to study various enzymes, including ATs.[22,27,28] GDH also has the advantages of being commercially available from a variety of sources and of using the α-kg/L-glutamate substrate/product pair that more than 160 different ATs spanning 31 unique serial numbers (E.C. 2.6.1.X) use,[29] broadening the

applicability of the assay. Finally, GDH was selected because its reaction utilizes the NADH coenzyme which absorbs at 340 nm, providing a convenient spectrophotometric reporter signal.

To develop a high-throughput assay that could be applied to the screening of either L- or D-amino acid specific aminotransferase mutant libraries, we elected to use the branched-chain aminotransferase (BCAT) from *E. coli*[30] and the D-amino acid aminotransferase (DAAT) from *Bacillus sp.* YM-1[31] as test enzymes. BCAT transfers the amino group of L-leucine to α-kg, resulting in L-glutamate and α-ketoisocaproate (Fig. 2.1A). L-glutamate is then oxidatively deaminated to α-kg by GDH, with concomitant production of NADH resulting in increased absorbance at 340 nm. On the other hand, DAAT transfers the amino group of D-glutamate to pyruvate, yielding α-kg and D-alanine (Fig. 2.1B). GDH can then reductively aminate α-kg to L-glutamate in the presence of ammonia while consuming NADH, resulting in an absorbance decrease at 340 nm. It should be noted that GDH is highly specific to L-glutamate and does not react with D-glutamate, allowing DAAT to be accurately assayed without significant interference from GDH.

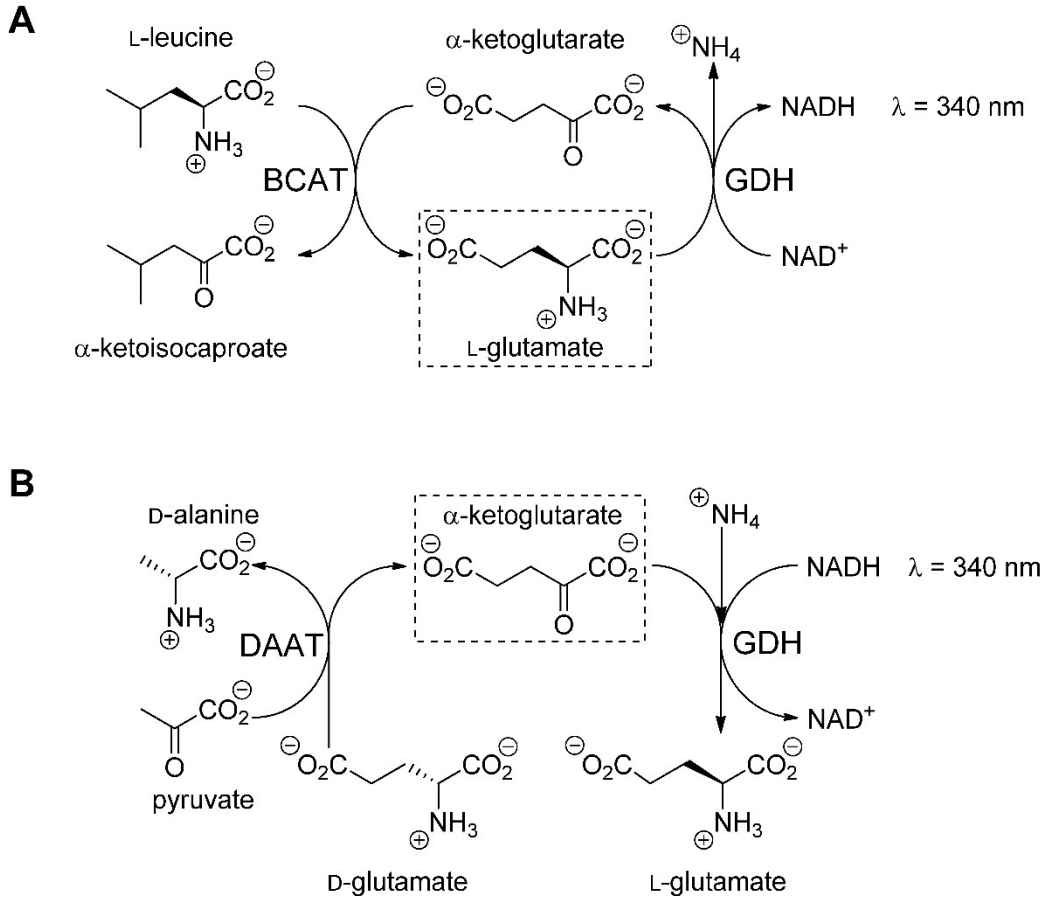

Figure 2.1 GDH coupled enzyme assay. (A) The transamination reaction catalyzed by BCAT produces L-glutamate (boxed), which is oxidatively deaminated by GDH in the presence of the coenzyme NAD^+. The coupled reaction generates NADH, resulting in an absorbance increase at 340 nm. (B) The transamination reaction catalyzed by DAAT produces α-ketoglutarate (boxed), which is converted by GDH into L-glutamate. This second reaction consumes the NADH coenzyme, resulting in an absorbance decrease at 340 nm. It should be noted that GDH is highly specific for L-glutamate and does not react with D-glutamate.

As a first step towards the development of our screening assay, we tested GDH coupled assay conditions using purified BCAT and DAAT. When performing coupled assays, it is crucial to optimize reaction conditions to ensure that the rate-limiting step is the enzyme reaction of interest (i.e., the aminotransferase reaction in this case), under all conditions tested. To ensure that this was the case, we used a 100-fold excess of the GDH coupling enzyme (1 U) relative to the amount of BCAT or DAAT (10 mU) and confirmed that the measured reaction rate did not vary significantly when the GDH concentration was either decreased two-fold or doubled. We also confirmed that the measured rates increased linearly with increasing amounts of aminotransferase (data not shown), demonstrating that the assay conditions were optimal for ensuring that the aminotransferase reaction was the rate-limiting step.

Using these optimized conditions (see Materials and Methods), we measured steady-state kinetics of BCAT and DAAT. The GDH assay allowed us to determine the apparent K_M and k_{cat} parameters for the donor and acceptor substrates of wild-type BCAT and DAAT. For the BCAT reaction, we tested the L-leucine donor and the α-kg acceptor, while for the DAAT reaction we tested the D-glutamate donor and the pyruvate acceptor. For BCAT, we obtained apparent K_M values of 0.35 ± 0.01 and 0.034 ± 0.002 mM and k_{cat} values of 0.26 ± 0.01 and 0.36 ± 0.01 s^{-1} for L-leucine (Table 2.1) and α-kg, respectively. For DAAT, we obtained apparent K_M values of 3.9 ± 0.2 and 0.4 ± 0.1 mM and k_{cat} values of 101 ± 2 and 77 ± 5 s^{-1} for D-glutamate (Table 2.2) and pyruvate, respectively. Michaelis-Menten plots reported in Fig. 2.2 show the expected hyperbolic relationship between initial rates and substrate concentrations, supporting the observation that the aminotransferase reaction was the rate-limiting step in the coupled assay.

Table 2.1 Apparent kinetic parameters of purified *E. coli* BCAT and its mutants for transamination of α-ketoglutarate with L-leucine.

	L-Leucine			
Enzyme	K_M (mM)	k_{cat} (s^{-1})	k_{cat}/K_M (s^{-1} M^{-1})	(k_{cat}/K_M wild-type) / (k_{cat}/K_M mutant)
Wild-type (WT)	0.35 ± 0.01	0.26 ± 0.01	740 ± 40	---
F36L	1.1 ± 0.1	0.18 ± 0.01	160 ± 20	5
F36Y	1.4 ± 0.1	0.21 ± 0.01	150 ± 10	5
F36M	1.5 ± 0.1	0.19 ± 0.01	130 ± 10	6
F36W	0.7 ± 0.1	0.071 ± 0.002	100 ± 20	7
F36V	0.55 ± 0.08	0.011 ± 0.001	20 ± 3	37
F36N	0.68 ± 0.08	0.0110 ± 0.0004	16 ± 2	46

Table 2.2 Apparent kinetic parameters of purified *Bacillus sp*. YM-1 DAAT and its mutants for transamination of pyruvate with D-glutamate.

Enzyme	D-Glutamate			
	K_M (mM)	k_{cat} (s^{-1})	k_{cat}/K_M (s^{-1} M^{-1})	(k_{cat}/K_M wild-type) / (k_{cat}/K_M mutant)
Wild-type (WT)	3.9 ± 0.2	101 ± 2	26,000 ± 1000	---
Y31L	2.9 ± 0.5	5.1 ± 0.4	1,800 ± 300	14
Y31V	3.8 ± 0.3	5.6 ± 0.1	1,500 ± 100	17
Y31F	3.0 ± 0.4	4.0 ± 0.2	1,300 ± 200	20
Y31A	2.2 ± 0.2	2.2 ± 0.1	1,000 ± 100	26
Y31G[a]	2.3 ± 0.1	0.85 ± 0.03	370 ± 20	70
Y31P[b]	0.37 ± 0.03	0.015 ± 0.003	41 ± 9	634

[a] This mutant exhibits substrate inhibition with a K_i of 10 ± 1 mM
[b] This mutant exhibits substrate inhibition with a K_i of 18 ± 4 mM.

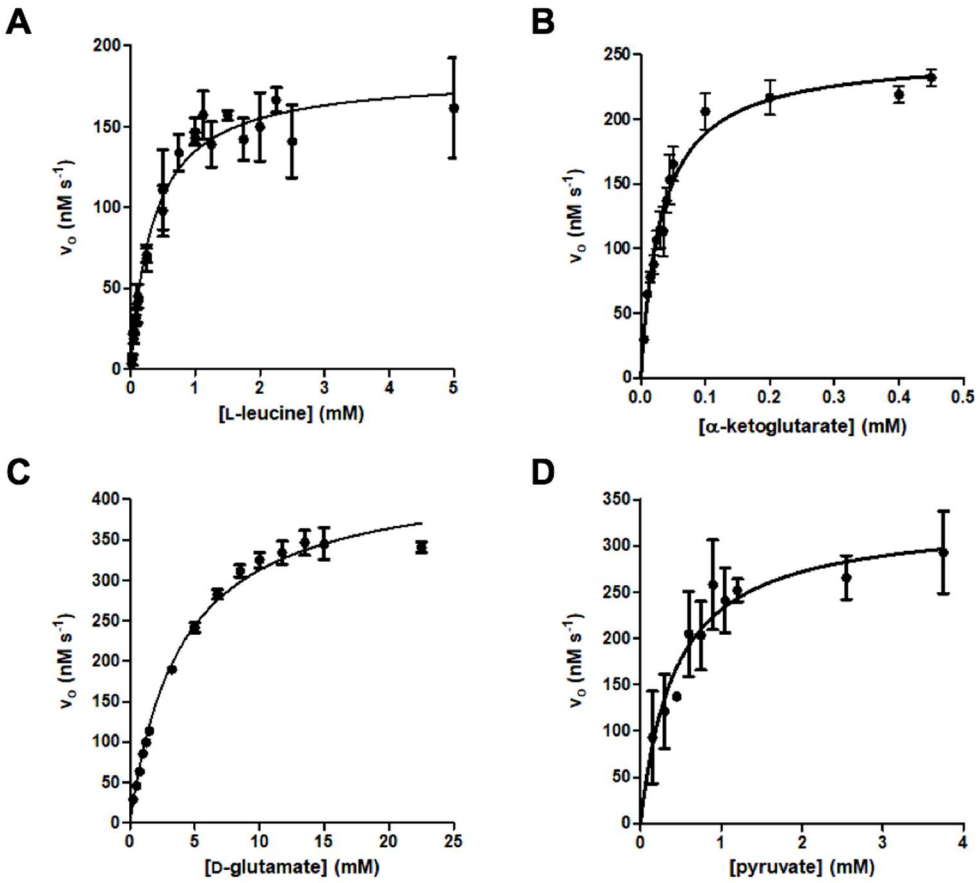

Figure 2.2 Steady-state kinetics of aminotransferase reactions using GDH coupled enzyme assay. Shown are Michaelis-Menton plots of initial rates versus L-leucine (A) or α-ketoglutarate (B) concentrations for the BCAT reaction and versus D-glutamate (C) or pyruvate (D) concentrations for the DAAT reaction. All experiments were performed in triplicate from a single enzyme sample. The data was fit using the Michaelis-Menten equation: $v_o = v_{max}[S]/(K_M + [S])$.

Next, we used these GDH assay conditions to develop a high-throughput screening procedure. To increase throughput, protein samples should be minimally processed. For example, the enzyme sample should not require purification for adequate detection to occur. Thus, clarified *E. coli* cell lysates containing overexpressed ATs were used as samples. Because these cell lysates likely contain molecules that could interfere with the GDH assay, such as NAD(H), L-glutamate/α-kg, ammonia, and endogenous BCAT, an appropriate negative control was essential. In our case, the negative controls were clarified lysates prepared from *E. coli* cells harboring an expression vector that did not contain the BCAT or DAAT genes. Thus, the negative control would not contain the overexpressed recombinant BCAT or DAAT but could contain any constitutively expressed endogenous aminotransferase. Because *E. coli* can produce endogenous BCAT, any endogenously expressed enzyme present in the lysates would be able to react with the L-leucine and α-kg substrates, allowing us to detect its presence in the negative control sample. On the other hand, DAAT is not encoded in the *E. coli* genome,[32] which should result in a lower background signal.

Using the clarified cell lysates prepared from *E. coli* cells overexpressing the BCAT and DAAT enzymes and from the negative controls described earlier, we performed the GDH coupled assay, as described in Materials and Methods. For the screening of BCAT, we used 5 mM L-leucine and 1 mM α-kg, whereas for the screening of DAAT, we used 10 mM D-glutamate and 5 mM pyruvate. These substrate concentrations are greater than 10 × K_M of each substrate for the wild-type enzymes, with the exception of D-glutamate. For D-glutamate, we used a concentration approximately 2.5 × K_M because of limitations imposed by its solubility. Nevertheless, the results, shown in Fig. 2.3 as black lines, clearly

demonstrate a large difference in absorbance increase or decrease between the lysates containing overexpressed wild-type ATs and the negative controls. It should be noted that the cell lysates were prepared from small volume (300-µL) *E. coli* cultures grown directly in 96-well plates. Thus, our assay is sufficiently sensitive to readily detect the catalytic activity of overexpressed ATs in complex mixtures containing small quantities of enzyme.

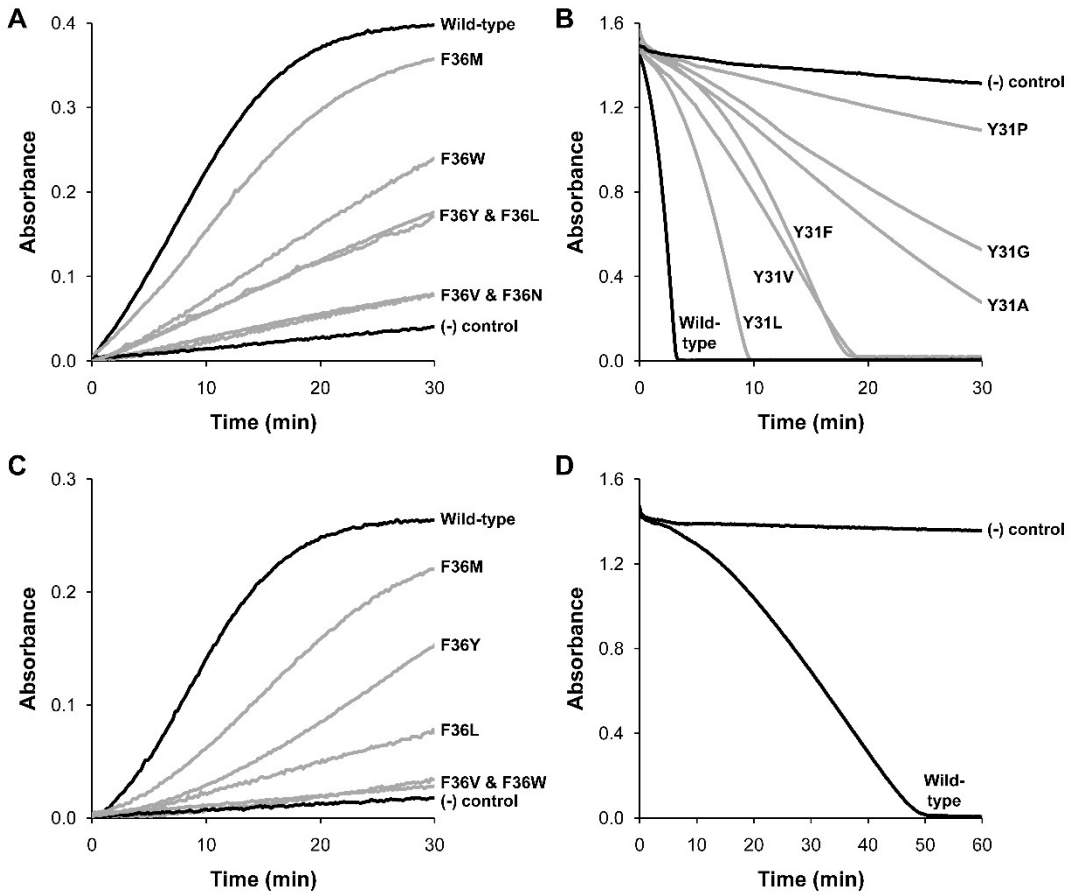

Figure 2.3 Mutant library screening. The GDH coupled assay was used to screen clarified *E. coli* lysates expressing the *E. coli* BCAT F36 and the *Bacillus sp.* YM-1 DAAT Y31 site saturation libraries. (A) Screening of the BCAT mutant library for transamination of α-ketoglutarate with the donor substrate L-leucine. (B) Screening of the DAAT mutant library for transamination of D-glutamate with the acceptor substrate pyruvate. (C) Screening of the BCAT mutant library for transamination of α-ketoglutarate with the non-native donor L-phenylalanine. (D) Screening of the DAAT mutant library for transamination of D-glutamate with the non-native acceptor phenylpyruvate. In all cases, black lines correspond to the positive and negative controls, which were a clarified cell lysate containing overexpressed wild-type aminotransferase and a lysate from cells that do not overexpress any aminotransferase, respectively. Grey lines correspond to active mutants detected by screening. All other mutants were indistinguishable from the negative control and were thus considered to be inactive. Screening of the DAAT mutant library for transamination of D-glutamate with phenylpyruvate (D) did not yield any active mutant. In the BCAT assays absorbance at 340 nm increases as NADH is produced by the coupling reaction, whereas in the DAAT assays, absorbance decreases as NADH is consumed.

As can be seen in Figure 2.3A, the negative control sample for the BCAT assays displays a small absorbance increase over the length of the assay. This absorbance increase likely results from the presence of reaction components such as L-glutamate or endogenous BCAT in the negative control lysate. However, the activity of the negative control (0.10 ± 0.03 nmol min^{-1}) is 14-fold lower than that of the lysate containing overexpressed wild-type BCAT (1.4 ± 0.3 nmol min^{-1}), suggesting that these reaction components are present in low quantities. In the case of DAAT (Fig. 2.3B), a large difference in activity is also readily observed between the negative control and the lysate containing overexpressed wild-type aminotransferase. In the sample containing wild-type DAAT, the absorbance at 340 nm decreases to zero in less than 5 minutes, indicating that the NADH present at the beginning of the reaction has been completely consumed. However, in the negative control sample, the absorbance at 340 nm decreases by less than 20% after a reaction time of 30 minutes, indicating the presence of a small amount of background reaction. Nonetheless, this background reaction, which can be attributed to the presence of α-kg in the cell lysate, yielded an activity (1.9 ± 0.5 nmol min^{-1}) that is approximately 20-fold lower than that of the lysates containing overexpressed wild-type DAAT (37 ± 5 nmol min^{-1}). Thus, although the clarified cell lysates used herein likely contain small quantities of the reagents utilized in our assay, these do not significantly interfere with our ability to detect the activity of overexpressed wild-type ATs.

2.4.2. Screening of site saturation mutagenesis libraries

To validate our assay as a high-throughput screening method, we prepared site-saturation libraries of both BCAT and DAAT and screened them to identify active mutants. To ensure that the libraries would contain mutants displaying different levels of catalytic activity, we

mutated a single active site residue that is directly interacting with the donor substrate to all twenty proteinogenic amino acids. For DAAT, we selected Y31 for site saturation mutagenesis (Fig. 2.4A) because this residue forms an H-bond interaction with the α-carboxyl group of the D-alanine donor substrate.[33] We hypothesized that this interaction would be necessary for maintaining the full catalytic activity of DAAT and that mutating it would result in mutants displaying a range of activities lower than that of the wild-type enzyme. Both DAAT and BCAT have similar aminotransferase fold type IV backbones that differ by a root mean square deviation of approximately 1.3 Å. Thus, we selected the BCAT F36 residue for site saturation mutagenesis because it is homologous to DAAT Y31 (Fig. 2.4B). We hypothesized that mutating the F36 residue in BCAT would also result in single mutants displaying a range of activities lower than that of the wild-type enzyme. Thus, site saturation mutagenesis was performed and colonies containing individual single mutants were inoculated into separate wells of a 96-well plate. These plates were then used to prepare the clarified cell lysates to be used in screening.

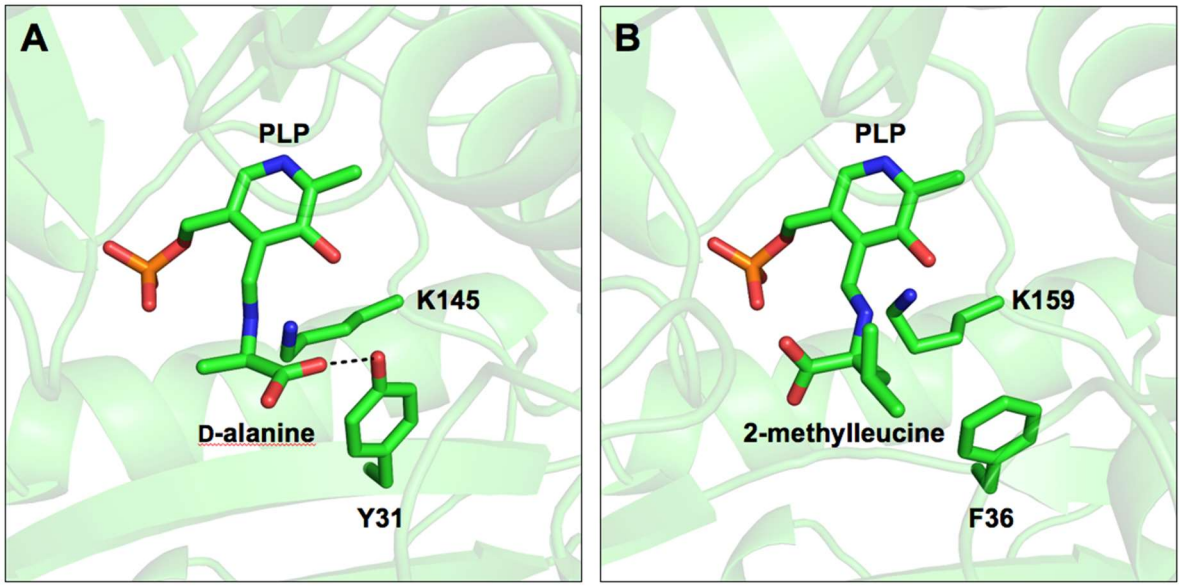

Figure 2.4 Crystal structures of aminotransferases. (A) The active site of *Bacillus sp.* YM-1 DAAT (PDB code: 3DAA) is shown in cartoon representation. The pyridoxal phosphate (PLP)-bound D-alanine donor substrate is shown in sticks, as are the catalytic residue K145 and the active site residue Y31. Y31 is H-bonded to the α-carboxyl group of the D-alanine substrate (dashed line). (B) The active site of *E. coli* BCAT (PDB code: 1I1L) is shown in cartoon representation. The pyridoxal phosphate-bound 2-methylleucine donor substrate analog is shown in sticks, as are the catalytic residue K159 and the active site residue F36. F36 is located directly next to the 2-methylleucine substrate analogue side chain, which is expected to bind to the active site pocket of BCAT in the same general orientation as that of the donor substrate L-leucine. Both DAAT and BCAT have similar backbones that belong to aminotransferase fold type IV.

Clarified cell lysates containing the mutants from the site saturation libraries were screened using the GDH assay, which allowed us to identify six BCAT (F36M, F36W, F36L, F36Y, F36N, and F36V) and six DAAT (Y31L, Y31V, Y31F, Y31A, Y31G, and Y31P) single mutants that displayed catalytic activity under the conditions tested (Fig. 2.3A and B). All other mutants tested yielded activities that could not be distinguished from that of the negative control and, thus, were considered to be inactive. It is important to note that we screened our libraries in triplicate by using lysates extracted from three different daughter plates prepared from the same mother plate, and that this resulted in the identification of the same 12 active mutants, demonstrating the reproducibility of our assay. All active mutants, shown as grey lines in Fig. 2.3, display lower activity than the wild-type enzymes, as expected. Furthermore, different activity levels were observed for each of the mutants, suggesting that different mutations affect catalytic efficiency differently. However, to ensure that the observed differences in activity reflect differences in catalytic efficiency and not variations in enzyme concentration resulting from different expression levels, we expressed and purified all active mutants and measured the apparent kinetic parameters for their donor substrate using the GDH assay. To do this, the donor substrate concentration was varied while keeping the acceptor concentration fixed at the value used during screening (1 and 5 mM for α-kg and pyruvate, respectively). This was done to remain consistent with the screening conditions, allowing a more direct comparison with the activities observed during screening. The apparent K_M and k_{cat} values are reported in Tables 2.1 and 2.2, for BCAT and DAAT mutants, respectively. As reflected by the lower activity observed during screening, all mutants display lower catalytic efficiencies than the wild-type enzyme, as demonstrated by lower k_{cat}/K_M values. This result is not surprising given

that mutants are often less active than their wild-type precursor, because the wild-type enzyme has been optimized by millions of years of evolution to perform its native catalytic activity with high efficiency.

The lowest activity BCAT mutant that we found by screening was F36N, which has a k_{cat}/K_M for the L-leucine donor that is decreased 46-fold from that of the wild-type. For DAAT, the lowest activity mutant, Y31P, had a 632-fold decrease in k_{cat}/K_M for the D-glutamate donor. Although lower activity mutants may be present in the 96-well plates, they may not have been detected under the conditions of our screening assay. If detection of lower activity mutants is desired, assay conditions may be made less stringent by increasing the amount of cell lysate used, by increasing the concentration of substrates, or by allowing the reaction to proceed for longer periods of time. Nonetheless, our current conditions allowed us to readily detect a mutant displaying a catalytic efficiency decreased by over two orders of magnitude, demonstrating the sensitivity of our assay.

2.4.3. Substrate specificity screening

An important goal of enzyme engineering is the creation of biocatalysts displaying altered substrate specificity. This is particularly important in cases where a natural enzyme that is capable of transforming the desired molecules has not been found. Our screening method can be readily adapted to the screening of mutants with altered substrate specificity by replacing the donor or acceptor substrate with a desired alternate compound. To demonstrate the utility of our screening method for this application, we screened the BCAT F36 site saturation library with potential donor L-phenylalanine. L-phenylalanine is not a native substrate of BCAT but can be used by the enzyme *in vitro* as a donor substrate in

the presence of the α-kg acceptor. However, the k_{cat}/K_M for transamination with this non-native substrate is 10-fold lower than for transamination with the native substrate L-leucine.[22] As shown in Fig. 2.3C, all of the BCAT variants that were found to be active with the natural substrate L-leucine, with the exception of F36N, were also found to be active with the L-phenylalanine donor substrate. However, their activities for transamination of α-kg with L-phenylalanine were lower than with L-leucine, which could explain why the activity of BCAT-F36N, the lowest activity mutant found by screening with L-leucine, could not be distinguished from that of the negative control. The activity of wild-type BCAT decreased 1.2-fold when screened with L-phenylalanine instead of L-leucine whereas that of the mutants decreased 1.2 to 2.3-fold, with the exception of BCAT-F36W, whose activity towards L-phenylalanine decreased 3.5-fold, almost three times higher than the observed decrease for the wild-type. This result suggested to us that BCAT-F36W may display altered donor substrate specificity as it appeared to be proportionally less active towards L-phenylalanine than the other active BCAT variants.

To investigate the possibility that the donor substrate specificity of BCAT-F36W was altered from that of the wild-type, we expressed and purified both proteins and measured their apparent kinetic parameters for transamination of α-kg with L-phenylalanine (Table 2.3). Wild-type BCAT displays a k_{cat}/K_M for L-phenylalanine that is 6-fold lower than for L-leucine. This result agrees with a previous study that reported a 10-fold decrease in k_{cat}/K_M for L-phenylalanine compared to L-leucine.[22] For BCAT-F36W, we could not achieve donor substrate saturation at 23 mM L-phenylalanine, preventing reliable determination of k_{cat} and K_M. Nonetheless, we were able to determine a k_{cat}/K_M of 0.32 s^{-1}

M^{-1}, a value 316-fold lower than for L-leucine, and ~400-fold lower than that of the wild-type enzyme for the transamination reaction with L-phenylalanine. Because the k_{cat}/K_M for the reaction of BCAT-F36W with L-leucine was only 7-fold lower than that of the wild-type enzyme, this single mutant is approximately 60-fold more specific for L-leucine relative to L-phenylalanine than the wild-type enzyme, confirming that the substrate specificity of BCAT-F36W was altered by the single mutation.

Table 2.3 Apparent kinetic parameters of purified *E.coli* BCAT and its F36W mutant for transamination of α-ketoglutarate with L-phenylalanine.

Enzyme	L-phenylalanine				
	K_M (mM)	k_{cat} (s^{-1})	k_{cat}/K_M (s^{-1} M^{-1})	(k_{cat}/K_M wild-type) / (k_{cat}/K_M mutant)	(k_{cat}/K_M L-leucine) / (k_{cat}/K_M L-phenylalanine)
Wild-type (WT)	0.27 ± 0.03	0.035 ± 0.001	130 ± 15	-	6
F36W	>23	ND	0.32 ± 0.01	406	316

Note: ND indicates that a value could not be determined because saturation with the donor substrate was not possible at the maximum concentration tested (23 mM).

We propose that the altered substrate specificity of BCAT-F36W results from the replacement of F36 with a bulkier tryptophan residue. A larger residue at position 36 may result in a steric clash with the donor substrate, which would be aggravated when the L-leucine donor is also replaced by a larger L-phenylalanine. As can be seen in the crystal structure of BCAT (Fig. 2.4B), the side chain of residue 36 is located directly next to the side chain of the donor substrate analogue 2-methylleucine, with its nearest atom 3.3 Å away. Thus, simultaneously increasing the size of residue 36 and of the donor substrate, by the introduction of the F36W mutation and by replacement of the L-leucine donor with L-phenylalanine, would likely result in a larger steric clash between the two, leading to the observed decrease in catalytic efficiency of more than three orders of magnitude when comparing transamination of α-kg with L-leucine for wild-type BCAT (k_{cat}/K_M = 743 s^{-1} M^{-1}) with transamination of L-phenylalanine for BCAT-F36W (k_{cat}/K_M = 0.32 s^{-1} M^{-1}).

We also screened the DAAT Y31 site-saturation library with the acceptor substrate phenylpyruvate. Phenylpyruvate was selected for screening because its product, D-phenylalanine, is known to be a poor donor substrate of DAAT in the reverse reaction.[34] Thus, we used our screening assay to determine whether we could identify a DAAT mutant displaying higher catalytic efficiency than the wild-type towards this acceptor substrate. As can be seen on Fig. 2.3D, only the wild-type enzyme was active when screened with the phenylpyruvate acceptor, and its activity was much lower than that obtained when screened with the native acceptor pyruvate (Fig. 2.3B). In the presence of phenylpyruvate, the reaction was complete after 50 minutes whereas with pyruvate the reaction was complete in less than 5 minutes. This observed lower activity level of DAAT towards phenylpyruvate agrees with a previous report where an approximately 70-fold decrease in

specific activity for DAAT was observed when the donor substrate D-alanine was replaced with the bulkier D-phenylalanine.[34] We measured the kinetic parameters of phenylpyruvate transamination with D-glutamate for wild-type DAAT and obtained apparent K_M and k_{cat} values of 0.19 ± 0.02 mM and 0.43 ± 0.01 s^{-1}, respectively. The resulting k_{cat}/K_M for phenylpyruvate, 2263 s^{-1} M^{-1}, is 85-fold lower than that of native substrate pyruvate, 192,500 s^{-1} M^{-1}, a result in agreement with the previous report by Fuchikami *et al.*.[34] Because all active DAAT mutants that were found by screening with the native substrate pyruvate have catalytic efficiencies decreased 15-fold or higher relative to the wild-type (Table 2.2), it is not surprising that none of these were found to be active when screened with the non-native acceptor phenylpyruvate.

2.4.4. Implementation of our assay in directed evolution

The assay developed here presents several advantages, allowing it to be applied to the directed evolution of ATs displaying altered substrate specificity. First, our assay is a high-throughput method because 96 samples can be tested at a time and more than 10^3 mutants can be screened in a matter of hours. This would enable the screening of large libraries prepared by random mutagenesis, increasing the likelihood of success of the directed evolution experiments. Second, our assay is modular because it can be used to screen DAAT with any desired α-keto acid. This modularity could facilitate the development of novel aminotransferase for the biocatalytic production of a wide range of desired enantiopure L- or D-amino acids. Finally, the conditions of our assay can be made more stringent by decreasing the substrate concentration, shortening the reaction time, or reducing the amount of clarified cell lysate used. Increasing the stringency gradually during

successive rounds of directed evolution would allow the activity of mutant ATs displaying altered substrate specificity to be optimized.

2.5. Conclusion

We have developed a continuous high-throughput assay that allowed us to screen mutant libraries of L- and D-amino acid specific aminotransferases. This assay is of broad utility as it may be used for the screening of any α-kg dependent aminotransferase with any desired donor or acceptor substrate. It is also sensitive as it allowed us to readily detect a mutant with 632-fold lower catalytic efficiency than the wild-type in a complex reaction mixture containing small quantities of enzyme. Finally, using this assay, we were able to identify a BCAT mutant, BCAT-F36W, that is ~60-fold more specific for L-leucine than L-phenylalanine compared to the wild-type. We expect that our high-throughput assay will be useful for the engineering of additional aminotransferases with increased catalytic activity or altered substrate specificity.

2.6. Acknowledgements

We thank Samantha Burugu for initial testing of the GDH assay. This work was supported by the Natural Sciences and Engineering Research Council of Canada, the University of Ottawa, and the Canada Foundation for Innovation.

2.7. Materials and Methods

2.7.1. Materials

All reagents used were of the highest available purity. Restriction enzymes and DNA modifying enzymes were obtained from New England Biolabs. Synthetic oligonucleotides were obtained from Integrated DNA Technologies, and Ni-NTA agarose resin was obtained from Promega. All aqueous solutions were prepared using water purified with a Barnstead Nanopure Diamond system. Enzyme substrates and cofactors were purchased from Sigma-Aldrich.

2.7.2. Mutagenesis

Codon-optimized *Eescherichia coli* BCAT and *Bacillus* sp. YM-1 DAAT genes synthesized by Integrated DNA Technologies were subcloned into pET11-a (Novagen) via *Nde*I/*Bam*HI. The plasmids were then transformed into *E. coli* XL-1 Blue (Stratagene). The entire *Nde*I/*Bam*HI fragments, including the whole coding region, were verified by DNA sequencing. Site saturation mutations were introduced into the BCAT and DAAT genes by overlap extension mutagenesis[35] using VentR DNA polymerase. Briefly, external primers were used in combination with sets of complementary pairs of oligonucleotides containing the NNS degenerate codon in individual polymerase chain reactions (PCR). The resulting overlapping fragments were gel-purified (Omega Biotek) and recombined by overlap extension PCR. The resulting amplicons were digested with *Nde*I/*Bam*HI, gel-purified, and ligated into pET11-a expression vector with T4 DNA ligase. Constructs were verified by sequencing the entire open reading frame.

2.7.3. Preparation of clarified cell lysates

The DNA libraries prepared as described above were transformed into chemically competent *E. coli* BL21-Gold (DE3) cells (Stratagene). Colonies were picked into individual wells of V96 MicroWell polypropylene plates (Nunc) containing 200 µL of medium (LB with 100 µg/mL ampicillin supplemented with 10% glycerol). The plates were covered with a sterile, breathable rayon membrane (VWR) and incubated overnight at 37°C with shaking. After incubation, these mother plates were used to inoculate sterile Nunc V96 MicroWell polypropylene plates ("daughter" plates) containing 300 µL of Overnight Express Instant TB media (Novagen) supplemented with ampicillin per well. Daughter plates were sealed with breathable membranes and incubated overnight (37 °C, 250 rpm). After incubation, the cells were harvested by centrifugation (3000g, 30 min, 4 °C) and the cell pellets were washed twice with phosphate-buffered saline (pH 7.4). Washed cell pellets were resuspended in lysis buffer (100 mM potassium phosphate buffer [pH 8] containing 1× Bug Buster Protein Extraction Reagent [Novagen], 25 U/mL Benzonase Nuclease [EMD], and 1 mg/mL lysozyme). The clarified lysate was collected following centrifugation and stored at 4 °C until used in the enzymatic assay.

2.7.4. Protein expression and purification

Proteins were expressed in 0.5 L cultures of *E. coli* BL21-Gold (DE3) cells transformed by a pET11-a vector containing the BCAT or DAAT gene. When the cultures reached an optical density at 600 nm of 0.6, 1 mM of isopropyl β-D-1-thiogalactopyranoside was added to the flasks to induce protein expression and cells were incubated with shaking for an additional 3 h at 37 °C. Following expression, cells were harvested by centrifugation and lysed with an EmulsiFlex-B15 cell disruptor (Avestin). The proteins were then

extracted and purified by immobilized metal affinity chromatography, according to manufacturer's protocol. Elution fractions containing the ATs were desalted by gel filtration using EconoPAC 10DG columns (Bio-Rad) into a final buffer solution of 100 mM potassium phosphate buffer (pH 8.0). The protein yields ranged from 70 to 157 mg/L and the purity was determined to be between 93–100%, as estimated by densitometry of Coomassie brilliant blue on an SDS-Page gel. Protein concentrations were quantified via a modified version of the Bradford assay, where the calibration curve is constructed as a plot of the ratio of the absorbance measurements at 590 nm and 450 nm versus concentration.[36]

2.7.5. Screening assays

All assays were performed in triplicate 200-µL reactions at 37 °C in 100 mM potassium phosphate buffer (pH 8). The standard reaction mixture for the BCAT screening assays contained final concentrations of 16 µM pyridoxal phosphate, 5 mM L-leucine, 1 mM α-kg, 1 U of GDH from bovine liver (Sigma), and 0.5 mM NAD^+. Plates containing the standard reaction mixture were preincubated at 37 °C for 10 min prior to initiation of the reaction by the addition of 25 µL of clarified cell lysates prepared as described earlier. For substrate specificity screening, L-leucine was replaced by 5 mM L-phenylalanine. For the DAAT screening assays, the standard reaction mixture contained final concentrations of 16 µM pyridoxal phosphate, 10 mM D-glutamate, 5 mM pyruvate, 1 U of GDH from bovine liver (Sigma), 15 mM ammonium chloride, and 0.5 mM NADH. Plates containing the standard reaction mixture were preincubated at 37 °C for 10 min prior to initiation of the reaction by the addition of 1 µL of clarified cell lysates prepared as described earlier. For substrate specificity screening, pyruvate was replaced by 5 mM phenylpyruvate. Enzyme reactions were monitored by measuring absorbance of NADH at 340 nm ($\varepsilon = 6220\ M^{-1}\ cm^{-}$

^{1}) every 12 s for 30 or 60 min in individual wells of 96-well plates (Greiner Bio-One) using an Infinite M1000 plate reader (Tecan).

2.7.6. Steady-state kinetics

All kinetic assays were performed in triplicate 200-µL reactions at 37 °C in 100 mM potassium phosphate buffer (pH 8). For these assays, reaction components were identical to those of the screening assays except for the following modifications. First, the concentration of the donor or acceptor substrate that was being kinetically characterized was varied, whereas the concentration of the other substrate was kept constant at 5, 1, 10, and 5 mM for L-leucine, α-kg, D-glutamate and pyruvate, respectively. In addition, the reaction was initiated by the addition of 1 to 10 mU of purified aminotransferase contained in 10 µL of potassium phosphate buffer. One unit (U) is the amount of enzyme that catalyzes the conversion of 1 µmol of substrate into product per minute. Separate reactions in which the aminotransferase was replaced by buffer, were used as blanks. Absorbance of NADH at 340 nm (ε = 6220 M^{-1} cm^{-1}) was measured every 12 s for 30 min in individual wells of 96-well plates (Greiner Bio-One) using an Infinite M1000 plate reader (Tecan). Path lengths for each well were calculated ratiometrically using the difference in absorbance of potassium phosphate buffer at 900 nm and 998 nm. Following a short lag apparent initial rates corresponding to the linear phase of the reaction were measured over a 144-s (12-data point) interval that gave a linear correlation. Non-linear regression analysis of the initial rates as a function of substrate concentrations fit to the Michaelis-Menten equation was performed with the GraphPad Prism software. For mutants displaying substrate inhibition, fitting of the kinetic data was done with a rate equation that takes into account substrate inhibition: $v_o = v_{max}$ [S] / (K_M+ [S] + [S]^2/ K_i).

2.8. References

(1) Eliot, A. C.; Kirsch, J. F. *Annu. Rev. Biochem.* **2004**, *73* (1), 383–415.
(2) Okada, K.; Hirotsu, K.; Hayashi, H.; Kagamiyama, H. *Biochemistry* **2001**, *40* (25), 7453–7463.
(3) Hayashi, H.; Inoue, K.; Nagata, T.; Kuramitsu, S.; Kagamiyama, H. *Biochemistry* **1993**, *32* (45), 12229–12239.
(4) Malashkevich, V. N.; Toney, M. D.; Jansonius, J. N. *Biochemistry* **1993**, *32* (49), 13451–13462.
(5) Sugio, S.; Petsko, G. a.; Manning, J. M.; Soda, K.; Ringe, D. *Biochemistry* **1995**, *34* (30), 9661–9669.
(6) Crismaru, C. G.; Wybenga, G. G.; Szymanski, W.; Wijma, H. J.; Wu, B.; Bartsch, S.; de Wildeman, S.; Poelarends, G. J.; Feringa, B. L.; Dijkstra, B. W.; Janssen, D. B. *Appl. Environ. Microbiol.* **2013**, *79* (1), 185–195.
(7) Kim, J.; Kyung, D.; Yun, H.; Cho, B.-K.; Seo, J.-H.; Cha, M.; Kim, B.-G. *Appl. Environ. Microbiol.* **2007**, *73* (6), 1772–1782.
(8) Rausch, C.; Lerchner, A.; Schiefner, A.; Skerra, A. *Proteins Struct. Funct. Bioinforma.* **2013**, *81* (5), 774–787.
(9) Rudat, J.; Brucher, B. R.; Syldatk, C. *AMB Express* **2012**, *2* (1), 11.
(10) Hwang, B.-Y.; Cha, M.; Park, H.-Y.; Kim, B.-G. *Biotechnol. Bioprocess Eng.* **2011**, *16* (4), 625–630.
(11) Savile, C. K.; Janey, J. M.; Mundorff, E. C.; Moore, J. C.; Tam, S.; Jarvis, W. R.; Colbeck, J. C.; Krebber, A.; Fleitz, F. J.; Brands, J.; Devine, P. N.; Huisman, G. W.; Hughes, G. J. *Science (80-.).* **2010**, *329* (5989), 305–309.
(12) Midelfort, K. S.; Kumar, R.; Han, S.; Karmilowicz, M. J.; McConnell, K.; Gehlhaar, D. K.; Mistry, A.; Chang, J. S.; Anderson, M.; Villalobos, A.; Minshull, J.; Govindarajan, S.; Wong, J. W. *Protein Eng. Des. Sel.* **2013**, *26* (1), 25–33.
(13) Cho, B.-K.; Park, H.-Y.; Seo, J.-H.; Kim, J.; Kang, T.-J.; Lee, B.-S.; Kim, B.-G. *Biotechnol. Bioeng.* **2008**, *99* (2), 275–284.
(14) Yano, T.; Oue, S.; Kagamiyama, H. *Proc. Natl. Acad. Sci. U. S. A.* **1998**, *95* (10), 5511–5515.
(15) Rothman, S. C.; Voorhies, M.; Kirsch, J. F. *Protein Sci.* **2004**, *13* (3), 763–772.
(16) Addington, T. A.; Mertz, R. W.; Siegel, J. B.; Thompson, J. M.; Fisher, A. J.; Filkov, V.; Fleischman, N. M.; Suen, A. A.; Zhang, C.; Toney, M. D. *J. Mol. Biol.* **2013**, *425* (8), 1378–1389.
(17) Schadewaldt, P.; Adelmeyer, F. *Anal. Biochem.* **1996**, *238*, 65–71.
(18) Cooper, A. J. L.; Conway, M.; Hutson, S. M. *Anal. Biochem.* **2002**, *308* (1), 100–105.
(19) Hopwood, J.; Truppo, M. D.; Turner, N. J.; Lloyd, R. C. *Chem. Commun.* **2011**, *47* (2), 773–775.
(20) Bommer, M.; Ward, J. M. *Enzyme Microb. Technol.* **2013**, *52* (4–5), 218–225.
(21) Luong, T. N.; Kirsch, J. F. *Anal. Biochem.* **1997**, *253* (1), 46–49.
(22) Kagamiyama, H.; Hayashi, H. In *Methods in Enzymology*; 2000; Vol. 324, pp 103–113.
(23) Schadewaldt, P. In *Methods in Enzymology*; Elsevier Science & Technology, 2000; pp 23–32.

(24) Yu, X.; Bresser, J.; Schall, I.; Djurdjevic, I.; Buckel, W.; Wang, X.; Engel, P. C. *Anal. Biochem.* **2012**, *431* (2), 127–131.
(25) Weinhandl, K.; Winkler, M.; Glieder, A.; Camattari, A. *Tetrahedron* **2012**, *68* (37), 7586–7590.
(26) Salerno, C.; Ovadi, J.; Keleti, T.; Fasella, P. *Eur. J. Biochem.* **1982**, *121* (3), 511–517.
(27) Day, N.; Keillor, J. W. *Anal. Biochem.* **1999**, *274* (1), 141–144.
(28) Smith, B. C.; Hallows, W. C.; Denu, J. M. *Anal. Biochem.* **2009**, *394* (1), 101–109.
(29) Schomburg, I.; Chang, A.; Placzek, S.; Söhngen, C.; Rother, M.; Lang, M.; Munaretto, C.; Ulas, S.; Stelzer, M.; Grote, A.; Scheer, M.; Schomburg, D. *Nucleic Acids Res.* **2012**, *41* (D1), D764–D772.
(30) Kuramitsu, S.; Ogawa, T.; Ogawa, H.; Kagamiyama, H. *J. Biochem.* **1985**, *97* (4), 993–999.
(31) Tanizawa, K.; Asano, S.; Masu, Y.; Kuramitsu, S.; Kagamiyama, H.; Tanaka, H.; Soda, K. *J. Biol. Chem.* **1989**, *264* (5), 2450–2454.
(32) Liu, L.; Yoshimura, T.; Endo, K.; Kishimoto, K.; Fuchikami, Y.; Manning, J. M.; Esaki, N.; Soda, K. *Biosci. Biotechnol. Biochem.* **1998**, *62* (1), 193–195.
(33) Peisach, D.; Chipman, D. M.; Van Ophem, P. W.; Manning, J. M.; Ringe, D. *Biochemistry* **1998**, *37* (14), 4958–4967.
(34) Fuchikami, Y.; Yoshimura, T.; Gutierrez, A.; Soda, K.; Esaki, N. *J. Biochem.* **1998**, *124* (5), 905–910.
(35) Heckman, K. L.; Pease, L. R. *Nat. Protoc.* **2007**, *2* (4), 924–932.
(36) Ernst, O.; Zor, T. *J. Vis. Exp.* **2010**, No. 38, 1–6.

Chapter 3.
Engineered aminotransferase for the production of D-phenylalanine derivatives using biocatalytic cascades.

The contents of this chapter were published in:
Walton, C.J.W., Parmeggiani, F., Barber, J.E.B., McCann, J.L., Turner, N.J. and Chica, R.A., Engineered Aminotransferase for the Production of D-Phenylalanine Derivatives Using Biocatalytic Cascades. *ChemCatChem*, **2018,** 10, 470–474.

3.1. Preface

In this chapter, we characterized the substrate scope of DAAT and identified that the enzyme has low catalytic efficiency for aromatic amino acids. We engineered the enzyme for enhanced catalytic efficiency towards aromatic amino acids and characterized the substrate specificity of the mutants. Lastly, we incorporated our high-efficiency DAAT mutant into a biocatalytic cascade to produce several D-phenylalanine derivatives with electron-donating or -withdrawing substituents at the *ortho*, *meta*, and *para* positions with high enantiomeric excess, percent conversion, and yield from ketoacids, racemates, and L-amino acids.

3.2. Contribution Statement

The contributions of all authors are outlined below:

Conception:

The initial concept of this article was conceived by Curtis J.W. Walton. Curtis J.W. Walton, Dr. Roberto A. Chica, Dr. Fabio Parmeggiani, and Dr. Nicholas J. Turner collaborated on the project direction, experimental design, and analysis of key results.

Writing:

The manuscript for this article was written by Curtis J.W. Walton, Dr. Fabio Parmeggiani, Janet E.B. Barber, Dr. Nicholas J. Turner, and Dr. Roberto A. Chica.

Experimental:

The experiments presented in this article were performed by Curtis J.W. Walton, Dr. Fabio

Parmeggiani, Dr. Janet E.B. Barber, and Jenna L. McCann. The DAAT mutants were prepared by Jenna L. McCann and Curtis J.W. Walton via site-directed mutagenesis and overlap extension PCR. The development and optimization of the D-aspartate oxidase assay was performed by Janet E.B. Barber. The screening and kinetic characterizations with wild-type and mutant DAATs were performed by Curtis J.W. Walton. The biotransformations (% conversion, *ee*, and yield), NMR, and HPLC experiments were performed by Fabio Parmeggiani.

3.3. Introduction

D-Phenylalanine and its derivatives are essential building blocks in the synthesis of many pharmaceuticals, which include antibiotics,[1] antidiabetics,[2] and chemotherapeutic agents for cancer treatment.[3] Although asymmetric Strecker reactions can be used to synthesize these compounds,[4] biocatalytic approaches are of great interest as they provide safer alternatives that exploit the unmatched selectivity of enzymes for the enantioselective synthesis of these chiral molecules. Previously, a fermentation process was developed to produce optically pure D-phenylalanine in *E. coli* cells.[5] However, this process relied on an aromatic amino acid biosynthetic pathway specific to the phenylpyruvate precursor of D-phenylalanine, which limited its applicability to the synthesis of a wide range of substituted D-phenylalanine derivatives. More recently, we developed chemoenzymatic and biocatalytic cascades that couple L-amino acid deaminase (LAAD) with either phenylalanine ammonia-lyase[6] or an engineered D-amino acid dehydrogenase[7] to enable the production of optically pure D-phenylalanine derivatives. Although these methods afford various D-phenylalanine derivatives with high enantiomeric excesses and

conversion rates, they suffer from limitations such as low reactivity with substrates that contain electron-donating substituents and requirement of a large excess of ammonia-borane reducing reagent,[6] or the need for an additional cofactor recycling step.[7] Attractive alternatives to these methods would be stereoinversion and deracemization cascades[8–12] in which LAAD is coupled with a D-phenylalanine-specific aminotransferase (Scheme 3.1). Such cascades would enable the one-pot enantioselective synthesis of a wide range of D-phenylalanine derivatives that contain electron-donating or withdrawing substituents from more easily accessed L- or racemic phenylalanine derivatives, and have the further benefit that they do not require the recycling of expensive cofactors. Although D-amino acid aminotransferases from various species have been shown to react with D-phenylalanine,[13] their activity towards this non-native substrate is low,[14–16] which motivated us to engineer more proficient biocatalysts to increase the efficiency and robustness of our targeted cascades.

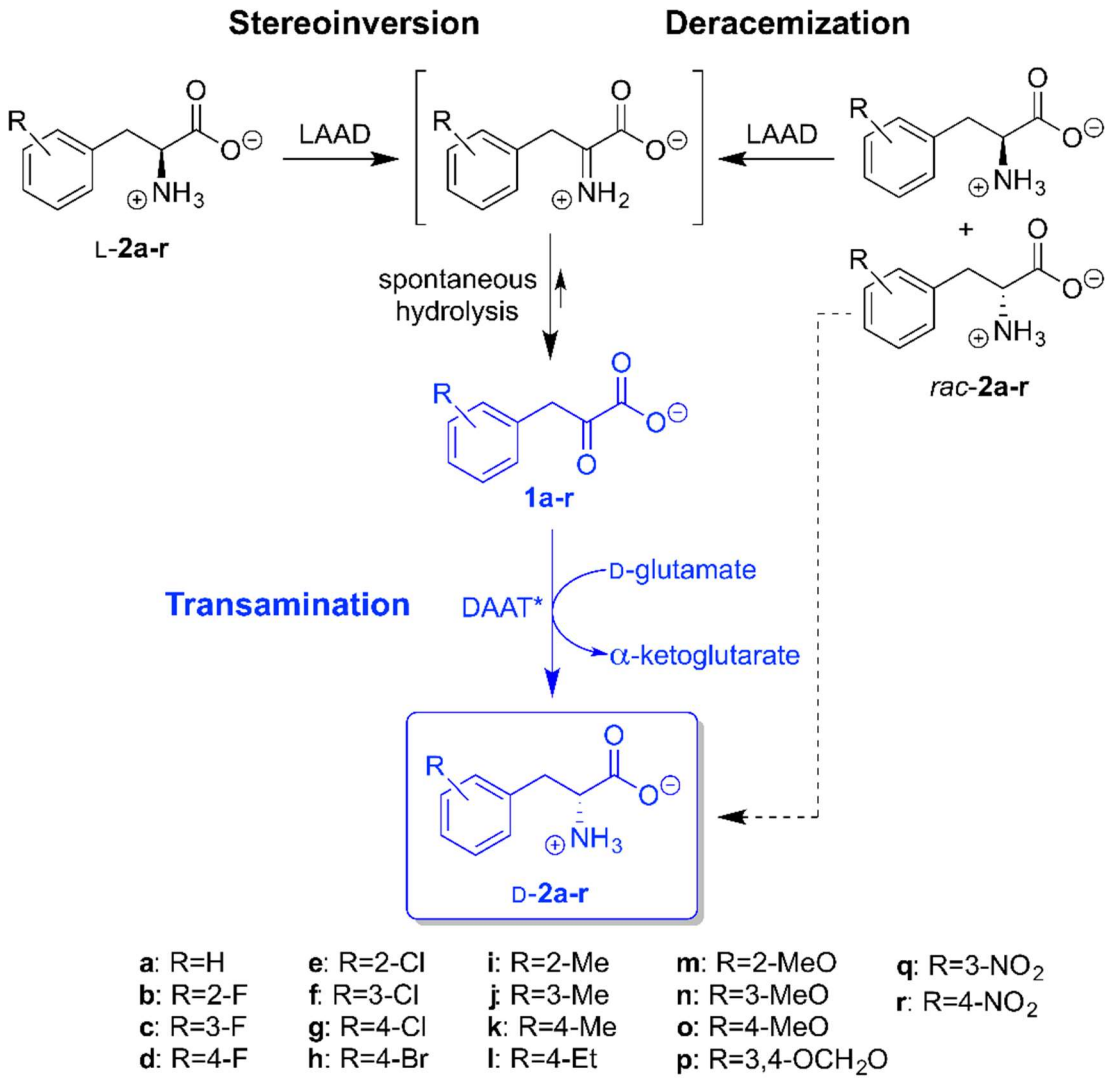

Scheme 3.1 Biocatalytic cascades for the asymmetric synthesis of D-phenylalanine derivatives. LAAD and DAAT* indicate L-amino acid deaminase and engineered D-amino acid aminotransferase, respectively.

3.4. Results and Discussion

As a starting point for biocatalyst engineering, we selected the D-amino acid aminotransferase (DAAT) from *Bacillus* sp. YM-1.[17,18] DAAT catalyzes the reversible transamination of D-alanine and α-ketoglutarate to yield D-glutamate and pyruvate. DAAT can also react with the oxaloacetate acceptor substrate (Supplementary Results, Table S3.1) as well as with a range of polar and aliphatic D-amino acid donors, albeit with reduced specific activity.[15] However, the specific activity of DAAT with D-phenylalanine is almost two orders of magnitude lower than with its native substrate D-alanine.[19] We postulated that this lower activity with aromatic compounds is because the side chain of the D-amino acid substrate sits in a pocket formed by residues V33, S240, and T242 in the DAAT active site[20] (Figure 3.1) that is too small to bind the bulky benzyl side chain of D-phenylalanine efficiently. Previously, we demonstrated that replacement of V33 to a smaller glycine residue increased the catalytic efficiency (k_{cat}/K_M) of DAAT towards phenylpyruvate by over three-fold,[21] an enhancement that was because of improved productive binding (K_M was decreased by approximately three-fold). This result supports our hypothesis and suggests that mutations that increase the size of the side-chain binding pocket in the active site will lead to more efficient binding of bulkier substrates. Although V33 is located on a β-strand, the two other residues that form the side-chain binding pocket (S240 and T242) are located on a loop formed by residues 240–243. This structural element is expected to be more flexible than β-strands, which lead us to hypothesize that substitution of these loop residues to glycine will permit a more efficient reshaping of the side-chain binding pocket for binding of bulkier substrates and thus result in more efficient biocatalysts for the synthesis of D-phenylalanine derivatives.

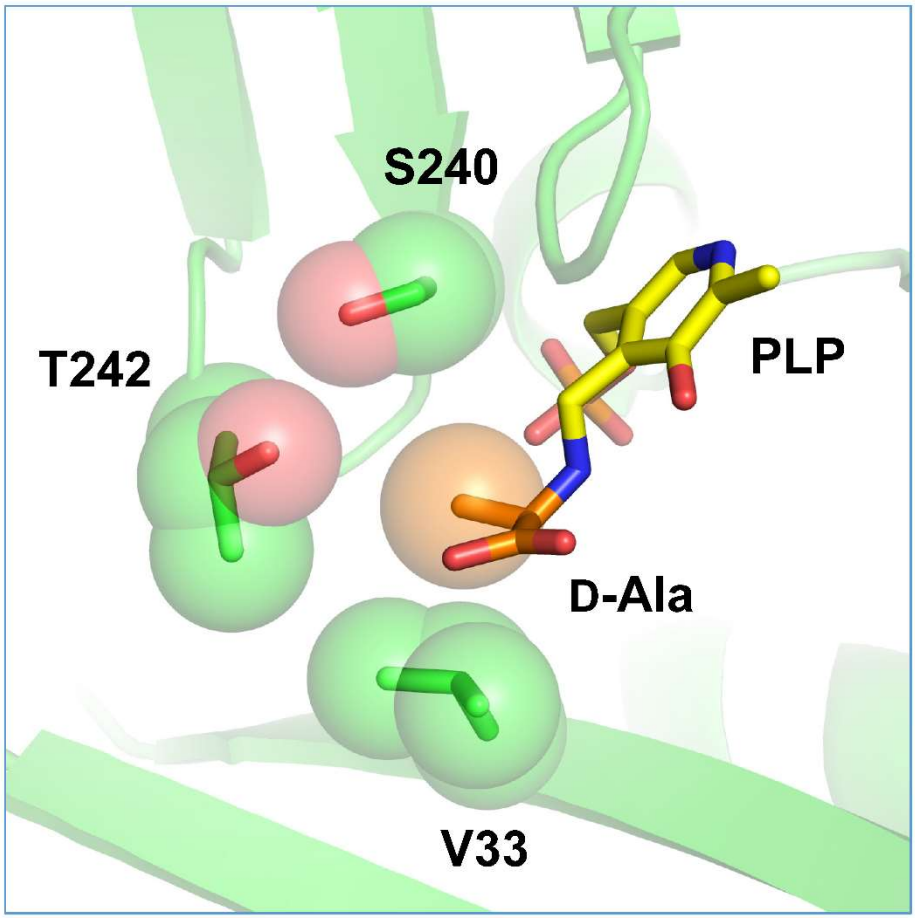

Figure 3.1 Active site of *Bacillus sp.* YM-1 DAAT. The side chain of the pyridoxal phosphate (PLP)-bound D-alanine donor substrate (orange) fits in a small cavity formed by residues V33, S240, and T242. PDB ID: 3DAA.[20]

To test our hypothesis, we prepared the S240G and T242G variants by site-directed mutagenesis and evaluated their ability to catalyze transamination with a library of D-amino acids, which included several D-phenylalanine derivatives. To perform this analysis in a high-throughput manner, we developed a microplate-based colorimetric assay in which bovine D-aspartate oxidase (DDO)[22,23] and horseradish peroxidase (HRP) are used as coupling enzymes (Scheme S3.1, Figures S3.1–S3.2, Table S3.1, Supplementary Results). We used this assay to measure the specific activity of wild-type and mutant DAATs towards a library of D-amino acids that contain aliphatic, polar uncharged, basic, or aromatic side chains (Figure 3.2, Table S3.2). As expected, wild-type DAAT displays high specific activity with its native substrate D-alanine, reacts less efficiently with various aliphatic and polar substrates, and shows no detectable activity towards aromatic amino acids. Next, we screened the S240G and T242G mutants against the D-amino acid library, and included in this analysis the V33G variant that we previously described.[21] We discovered that all three DAAT mutants display broader substrate specificity than the wild-type enzyme, and the V33G has the broadest specificity as it reacts with all amino acids tested except for D-phenylglycine. Interestingly, none of the variants reacted with this aromatic amino acid, which can be rationalized by the absence of the methylene group that bridges the main chain and phenyl ring in D-phenylglycine that is likely required to alleviate steric clashes of this ring with the loop formed by residues 240–243. All three mutants reacted with all D-phenylalanine derivatives tested with a specific activity >10 mU mg^{-1}, with the exception of S240G with D-**2k**. Of all the mutants, T242G had the highest specific activity with D-phenylalanine (1210 ± 60 mU mg^{-1}), a value that is the same within error to that of the wild type with its native substrate D-alanine (1100 ± 100 mU mg^{-1}).

T242G is also highly active with all D-phenylalanine derivatives tested, which suggests that we engineered an efficient aminotransferase biocatalyst for the synthesis of D-phenylalanine and its derivatives.

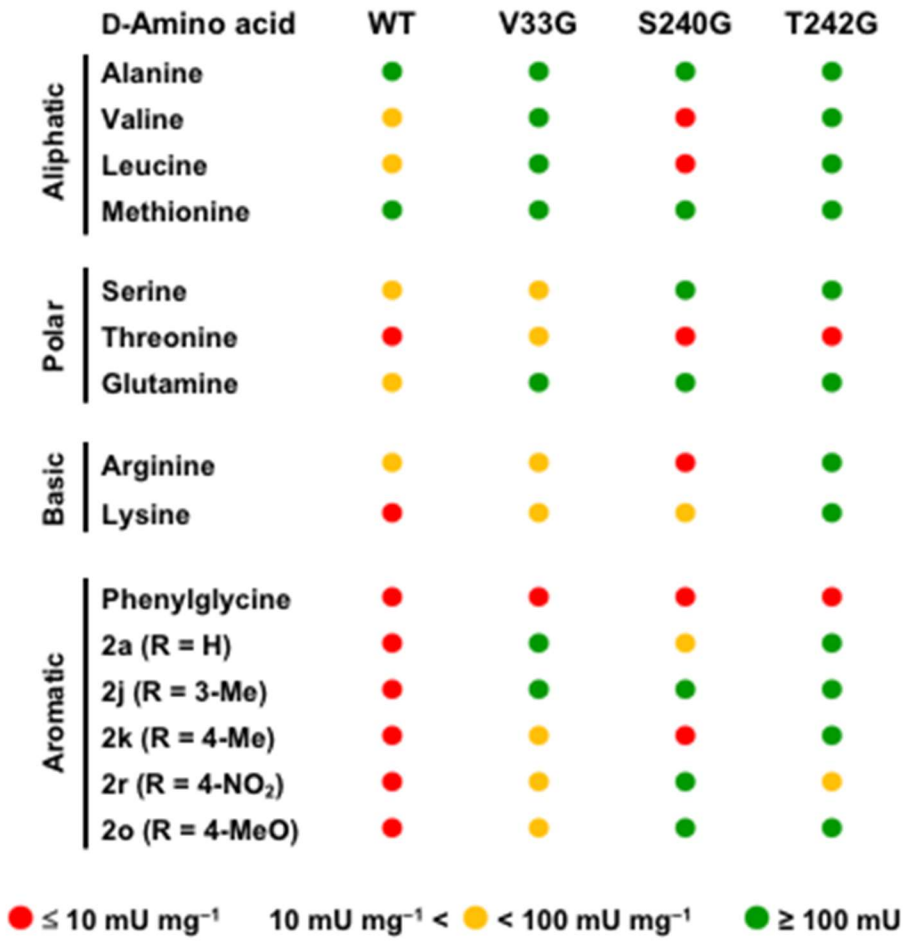

Figure 3.2 Substrate-specificity profiles of wild-type and mutant DAAT enzymes. Each dot represents a unique aminotransferase–amino acid combination and is colored based on the specific activity of the resulting enzymatic reaction. The acceptor substrate for each reaction was oxaloacetate.

To gain a better understanding of the underlying reason for the increased activity of these mutants towards D-phenylalanine derivatives, we determined steady-state kinetic parameters of wild-type and mutant DAATs for transamination of six representative substrates that contain either electron-donating or -withdrawing substituents at the *ortho*, *meta*, or *para* positions of the phenyl ring (Table 3.1). For wild-type DAAT, we were unable to achieve saturation with D-phenylalanine within its solubility limit, which prevented reliable determination of K_M and k_{cat}. However, we were able to measure a catalytic efficiency of 0.65 M^{-1} s^{-1} for this substrate, a value that is over three orders of magnitude lower than that for the native substrate D-alanine (Table S3.1). All other D-phenylalanine derivatives tested with wild-type DAAT also gave low catalytic efficiencies (≤10 M^{-1} s^{-1}), which confirms that wild-type DAAT is a poor biocatalyst for transamination of aromatic D-amino acids. However, all three DAAT mutants displayed an enhanced catalytic efficiency towards aromatic D-amino acids compared to the wild type, as observed during screening. Surprisingly, the higher catalytic efficiencies result mostly from improved k_{cat} and not K_M, which suggests that these mutations enhance catalytic activity without improving productive binding significantly, contrary to our hypothesis. In agreement with our screening results, the T242G mutant had the highest catalytic efficiency for D-phenylalanine (400 M^{-1} s^{-1}), which represents a 615-fold increase compared to the wild type. Importantly, this k_{cat}/K_M value is only 4.6-fold lower than that of the wild type with its native substrate D-alanine (Table S3.1), and the k_{cat} of the mutant (1.8 ± 0.1 s^{-1}) is 1.5-fold greater than that of the wild type with its native substrate (1.18 ± 0.03 s^{-1}). Taken together, these results confirm that we have successfully engineered an aminotransferase with native-like catalytic activity towards D-phenylalanine and its derivatives.

Table 3.1 Apparent kinetic parameters for the transamination of various D-phenylalanine derivatives by wild-type and mutant DAATs.

Enzyme	Substrate[a]	R	K_M (mM)	k_{cat} (s^{-1})	k_{cat}/K_M ($M^{-1} s^{-1}$)	Relative k_{cat}/K_M
Wild type	D-**2a**	H	N.D.[b]	N.D.[b]	0.65 ± 0.02	1
	D-**2i**	2-Me	>50	<0.0006	<0.01	1
	D-**2j**	3-Me	N.D.[b]	N.D.[b]	1.5 ± 0.1	1
	D-**2n**	3-MeO	3.7 ± 0.4	0.038 ± 0.001	10 ± 1	1
	D-**2q**	3-NO_2	2.4 ± 0.3	0.025 ± 0.001	10 ± 1	1
	D-**2k**	4-Me	1.4 ± 0.5	0.006 ± 0.001	4 ± 2	1
V33G	D-**2a**	H	8.8 ± 0.4	0.27 ± 0.01	31 ± 2	48
	D-**2i**	2-Me	18 ± 2	0.59 ± 0.04	33 ± 4	>3300
	D-**2j**	3-Me	17.8 ± 0.8	2.60 ± 0.05	146 ± 7	97
	D-**2n**	3-MeO	8.9 ± 0.9	0.43 ± 0.02	48 ± 5	5
	D-**2q**	3-NO_2	8.5 ± 0.8	1.44 ± 0.06	169 ± 17	17
	D-**2k**	4-Me	4 ± 2	0.024 ± 0.002	6 ± 3	1.5
S240G	D-**2a**	H	15 ± 2	0.58 ± 0.04	39 ± 6	60
	D-**2i**	2-Me	>50	<0.0006	<0.01	1
	D-**2j**	3-Me	16 ± 2	1.6 ± 0.1	100 ± 14	67
	D-**2n**	3-MeO	4.0 ± 0.8	0.26 ± 0.02	65 ± 17	6.5
	D-**2q**	3-NO_2	3.0 ± 0.5	0.30 ± 0.02	100 ± 18	10
	D-**2k**	4-Me	26 ± 5	0.8 ± 0.1	31 ± 7	8
T242G	D-**2a**	H	4.5 ± 0.8	1.8 ± 0.1	400 ± 75	615
	D-**2i**	2-Me	16 ± 1	0.74 ± 0.03	45 ± 3	>4500
	D-**2j**	3-Me	3.7 ± 0.7	2.6 ± 0.1	703 ± 136	468
	D-**2n**	3-MeO	6 ± 2	2.2 ± 0.4	367 ± 139	37
	D-**2q**	3-NO_2	5.3 ± 0.7	0.44 ± 0.01	83 ± 11	8
	D-**2k**	4-Me	5 ± 1	2.2 ± 0.2	449 ± 97	112

[a] For all reactions, the acceptor substrate was 5 mM oxaloacetate (mean ± s.d., n = 3). [b] N.D.: could not be determined as substrate saturation was not possible within its solubility limit.

Next, we performed a series of transamination reactions with our most active mutant, DAAT-T242G, to synthesize D-phenylalanine derivatives. An *E. coli* whole-cell that expresses DAAT-T242G was incubated with a panel of phenylpyruvate analogs that contain electron-donating or -withdrawing substituents of different sizes and at different positions on the phenyl ring as acceptor substrates, along with the D-glutamate donor. All phenylpyruvate analogs tested were transformed into the corresponding D-phenylalanine derivatives with high conversion rates (≥94%) over a 12-hour period (Table 3.2), which confirms the broad specificity of our biocatalyst. The enantiomeric excess (*ee*) values of these transamination reactions were also high (92–99%), with the exception of the transamination of **1h**, which resulted in an *ee* value of 80%. It is unclear what caused the lower *ee* obtained with this substrate as the enzyme displays near-perfect enantioselectivity (e.g., *ee* ≥98% for all transamination reactions using purified enzyme, Table 3.2), but it may result from unrelated enzymatic processes that occur in *E. coli* cells during the 12 h incubation.

After we had confirmed that our DAAT-T242G whole-cell biocatalyst could be used to synthesize a variety of D-phenylalanine derivatives from their corresponding keto acids, we combined it with an *E. coli* whole-cell biocatalyst that expressed LAAD from *Proteus mirabilis*[24] to test our targeted stereoinversion and deracemization cascades (Scheme 3.1). These cascades should enable the one-pot tandem oxidative deamination and reductive amination of L-amino acids into D-amino acids. If we started from racemic or L-phenylalanine derivatives that contain electron-withdrawing (**2b-h**) or donating (**2i-k, n**) substituents at the *ortho*, *meta*, or *para* positions of the phenyl ring, our biocatalytic cascades yielded the corresponding D-phenylalanine derivatives with excellent *ee* values

(90 to >99%) in 4 h (Table 3.2). Even in the case where transamination of the corresponding phenylpyruvate does not proceed with high enantioselectivity (e.g., **1h**), very high *ee* can be obtained because repeated deracemization cycles ultimately result in complete consumption of the L-enantiomer and accumulation of enantiopure D product. Furthermore, no accumulation of the corresponding phenylpyruvate was observed during deracemization (Figure S3.3), which suggest strongly that the undesired L enantiomer was converted to the D enantiomer and not simply oxidized by LAAD. Thus, our biocatalytic processes are true stereoinversion and deracemization cascades and not kinetic resolution processes.

Table 3.2 Biocatalytic production of D-phenylalanine derivatives.

Substrate	R	Conv. (%)[a]	*ee* D-2 (%)[b]
Transamination[c]			
1a	H	>99	95 (99)
1d	4-F	>99	92 (>99)
1e	2-Cl	>99	92 (>99)
1h	4-Br	98	80 (98)
1i	2-Me	94	99 (>99)
1k	4-Me	98	93 (98)
1l	4-Et	>99	97 (>99)
1m	2-MeO	97	98 (98)
1o	4-MeO	>99	99 (>99)
1p	3,4-OCH_2O	98	96 (>99)
Stereoinversion/Deracemization[d]			
rac-**2a**	H	–	>99 (94)
rac-**2b**	2-F	–	>99 (98)
rac-**2c**	3-F	–	99 (97)
rac-**2d**	4-F	–	99 (97)
L-**2e**	2-Cl	–	98 (83)
L-**2f**	3-Cl	–	99 (89)
rac-**2g**	4-Cl	–	>99 (97)
rac-**2h**	4-Br	–	>99 (>99)
L-**2i**	2-Me	–	90 (86)
L-**2j**	3-Me	–	96 (76)
L-**2k**	4-Me	–	93 (79)
L-**2n**	3-MeO	–	98 (83)

[a] Conversion of **1** to **2** measured by reverse-phase HPLC on a non-chiral stationary phase. [b] For transamination, the values given are after 12 h incubation with whole-cell biocatalyst (values in parenthesis are with purified enzyme) whereas for stereoinversion/deracemization, the values are after 4 h (values in parenthesis are after 2 h). [c] Reaction conditions: 5 mM **1**, 20 mM D-Glu, 0.5 mM PLP, 1% v/v DMSO, 20 mg mL^{-1} DAAT-T242G wet cells (or 1 mg mL^{-1} purified enzyme), 100 mM potassium phosphate buffer, pH 8.0, 37 °C, 12 h. [d] Reaction conditions: 10 mM **2**, 30 mM D-Glu, 20 mg mL^{-1} LAAD wet cells, 20 mg mL^{-1} DAAT-T242G wet cells, 100 mM potassium phosphate buffer, pH 8.0, 37 °C, 4 h.

To confirm this result and demonstrate the practical utility of our biocatalytic cascades for the synthesis of valuable D-phenylalanine derivatives, we performed a preparative scale test of the deracemization cascade with *rac*-**2d** and the D-glutamate donor to produce D-4-fluorophenylalanine, a building block of melanocortin-4 receptor agonists used as antiobesity agents.[25] To favor the complete conversion of racemic **2d** into enantiopure D-**2d,** an excess of D-glutamate was used (3 equivalents). Although complete deracemization was observed (99% *ee*), the unreacted excess D-glutamate could not be separated from D-**2d** by adsorption on ion-exchange resin, our standard procedure for amino acid purification (Figure S3.4a). To address this issue, we incubated the reaction mixture with DDO upon the completion of the deracemization process to transform the unreacted donor substrate into its corresponding keto acid, which can be removed readily by using ion-exchange purification. We tested the addition of wet *E. coli* cells expressing DDO (20 or 80 mg mL^{-1} for 24 or 8 h, respectively) on deracemization mixtures prepared using excess D-glutamate or D-aspartate. D-Aspartate was included in our tests because it is the preferred substrate of DDO (Figure S3.1a) and good donor substrate of DAAT.[26] DDO treatment enabled the complete removal of excess D-aspartate but not D-glutamate after deracemization of *rac*-**2d** under these conditions (Figure S3.4), a result that can be explained by the eightfold higher catalytic efficiency of DDO towards D-aspartate (Table S3.1). We were able to use this procedure with the D-aspartate donor to obtain 76.9 mg of optically pure D-**2d** (99% *ee*), which represents an isolated yield of 84%. These results confirm that our deracemization cascade can be used for the preparative-scale synthesis of valuable enantiopure D-phenylalanine derivatives with high yield.

3.5. Conclusion

We have developed one-pot biocatalytic processes for the synthesis of valuable enantiopure D-phenylalanine derivatives that contain electron-donating or -withdrawing substituents of various sizes, and at different positions on the phenyl ring from more accessible starting materials. To do this, we engineered an aminotransferase that shows a high catalytic activity towards D-phenylalanine. In comparison with previous biocatalytic cascades used to synthesize similar compounds, our cascades have the benefit that they do not require expensive cofactors,[7] which removes the need for a cofactor regeneration system, or large excesses of chemical reducing agents.[6] However, our cascades require stoichiometric amounts of the D-glutamate or D-aspartate donor substrate, which may represent a disadvantage for certain applications. This disadvantage can be eliminated by generating the donor substrate *in situ* with a glutamate or aspartate racemase,[27,28] and by replacing LAAD from *Proteus mirabilis* with that from *Proteus myxofaciens*, which has been shown to not deaminate L-glutamate or L-aspartate.[29,30]Although we focused on the synthesis of D-phenylalanine derivatives in this study, other D-amino acids could also be synthesized using our cascades as all three DAAT variants reported here display increased activity relative to the wild type towards a series of D-amino acids that have aliphatic or polar side chains. Our cascades thus complement other biocatalytic processes reported previously,[5–7,31] and represent useful additions to the D-amino acid synthesis toolbox.

3.6. Acknowledgements

R.A.C. acknowledges an Early Researcher Award from the Ontario Ministry of Economic Development & Innovation (ER14-10-139) and grants from the Natural Sciences and Engineering Research Council of Canada (RGPIN-2016-04831) and the Canada Foundation for Innovation (26503). F.P. was supported by the Biotechnology and Biological Sciences Research Council (BBSRC) and Glaxo-SmithKline (GSK) under the strategic Longer and Larger (sLoLa) grant initiative ref. BB/K00199X/1. N.J.T. thanks the Royal Society for a Wolfson Research Merit Award.

3.7. Supplemental Information

3.7.1. Supplementary results

3.7.1.1. DDO assay development

To evaluate the range of D-amino acid donors that our DAAT mutants can react with, we developed a continuous, colorimetric assay based on the use of *Bos taurus* D-aspartate oxidase (DDO)[22] as the coupling enzyme. DDO was selected as the coupling enzyme because it oxidizes D-aspartate and D-glutamate while displaying minimal activity towards a range of amino acids having aliphatic, aromatic, polar uncharged, and basic side chains (Fig. S3.1a). Furthermore, DDO displays maximum activity at pH 8.0 (Fig. S3.1b), which is the optimal pH of DAAT.[32] Although DDO can react favorably with both D-aspartate and D-glutamate, its k_{cat}/K_M for D-aspartate is approximately 8-fold higher than for D-glutamate (Table S3.1), which results mostly from improved k_{cat}. Because of this, we selected oxaloacetate rather than α-ketoglutarate as the DAAT acceptor substrate in our development of the DDO coupled assay.

In the DDO assay (Scheme S3.1), DAAT transfers the amino group of a D-amino acid to oxaloacetate, producing D-aspartate and an α-keto acid. D-Aspartate is oxidized back to oxaloacetate by DDO in the presence of molecular oxygen and water with concomitant release of ammonium and hydrogen peroxide, which can be detected colorimetrically by the addition of horseradish peroxidase (HRP) and *o*-dianisidine. Thus, the DDO coupled assay enables testing of many D-amino acids as DAAT donor substrates, making it complementary to our previously reported assay based on *Trigonopsis variabilis* D-amino acid oxidase[21] that allows testing of a wide range of keto acids as potential acceptor substrates of DAAT.

As a first step in the development of the DDO assay, reaction conditions were optimized using purified wild-type DAAT, DDO, and HRP to ensure that the DAAT reaction was the rate-limiting step. To do this, we initially assayed 2 mU of DAAT with large excesses of the coupling enzymes (≥100-fold) and reagent concentrations that we previously determined to be optimal for a similar oxidase/HRP-based coupled assay (16 μM pyridoxal phosphate [PLP], 1 μM flavin adenine dinucleotide [FAD], 0.5 mM *o*-dianisidine).[21] As shown on Figure S3.2a, no significant changes in rate were observed when the concentration of FAD, *o*-dianisidine, or HRP (5 U) was doubled from their starting amounts. However, the rate increases linearly with increased DAAT concentration (Fig. S3.2b), demonstrating that assay conditions are optimal for ensuring that the DAAT reaction is the rate-limiting step. This observation is further supported by the fact that Michaelis-Menten plots (Fig. S3.2c) show the expected hyperbolic relationship between initial rates and aminotransferase substrate concentrations, allowing for apparent kinetic parameters of the DAAT-catalyzed transamination of oxaloacetate or α-ketoglutarate with

D-alanine to be determined (Table S3.1). Importantly, the catalytic efficiency of DAAT with the oxaloacetate acceptor is only two-fold lower than with α-ketoglutarate, which should provide robust activity measurements when using the DDO assay with this acceptor substrate.

3.7.1.2. Supplementary tables

Table S3.1 Apparent kinetic parameters of *Bos taurus* DDO and *Bacillus sp.* YM-1 DAAT.

Enzyme	Substrate	K_M (mM)	k_{cat} (s^{-1})	k_{cat}/K_M (M^{-1} s^{-1})
DDO[†]	D-glutamate	0.7 ± 0.1	0.093 ± 0.002	130 ± 20
	D-aspartate	0.52 ± 0.05	0.54 ± 0.01	1000 ± 100
DAAT[‡]	D-alanine	0.64 ± 0.05	1.18 ± 0.03	1800 ± 200
	α-ketoglutarate	0.56 ± 0.05	1.18 ± 0.03	2100 ± 200
	oxaloacetate	0.97	1.01	1000

[†] Reaction conditions: 2 mU DDO, 1 μM FAD, 0.5 mM *o*-dianisidine, and 5 U HRP. Experiments were performed in triplicate using DDO from three independent protein preparations (mean ± s.d.).

[‡] Reaction conditions: 2 mU DAAT, 200 mU DDO, 16 μM PLP, 1 μM FAD, 0.5 mM *o*-dianisidine, and 5 U HRP. For D-alanine kinetics, the acceptor substrate was α-ketoglutarate (5 mM). For kinetics of α-ketoglutarate and oxaloacetate, the donor substrate was D-alanine (10 mM). Experiments were performed in triplicate using DAAT from three independent protein preparations (mean ± s.d.), except for oxaloacetate kinetics, where a single protein preparation was used.

Table S3.2 Specific activities of wild-type (WT) and mutant DAATs for various D-amino acids.

D-amino acid	WT (mU mg^{-1})	V33G (mU mg^{-1})	S240G (mU mg^{-1})	T242G (mU mg^{-1})
alanine	1100 ± 100	800 ± 100	20000 ± 1000	9600 ± 600
valine	31 ± 1	1200 ± 100	<1	109 ± 3
leucine	62 ± 5	200 ± 10	<1	900 ± 200
methionine	240 ± 30	2100 ± 100	1900 ± 200	11100 ± 400
serine	20 ± 10	90 ± 30	240 ± 30	330 ± 40
threonine	<1	80 ± 8	<1	<1
glutamine	80 ± 20	600 ± 50	300 ± 60	500 ± 90
arginine	30 ± 20	60 ± 10	<1	310 ± 90
lysine	9 ± 4	60 ± 20	70 ± 50	250 ± 40
phenylglycine	<1	<1	<1	<1
2a (R = H)	<1	590 ± 30	90 ± 10	1210 ± 60
2j (R = 3-Me)	<1	1350 ± 60	520 ± 60	510 ± 20
2k (R = 4-Me)	<1	70 ± 20	<1	2120 ± 20
2r (R = 4-NO_2)	<1	33 ± 9	800 ± 100	90 ± 20
2o (R = 4-MeO)	<1	20 ± 10	200 ± 100	320 ± 40

In all cases, the acceptor substrate was 5 mM oxaloacetate.
All experiments were performed in triplicate (mean ± s.d.).

3.7.1.3. Supplementary scheme and figures

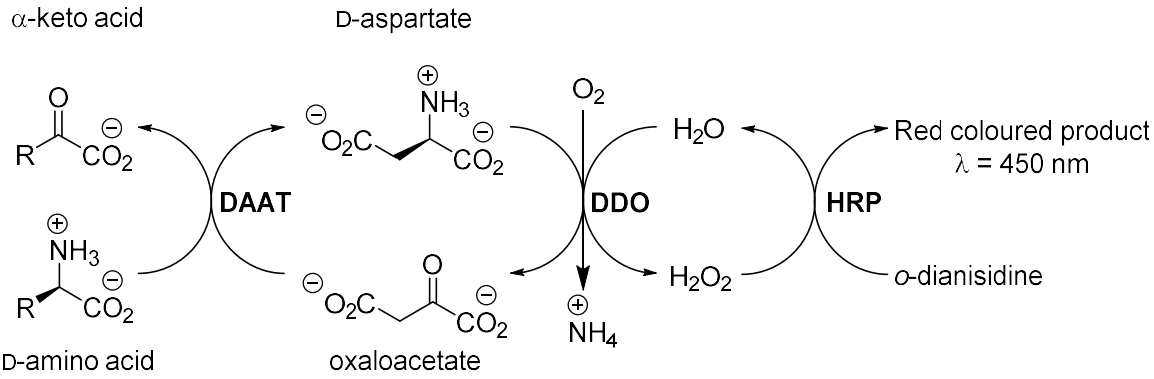

Scheme S3.1 DDO coupled enzyme assay. The transamination reaction catalyzed by DAAT produces D-aspartate, which is oxidized back to oxaloacetate by DDO in the presence of molecular oxygen and water. The DDO reaction produces hydrogen peroxide, which is used by HRP to oxidize *o*-dianisidine into a red-colored product. By varying the donor D-amino acid, the substrate specificity of DAAT can be evaluated.

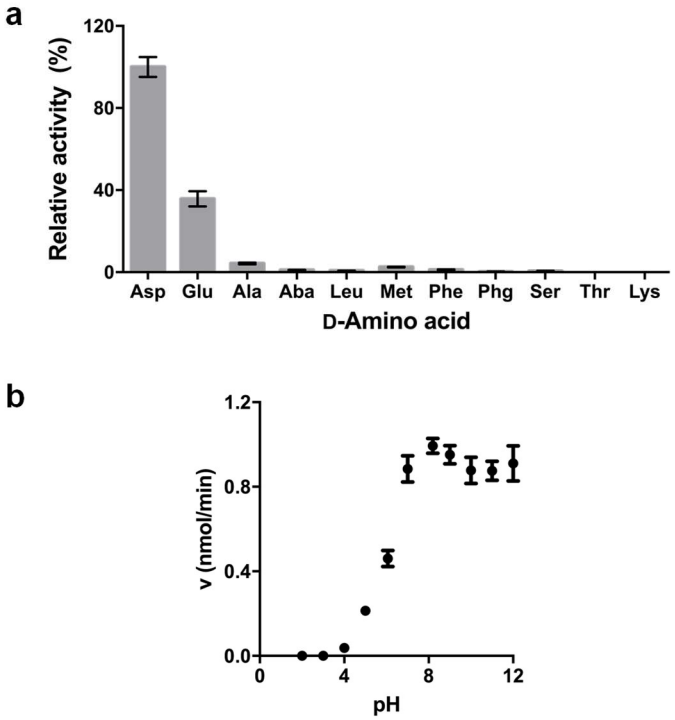

Figure S3.1 Properties of *Bos taurus* DDO. (a) Substrate specificity profile. Activity values for various D-amino acids relative to that of the native substrate D-aspartate are reported. D-2-aminobutyric acid and D-phenylglycine are identified as Aba and Phg, respectively. (b) pH profile using 10 mM D-glutamate in Britton-Robinson buffer over a pH range of 2–12. In all cases, mean ± s.d. is reported (n = 3).

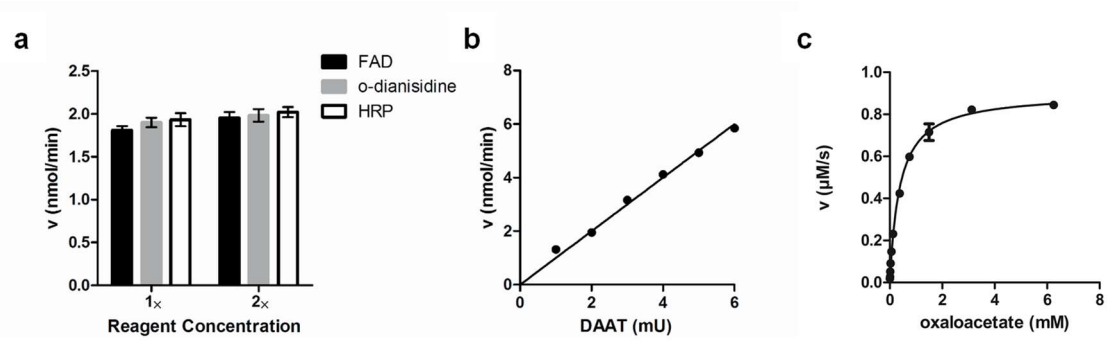

Figure S3.2 DDO coupled enzyme assay optimization. (a) Rates obtained for DAAT when the following reagent concentrations are doubled: FAD, 1 μM; *o*-dianisidine, 0.5 mM; HRP, 5 U. One unit (U) is the amount of enzyme that catalyzes the conversion of 1 μmol of substrate into product per minute. (b) Rates obtained when increasing amounts of DAAT are assayed under optimal conditions. (c) Rates obtained when increasing amounts of DAAT acceptor substrate are assayed under optimal conditions show the expected saturation at high concentrations. In all cases, mean ± s.d. is reported (n = 3).

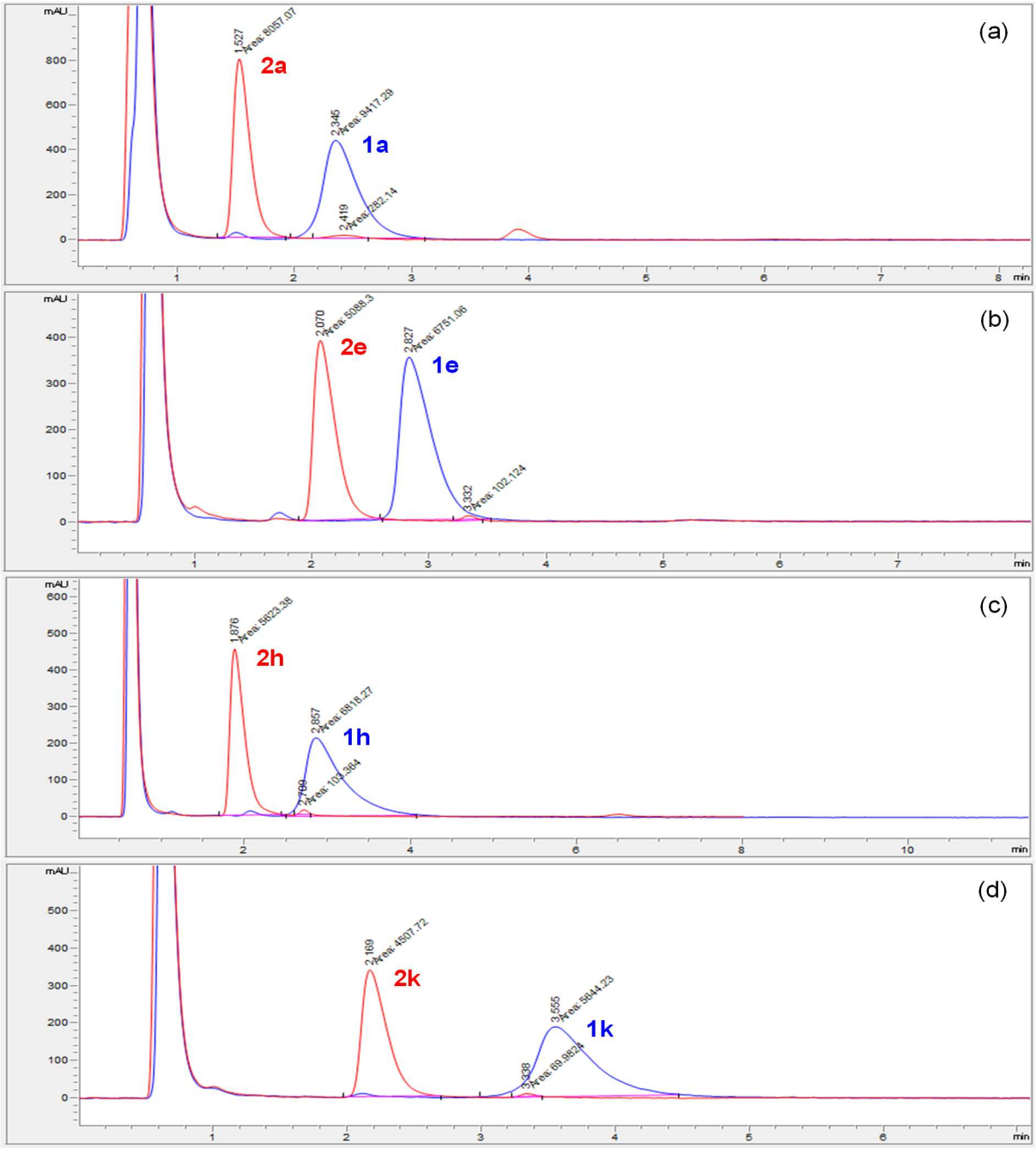

Figure S3.3 Representative HPLC traces (on a non-chiral stationary phase) for stereoinversion or deracemization with LAAD/DAAT-T242G. Biotransformation samples after 4 h (red traces) are compared with chemically synthesized standards of the corresponding arylpyruvic acids (blue traces). The chromatograms show the formation of negligible amounts of the arylpyruvic acids 1 during the biotransformations, giving an almost quantitative analytical yield of 2. (a) deracemization of *rac*-2a. (b) stereoinversion of L-2e. (c) deracemization of *rac*-2h. (d) stereoinversion of L-2k.

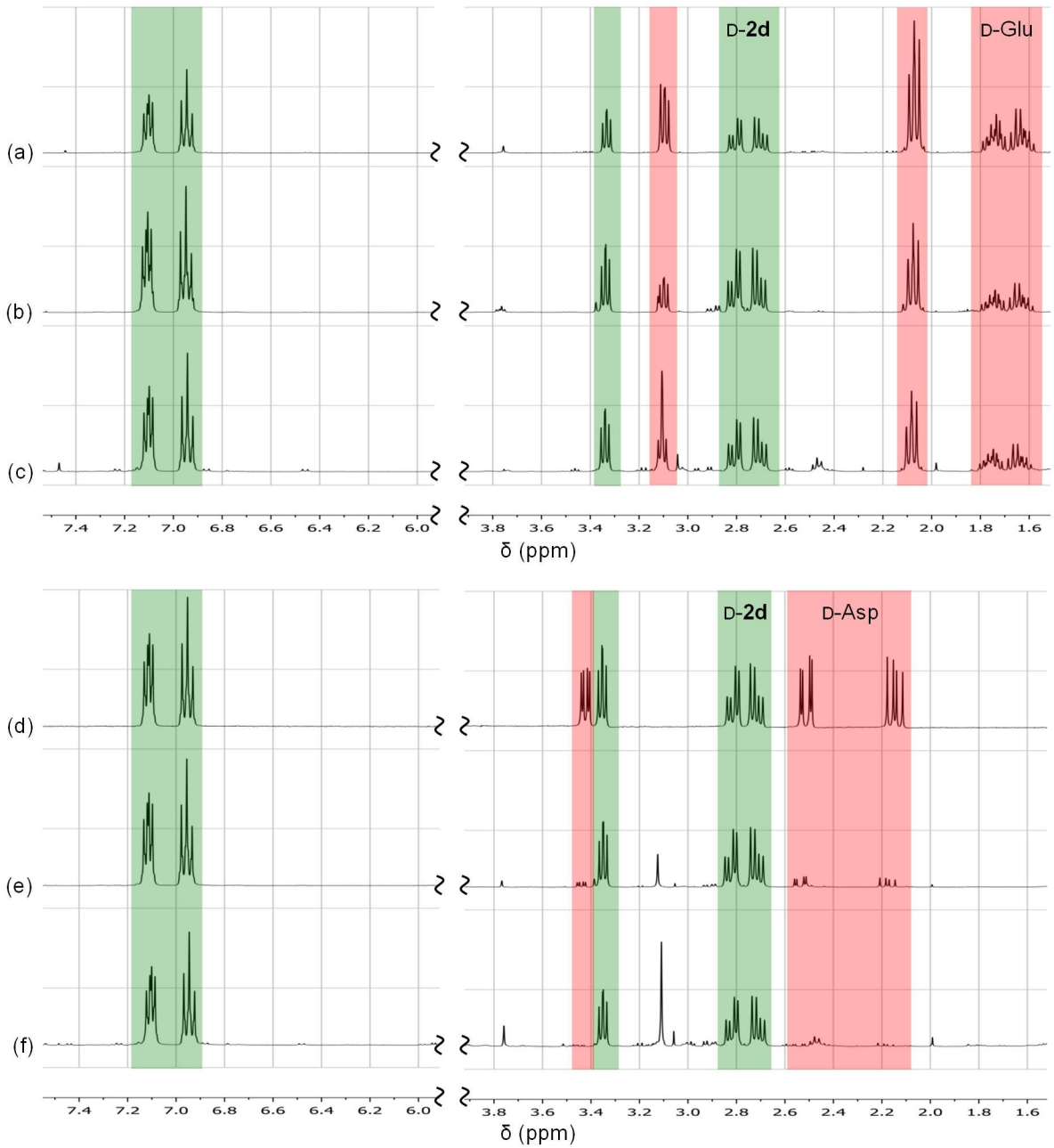

Figure S3.4 Removal of excess amine donor with DDO after deracemization of *rac*-2d with D-Glu or D-Asp as amine donors. Each trace shows the ^{1}H-NMR spectrum of ion-exchange purified D-2d (green) after deracemization with LAAD/DAAT-T242G with or without treatment with DDO, showing different amounts of unreacted D-Glu or D-Asp (red). (a) 3 equiv. D-Glu, no treatment with DDO. (b) 3 equiv. D-Glu, incubation with DDO (20 mg mL^{-1} wet cells, 24 h, 37 °C). (c) 3 equiv. D-Glu, incubation with DDO (80 mg mL^{-1} wet cells, 8 h, 37 °C). (d) 3 equiv. D-Asp, no treatment with DDO. (e) 3 equiv. D-Asp, incubation with DDO (20 mg mL^{-1} wet cells, 24 h, 37 °C). (f) 3 equiv. D-Asp, incubation with DDO (80 mg mL^{-1} wet cells, 8 h, 37°C).

3.7.2. Materials

All reagents used were of the highest available purity. Synthetic oligonucleotides were purchased from Eurofins MWG Operon. Restriction enzymes and DNA-modifying enzymes were purchased from New England Biolabs. HRP was purchased from Sigma-Aldrich. Ni-NTA agarose resin was purchased from Bio-Rad Laboratories. All aqueous solutions were prepared using water purified with a Barnstead Nanopure Diamond system.

3.7.3. Chemicals

Substrates and chemicals for activity assays: D-alanine (Sigma-Aldrich, >99%), D-valine (Sigma-Aldrich, >99%), D-leucine (Sigma-Aldrich, >99%), D-methionine (Sigma-Aldrich, >99%), D-serine (Sigma-Aldrich, >99%), D-threonine (Sigma-Aldrich, >99%), D-glutamine (Sigma-Aldrich, >99%), D-arginine (Sigma-Aldrich, >99%), D-lysine (Sigma-Aldrich, >99%), D-phenylalanine D-**2a** (Sigma-Aldrich, >97%), 2-methyl-D-phenylalanine D-**2i** (Alfa Aesar >94%), 3-methyl-D-phenylalanine D-**2j** (Alfa Aesar, >97%), 4-methyl-D-phenylalanine D-**2k** (Alfa Aesar, >97%), 3-methoxy-D-phenylalanine D-**2n** (Asta Tech, >96%), 4-methoxy-D-phenylalanine D-**2o** (Santa Cruz Biotechnology, >94%), 3-nitro-D-phenylalanine D-**2q** (Alfa Aesar, >94%), 4-nitro-D-phenylalanine D-**2r** (Sigma-Aldrich, >99%), oxaloacetate (Sigma-Aldrich, >96%), *o*-dianisidine (Sigma-Aldrich, >94%), FAD (Sigma-Aldrich, >94%), PLP (Acros Organics, 99%). Biotransformation substrates: DL-phenylalanine *rac*-**2a** (Sigma-Aldrich, >99%), 2-fluoro-DL-phenylalanine *rac*-**2b** (Alfa Aesar, >98%), 3-fluoro-DL-phenylalanine *rac*-**2c** (Alfa Aesar, >98%), 4-fluoro-DL-phenylalanine *rac*-**2d** (Alfa Aesar, >99%), 2-chloro-L-phenylalanine L-**2e** (Alfa Aesar, >98%), 3-chloro-L-phenylalanine L-**2f** (Alfa Aesar, >95%), 4-chloro-DL-phenylalanine *rac*-**2g** (Alfa Aesar, >98%), 4-bromo-DL-phenylalanine *rac*-**2h** (Sigma-Aldrich, >99%), 2-

methyl-DL-phenylalanine L-**2i** (Alfa Aesar, >97%), 3-methyl-DL-phenylalanine L-**2j** (Fluorochem, >98%), 4-methyl-L-phenylalanine L-**2k** (Fluorochem, >98%), 3-methoxy- L-phenylalanine L-**2n** (Fluorochem, >99%), D-aspartic acid (Sigma-Aldrich, >99%), D-glutamic acid (Sigma-Aldrich, >99%). Arylpyruvic acids were synthesized according to a previously published procedure.[7]

3.7.4. Cloning and mutagenesis

Codon-optimized (*E. coli*) and his-tagged genes for *Bacillus sp.* YM-1 DAAT (GenBank: J04460.1) and *Bos taurus* DDO (GenBank: CAA64622.1) were purchased from Integrated DNA Technologies and GenScript, respectively. These genes were subcloned into the pET-11a expression vector (Novagen) via the *Nde*I/*Bam*HI restriction sites, and the resulting plasmids were transformed into chemically-competent *E. coli* XL1-Blue cells (Stratagene). Mutations were introduced into the DAAT gene by overlap extension mutagenesis[33] using VentR DNA Polymerase. Briefly, external primers were used in combination with sets of complementary pairs of oligonucleotides containing the mutated codon in individual polymerase chain reactions (PCRs). The resulting overlapping fragments were gel-purified (Omega Biotek) and recombined by overlap extension PCR. The resulting amplicons were digested with *Nde*I/*Bam*HI, gel-purified, and ligated into pET-11a expression vector with T4 DNA ligase. Constructs were verified by sequencing the entire open reading frame, and were transformed into chemically-competent *E. coli* BL21-Gold(DE3) cells (Stratagene) for protein expression.

3.7.5. Protein expression and purification

Proteins were expressed in 1-L cultures (Luria-Bertani broth supplemented with 100 μM ampicillin) of *E. coli* BL21-Gold(DE3) cells transformed by a pET-11a vector containing his-tagged wild-type or mutant DAAT genes or the DDO gene. Upon reaching an optical density at 600 nm of 0.6 (37 °C, 250 rpm), the cultures were chilled to 15 °C and protein production was induced by the addition of isopropyl β-D-1-thiogalactopyranoside to a final concentration of 0.1 mM. Following overnight incubation with shaking at 15 °C, cells were harvested by centrifugation and lysed with an EmulsiFlex-B15 cell disruptor (Avestin). Proteins were then extracted and purified by immobilized metal affinity chromatography according to the manufacturer's protocol. Elution fractions containing the enzymes were desalted by gel filtration using EconoPAC 10DG columns (Bio-Rad) into a final buffer solution of 100 mM potassium phosphate buffer (pH 8.0). The protein yields ranged from 12–42 mg/L and the purity was determined to be ≥ 90%, as estimated by densitometry of Coomassie brilliant blue on an SDS-Page gel. Protein concentrations were quantified via a modified version of the Bradford assay, where the calibration curve is constructed as a plot of the ratio of the absorbance measurements at 590 and 450 nm versus concentration.[34]

3.7.6. D-amino acid screening assay

All assays were performed using the DDO coupled enzyme assay (Scheme S3.1) in triplicate 200-μL reactions at 37 °C in 100 mM potassium phosphate buffer (pH 8.0). Reaction conditions: 2 mU of purified wild-type or mutant DAAT, 10 mM D-amino acid donor, 5 mM oxaloacetate acceptor, 16 μM PLP, 25 mU purified DDO, 1 μM FAD, 0.5 mM *o*-dianisidine, and 5 U HRP. Negative controls containing all reaction components except DAAT were used. Solution mixtures were pre-incubated at 37 °C for 30 minutes

prior to initiating the reaction by the addition of DAAT. The enzymatic reaction was monitored as described above.

3.7.7. Kinetics assays

For steady-state kinetics of DAAT, reaction components were identical to the D-amino acid screening assay except for the following modifications: the concentration of the donor amino acid being kinetically characterized was varied and the amount of DDO was increased to 200 mU. For steady-state kinetics of DDO, reaction components were identical to DDO substrate specificity profile assay but with varying concentrations of the substrate being kinetically characterized. Non-linear regression analysis of the initial rates as a function of substrate concentration were fit to the Michaelis-Menten equation using the GraphPad Prism software.

3.7.8. DDO substrate specificity and pH profile

All assays were performed in triplicate 200-μL reactions at 37 °C in 100 mM potassium phosphate (pH 8.0) or 40 mM Britton-Robinson (pH 2–12)[35] buffer for substrate specificity or pH profiles, respectively. Reaction conditions: 2 mU DDO, 10 mM D-amino acid (Fig. S3.1), 1 μM FAD, 0.5 mM *o*-dianisidine, and 5 U HRP. One unit (U) is the amount of enzyme that catalyzes the conversion of 1 μmol of substrate into product per minute. Negative controls containing all reaction components except DDO were used. Solution mixtures were pre-incubated at 37 °C for 30 minutes prior to initiating the reaction by the addition of DDO. The enzymatic reaction was monitored by measuring the absorbance of the bisazobiphenyl species[36] produced by HRP-mediated oxidization of *o*-dianisidine (λ = 450 nm, ε = 11.3 mM^{-1} cm^{-1})[37] in 96-well plates (Greiner Bio-One) using an Infinite

M1000 plate reader (Tecan). The path length of each well was calculated using the difference in absorbance of water at 900 nm and 998 nm.

3.7.9. Synthesis of D-phenylalanine derivatives by transamination reactions

The suitable arylpyruvic acid **1a-r** (5 mM, added as 10 µL of a 500 mM solution in DMSO) and PLP (0.5 mM, added as 10 µL of a 50 mM solution in water) were added to potassium phosphate buffer (1 mL, 100 mM, pH 8.0) containing D-glutamic acid (20 mM). Wet whole *E. coli* cells producing DAAT-T242G (final conc. 20 mg mL^{-1}) were added, and the mixture was incubated at 37 °C for 12 h with vigorous shaking (180 rpm). Samples (300 µL) were taken at specified intervals, diluted with MeOH (300 µL), centrifuged to remove insoluble materials (13,000 rpm, 2 min) and transferred to a filter vial for HPLC analysis. A similar protocol was used for reactions with purified enzyme, with the exception that *E. coli* cells were replaced by 1 mg mL^{-1} of enzyme.

3.7.10. Synthesis of D-phenylalanine derivatives by stereoinversion/deracemization cascades

The suitable racemic or L-arylalanine **2a-r** (10 mM final concentration) was added to potassium phosphate buffer (5 mL, 100 mM, pH 8.0) containing the required amine donor (D-glutamic acid or D-aspartic acid, 30 mM). Wet E. coli cells producing LAAD (final conc. 20 mg mL^{-1}) and wet E. coli cells producing DAAT-T242G (final conc. 20 mg mL^{-1}) were added, and the mixture was incubated at 37 °C for 4 h with vigorous shaking (180 rpm). Samples (300 µL) were taken at specified intervals, diluted with MeOH (300 µL), centrifuged to remove insoluble materials (13,000 rpm, 2 min) and transferred to a filter vial for HPLC analysis.

3.7.11. Representative preparative scale synthesis of D-2d

Racemic 4-fluorophenylalanine *rac*-**2d** (91.6 mg, 0.5 mmol) and D-aspartic acid (99.8 mg, 0.75 mmol, 1.5 equiv. with respect to the L-enantiomer of 4-fluorophenylalanine) were dissolved in potassium phosphate buffer (40 mL, 100 mM, pH 8.0). Wet *E. coli* cells producing LAAD (final conc. 50 mg mL^{-1}) and wet *E. coli* cells producing DAAT-T242G (final conc. 50 mg mL^{-1}) were added, and the mixture was incubated at 37 °C for 12 h with vigorous shaking (180 rpm). Complete deracemization was confirmed by HPLC. The suspension was heat-treated to inactivate the enzymes (95 °C, 5 min) then centrifuged to remove insoluble materials (4000 rpm, 10 min). In order to remove unreacted D-aspartic acid, wet cells producing DDO (final conc. 80 mg mL^{-1}) were added to the supernatant, and the mixture was incubated at 37 °C for 8 h with vigorous shaking (180 rpm). After acidification to pH < 2.0 by addition of aqueous H_2SO_4 (10% w/v), the suspension was centrifuged (4000 rpm, 10 min). Dowex 50WX8 hydrogen form (2.0 g) was washed with deionized water (30 mL) and aqueous H_2SO_4 (20 mL, 10% w/v). The acidified supernatant from the biotransformation was loaded onto the resin (1 mL min^{-1}). The resin was washed repeatedly with deionized water (until pH ~7.0), then the product was eluted with aqueous NH_4OH (30 mL, 10% w/v). Fractions containing the product were pooled and evaporated in a centrifugal evaporator, to afford amino acid D-**2d** as a white solid (76.9 mg, 84% isolated yield, 99% ee). NMR data are consistent with previously reported values.[7]

3.7.12. HPLC methods and representative traces

Conversions (for transamination reactions) were measured by HPLC on a non-chiral reverse-phase Zorbax Extend C18 column (50 mm × 4.6 mm × 3.5 μm, Agilent), flow rate 1.0 mL min^{-1}, temperature 40 °C, detection wavelength 210 nm, mobile phase aq. NH_4OH

0.1 M pH 10.0 / MeOH (ratio specified in the following table). Enantiomeric excess values of the phenylalanine products were measured on a reverse-phase Crownpak CR(+) column (150 mm × 4 mm × 3.5 μm, Daicel). Flow rate 1.0 mL min^{-1}, temperature 25 °C, detection wavelength 210 nm, mobile phase: aq. $HClO_4$ 1.14% w/v / MeOH (ratio specified in the following tables).

Table S3.3 Retention times for non-chiral HPLC analyses.

	R	MeOH [%]	t_R (amino acid 2) [min]	t_R (keto acid 1) [min]
a	H	10	2.7	4.4
d	4-F	10	3.3	5.9
e	2-Cl	20	2.3	3.0
h	4-Br	20	4.2	7.0
i	2-Me	20	2.2	3.0
k	4-Me	20	2.4	3.7
l	4-Et	20	6.4	10.5
m	2-MeO	10	6.3	9.2
o	4-MeO	10	4.1	8.4
p	3,4-OCH_2O	10	3.5	6.6

Table S3.4 Retention times for chiral HPLC analyses.

	R	MeOH [%]	t_R (D-2) [min]	t_R (L-2) [min]
a	H	4	5.6	7.4
b	2-F	4	6.2	8.4
c	3-F	4	6.8	9.1
d	4-F	4	7.2	9.0
e	2-Cl	14	8.5	10.9
f	3-Cl	14	11.4	17.4
g	4-Cl	14	11.8	15.3
h	4-Br	14	17.0	22.2
i	2-Me	14	7.2	9.2
j	3-Me	14	8.5	12.3
k	4-Me	14	8.6	12.0
n	3-MeO	4	10.5	14.5

3.7.13. Representative HPLC traces

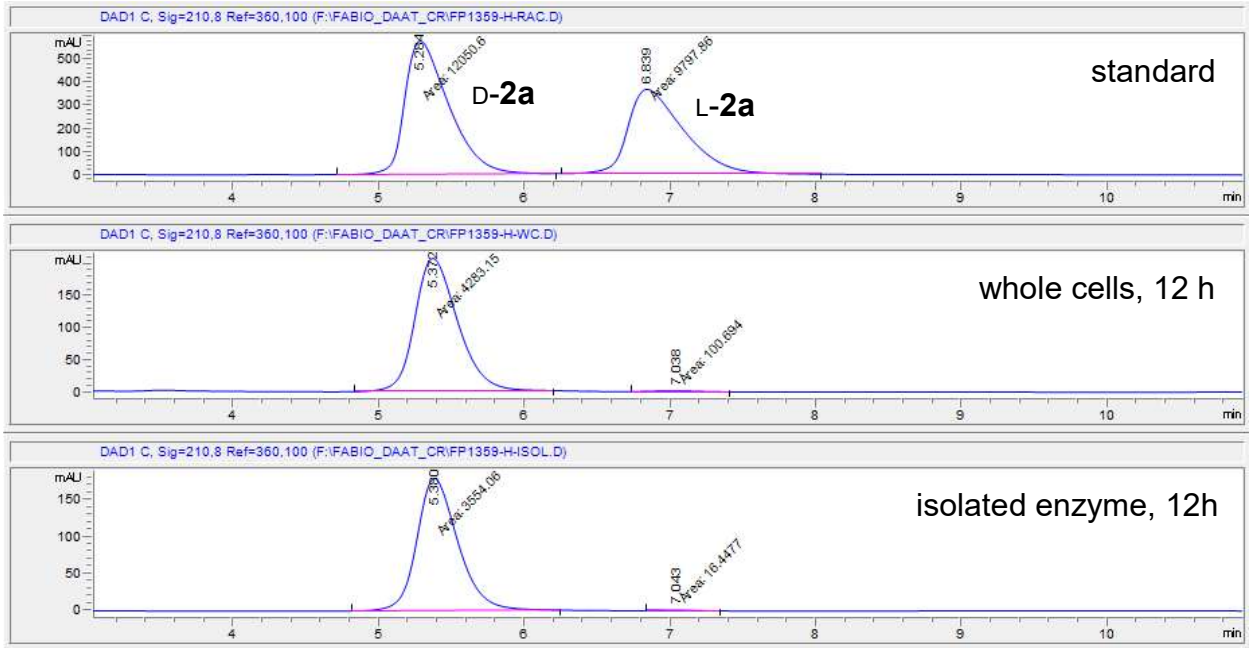

Figure S3.5 Transamination of 1a with DAAT-T242G.

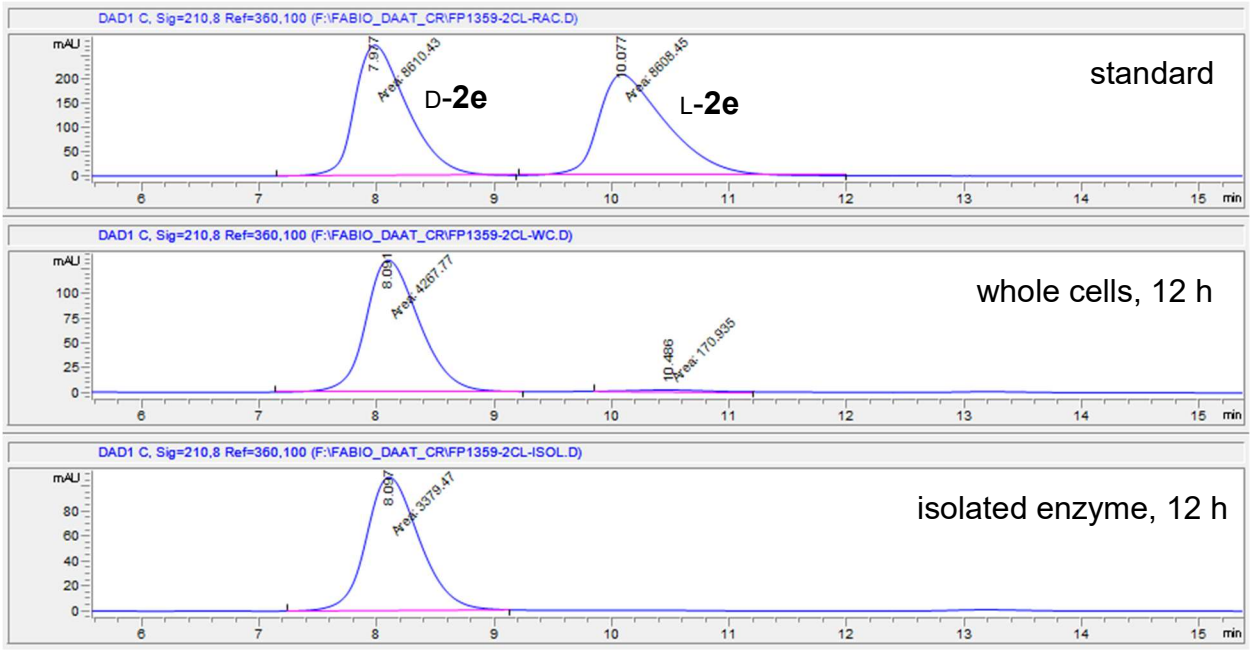

Figure S3.6 Transamination of 1e with DAAT-T242G.

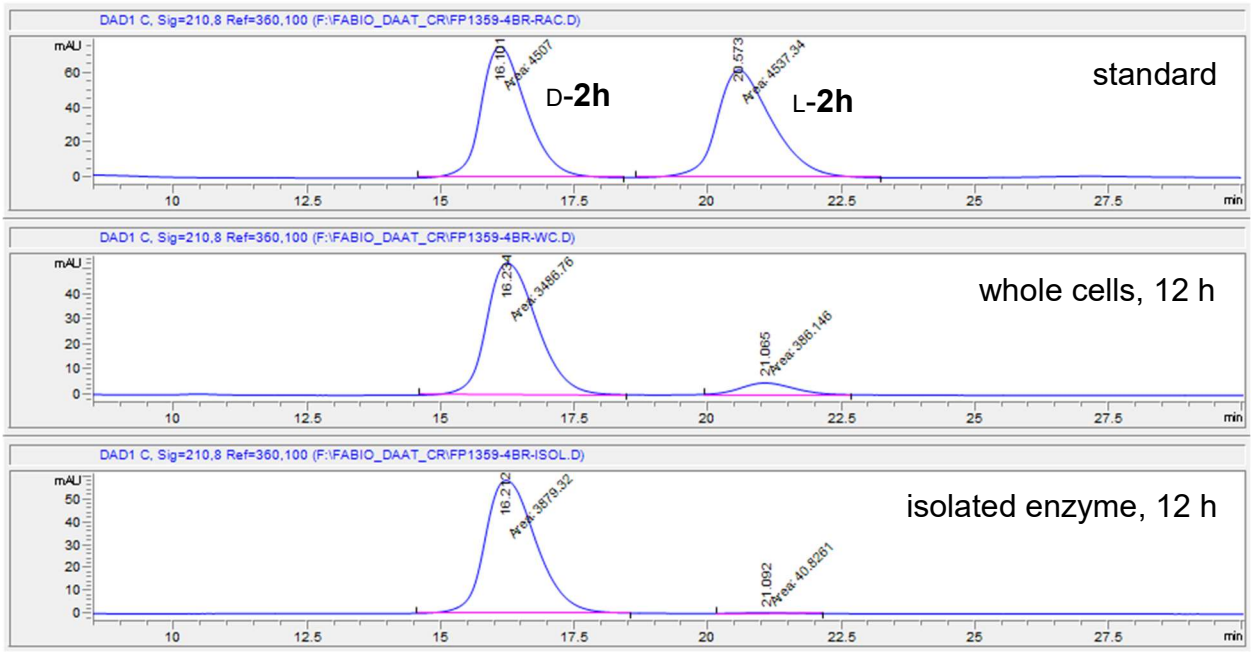

Figure S3.7 Transamination of 1h with DAAT-T242G.

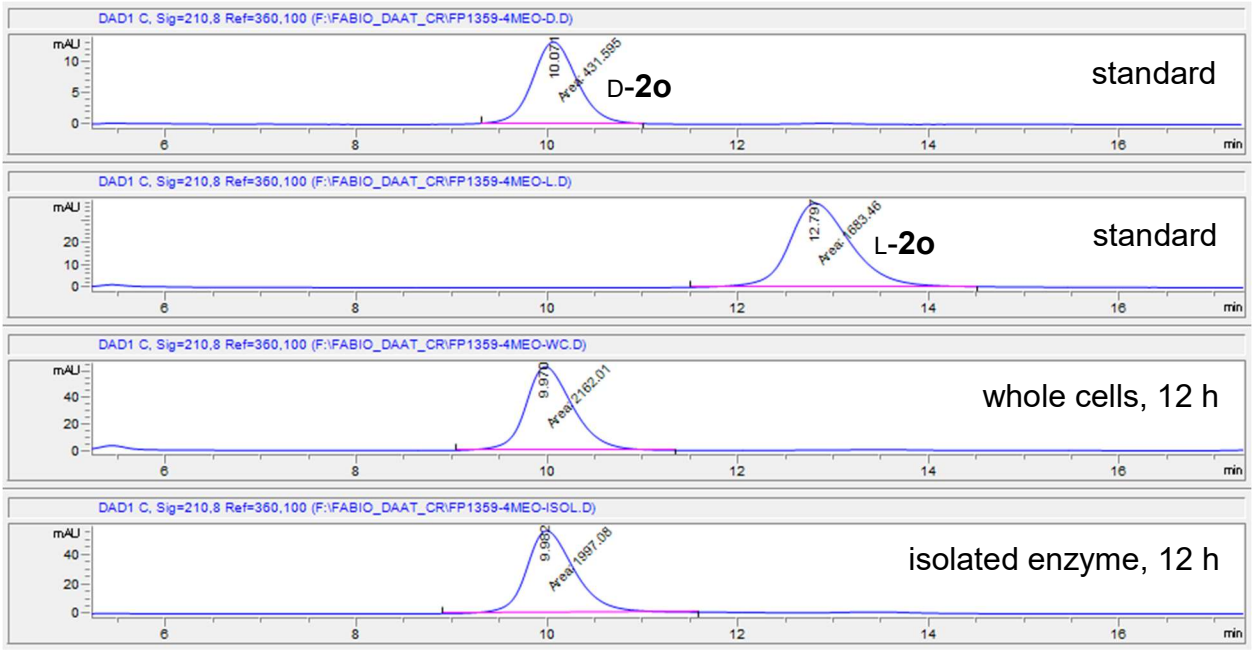

Figure S3.8 Transamination of 1o with DAAT-T242G.

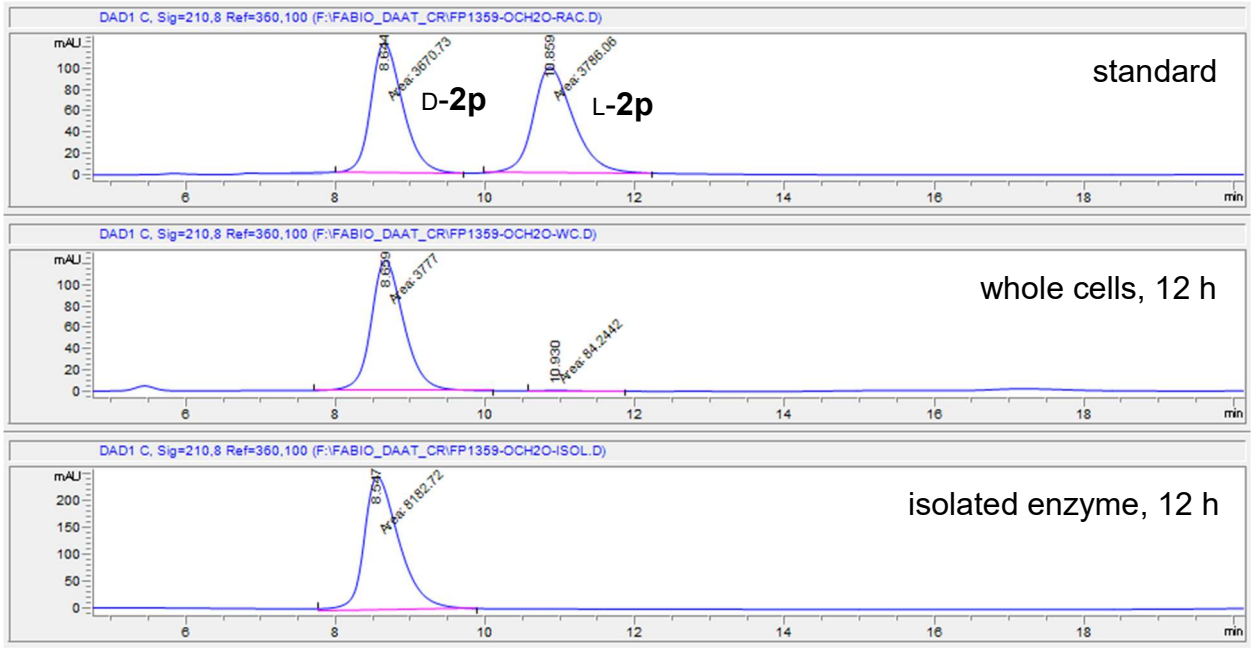

Figure S3.9 Transamination of 1p with DAAT-T242G.

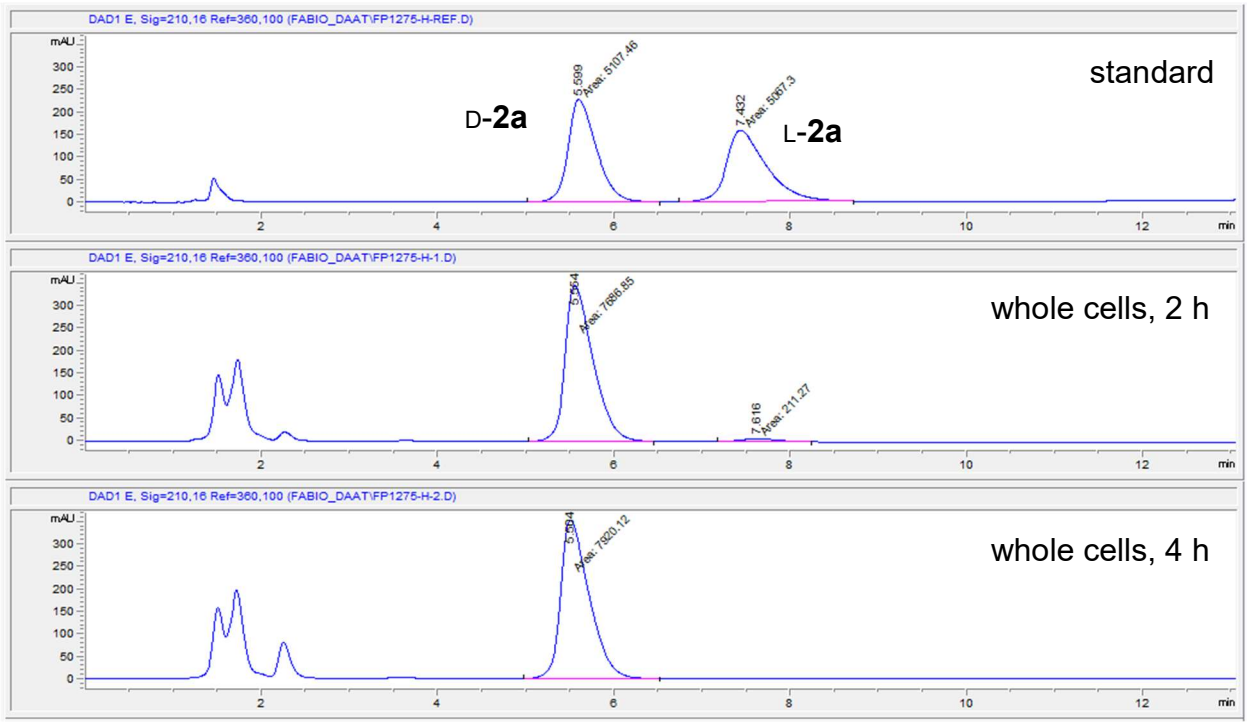

Figure S3.10 Deracemization of DL-2a with LAAD/DAAT-T242G.

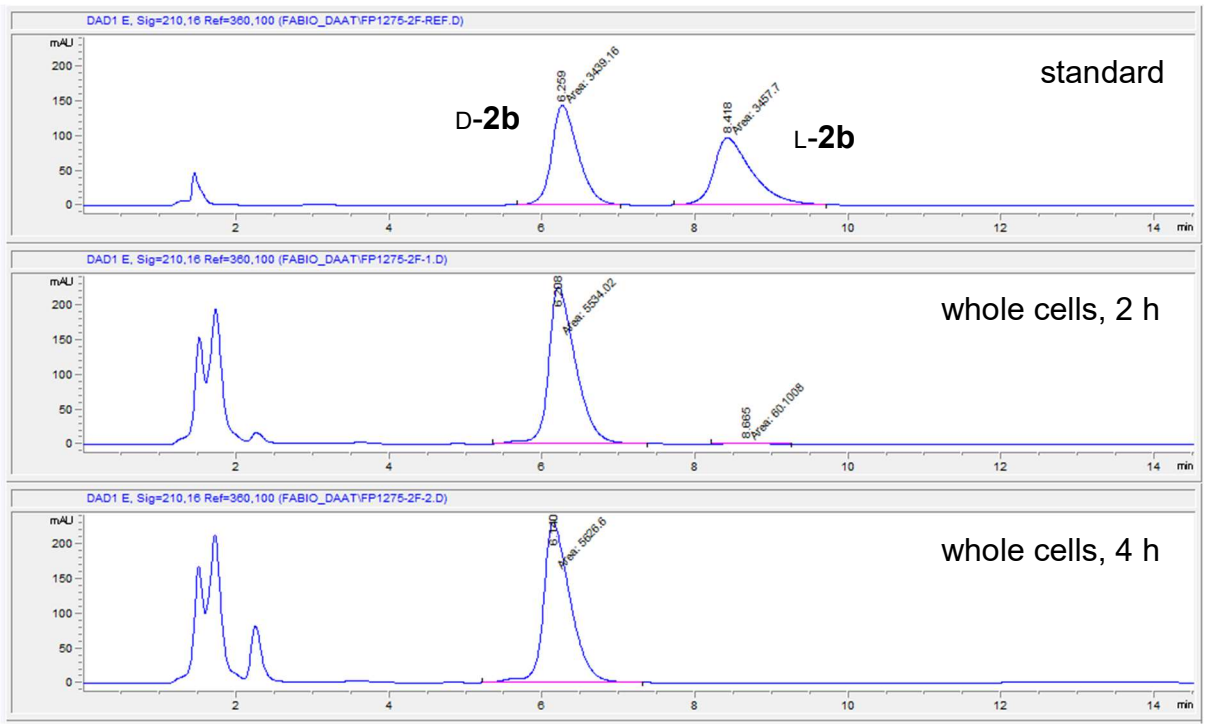

Figure S3.11 Deracemization of DL-2b with LAAD/DAAT-T242G.

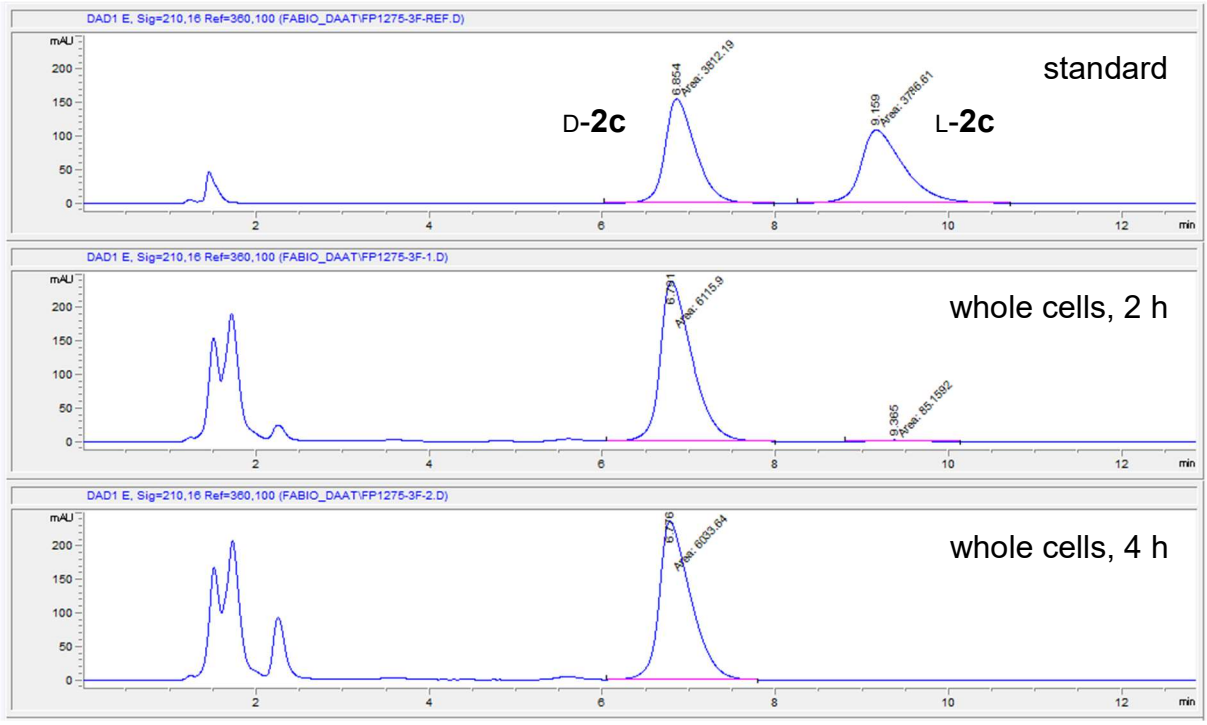

Figure S3.12 Deracemization of DL-2c with LAAD/DAAT-T242G.

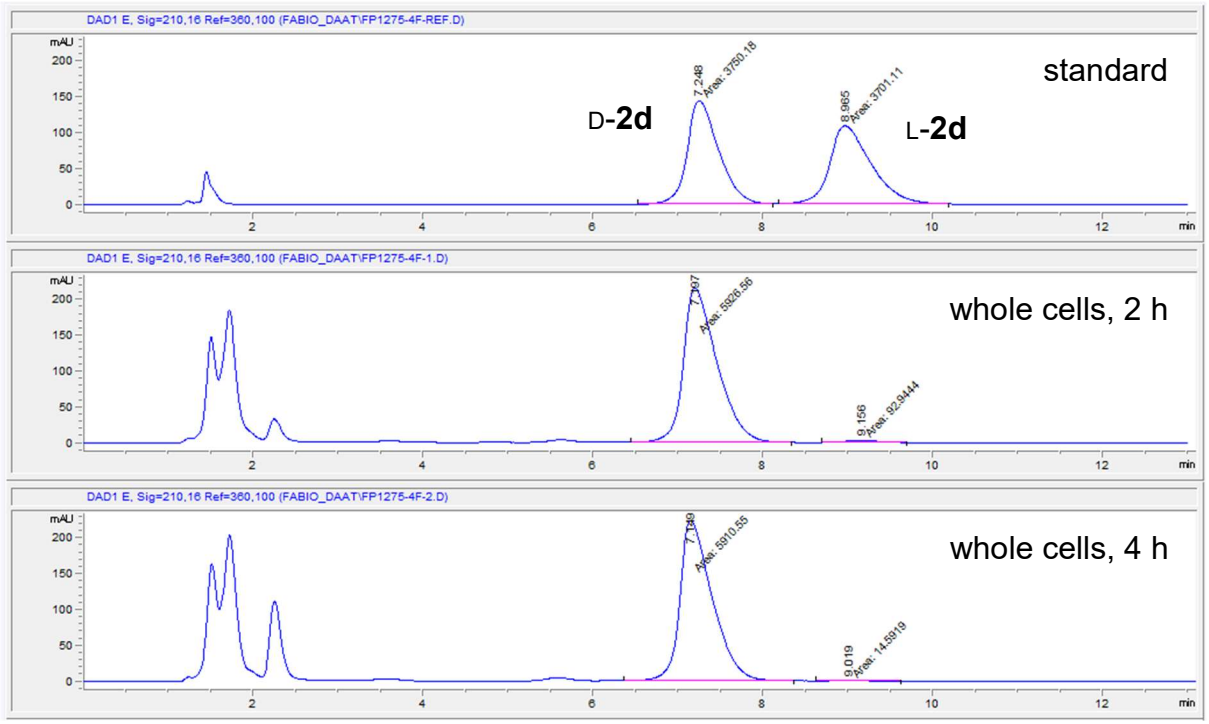

Figure S3.13 Deracemization of DL-2d with LAAD/DAAT-T242G.

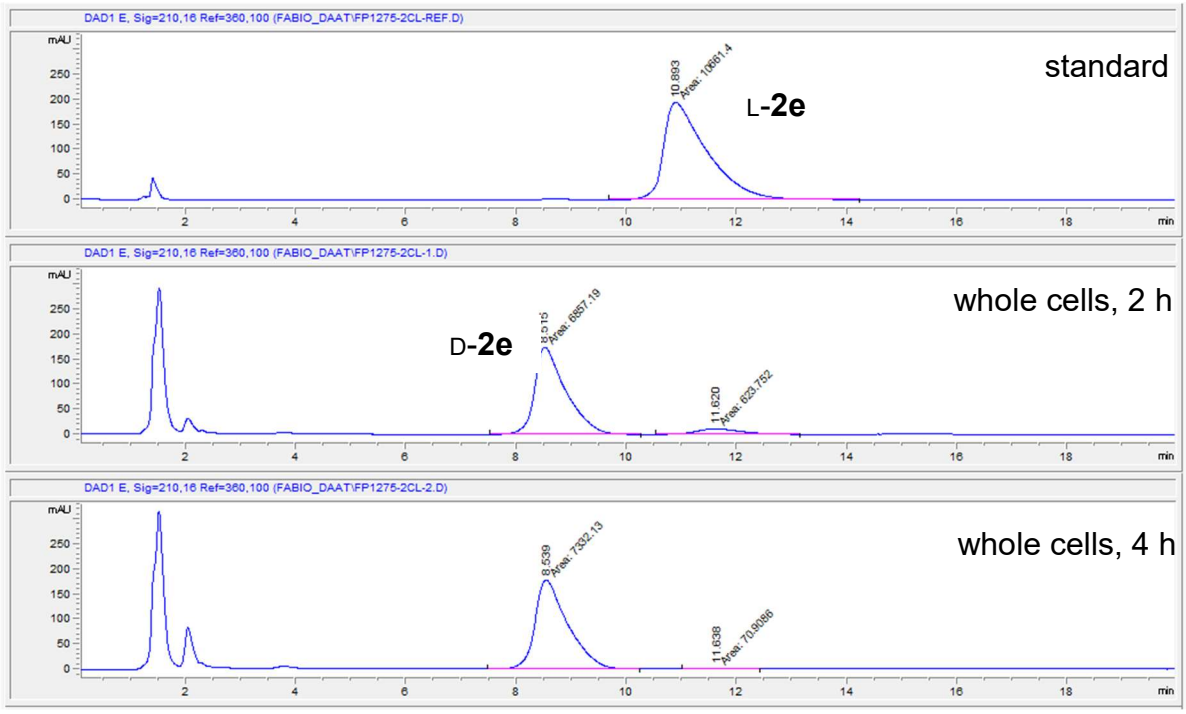

Figure S3.14 Stereoinversion of L-2e with LAAD/DAAT-T242G.

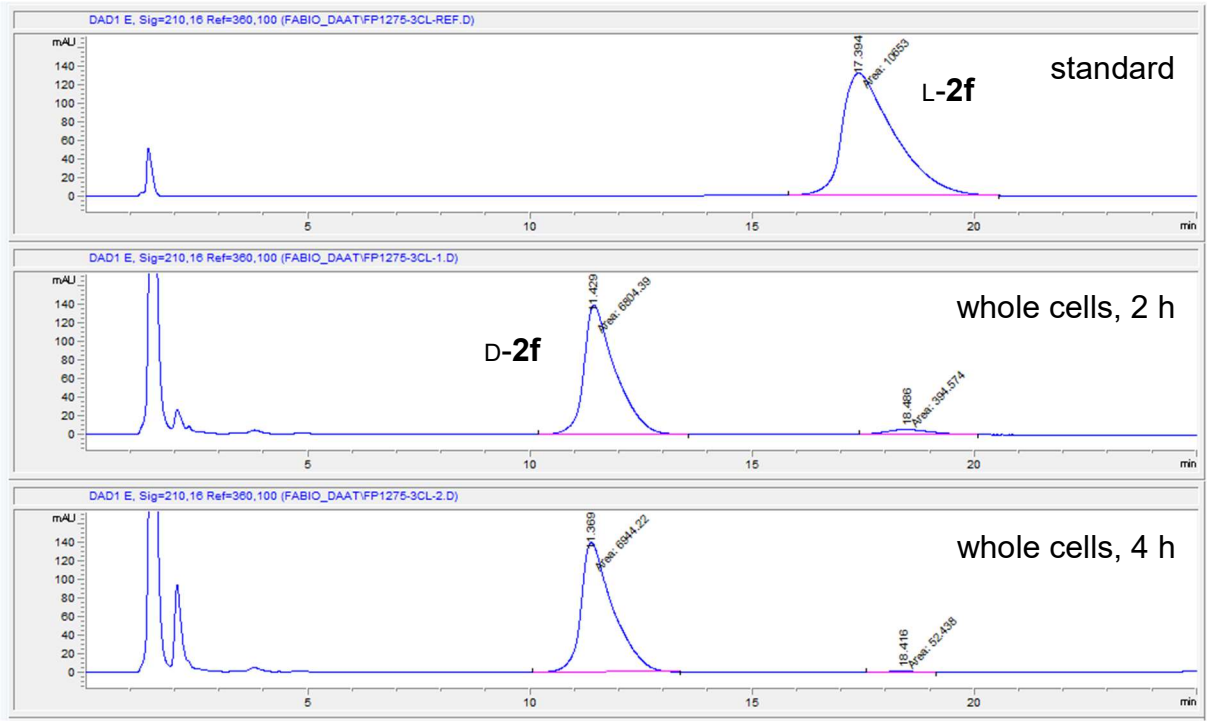

Figure S3.15 Stereoinversion of L-2f with LAAD/DAAT-T242G.

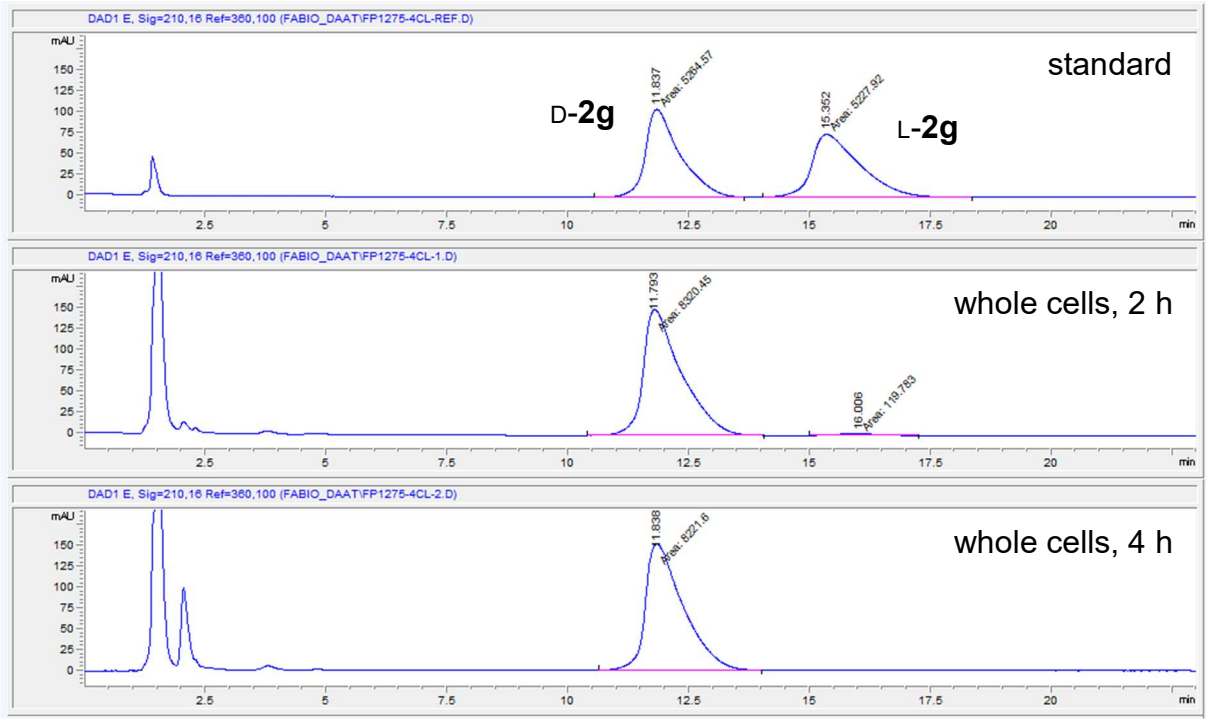

Figure S3.16 Deracemization of DL-2g with LAAD/DAAT-T242G.

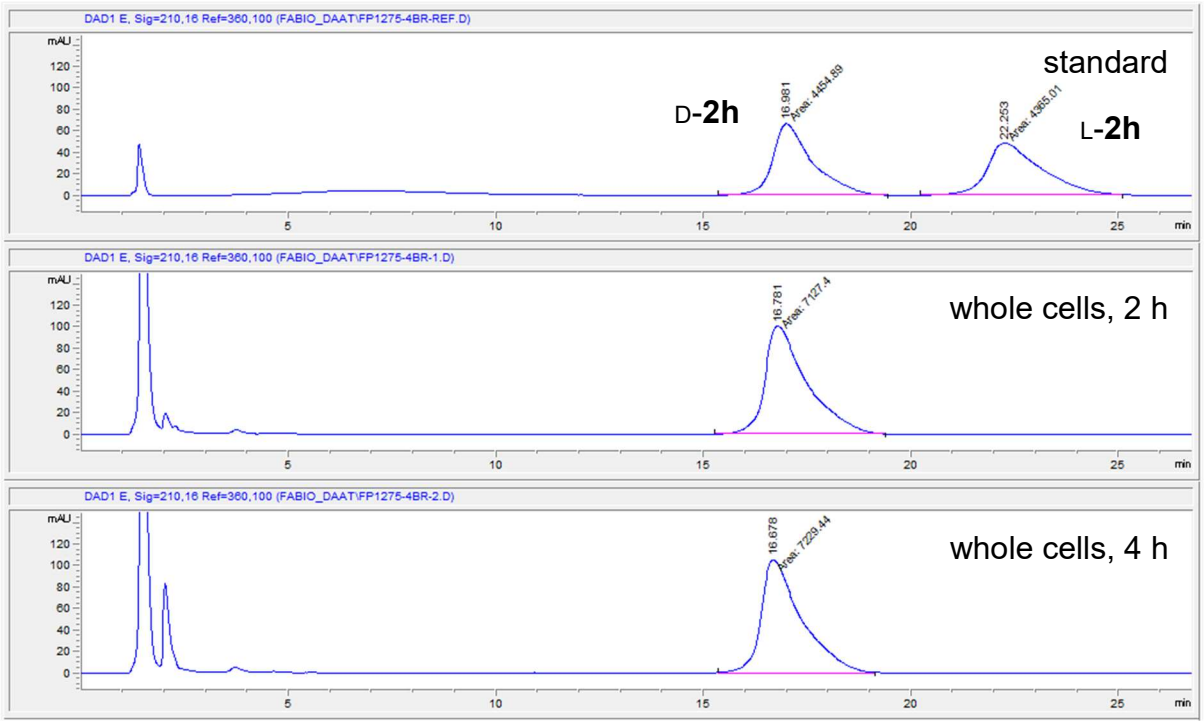

Figure S3.17 Deracemization of DL-2h with LAAD/DAAT-T242G.

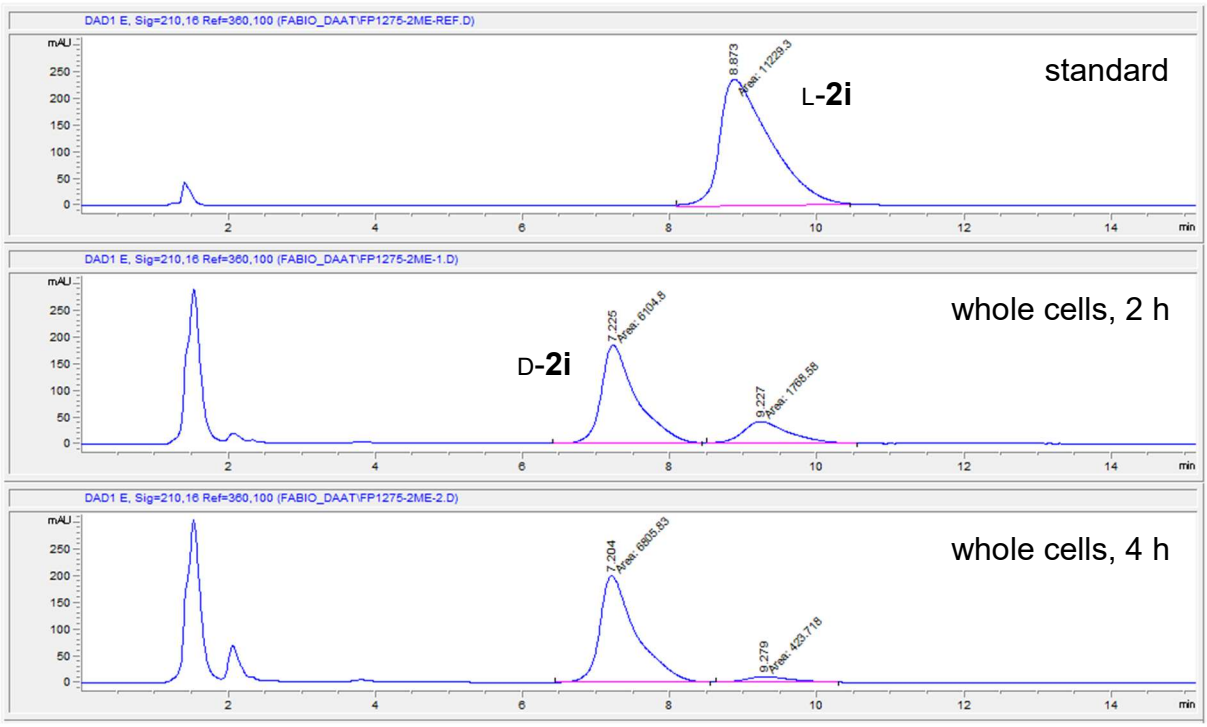

Figure S3.18 Stereoinversion of L-2i with LAAD/DAAT-T242G.

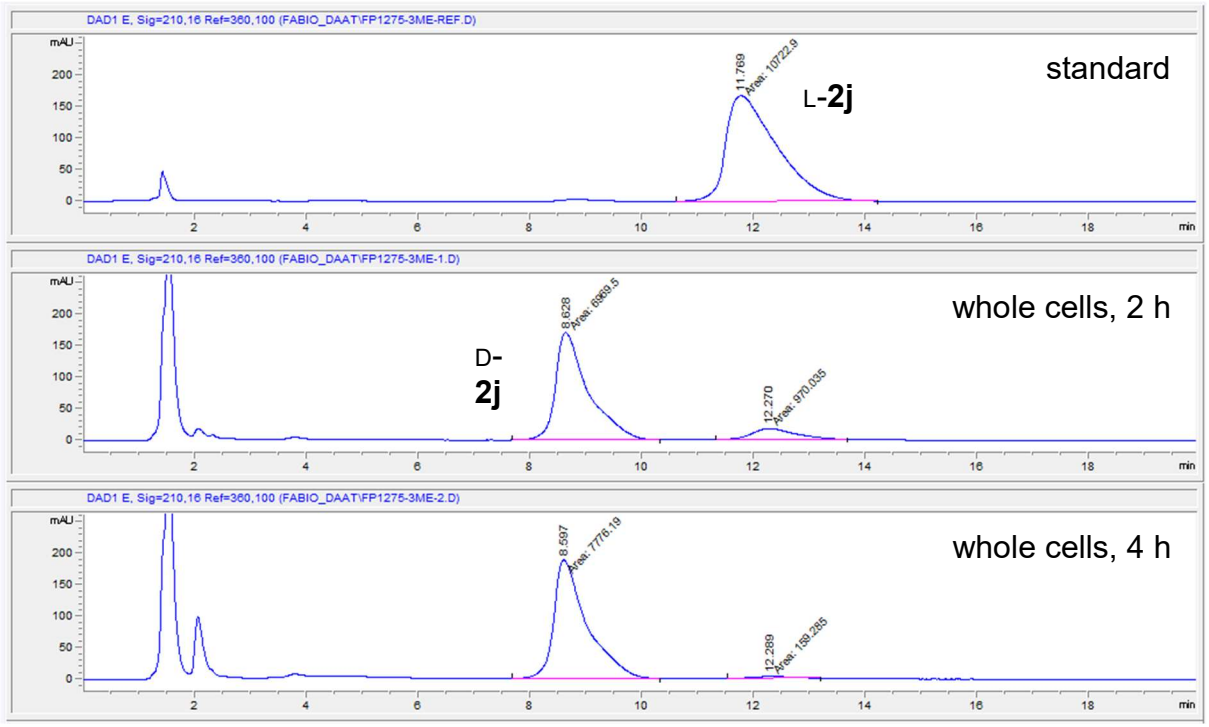

Figure S3.19 Stereoinversion of L-2j with LAAD/DAAT-T242G.

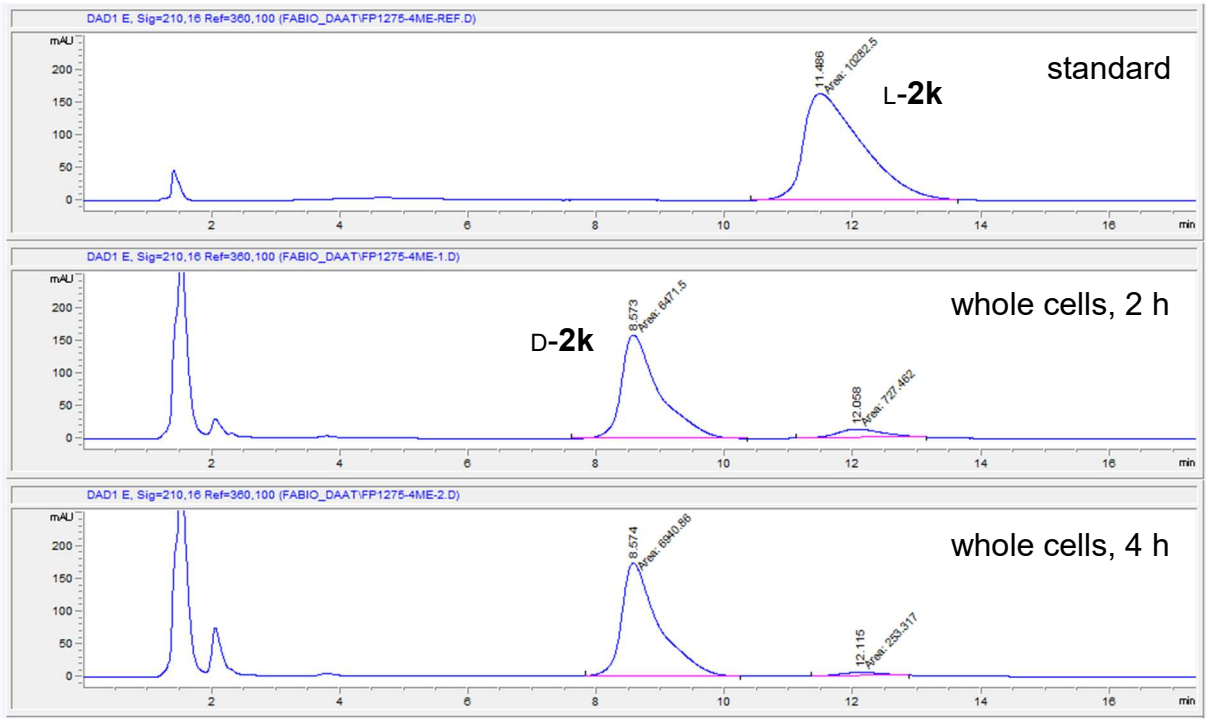

Figure S3.20 Stereoinversion of L-2k with LAAD/DAAT-T242G.

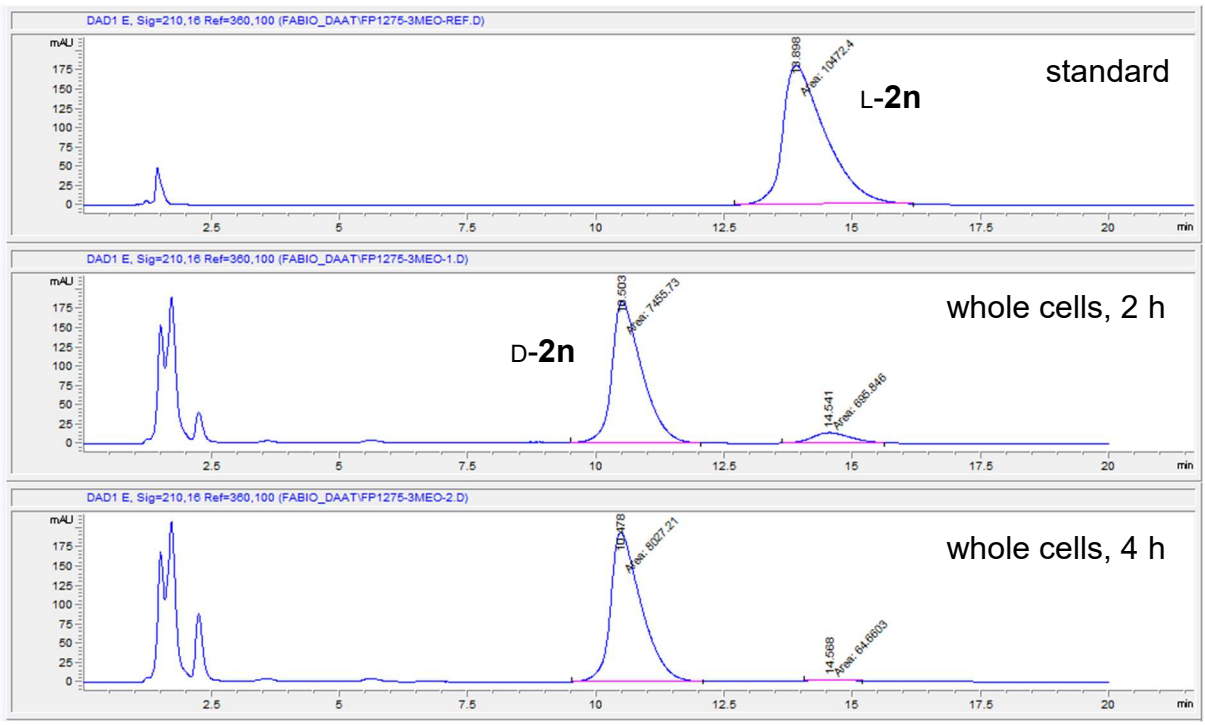

Figure S3.21 Stereoinversion of L-2n with LAAD/DAAT-T242G.

3.8. References

(1) Miyao, K. *Bull. Agric. Chem. Soc. Japan* **1960**, *24* (1), 23–30.
(2) Tentolouris, N.; Voulgari, C.; Katsilambros, N. *Vasc. Health Risk Manag.* **2007**, *3* (6), 797–807.
(3) Kovacs, M. *Proc. Natl. Acad. Sci.* **2001**, *98* (4), 1829–1834.
(4) Wang, J.; Liu, X.; Feng, X. *Chem. Rev.* **2011**, *111* (11), 6947–6983.
(5) Fotheringham, I. G.; Taylor, P. P.; Ton, J. L. Preparation of d-amino acids by direct fermentative means, 1998.
(6) Parmeggiani, F.; Lovelock, S. L.; Weise, N. J.; Ahmed, S. T.; Turner, N. J. *Angew. Chemie - Int. Ed.* **2015**, *54* (15), 4608–4611.
(7) Parmeggiani, F.; Ahmed, S. T.; Thompson, M. P.; Weise, N. J.; Galman, J. L.; Gahloth, D.; Dunstan, M. S.; Leys, D.; Turner, N. J. *Adv. Synth. Catal.* **2016**, *358* (20), 3298–3306.
(8) Schrittwieser, J. H.; Velikogne, S.; Hall, M.; Kroutil, W. *Chem. Rev.* **2018**, *118* (1), 270–348.
(9) France, S. P.; Hepworth, L. J.; Turner, N. J.; Flitsch, S. L. *ACS Catal.* **2017**, *7* (1), 710–724.
(10) Santacoloma, P. A.; Sin, G.; Gernaey, K. V; Woodley, J. M. *Org. Process Res. Dev.* **2011**, *15* (1), 203–212.
(11) Ricca, E.; Brucher, B.; Schrittwieser, J. H. *Adv. Synth. Catal.* **2011**, *353* (13), 2239–2262.
(12) Oberleitner, N.; Peters, C.; Muschiol, J.; Kadow, M.; Saß, S.; Bayer, T.; Schaaf, P.; Iqbal, N.; Rudroff, F.; Mihovilovic, M. D.; others. *ChemCatChem* **2013**, *5* (12),

3524–3528.
(13) Liu, R. X.; Liu, S. P.; Cheng, S.; Zhang, L.; Ding, Z. Y.; Gu, Z. H.; Shi, G. Y. *Appl. Biochem. Microbiol.* **2015**, *51* (6), 695–703.
(14) Yonaha, K.; Misono, H.; Yamamoto, T.; Soda, K. *J. Biol. Chem.* **1975**, *250* (17), 6983–6989.
(15) Kobayashi, J.; Shimizu, Y.; Mutaguchi, Y.; Doi, K.; Ohshima, T. *J. Mol. Catal. B Enzym.* **2013**, *94*, 15–22.
(16) Khorsand, F.; Murphy, C. D.; Whitehead, A. J.; Engel, P. C. *Green Chem.* **2017**, *19* (2), 503–510.
(17) Tanizawa, K.; Asano, S.; Masu, Y.; Kuramitsu, S.; Kagamiyama, H.; Tanaka, H.; Soda, K. *J. Biol. Chem.* **1989**, *264* (5), 2450–2454.
(18) Tanizawa, K.; Masus, Y.; Asano, S.; Tanaka, H.; Sodas, K. *J. Biol. Chem.* **1989**, *264* (5), 2445–2449.
(19) Fuchikami, Y.; Yoshimura, T.; Gutierrez, A.; Esaki, N.; Soda, K.; Esaki, N. *J. Biochem.* **1998**, *124* (5), 905–910.
(20) Peisach, D.; Chipman, D. M.; Van Ophem, P. W.; Manning, J. M.; Ringe, D. *Biochemistry* **1998**, *37* (14), 4958–4967.
(21) Barber, J. E. B.; Damry, A. M.; Calderini, G. F.; Walton, C. J. W.; Chica, R. A. *Anal. Biochem.* **2014**, *463*, 23–30.
(22) Simonic, T.; Stefano, D.; Negri, A.; Tedeschi, G.; Malcovati, M.; Tenchini, M. L.; Ronchi, S. *Biochem. J.* **1997**, *322* (3), 729–735.
(23) Negri, A.; Tedeschi, G.; Ceciliani, F.; Ronchi, S. *Biochim. Biophys. Acta (BBA)-Protein Struct. Mol. Enzymol.* **1999**, *1431* (1), 212–222.
(24) Massad, G.; Zhao, H.; Mobley, H. L. *J. Bacteriol.* **1995**, *177* (20), 5878–5883.
(25) Tian, X.; Switzer, A. G.; Derose, S. A.; Mishra, R. K.; Solinsky, M. G.; Mumin, R. N.; Ebetino, F. H.; Jayasinghe, L. R.; Webster, M. E.; Colson, A.-O.; others. *J. Med. Chem.* **2008**, *51* (19), 6055–6066.
(26) Gutierrez, a; Yoshimura, T.; Fuchikami, Y.; Soda, K.; Esaki, N. *Protein Eng.* **1998**, *11* (1), 53–58.
(27) Ahn, J.-W.; Chang, J. H.; Kim, K.-J. *FEBS Lett.* **2015**, *589* (24), 3842–3847.
(28) Washio, T.; Kato, S.; Oikawa, T. *Extremophiles* **2016**, *20* (5), 711–721.
(29) Motta, P.; Molla, G.; Pollegioni, L.; Nardini, M. *J. Biol. Chem.* **2016**, *291* (20), 10457–10475.
(30) Taylor, P. P.; Pantaleone, D. P.; Senkpeil, R. F.; Fotheringham, I. G. *Trends Biotechnol.* **1998**, *16* (10), 412–418.
(31) Bommarius, A. S.; Schwarm, M.; Drauz, K. *Chim. Int. J. Chem.* **2001**, *55* (1–2), 50–59.
(32) Kishimoto, K.; Yoshimura, T.; Soda, K.; Esaki, N. *J. Biochem.* **1997**, *122* (6), 1182–1189.
(33) Heckman, K. L.; Pease, L. R. *Nat. Protoc.* **2007**, *2* (4), 924–932.
(34) Ernst, O.; Zor, T. *J. Vis. Exp.* **2010**, No. 38, 1–6.
(35) Wybenga, G. G.; Crismaru, C. G.; Janssen, D. B.; Dijkstra, B. W. *J. Biol. Chem.* **2012**, *287* (34), 28495–28502.
(36) Moller, K. M.; Ottolenghi, P. *C. R. Trav. Lab. Carlsberg* **1966**, *35* (16), 369–389.
(37) Keyhani, E.; Zarei, M. A.; Lashgarblooki-Livani, T. *FEBS Lett.* **1999**, *452* (3), 233–236.

Chapter 4.
Structural and kinetic analysis of the stereo-inverting D-phenylglycine aminotransferase from *Pseudomonas stutzeri*

4.1. Preface

In this chapter, a PLP-dependent aminotransferase with a rare stereo-inverting activity is investigated because it may hold biocatalytic potential for the synthesis of non-canonical D-amino acids from prochiral keto acids and inexpensive L-glutamate. A crystal structure of the apo enzyme is solved and compared to structurally similar enzymes to identify active site residues. This enabled the development of a binding hypothesis for how the aminotransferase enzyme achieves the L- to D- stereo-inversion to produce D-phenylglycine. Finally, we kinetically characterize the wild-type enzyme and three mutants, which provides evidence for our binding hypothesis and helps identify residues amenable to substitution in the O-pocket that may alter the enzyme's substrate specificity for alternate D-amino acids.

4.2. Contribution Statement

The contributions of all authors are outlined below:

Conception:

The initial concept of this article was conceived by Dr. Roberto A. Chica. Curtis J.W. Walton and Dr. Roberto A. Chica collaborated on the project's direction, experimental design, and analysis of key results.

Writing:

The manuscript for this article was written by Curtis J.W. Walton and Dr. Roberto A. Chica.

Experimental:

The experiments presented in this article were performed by Curtis J.W. Walton, Dr. Frédéric Thiebaut, and Dr. Jean-François Couture. The DPAT mutants were prepared by Dr. Frédéric Thiebaut and Curtis J.W. Walton. The crystallization experiments and harvestings of protein crystals were performed by Curtis J.W. Walton. The crystal structure was solved by Dr. Jean-François Couture. The screening and kinetic characterizations with wild-type and mutant DPAT enzymes were performed by Curtis J.W. Walton.

4.3. Introduction

D-amino acids are important building blocks in the synthesis of many pharmaceuticals[1] and bioactive peptides[2] used for the treatment of microbial infections[3], hypertension[4], and cancer.[5] The production of optically pure D-amino acids by chemoenzymatic and biocatalytic strategies offer significant advantages compared to chemical syntheses.[6,7] Biocatalytic cascades performed with whole bacterial cells are particularly useful for the asymmetric synthesis of amino acids as they increase process efficiency by catalyzing multiple steps in one-pot reactions without requiring intermediate work-ups, cofactor recycling, or toxic metals.[8] We recently developed a biocatalytic cascade to produce unnatural aromatic D-amino acids that couples L-amino acid deaminase (LAAD) with a D-amino acid aminotransferase (DAAT) variant that we engineered to display high activity towards D-phenylalanine.[9] Although this method enables the synthesis of various D-phenylalanine derivatives with high conversion rates and enantiomeric excesses, it requires a sacrificial D-amino acid donor substrate to produce the desired D-amino acid product because of the strict stereospecificity of DAAT.[10,11] To increase the efficiency of our

LAAD/DAAT biocatalytic cascade, a biocatalyst capable of performing a stereo-inverting transamination reaction to produce a desired D-amino acid product from an inexpensive and abundant L-amino acid sacrificial amine donor is highly desirable.

D-phenylglycine aminotransferase (DPAT) from *Pseudomonas stutzeri* ST-201 and *Pseudomonas putida* are, to our knowledge, the only presently known L to D stereo-inverting ATs (E.C. 2.6.1.72).[12] DPAT catalyzes the reversible transamination of benzoylformate or *p*-hydroxybenzoylformate with L-glutamate (L-Glu), which yields α-ketoglutarate (α-kg) and D-phenylglycine (D-Phg) or D-4-hydroxyphenylglycine (Figure 4.1). Although DPAT has been used in several biocatalytic applications,[13,14] the mechanism by which it can catalyze its stereo-inverting transamination reaction is unknown. In addition, no detailed structural analysis has been published on the enzyme, although a partial crystal structure has been deposited in the Protein Data Bank (PDB ID: 2CY8).[15] However, the deposited structure contains eight unexplained amino acid substitutions that deviate from the Genbank sequence (Protein ID: AAQ82900.1).

To gain a better understanding of the structural determinants of its stereo-inverting activity, the identity of DPAT's substrate binding residues and their interactions with donor and acceptor substrates are necessary. Herein, we report the crystal structure of *Pseudomonas stutzeri* ST-201 DPAT, which we used to identify active-site residues involved in substrate specificity. Saturation mutagenesis of these residues coupled to kinetic characterization of active mutants with several donor substrates enabled us to propose a model for the dual L/D specificity of DPAT. The results presented here open the door to the engineering of

Pseudomonas stutzeri ST-201 DPAT in order to produce variants capable of synthesizing a variety of valuable D-amino acids from inexpensive and abundant L-amino acids.

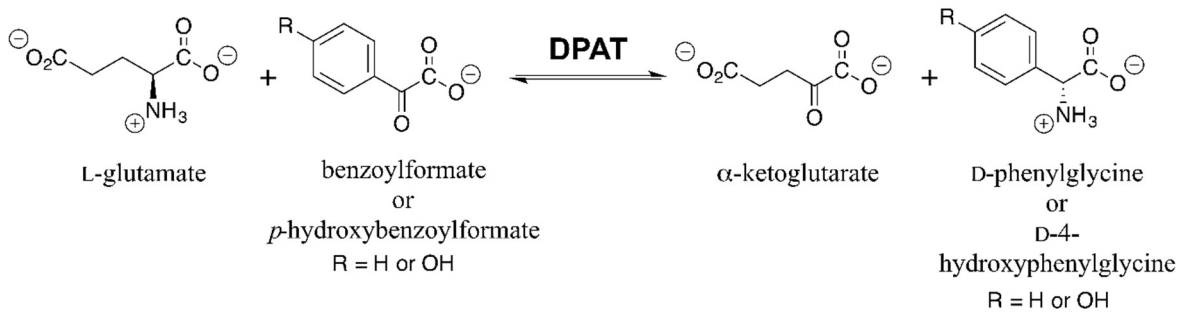

Figure 4.1 Stereo-inverting transamination reaction catalyzed by DPAT.

4.4. Results and Discussion

4.4.1. Expression and purification

The codon-optimized and His-tagged DPAT gene from *Pseudomonas stutzeri* ST-201 was subcloned into a pET11a expression vector and transformed into *E. coli* BL21-Gold(DE3) cells. Expression of the protein under standard conditions (37 °C, 3 h induction, 1 mM isopropyl β-D-1-thiogalactopyranoside (IPTG)) resulted in large quantities of aggregated recombinant protein in the cell pellet (data not shown). To enable production of soluble protein, expression was performed at lower temperature and IPTG concentration (15 °C, overnight, 0.1 mM IPTG). Under these conditions, 12 ± 5 mg L^{-1} of DPAT with a specific activity of 4.7 ± 0.2 U mg^{-1} was obtained (Fig. 4.2, see materials and methods for purification procedure).

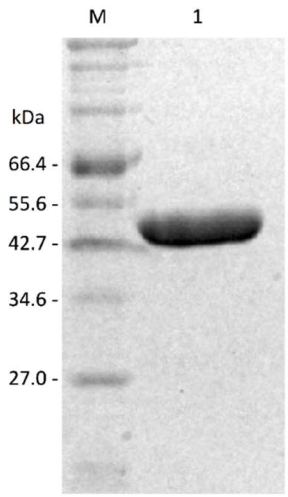

Figure 4.2 12.5% SDS-PAGE gel of purified DPAT. M: NEB Broad Range Protein Marker, 1: Immobilized metal affinity chromatography purified DPAT (molecular weight = 49.9 kDa).

4.4.2. Crystal structure

Following purification, DPAT crystals were generated using the sitting drop vapour-diffusion method at room temperature (complete crystallization conditions listed under Methods). The enzyme crystallized into trigonal crystals in approximately 2 weeks (Fig. S4.1). The structure of DPAT was solved by molecular replacement to R_{work} and R_{free} factors of 17.4 and 20.9, respectively. The data collection and refinement statistics are summarized in Table S1. The apoenzyme crystallized in the space group $P3_121$ and the structure was elucidated and refined to 1.82 Å resolution. In addition to nine C-terminal residues (445–453), the structure contains three disordered regions in the apo state for which no electronic density was observed (residues 27–39, 146–178, and 291–305), which together represent approximately 15% of the total polypeptide chain (Fig. 4.3). A comparison to the 2CY8 structure revealed six of the eight mutations are located at both end of the disordered loop region (145–178) with the two structures having a backbone Cα

RMSD of < 0.28 Å. Additionally, there are no phosphate ions resolved in the active site of the 2CY8 structure. Attempts to acquire a crystal structure of the holoenzyme with cofactor and substrate bound were unsuccessful as co-crystallization and substrate soaking experiments resulted in uncontrolled protein precipitation and no cofactor or substrate being observed in the active site, respectively.

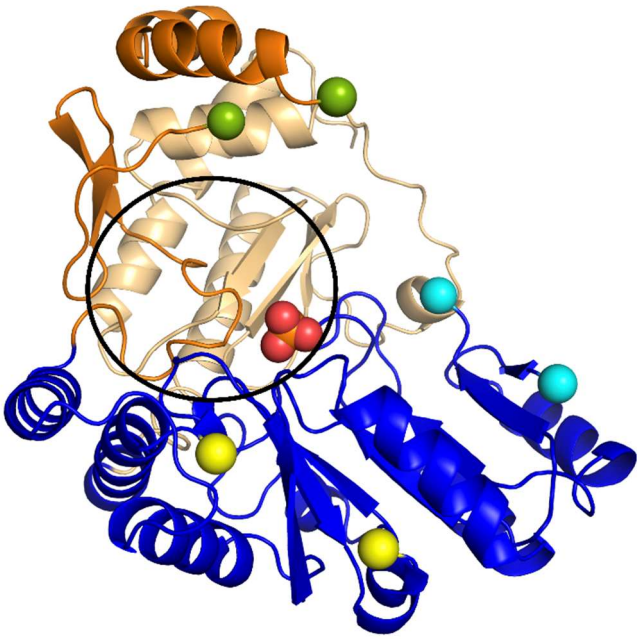

Figure 4.3 A DPAT subunit showing the active site cleft with a phosphate ion bound. Pairs of spheres indicate the backbone breaks for regions 27–39, 146–178, and 291–305 in green, yellow, and cyan, respectively. A phosphate ion is bound in the PLP binding site which is shown in a space-filling model. The black circle indicates the location of the active site.

4.4.3. Structural classification

DPAT is a member of the PLP-dependent enzyme superfamily, with a structural classification of fold-type I. The archetype of this fold is the well characterized aspartate aminotransferase (PDB ID: 1BKG; RMSD of 3.3 Å for 244 Cα atoms; 16% sequence identity).[16,17] The subunit of DPAT is comprised of a large and small domain and forms an obligate homodimer with one active site per subunit positioned in the cleft formed by the two domains (Fig. 4.4A&B). The large domain forms a 3-layered α/β/α sandwich comprised of a 7-stranded mixed β-sheet (strands β4-β11-β10-β9-β7-β5-β6) with β11 being the sole anti-parallel strand (Fig. 4.4C). The small domain is comprised of two 3-stranded anti-parallel β-sheets with 6 α-helices. The N-terminal lobe is formed by strands β1–3 and capped by helices α1 and α2. The C-terminal lobe is formed by β12, β13, and β15, which are surrounded by helices α12–15. Structural segments for which no electronic density was observed are indicated on the topology diagram by red lines.

The PLP-dependent fold-type I family can be further divided into subclasses based on structural and sequence classifications. DPAT belongs to class III ATs or "Ornithine AT-like" class.[18] The defining traits of this class include the 3-stranded antiparallel β-sheet of the N-terminus (β1–3) which is suspected to be responsible for partial suppression of large-scale domain rearrangements that are observed upon ligand binding in other AT classes.[19–21] Class III ATs have a rare *si*-facing left-handed α-helix (residues 64–67) that are coordinated by the highly conserved D61 and R248 residues (Fig. 4.5). The final defining trait of class III ATs is conservation of a threonine residue (T303 in the case of DPAT), which is involved in PLP binding and potentially catalysis through an H-bonding

interaction with the catalytic K269 residue.[22] Interestingly, the three disordered or dynamic regions located in or near the enzyme cleft are expected to contribute residues to the active site (Fig. 4.3). In the absence of structural information for these regions, we compared DPAT to homologous enzymes in order to gain insights on active-site organization and possible substrate binding modes.

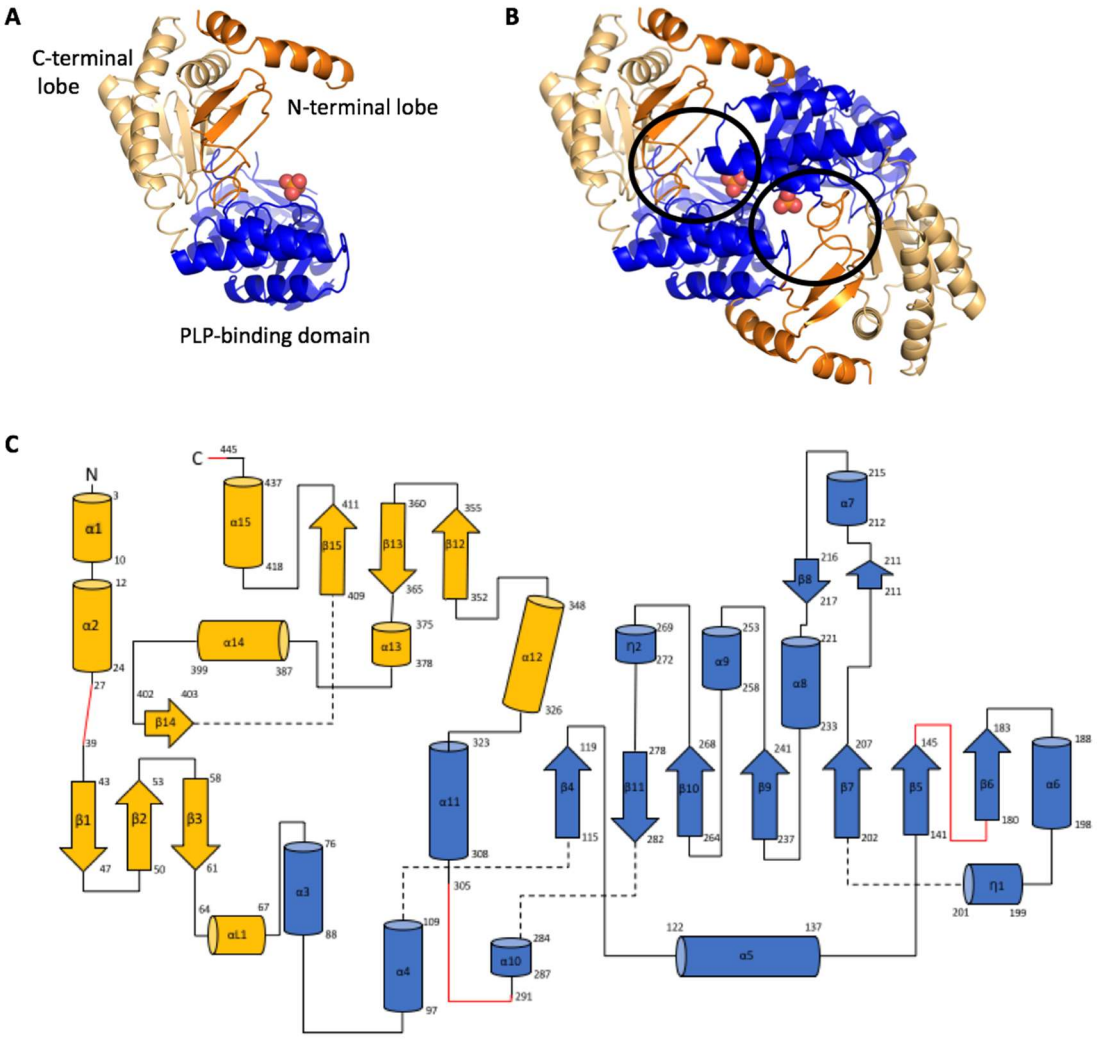

Figure 4.4 The crystal structure of DPAT. (A) DPAT subunit. The large PLP binding domain (residues 75–322) is coloured blue, whereas the smaller NC domain (residues 1–74 and 323–453) is divide into two lobes coloured orange and light orange. A phosphate ion is bound in the phosphate binding subsite. (B) DPAT dimer with one active site (indicated by circle) per subunit. A phosphate ion (shown as space-filling model) is bound in the PLP binding site. (C) Topology diagram of the DPAT structure. α-helices, β-strands, and loops are represented by cylinders, arrows, and black lines, respectively. The missing regions are indicated with red lines. Dashed lines are used when two lines intersect.

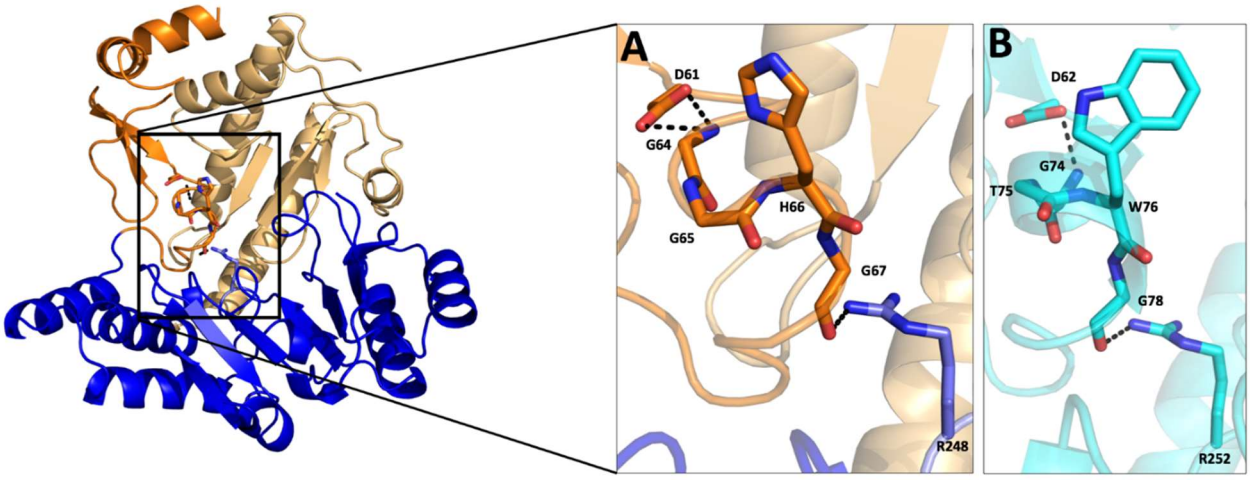

Figure 4.5 Left-handed α-helices of class III ATs. (A) The partial left-handed α-helix of DPAT is stabilized by hydrogen bonds made by the side chains of D61 or R248 with the backbone amide of G64 or backbone carbonyl of G67, respectively. (B) The left-handed α-helix of GSAM from *Synechococcus elongates* is stabilized by hydrogen bonds made by the side chains of D62 or R252 with the backbone amide of G74 or backbone carbonyl of G78, respectively (PDB ID: 2HP2)[23].

4.4.4. Comparison with homologous enzymes

We performed sequence and structural alignments of DPAT using PDBeFold to identify similar structures in the Protein Data Bank (Table S4.2).[17] The highest scoring, and thereby most structurally similar structure, was glutamate-1-semialdehyde-2,1-aminomutase (GSAM) from *Synechococcus elongates* (PDB ID: 2HOY; RMSD of 1.6 Å for 348 Cα atoms; 28% sequence identity).[23] The highest scoring aminotransferase was a β-AT: β-phenylalanine aminotransferase (MesAT) from *Mesorhizobium sp. LUK* (PDB ID: 2YKX; RMSD of 1.9 Å for 353 Cα atoms; 30% sequence identity).[24] These homologous enzymes are classified as PLP-dependent fold-type I and class III ATs, and share many common structural (Fig. S4.2 and Fig. S4.3) and sequence features with DPAT (Fig. 4.6).[25–28]

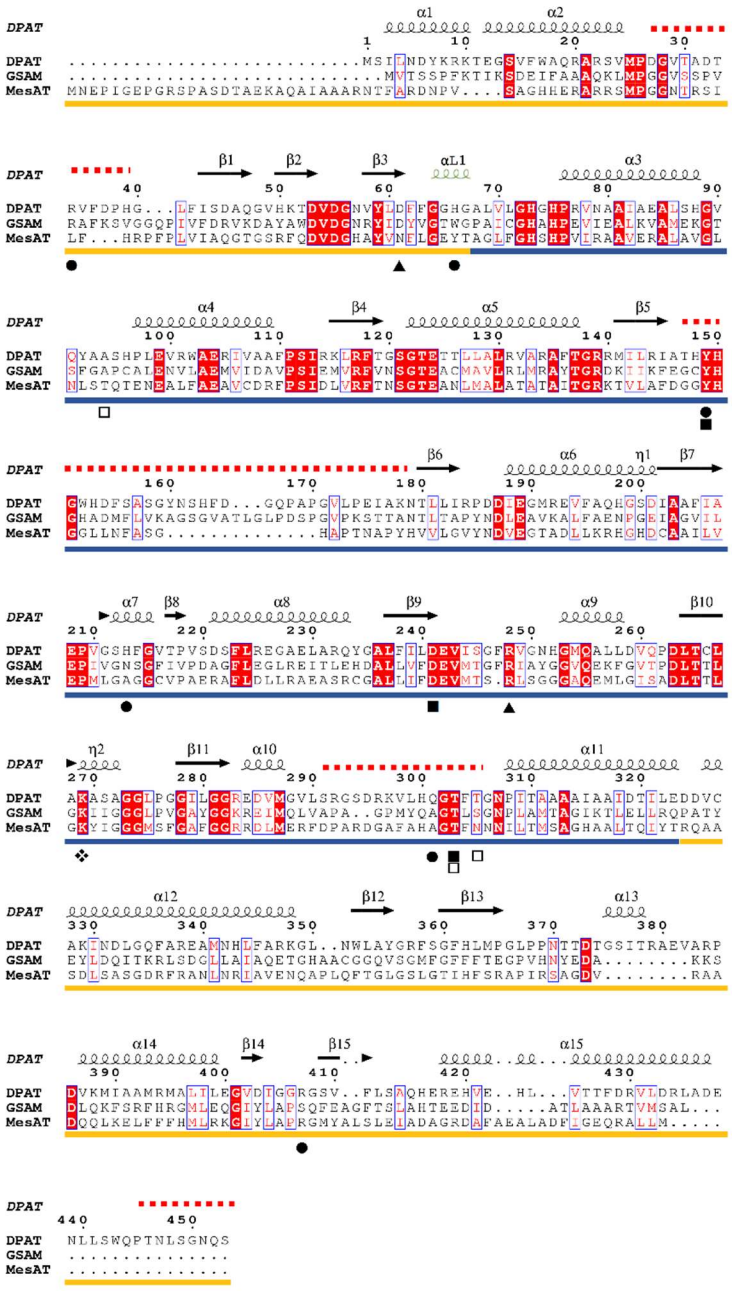

Figure 4.6 Sequence alignment of DPAT with homologous enzymes. Fully and partially conserved residues are indicated by white letters on a red background or red letters, respectively. Red dotted lines indicate disordered regions for which no electronic density was observed in the apo state. Coloured lines below alignment indicate the NC domain (orange) and the PLP-binding domain (blue). The catalytic lysine is indicated by ❖. Residues that bind PLP, stabilize the left-handed α-helix, participate in substrate binding, or bind R34 are indicated by ■, ◆, ●, or □ respectively. The α-helices, β-strands, the left-handed α-helix, and 310 helices are labelled α, β, αL1, and η, respectively. The sequence alignment was generated using ESPript 3.0 (http://espript.ibcp.fr).[28]

4.4.4.1. Binding pockets of ATs

ATs have evolved ways to accommodate two substrates with side chains of different shapes and properties at the same active site while discriminating against other molecules. Molecular recognition by ATs is typically controlled by a carboxylate binding pocket, which binds the α-carboxylate of amino acid substrates, and a side-chain binding pocket, which can bind the charged δ-carboxylate group of L-Glu and a neutral or charged side-chain of another substrate. The dual substrate recognition of the side-chain binding pocket is commonly achieved through one of two strategies: an arginine switch or hydrogen-bond network rearrangement.[29] In the case of DPAT, the enzyme also needs to achieve the L to D stereo-inversion to produce D-Phg. Previously, the C-4′ hydrogen transfer required for transamination in DPAT was shown to occur exclusively on the *si*-face of the PLP cofactor.[30] Therefore, to achieve the stereo-inversion, D-Phg must bind in a flipped orientation relative to L-Glu. In this orientation, the D-Phg phenyl side-chain would be bound in the carboxylate pocket that binds the L-Glu α-carboxylate group, while the α-carboxylate of D-Phg would be bound in the side-chain pocket, where the δ-carboxylate group of L-Glu also binds. Thus, binding of D-Phg and L-Glu by DPAT may require both the carboxylate and side-chain binding pockets to undergo some structural rearrangement, in contrast to most other ATs, who only require rearrangement of the side-chain binding pocket. This hypothesis is supported by the missing electron density observed in each pocket in our structure of the DPAT apo state, which suggests a high degree of conformational flexibility in these regions. As each pocket in DPAT may bind an α-carboxylate group (of either D-Phg or L-Glu), we will use the O- and P-pocket nomenclature to analyze the binding pockets of DPAT instead of the traditional

carboxylate/side-chain binding pocket nomenclature.[24] In this nomenclature, the O- and P-pockets are defined by being located on the 3′-O or phosphate group side of PLP.

We started our analysis by superimposing substrate-bound structures of GSAM (PDB ID: 2HP2) or MesAT (PDB ID: 2YKX) with that of DPAT (Fig. 4.7) Inspection of the superimposed structures allowed us to identify DPAT residues H66, H213, and R407 as potential substrate binding residues in the O-pocket. For the P-pocket however, this was not possible as the crystal structure of DPAT is missing electron density in this region of the active site (residues 27–39, 291–305). Therefore, it was necessary to rely on the sequence alignments (Fig. 4.6) to identify potential substrate-binding residues in DPAT's P-Pocket. Both GSAM and MesAT utilize an arginine residue in the P-pocket to coordinate the carboxylate of their respective substrates. This arginine residue in GSAM aligns with R34 of DPAT, whereas the arginine residue in MesAT is located 3 residues upstream in the sequence alignment. The sequence and structural comparison of DPAT to the homologous enzymes indicates that the P-pocket of DPAT is organized in an arrangement similar to that of GSAM (see SI, Fig. S4.4). Inspection of the P-pockets of GSAM and MesAT show that they both contain an Ala residue whose side chain is in close proximity to the substrate. Interestingly, the residue at the corresponding position in DPAT is a Gln (Q301*, * indicates a residue from the second subunit), which rare among other class III ATs.

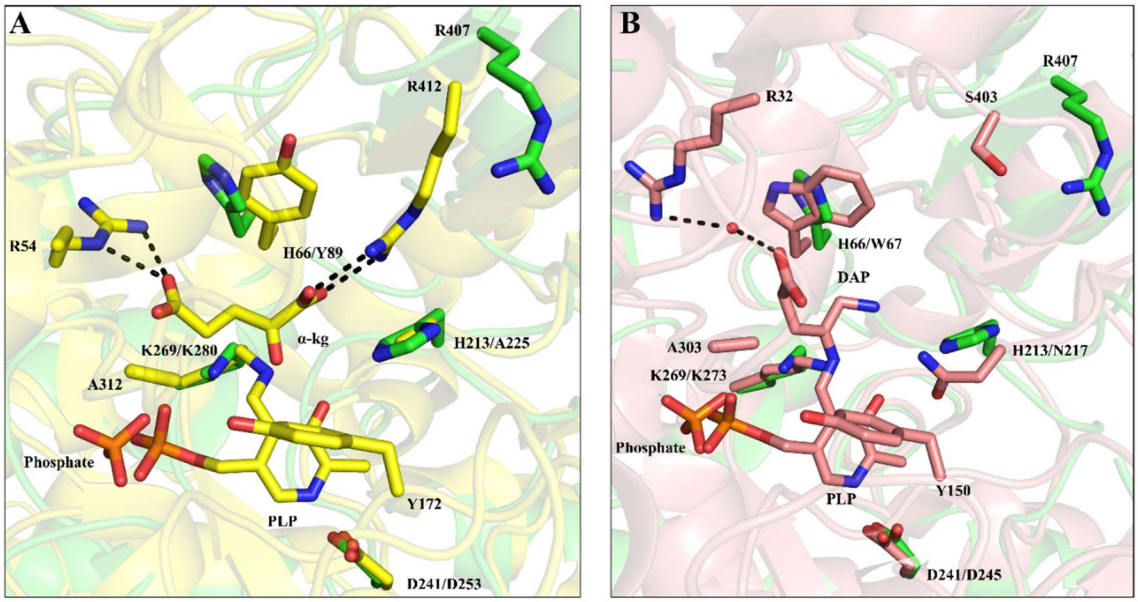

Figure 4.7 Active site comparison of DPAT with homologous enzymes. (A) The active site of MesAT (yellow, PDB ID: 2YKX) with α-kg and PLP bound, superimposed with DPAT (green). The α-kg H-bonds with R54 and R412 of MesAT, indicated by dashed black lines. (B) The active site of GSAM (salmon, PDB ID: 2HP2, chain A) with the pyridoxal phosphate-bound (ketimine) (4*S*)-4,5-diaminopentanoic acid (DAP), superimposed with DPAT (green). The R32 of GSAM forms a water-mediated H-bond with DAP, indicated by dashed black lines.

4.4.4.2. Probing the active site of DPAT

Based on our comparison of DPAT with the homologous enzymes, we performed saturation mutagenesis to produce five libraries of the P- (R34, Q301) and O-Pockets (H66, H213, R407). Library screening was performed in 96-well plates using the glutamate dehydrogenase (GDH) assay that we previously developed.[31] However, due to the low solubility of wild-type DPAT, expression in 96-well plate format did not yield sufficient quantities of the enzyme to distinguish its activity from the negative control containing no DPAT. To solve this issue, we introduced two surface mutations (N439D/Q444E) in DPAT, which were previously shown to improve the solubility without causing significant changes to the specific activity of the enzyme.[32] Introduction of these mutations into our saturation libraries resulted in an increased amount of soluble protein produced in 96-well format, which was sufficient to enable screening of clarified lysates.

Screening results of the R34 and R407 libraries for transamination activity with D-Phg as the amine donor and α-kg as acceptor yielded no active mutants. Activity levels in all mutants present in both libraries were indistinguishable from that of the negative controls, demonstrating that R34 and R407 are essential for the transamination reaction. This result suggests that these two arginine residues may bind the carboxylate groups of both donor and acceptor substrates. A similar result was observed for MesAT when R412 was mutated to an Ala residue, which caused a large decrease in specific activity (<1% relative to wild-type).[24] Next, we screened the H66, Q301, and H213 saturation libraries for transamination activity. In contrast with the R34 and R407 library screening results, several mutations that retained the ability of DPAT to perform the transamination reaction were identified (H66N, H66Q, H66M, H213N, H213Q, H213L, H213I, H213S, H213A, Q301G, Q301S, and

Q301A), albeit with reduced activity levels compared to the wild type. Nevertheless, these results suggest that residues H66, H213, and Q301 are not essential to DPAT catalytic activity, unlike R34 and R407.

4.4.5. Substrate binding model

Based on our sequence and structural comparison of DPAT with its homologous enzymes and screening results, we propose the following binding model for DPAT. The P- and O-pocket perform dual molecular recognition by adopting one of two binding modes (Fig. 4.8). The dual recognition performed by the P-pocket distinguishes between the binding of the δ-carboxylate of L-Glu (configuration 1) and the α-carboxylate of D-Phg (configuration 2). In configuration 1, R34 is responsible for binding the δ-carboxylate of L-Glu, in a similar way to R32 in GSAM, which forms a water mediated H-bond to the carboxylate group of the (4*S*)-4,5-diaminopentanoic acid substrate (Fig. S4.4A). However, R34 in DPAT is expected to be at least 6 Å away from the α-carboxylate of D-Phg. Therefore, a rearrangement of the hydrogen bond network may be necessary to accommodate the shorter α-carboxylate of D-Phg. This rearrangement could be mediated by Q301*, which is positioned close enough to directly H-bond to the α-carboxylate group of D-Phg.

In the O-pocket, the dual recognition distinguishes between the α-carboxylate of L-Glu (configuration 1) and a hydrophobic phenyl ring of D-Phg (configuration 2). In configuration 1, the α-carboxylate of L-Glu is bound by a salt bridge with R407. The sequence and structural alignments indicate R407 of DPAT is conserved with the R412 of MesAT, which participates in an arginine switch mechanism to bind the phenyl ring of (*S*)-

3-phenyl-β-alanine or α-carboxylate of L-Glu (Fig 4.6, Fig S4.4).[24] A similar arginine switch is also observed in the β-AT from *Variovorax paradoxus* (VPAT; PDB ID: 4AO9; RMSD of 1.57 Å for 350 Cα atoms; 30% sequence identity).[33] We propose that the R407 residue undergoes a conformational change or "arginine switch" similar to those observed in β-ATs, moving out of the O-Pocket when D-Phg is bound, leaving a hydrophobic pocket comprised of Y149, H66, and H213 (configuration 2). In our crystal structure of DPAT, the O-pocket is in configuration 2 with R407 switched out of the pocket, since no substrate is bound in the apo state. Although no electron density is observed for the Y149 residue in our crystal structure, this residue is moderately conserved across class III ATs as it is involved in PLP binding and contributes to the hydrophobic O-pocket.[22]

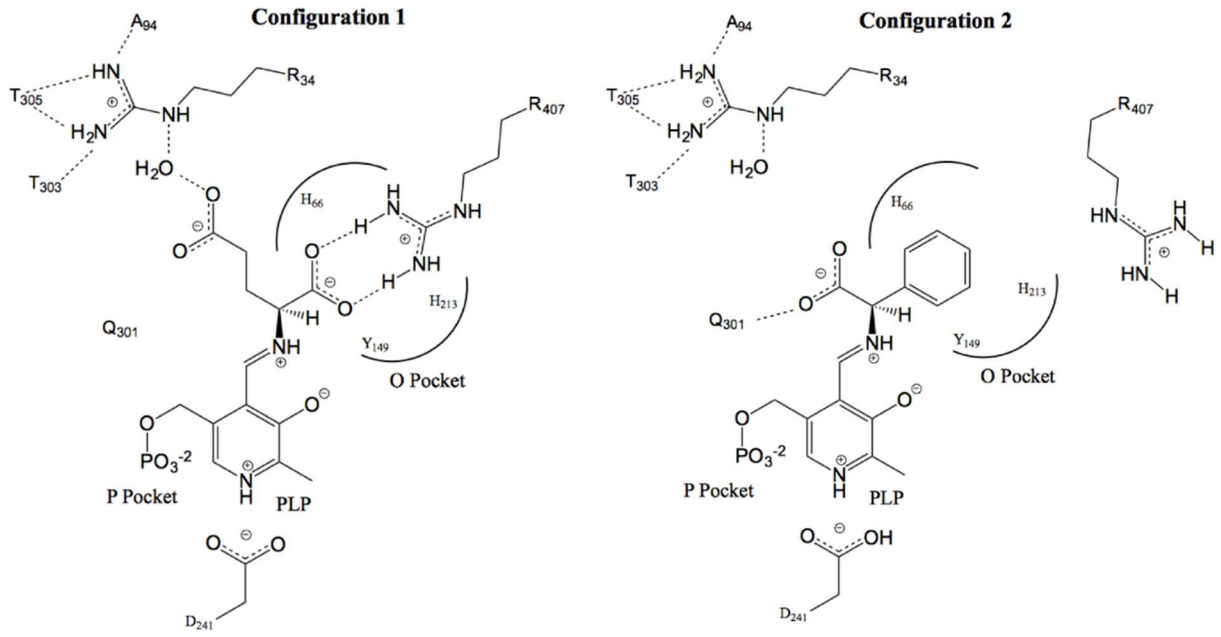

Figure 4.8 Hypothetical schematic representation of DPAT's active site with L-Glu and D-Phg bound to PLP. Configuration 1. L-Glu is bound with the α-carboxylate in the O-pocket and side-chain in the P-pocket. The R407 residue is in the "flipped in" conformation. Configuration 2. D-Phg is bound to the active site with the α-carboxylate bound in the P-pocket and the side-chain in the O-pocket. The R407 residue is in the "flipped out" conformation.

4.4.6. Substrate specificity of DPAT

The proposed binding modes described in the previous section agree with the narrow specificity reported for DPAT. Wiyakrutta *et al.* showed that DPAT is highly specific towards D-Phg and L-Glu, as it did not react with D-Phe, D-Tyr, D-Ala, D-Val, D-Leu, D-Glu, D-Asp, DL-Ile, DL-Ser, L-Asp, or L-Ala when used as amine donors.[12] The specificity of DPAT was probed using an HPLC-based assay, which limited the number of molecules tested as potential substrates of the enzyme. To perform a more thorough analysis of the substrate profile for DPAT, we tested the wild-type enzyme against a library of 17 D-amino acids, 4 L-amino acids, 1 β-amino acid, 1 γ-amino acid, and the achiral molecule aminomalonate using our microplate-based GDH assay (Fig. 4.9). In agreement with previous observations,[12] DPAT displayed high activity with its native substrate D-Phg (Fig. 4.9, Table S4.3) and over two orders of magnitude lower activity towards D-Phe. Surprisingly, our results show that DPAT reacts with D-leucine, D-methionine, and D-tryptophan with an activity that is approximately 10-fold higher than with D-Phe, even though these substrates are less structurally similar to the native substrate D-Phg.

In the panel of amino acids that were tested, we included two D-Phg analogs, *(S)*-3-phenyl-β-alanine and (*S*)-4-phenyl-4-aminobutyric acid (Fig 4.10), which contain one or two additional methylene groups bridging the main chain and phenyl ring, respectively. We postulated that the phenyl group of these analogs would bind in the O-pocket in a similar way to the phenyl ring of D-Phg, allowing us to probe the ability of the P-pocket to discriminate between carboxyl groups separated from the phenyl ring by carbon chains of different lengths. The carboxyl group of (*S*)-4-phenyl-4-aminobutyric acid is expected to

mimic the side-chain of L-Glu. This is not the case for the carboxyl group of (*S*)-3-phenyl-β-alanine, whose distance from the phenyl ring is lower than in (*S*)-4-phenyl-4-aminobutyric acid but longer than in D-Phg. Thus, use of these analogs in combination with mutagenesis would allow us to probe the structural determinants of specificity in the P-pocket of DPAT.

The specific activity of wild-type DPAT for (*S*)-3-phenyl-β-alanine decreased by more than an order of magnitude compared to D-Phg (Table S3). However, the specific activity for (*S*)-4-phenyl-4-aminobutyric acid was within error to that of D-Phg. The lower activity obtained with (*S*)-3-phenyl-β-alanine compared to both D-Phg and (*S*)-4-phenyl-4-aminobutyric acid suggests that the carboxylate of the lower activity substrate is not optimally positioned to participate in the coordinated hydrogen bond network established in the P-pocket. Nonetheless, this is the first report that DPAT can function with β- and γ-amino acids, classifying DPAT as an ω-AT with promiscuous activity for β-amino acids.

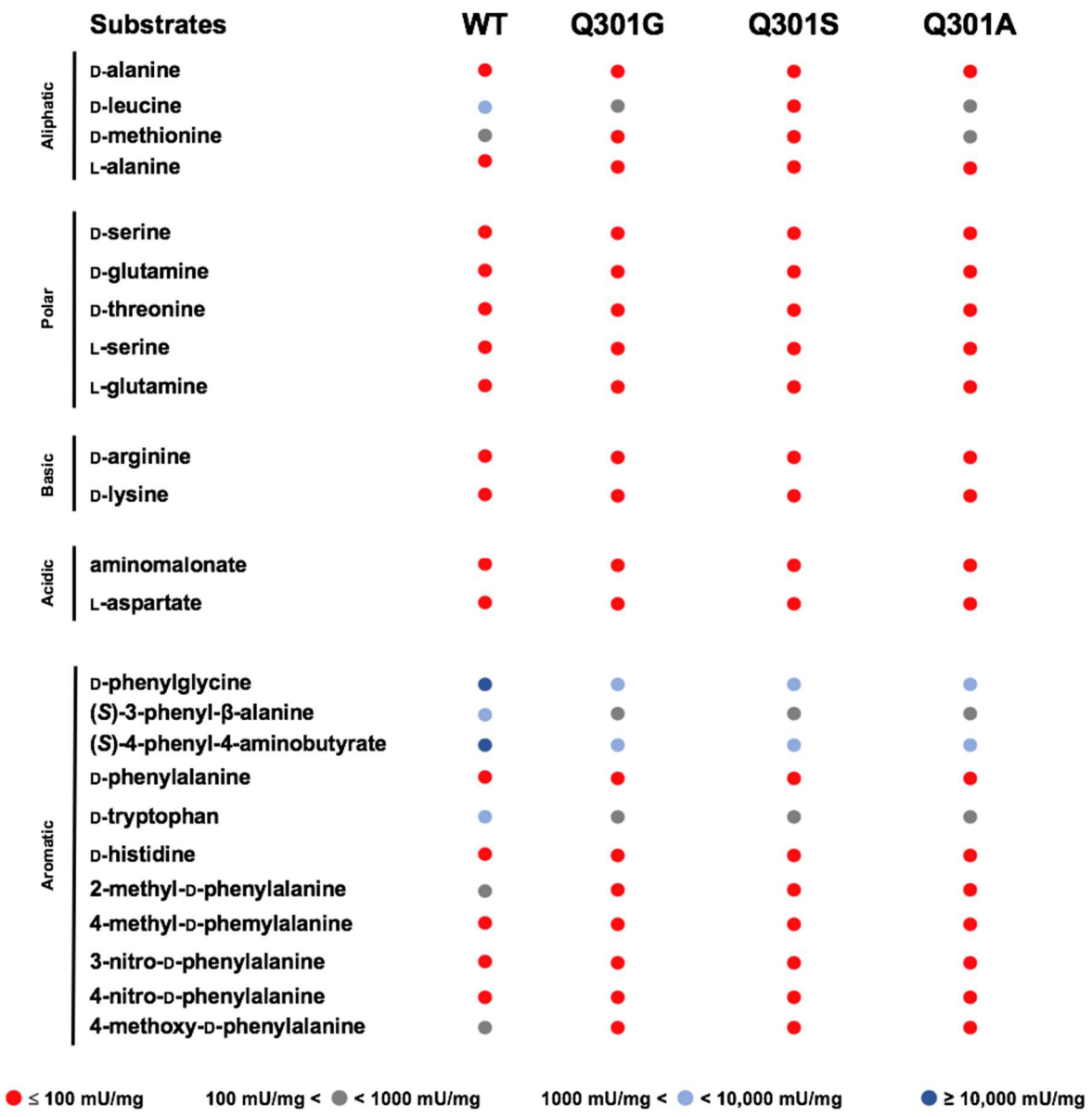

Figure 4.9 Substrate-specificity profiles of wild-type and mutant DPAT enzymes. Each dot represents a unique aminotransferase-amine donor pair. The colour is based on the specific activity of the resulting enzymatic reaction. In all cases, the acceptor substrate is α-kg at 1 mM.

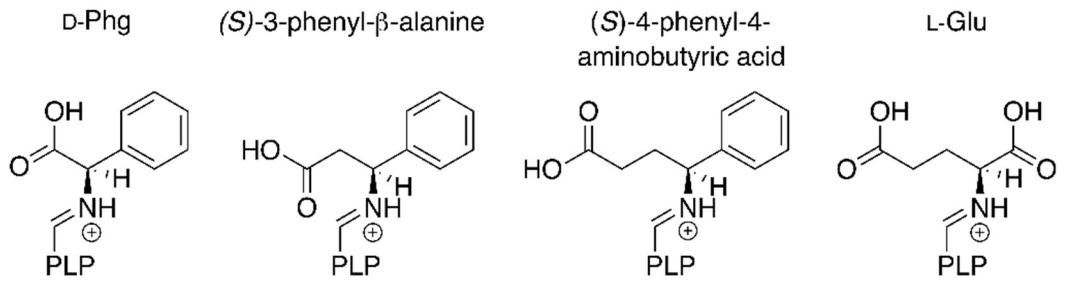

Figure 4.10 Representation of DPAT substrates bound to PLP in external aldimine form.

Based on our binding model (Fig. 4.8), we postulated that mutations to the O-pocket will be required to alter the specificity of DPAT to increase its activity towards alternative D-amino acids. Our mutagenesis results showing that several H66 and H213 mutants retain catalytic activity indicate that the O-pocket is tolerant to mutation and therefore amenable to engineering for alteration of DPAT's substrate specificity.

4.4.7. Characterization of DPAT and Q301 mutants

The Q301G, Q301A, and Q301S mutants retained varying levels of activity with D-Phg (Fig. S4.6), demonstrating that this residue is not essential for the transamination reaction. Yet, these mutants may be useful in elucidating the role of Q301 in binding substrates in the P-pocket, and could allow us to test our binding model. Therefore, we screened the Q301 mutants with the panel of amine donors, with particular interest in the D-Phg analogs. Generally, the mutants experienced a decrease in specific activity for the D-amino acids compared to the wild type (Fig. 4.9, Table S4.3). These results were expected, as the mutation is located in the P-pocket and our proposed binding model dictates that the O-pocket controls specificity for D-amino acids. The Q301A mutant displayed the largest decrease in specific activity for D-Phg at approximately 12-fold. The Q301G and Q301S

mutants displayed a 1.7 and 3-fold decrease, respectively. A similar decrease in specific activity was observed for (*S*)-4-phenyl-4-aminobutyrate with the three DPAT mutants. This result was unexpected as we are proposing that Q301 is involved in binding the shorter α-carboxylate of D-Phg and not longer-chain carboxylates. Therefore, to gain a better understanding of the functional role of Q301, we kinetically characterize the wild type and mutants with D-Phg, *(S)*-3-phenyl-β-alanine, (*S*)-4-phenyl-4-aminobutyrate, and α-kg.

Using the GDH assay, we determined the apparent steady-state kinetic parameters of the wild type and Q301 mutants (Table 4.1). Importantly, the Q301 variants also contain the two solubility enhancing mutations (N439D/Q444E), unlike the wild type. These mutations are located on the surface of the protein and have been shown to not affect catalytic activity.[32] For the wild type, we obtained apparent K_M values of 0.27 ± 0.04 and 0.16 ± 0.01 mM and k_{cat} values of 5.0 ± 0.2 and 6.5 ± 0.7 s^{-1} for D-Phg and α-kg, respectively. Catalytic efficiencies (k_{cat}/K_M) for *(S)*-3-phenyl-β-alanine and (*S*)-4-phenyl-4-aminobutyrate were determined to be approximately 60- and 6-fold lower compared to D-Phg, respectively. In the case of the three Q301 mutants, catalytic efficiencies are between 6 to 24-fold lower with D-Phg and 4 to 10-fold lower for α-kg, compared to the wild type. For the Q301A and Q301S mutants, the apparent K_M of α-kg was not significantly impacted by the mutations, but the apparent K_M for D-Phg increased by approximately 3-fold. In the case of Q301G, the apparent K_M for α-kg and D-Phg increased by approximately 2- and 4-fold, respectively. The observed larger effect of the Q301 mutations on apparent K_M for D-Phg than for α-kg supports our hypothesis that this residue plays a role in productive binding of D-Phg and not α-kg, which instead is bound through a water-mediated H-bond to R34, as in GSAM (Fig. S4.4).

Additionally, the apparent K_M and k_{cat} values for all Q301A and Q301S mutants with (*S*)-4-phenyl-4-aminobutyrate were within error to those of the wild type, suggesting that these variants are as efficient as the wild type at catalyzing transamination of this amino acid with α-kg. This result contrasts with our substrate library screening results (Fig. 4.9 and Table S4.3), where large decreases (4 to 11-fold) in specific activity with this substrate were observed for the Q301 mutants relative to the wild type. This result can be explained by substrate inhibition of the mutants under the conditions of the screening assay (K_i values are reported in Table 4.1). Similarly, catalytic efficiency of the three Q301 mutants with the *(S)*-3-phenyl-β-alanine substrate shows no significant change compared to the wild type, although in all cases the k_{cat}/K_M is 3 to 9-fold lower than with the native substrate D-Phg. Taken together, these results support our hypothesis that R34 is fixed in a conformation similar to that of R32 in GSAM, and unable to move closer to interact with the carboxylate of *(S)*-3-phenyl-β-alanine, which is one methylene group further away. However, the side chain of Q301 is positioned close enough to establish a hydrogen bond with the short α-carboxylate of D-Phg, but would not be required for productive binding of the longer chain (*S*)-4-phenyl-4-aminobutyrate or α-ketoglutarate substrates.

Table 4.1. Apparent kinetic parameters for the transamination reaction of DPAT and Q301 mutants.

Substrate	Kinetic Parameter	WT	Q301G	Q301A	Q301S
α-ketoglutarate[a]	K_M (mM)	0.16 ± 0.01	0.33 ± 0.05	0.23 ± 0.01	0.17 ± 0.04
	k_{cat} (s^{-1})	6.5 ± 0.7	3.5 ± 0.2	0.92 ± 0.01	2.3 ± 0.2
	k_{cat}/K_M (M^{-1} s^{-1})	41,000 ± 5,000	11,000 ± 1,700	4,000 ± 200	14,000 ± 3,400
D-phenylglycine	K_M (mM)	0.27 ± 0.04	1.14 ± 0.02	0.9 ± 0.1	0.9 ± 0.1
	k_{cat} (s^{-1})	5.0 ± 0.2	3.57 ± 0.03	0.71 ± 0.05	2.4 ± 0.1
	k_{cat}/K_M (M^{-1} s^{-1})	19,000 ± 3,000	3,130 ± 60	800 ± 100	3,000 ± 300
(*S*)-3-phenyl-β-alanine	K_M (mM)	2.7 ± 0.3	4.4 ± 0.6	3.0 ± 0.3	3.7 ± 0.3
	k_{cat} (s^{-1})	0.86 ± 0.03	1.60 ± 0.09	0.75 ± 0.02	1.30 ± 0.05
	k_{cat}/K_M (M^{-1} s^{-1})	320 ± 40	360 ± 60	250 ± 30	360 ± 30
(*S*)-4-phenyl-4-aminobutyrate	K_M (mM)	0.64 ± 0.05	1.2 ± 0.3	0.89 ± 0.08	0.64 ± 0.06
	k_{cat} (s^{-1})	2.6 ± 0.1	3.2 ± 0.5	3.7 ± 0.2	3.0 ± 0.2
	k_{cat}/K_M (M^{-1} s^{-1})	4,000 ± 400	2,700 ± 900	4,200 ± 400	4,700 ± 500
	K_i (mM)	16 ± 2	9 ± 3	5.7 ± 0.5	9 ± 1

[a] donor substrate is 5 mM D-Phg.

4.5. Conclusion

The partial apo structure of DPAT has been solved and based on a comparison with the structures of homologous enzymes, several active site residues were identified and subjected to saturation mutagenesis. The saturation libraries helped us identify two arginine residues (R34 and R407), one in each binding pocket, that are essential to catalysis. Mutagenesis also revealed that O-pocket residues H66 and H213 are amenable to substitution and may provide a route to engineering the specificity of DPAT for other D-amino acids.

Next, a binding model was proposed based on comparison of DPAT's sequence and structure to that of the homologous enzymes GSAM and MesAT, and on the screening results. The kinetic parameters of the wild type and Q301 mutants were measured to support the proposed binding model. Our kinetic results demonstrate that Q301 is involved in productive binding of the α-carboxylate group of D-Phg but not of longer-chain carboxylates. However, crystal structures of the holo form of DPAT with either D-Phg and α-kg bound at the active site will be required to confirm our proposed binding model. Finally, substrate specificity profiles of the wild type and Q301 mutants were determined, which allowed us to demonstrate that DPAT acts as an ω-AT.

4.6. Acknowledgements

We would like to thank Sarah Mavula and Maja Mujcin for their initial testing of DPAT recombinant expression protocols.

4.7. Supplemental Information

4.7.1. Supplementary results

4.7.1.1. Structural analysis of the GSAM and MesAT P-pockets

GSAM (PDB ID: 2HP1, 2HP2)[23] has been crystallized with the (4*S*)-4,5-diaminopentanoic acid (DAP) substrate bound in the active site either covalently (ketimine) or non-covalently. When covalently bound, the carboxylate side chain extends into the P-pocket, where it hydrogen bonds with a water molecule coordinated by R32 (Fig. S4.4A). This arginine residue is located at the C-terminus of an α-helix corresponding to residues 30-35 in DPAT, with its side chain extending into the P-pocket. The guanidinium group of R32 is anchored in place through hydrogen bonds to the backbone carbonyl groups of T305*, S307*, and A95*, which form a coordination pocket. In the GSAM subunit with non-covalently bound DAP (chain B in 2HP1), this coordination pocket undergoes a minor conformational change compared to covalently bound subunit, shifting from the direct coordination of R32 with the backbone carboxylate of A95* to a water-mediated bridge. When DAP is not covalently bound, the carboxylate directly interacts with the guanidinium group of R32 which remains fixed in the coordination pocket.

In the crystal structure of MesAT (PDB ID: 2YKX),[24] the δ-carboxylate of α-kg forms a direct hydrogen bond with R54 (Fig. S4.4B). Because the R54 residue of MesAT is located three residues upstream to the R34 residue of DPAT in the sequence alignment (Fig. 4.6), it is located in the middle of the α-helix, with its side chain at the bottom of the matching structural element in GSAM and extending perpendicularly to the α-helix and into the P-

pocket. The R54 residue is coordinated by a salt bridge with E88 and H-bonds with the side-chain of N317* in a configuration that would not be possible in DPAT.

A comparison of the residues responsible for coordinating the arginine residue in GSAM and MesAT indicate that the DPAT R34 residue is likely configured similarly to R32 in GSAM. The MesAT residues E88 and N317*, which are responsible for coordinating R54, are not conserved in DPAT. The R34 residue in DPAT is likely positioned to bind the δ-carboxylate of L-Glu/α-kg through a coordinated water molecule or directly through salt bridge formation similar to the observed binding modes in GSAM. The arginine coordinating residues in GSAM are conserved with DPAT, with T305* being the sole exception. However, the missing interaction is replaced by an H-bond with the backbone carbonyl of S303*.

4.7.2. Supplementary figures

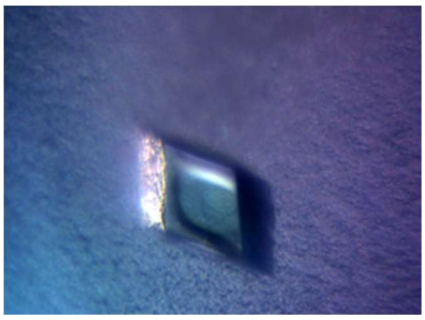

Figure S4.1. Trigonal protein crystal of DPAT.

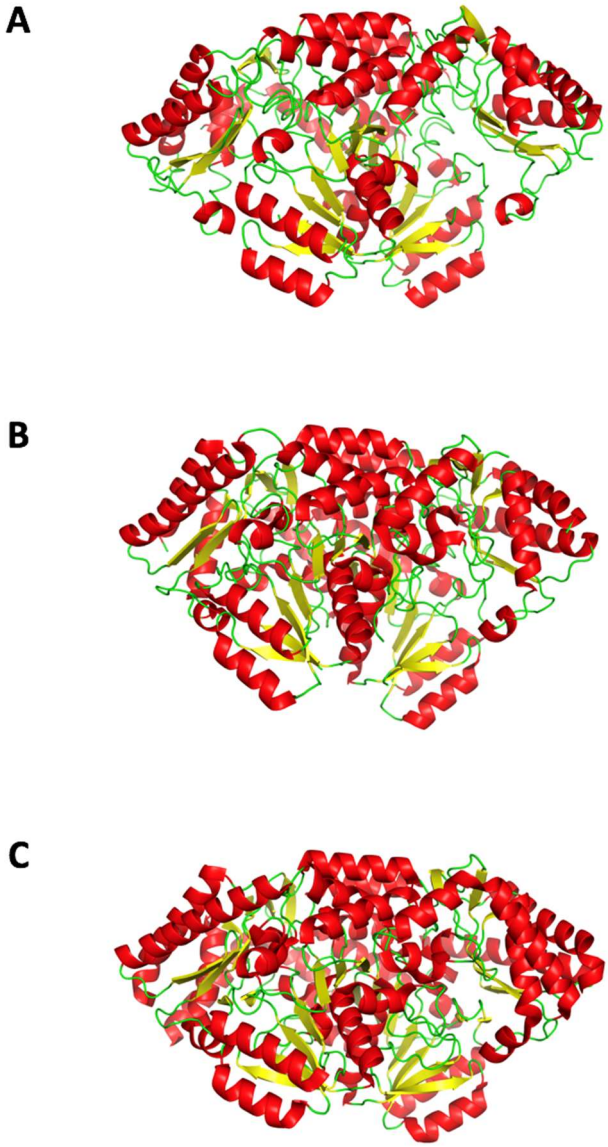

Figure S4.2 Crystal Structures of DPAT and Homologous enzymes. (A) Dimer structure of DPAT from *Pseudomonas stutzeri* ST-201. (B) Dimer structure of GSAM from *Synechococcus elongates* (PDB ID: 2HOY).[23] (C) Dimer structure of MesAT from *Mesorhizobium sp. LUK* (PDB: 2YKX).[24]

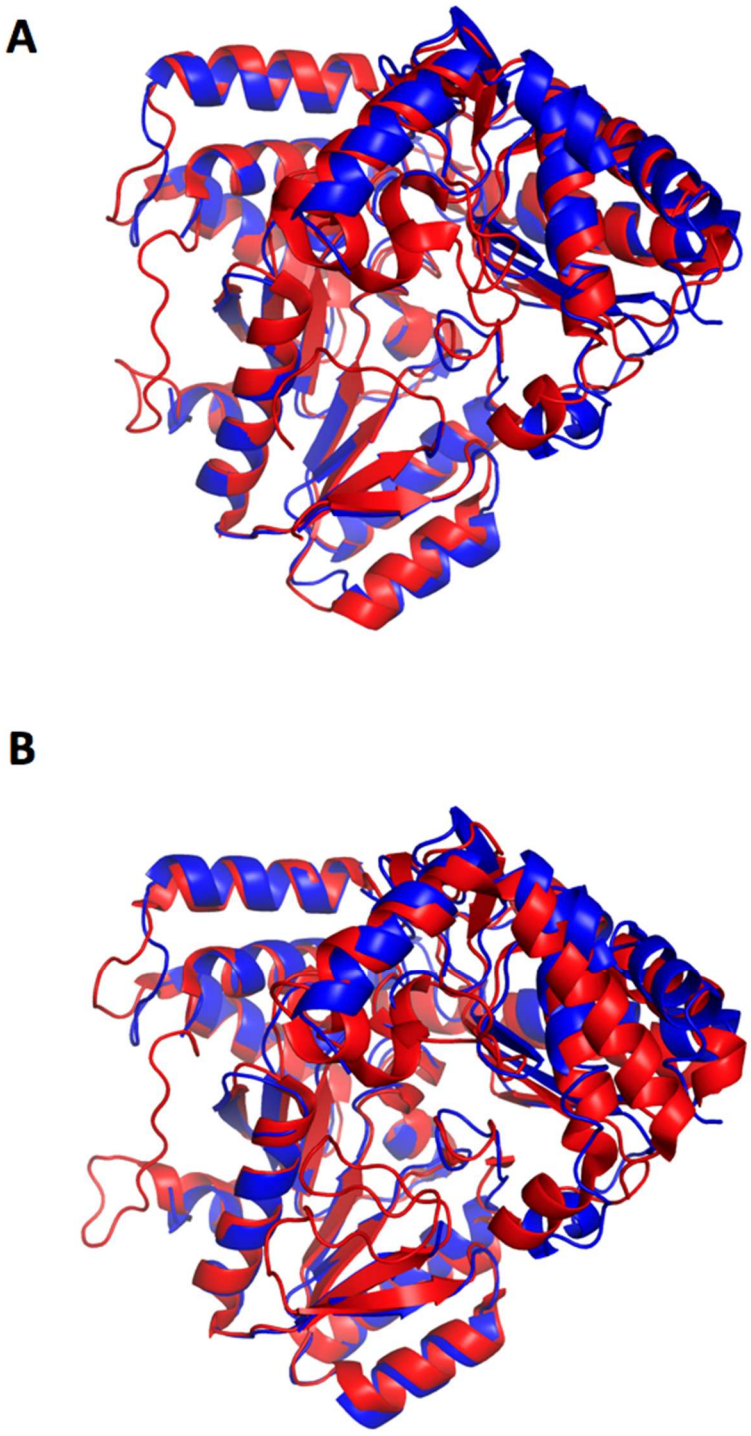

Figure S4.3 Comparison of DPAT subunit with that of homologous class III ATs. The DPAT subunit (blue) is structurally similar to (A) GSAM subunit (PDB ID: 2HOY) and (B) MesAT (PDB: 2YKX) shown in red.

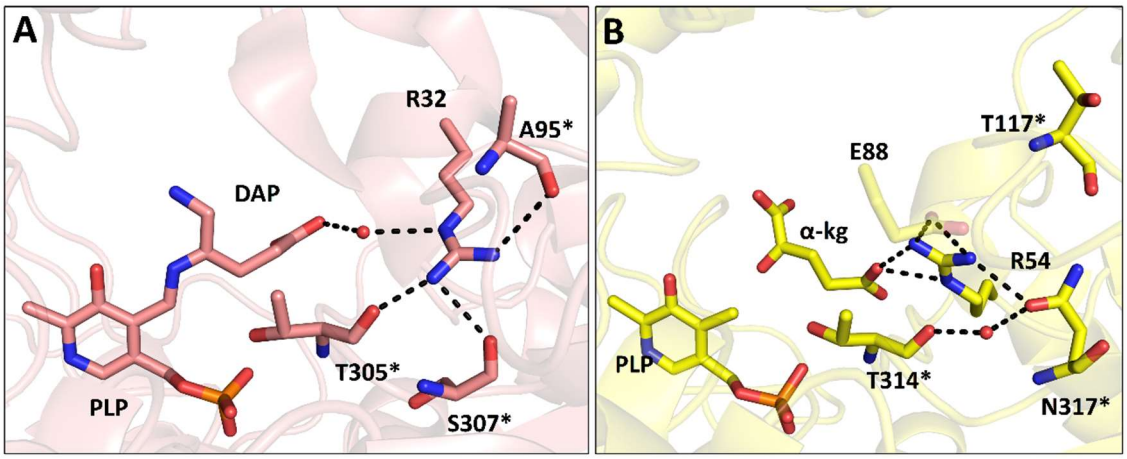

Figure S4.4 P-pocket comparison of homologous enzymes of DPAT. (A) P-pocket of GSAM (PDB ID: 2HP2, chain A) with pyridoxal phosphate-bound (4*S*)-4,5-diaminopentanoic acid (DAP). The R32 residue of GSAM coordinates a water molecule that interacts with the carboxylate of DAP. The R32 residue is coordinated by A95*, T305*, and S307*. (B) P-pocket of MesAT with bound PLP and α-kg. The R54 residue interacts with the δ-carboxylate of α-kg. The R54 residue is coordinated with E88 and N317*.

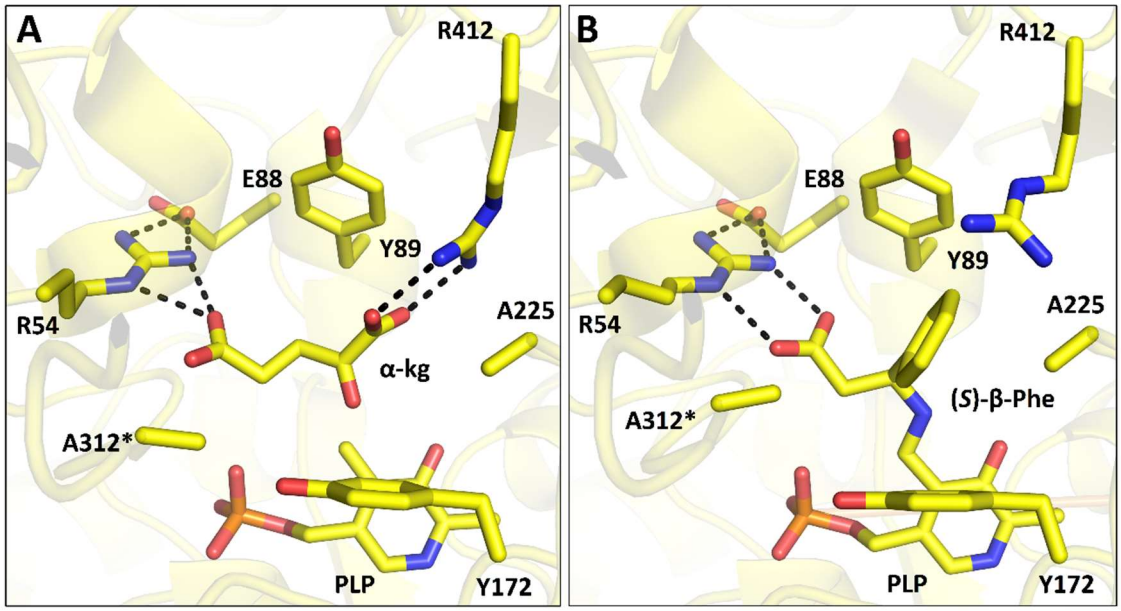

Figure S4.5 Active site comparison of MesAT with α-kg and (*S*)-3-phenyl-β-alanine ((*S*)-β-Phe). (A) The active site of MesAT with α-kg bound (PDB ID: 2YKX). The R412 residue is in the flipped in conformation forming a salt bridge with the α-carboxylate of α-kg. The R54 residue is coordinated by E88. (B) The active site of MesAT with (*S*)-β-Phe bound (PDB ID: 2YKY). The R412 residue undergoes a switch out of the O-pocket leaving a hydrophobic pocket of Y89, Y172, and A225. The R54 remains coordinated by E88.

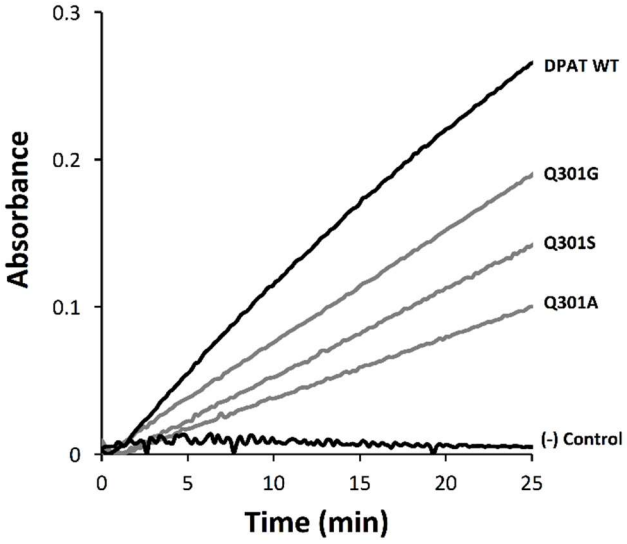

Figure S4.6 Screening of DPAT Q301 mutant library. The screening of the library was performed with D-Phg and α-kg as donor and acceptor substrates, respectively. The black lines indicated positive and negative controls, which contain wild-type DPAT (WT) or no aminotransferase. The grey lines correspond to active mutants detected by screening. The activities of all other mutants were indistinguishable from the negative control. Abs = 340 nm.

4.7.3. Supplementary tables

Table S4.1. Data collection and refinement statistics of DPAT.

Parameters	DPAT apo [a]
Data Collection	
Space group	$P3_121$
Cell dimensions	
a, b, c (Å)	74.64, 74.64, 149.9
A, β, γ (°)	90, 90, 120
Resolution	49.98 – 1.82 (2.04 – 1.82)
R_{meas}	6.7 (71.1)
I / σI	24.7 (3.1)
Completeness (%)	100 (100)
Redundancy	9.2 (9.3)
Refinement	
Resolution (Å)	49.98 – 1.82
No. reflections	44043
R_{work} / R_{free}	17.4/20.9
No. Atoms	
Protein	2954
Sulfate	10
Water	249
B-factors (Å^2)	
Protein	33.4
Sulfate	36.3
Water	44.8
Rmsds	
Bond lengths (Å)	0.019
Bond angles (°)	1.55
Molprobity scores	1.18
Ramachandran favored (%)	97.4
Ramachandran allowed (%)	2.6

[a] Values in () are for the last resolution shell.

Table S4.2. Structure Alignment Results of DPAT Crystal structure from PDBeFold.

	Scoring								
	Q	**P**	**Z**	**RMSD**	**Nalign**	**Ng**	**%seq**	**PDB**	**Enzyme**
1	0.93	78.6	26.7	0.37	382	3	99	2cy8:A	CRYSTAL STRUCTURE OF D-PHENYLGLYCINE AMINOTRANSFERASE (D-PHGAT) FROM PSEUDOMONAS STRUTZERI ST-201
2	0.63	34.5	18.3	1.56	348	12	28	2hoy:B	INTER-SUBUNIT SIGNALING IN GSAM
3	0.62	31.3	17.3	1.60	331	9	32	2cfb:A	GLUTAMATE-1-SEMIALDEHYDE 2,1-AMINOMUTASE FROM THERMOSYNECHOCOCCUS ELONGATUS
4	0.62	29.3	16.9	1.60	348	15	28	2hp1:B	INTER-SUBUNIT SIGNALING IN GSAM
5	0.62	33.8	18.1	1.56	347	12	28	3usf:B	CRYSTAL STRUCTURE OF DAVA-4
6	0.61	34.1	18.1	1.53	345	13	28	2hoy:A	INTER-SUBUNIT SIGNALING IN GSAM
7	0.61	34.2	18.1	1.51	344	11	33	4e77:A	2.0A CRYSTAL STRUCTURE OF A GLUTAMATE-1-SEMIALDEHYDE AMINOTRANSFERASE FROM YERSINIA PESTIS CO92
8	0.60	33.2	17.9	1.48	346	15	30	3k28:D	CRYSTAL STRUCTURE OF A GLUTAMATE-1-SEMIALDEHYDE AMINOTRANSFERASE FROM BACILLUS ANTHRACIS WITH BOUND PYRIDOXAL 5'PHOSPHATE
9	0.60	34.8	18.2	1.51	332	10	30	4zm3:C	CRYSTAL STRUCTURE OF PLP-DEPENDENT 3-AMINOBENZOATE SYNTHASE PCTV WILD- TYPE
10	0.60	38.5	19.4	1.52	350	11	30	3l44:A	CRYSTAL STRUCTURE OF BACILLUS ANTHRACIS HEML-1, GLUTAMATE SEMIALDEHYDE AMINOTRANSFERASE
11	0.59	33.5	17.9	1.48	345	15	30	3k28:C	CRYSTAL STRUCTURE OF A GLUTAMATE-1-SEMIALDEHYDE AMINOTRANSFERASE FROM BACILLUS ANTHRACIS WITH BOUND PYRIDOXAL 5'PHOSPHATE
12	0.59	33.7	17.9	1.52	329	9	30	4zm3:B	CRYSTAL STRUCTURE OF PLP-DEPENDENT 3-AMINOBENZOATE SYNTHASE PCTV WILD- TYPE
13	0.59	38.2	19.2	1.52	351	11	30	3l44:B	CRYSTAL STRUCTURE OF BACILLUS ANTHRACIS HEML-1, GLUTAMATE SEMIALDEHYDE AMINOTRANSFERASE
14	0.59	32.9	17.9	1.52	346	15	30	3k28:A	CRYSTAL STRUCTURE OF A GLUTAMATE-1-SEMIALDEHYDE AMINOTRANSFERASE FROM BACILLUS ANTHRACIS WITH BOUND PYRIDOXAL 5'PHOSPHATE
15	0.59	32.8	17.9	1.53	346	15	30	3k28:B	CRYSTAL STRUCTURE OF A GLUTAMATE-1-SEMIALDEHYDE AMINOTRANSFERASE FROM BACILLUS ANTHRACIS WITH BOUND PYRIDOXAL 5'PHOSPHATE
16	0.59	30.4	17.3	1.56	347	16	29	5i92:B	CRYSTAL STRUCTURE OF GLUTAMATE-1-SEMIALDEHYDE 2,1-AMINOMUTASE (GSA) FROM PSEUDOMONAS AERUGINOSA
17	0.59	31.4	17.8	1.57	347	14	29	5i92:C	CRYSTAL STRUCTURE OF GLUTAMATE-1-SEMIALDEHYDE 2,1-AMINOMUTASE (GSA) FROM PSEUDOMONAS AERUGINOSA
18	0.59	34.6	18.3	1.53	347	12	29	3fqa:B	GABACULIEN COMPLEX OF GABACULINE RESISTANT GSAM VERSION

19	0.59	34.6	18.4	1.53	347	12	29	3fqa:A	GABACULIEN COMPLEX OF GABACULINE RESISTANT GSAM VERSION
20	0.58	30.7	17.1	1.82	361	12	30	2ykx:C	STRUCTURAL DETERMINANTS OF THE BETA-SELECTIVITY OF A BACTERIAL AMINOTRANSFERASE
21	0.58	33.8	18.0	1.50	330	10	30	4zm3:A	CRYSTAL STRUCTURE OF PLP-DEPENDENT 3-AMINOBENZOATE SYNTHASE PCTV WILD- TYPE
22	0.58	35.2	18.4	1.55	348	12	28	2gsa:B	CRYSTAL STRUCTURE OF GLUTAMATE-1-SEMIALDEHYDE AMINOMUTASE (AMINOTRANSFERASE, WILD-TYPE FORM)
23	0.58	29.2	17.1	1.57	347	15	29	5i92:D	CRYSTAL STRUCTURE OF GLUTAMATE-1-SEMIALDEHYDE 2,1-AMINOMUTASE (GSA) FROM PSEUDOMONAS AERUGINOSA
24	0.58	33.7	18.0	1.56	348	15	28	3fq8:B	M248I MUTANT OF GSAM
25	0.58	29.5	17.5	1.55	346	15	29	5i92:A	CRYSTAL STRUCTURE OF GLUTAMATE-1-SEMIALDEHYDE 2,1-AMINOMUTASE (GSA) FROM PSEUDOMONAS AERUGINOSA
26	0.58	28.8	17.1	1.62	348	14	29	5i92:F	CRYSTAL STRUCTURE OF GLUTAMATE-1-SEMIALDEHYDE 2,1-AMINOMUTASE (GSA) FROM PSEUDOMONAS AERUGINOSA
27	0.58	34.8	18.3	1.54	347	13	28	4gsa:B	CRYSTAL STRUCTURE OF GLUTAMATE-1-SEMIALDEHYDE AMINOMUTASE (AMINOTRANSFERASE) REDUCED WITH CYANOBOROHYDRATE
28	0.58	33.4	17.8	1.54	330	10	31	4zm3:D	CRYSTAL STRUCTURE OF PLP-DEPENDENT 3-AMINOBENZOATE SYNTHASE PCTV WILD- TYPE
29	0.58	36.2	18.1	1.59	350	14	30	4aoa:A	BIOCHEMICAL PROPERTIES AND CRYSTAL STRUCTURE OF A NOVEL BETA-PHENYLALANINE AMINOTRANSFERASE FROM VARIOVORAX PARADOXUS
30	0.58	31.0	17.5	1.57	345	15	29	5i92:E	CRYSTAL STRUCTURE OF GLUTAMATE-1-SEMIALDEHYDE 2,1-AMINOMUTASE (GSA) FROM PSEUDOMONAS AERUGINOSA
31	0.58	36.8	18.1	1.57	350	14	30	4ao9:B	BIOCHEMICAL PROPERTIES AND CRYSTAL STRUCTURE OF A NOVEL BETA-PHENYLALANINE AMINOTRANSFERASE FROM VARIOVORAX PARADOXUS
32	0.58	35.3	18.6	1.55	347	11	29	3usf:A	CRYSTAL STRUCTURE OF DAVA-4
33	0.58	31.7	17.6	1.61	346	13	28	2hoz:B	INTER-SUBUNIT SIGNALING IN GSAM
34	0.58	31.8	17.7	1.55	346	14	28	3fq8:A	M248I MUTANT OF GSAM
35	0.58	30.2	17.6	1.58	344	12	29	4zm4:F	COMPLEX STRUCTURE OF PCTV K276R MUTANT WITH PMP AND 3-DEHYDROSHKIMATE
36	0.58	32.9	17.9	1.52	345	14	30	5hdm:B	CRYSTAL STRUCTURE OF ARABIDOPSIS THALIANA GLUTAMATE-1-SEMIALDEHYDE-2, 1-AMINOMUTASE
37	0.58	33.7	18.1	1.56	345	11	34	2e7u:A	CRYSTAL STRUCTURE OF GLUTAMATE-1-SEMIALDEHYDE 2,1-AMINOMUTASE FROM THERMUS THERMOPHILUS HB8
38	0.58	36.7	18.5	1.57	350	11	30	5d95:B	STRUCTURE OF THERMOSTABLE OMEGA-TRANSAMINASE
39	0.58	35.3	18.4	1.51	344	11	28	3gsb:B	CRYSTAL STRUCTURE OF GLUTAMATE-1-SEMIALDEHYDE

									AMINOMUTASE IN COMPLEX WITH GABACULINE
40	0.58	31.0	17.8	1.59	344	12	29	4zm4:A	COMPLEX STRUCTURE OF PCTV K276R MUTANT WITH PMP AND 3-DEHYDROSHKIMATE
41	0.58	35.9	17.9	1.62	351	14	30	4ao9:A	BIOCHEMICAL PROPERTIES AND CRYSTAL STRUCTURE OF A NOVEL BETA-PHENYLALANINE AMINOTRANSFERASE FROM VARIOVORAX PARADOXUS
42	0.58	34.6	17.7	1.65	352	13	30	4aoa:B	BIOCHEMICAL PROPERTIES AND CRYSTAL STRUCTURE OF A NOVEL BETA-PHENYLALANINE AMINOTRANSFERASE FROM VARIOVORAX PARADOXUS
43	0.57	33.4	18.1	1.55	345	11	28	3gsb:A	CRYSTAL STRUCTURE OF GLUTAMATE-1-SEMIALDEHYDE AMINOMUTASE IN COMPLEX WITH GABACULINE
44	0.57	32.7	17.8	1.61	348	11	28	3fq7:B	GABACULINE COMPLEX OF GSAM
45	0.57	31.0	17.8	1.62	344	11	29	4zm4:C	COMPLEX STRUCTURE OF PCTV K276R MUTANT WITH PMP AND 3-DEHYDROSHKIMATE
46	0.57	32.6	17.8	1.57	346	13	29	5hdm:A	CRYSTAL STRUCTURE OF ARABIDOPSIS THALIANA GLUTAMATE-1-SEMIALDEHYDE-2, 1-AMINOMUTASE
47	0.57	32.7	17.9	1.60	347	11	28	3fq7:A	GABACULINE COMPLEX OF GSAM
48	0.57	37.4	18.5	1.59	350	11	30	5d95:A	STRUCTURE OF THERMOSTABLE OMEGA-TRANSAMINASE
49	0.57	35.0	18.5	1.55	345	11	29	2hp2:B	INTER-SUBUNIT SIGNALING IN GSAM
50	0.57	33.4	18.1	1.55	344	12	28	2gsa:A	CRYSTAL STRUCTURE OF GLUTAMATE-1-SEMIALDEHYDE AMINOMUTASE (AMINOTRANSFERASE, WILD-TYPE FORM)
51	0.57	33.2	18.0	1.59	346	11	29	2hp2:A	INTER-SUBUNIT SIGNALING IN GSAM
52	0.57	33.0	18.0	1.53	343	10	28	4gsa:A	CRYSTAL STRUCTURE OF GLUTAMATE-1-SEMIALDEHYDE AMINOMUTASE (AMINOTRANSFERASE) REDUCED WITH CYANOBOROHYDRATE
53	0.57	30.5	17.7	1.56	343	12	29	4zm4:B	COMPLEX STRUCTURE OF PCTV K276R MUTANT WITH PMP AND 3-DEHYDROSHKIMATE
54	0.57	33.2	17.9	1.81	353	13	32	2zsm:C	CRYSTAL STRUCTURE OF GLUTAMATE-1-SEMIALDEHYDE 2,1-AMINOMUTASE FROM AEROPYRUM PERNIX, HEXAGONAL FORM
55	0.57	32.1	17.7	1.59	345	12	28	2hp1:A	INTER-SUBUNIT SIGNALING IN GSAM
56	0.57	35.5	18.6	1.83	353	13	33	2zsm:B	CRYSTAL STRUCTURE OF GLUTAMATE-1-SEMIALDEHYDE 2,1-AMINOMUTASE FROM AEROPYRUM PERNIX, HEXAGONAL FORM
57	0.57	30.7	17.7	1.58	343	11	29	4zm4:E	COMPLEX STRUCTURE OF PCTV K276R MUTANT WITH PMP AND 3-DEHYDROSHKIMATE
58	0.56	31.4	16.9	1.76	318	14	25	4ade:B	STRUCTURAL AND FUNCTIONAL STUDY OF SUCCINYL-ORNITHINE TRANSAMINASE FROM E. COLI
59	0.56	31.6	17.6	1.63	345	11	29	2hoz:A	INTER-SUBUNIT SIGNALING IN GSAM
60	0.56	33.4	18.0	1.78	349	13	33	2zsl:A	CRYSTAL STRUCTURE OF GLUTAMATE-1-SEMIALDEHYDE 2,1-AMINOMUTASE FROM AEROPYRUM PERNIX

Table S4.3. Specific activities (mU mg^{-1}) of wild-type and mutant DPAT for various donor substrates.

Substrates	Enzyme			
	Wild type	**Q301G**	**Q301S**	**Q301A**
D-alanine	17 ± 2	0	0	0
D-leucine	1160 ± 60	160 ± 50	120 ± 30	240 ± 30
D-methionine	940 ± 30	64 ± 8	110 ± 20	180 ± 10
L-alanine	29 ± 1	0	7 ± 3	22 ± 3
D-serine	0	0	0	0
D-threonine	0	0	0	0
D-glutamine	23 ± 4	0	0	12 ± 2
L-glutamine	24 ± 4	0	0	11 ± 1
L-serine	20 ± 10	0	0	7 ± 3
L-aspartate	12 ± 9	0	90 ± 30	30 ± 3
D-arginine	0	0	0	2 ± 1
D-lysine	0	0	0	5 ± 1
aminomalonate	20 ± 10	0	0	3 ± 1
D-phenylglycine	14000 ± 4000	8450 ± 40	4690 ± 30	1190 ± 30
(*S*)-3-phenyl-β-alanine	1173 ± 8	970 ± 10	715 ± 4	232 ± 1
(*S*)-4-phenyl-4-aminobutyrate	11500 ± 200	2690 ± 20	3192 ± 3	1090 ± 20
D-histidine	0	0	0	0
D-tryptophan	1200 ± 40	100 ± 10	151 ± 5	238 ± 1
D-phenylalanine	99 ± 8	0	0	22 ± 3
2-methyl-D-phenylalanine	570 ± 30	0	18 ± 6	55 ± 4
3-nitro-D-phenylalanine	0	0	0	0
4-methyl-D-phenylalanine	0	0	0	15 ± 1
4-nitro-D-phenylalanine	0	0	0	20 ± 2
***4*-methoxy-D-phenylalanine**	140 ± 20	0	12 ± 5	25 ± 5

[a] 1 mU is defined as 1 nmol of product produced per minute.

4.7.4. Materials and methods

4.7.4.1. Materials

All reagents used were of the highest available purity. Restriction enzymes and DNA modifying enzymes were obtained from New England Biolabs. Synthetic oligonucleotides were obtained from Integrated DNA Technologies, and Ni-NTA resin was obtained from Bio-Rad. All aqueous solutions were prepared using water purified with a Barnstead Nanopure Diamond system. The enzyme substrates and cofactors were purchased from Sigma-Aldrich with the exception of 2-methyl-D-phenylalanine (Alfa Aesar, >94%), 3-nitro-D-phenylalanine (Alfa Aesar, >94%), 4-methyl-D-phenylalanine (Alfa Aesar, >97%), 4-methoxy-D-phenylalanine (Santa Cruz Biotechnology, >94%), (*S*)-3-Phenyl-β-alanine (Toronto Research Chemicals, >95%), and (*S*)-4-phenyl-4-aminobutyrate (J & W PharmLab LLC, 97%).

4.7.4.2. DPAT gene cloning

The codon-optimized (E. coli) gene of Pseudomonas stutzeri ST-201 DPAT (GenBank ID: AY319935.1) was purchased from Genscript and subcloned into the pET11-a (N-terminal his-tag) or pCDFDuet-1 (C-terminal TEV protease cleavage site followed by his-tag) expression vectors (Novagen) via the NdeI/BamHI or NdeI/XhoI restrictions sites, respectively. The resulting plasmids were then transformed into chemically-competent E. coli XL-1 Blue cells (Stratagene). The entire reading frame of each plasmid was verified by DNA sequencing, after which the plasmids were transformed into chemically-competent E. coli BL21-Gold(DE3) cells (Stratagene) for protein expression.

4.7.4.3. Mutagenesis

Mutations were introduced into the DPAT gene by overlap extension mutagenesis using VentR DNA Polymerase.[34] Briefly, external primers were used in combination with sets of complementary pairs of oligonucleotides containing the mutated codon in individual polymerase chain reactions (PCRs). The resulting overlapping fragments were gel-purified (Omega Biotek) and recombined by overlap extension PCR. The resulting amplicons were digested with NdeI/BamHI, gel-purified, and ligated into pET-11a expression vector with T4 DNA ligase. Constructs were verified by sequencing the entire open reading frame, and were transformed into chemically-competent E. coli BL21-Gold(DE3) cells (Stratagene) for protein expression.

4.7.4.4. Protein expression and purification

Proteins were expressed in 1 L cultures of *E. coli* BL21-Gold(DE3) cells transformed with a pET11-a or pCDFDuet-1 vector containing the DPAT gene, respectively. When the cultures reached an optical density at 600 nm of 0.6, the temperature was reduced from 37 to 15 °C. Upon reaching the induction temperature, 0.1 mM of isopropyl β-D-1-thiogalactopyranoside was added to the flasks to induce protein expression and the cells were incubated with shaking for 18 hours. Following expression, cells were harvested by centrifugation and lysed with an EmulsiFlex-B15 cell disruptor (Avestin). The proteins were then extracted and purified by immobilized metal affinity chromatography (IMAC), according to manufacturer's protocol. Elution fractions containing the aminotransferases were desalted by gel filtration using EconoPAC 10DG columns (Bio-Rad) into a final buffer solution of 100 mM potassium phosphate (pH 8.0) or 100 mM *N*-cyclohexyl-2-aminoethanesulfonic acid (CHES) buffer (pH 9.0) for samples used in crystallography or

enzyme assays, respectively. Protein concentrations were quantified using a modified version of the Bradford assay, where the calibration curve is constructed as a plot of the ratio of the absorbance measurements at 590 nm and 450 nm versus concentration.[35] This procedure yielded 12 ± 5 mg L^{-1} of wild-type DPAT, and approximately 8 mg L^{-1} of each of the Q301 mutants. The purity was determined to be >99% estimated by densitometry of coomassie brilliant blue on an SDS-Page gel.

4.7.4.5. Protein crystallization

The initial enzyme purification was performed as described above. Additional steps were taken to increase the purity of the wild-type DPAT sample for crystallography. The IMAC purified sample was dialyzed in 4 L of 100 mM potassium phosphate buffer (pH 8), 0.5 mM EDTA, and 1 mM dithiothreitol, overnight at 4 °C with stirring in the presence of TEV protease to cleave the C-terminal his-tag. Following cleavage of the his-tag, the sample was centrifuged (3000 × g, 30 minutes, 4 °C) to remove any precipitate. Finally, the protein was purified on a Bio-Rad Biologic Duoflow system using a Bio-Rad Enrich SEC 650 size exclusion column with a flow rate of 0.5 mL min^{-1} of 100 mM Tris-Cl Buffer (pH 7.4) supplemented with 100 mM sodium chloride. Fractions containing the enzyme were pooled and concentrated to 10 mg mL^{-1} using Amicon Ultra centrifugal filters. Trigonal crystals were grown in 0.2 M sodium phosphate buffer, pH 6.2 or 6.6, with 0.2–1.3 M ammonium sulfate using vapour diffusion. The crystals grew in 2 to 3 weeks and were transferred to a 35% cryoprotection solution of ethylene glycol with mother liquor. Crystals were subsequently flash-frozen with liquid nitrogen.

4.7.4.6. Crystal data collection and processing

A full data set was collected at the 17-ID-D beamline of LS-CAT (Advanced Photon Source, Argonne National Laboratories). The data set was indexed with XDS and scaled using Aimless.[36,37] A molecular replacement solution was found with Phaser using the available DPAT structure as a search model (PDB ID: 2CY8).[38] The model was completed using iterative rounds of refinement and model building using PHENIX and Coot, respectively.[39,40] Quality of the models was assessed using MolProbity.[41] The 17-ID-D beamline of LS-CAT (Advanced Photon Source, Argonne National Laboratories) collected the data set which was indexed with XDS, and scaled using Aimless.[36,42]

4.7.4.7. Preparation of clarified lysate

DNA libraries of saturation mutants were transformed into chemically competent *E. coli* BL21-Gold(DE3) cells (Stratagene). Colonies were picked into individual wells of V96 MicroWell polypropylene plates (Nunc) containing 200 µL of medium (Luria-Bertani with 100 µg/mL ampicillin supplemented with 10% glycerol). The plates were covered with a sterile, breathable rayon membrane (VWR) and incubated overnight at 37 °C with shaking. After incubation, these mother plates were used to inoculate sterile Nunc V96 MicroWell polypropylene plates ("daughter" plates) containing 300 µL of Overnight Express Instant TB media (Novagen) supplemented with ampicillin. Daughter plates were sealed with breathable membranes and incubated overnight (37 °C, 250 rpm). Cells were harvested by centrifugation (3000 × g, 30 minutes, 4 °C) and the resulting pellets were washed twice with phosphate buffered saline pH 7.4. Washed cell pellets were resuspended in lysis buffer (100 mM CHES buffer, pH 9, containing 1× Bug Buster Protein Extraction Reagent

(Novagen), 25 U mL^{-1} Benzonase Nuclease (EMD), and 1 mg mL^{-1} lysozyme). The clarified lysate was collected following centrifugation and stored at 4 °C until used in the screening assay.

4.7.4.8. Mutant library screening assay

The screening assay is fully described in reference [31]. Briefly, triplicate 200-µL reactions at 37 °C in 100 mM CHES buffer (pH 9.0) were prepared. The reaction mixture contained 16 µM pyridoxal phosphate, 5 mM D-phenylglycine, 1 mM α-kg, 1 U of GDH from bovine liver (Sigma), 0.5 mM NAD^+. Reactions were initiated by addition of 10 µL clarified cell lysate prepared as described earlier, and monitored by measuring the absorbance of NADH at 340 nm (extinction coefficient = 6220 M^{-1} cm^{-1}) for 30 minutes in individual wells of 96-well plates (Greiner Bio-One) using an Infinite M1000 plate reader (Tecan).

4.7.4.9. Substrate specificity profile screening

The substrate specificity profile for each DPAT variant was determined as described in the previous paragraph with the following modifications. The reaction mixture contained 10 mM amine donor. Reactions were initiated using 2 mU of purified enzyme (activity determined using 5 mM of D-phenylglycine, 1 mM α-ketoglutarate, 1 U of glutamate dehydrogenase from bovine liver, and 0.5 mM NAD^+ in CHES buffer, pH 9, 37 °C). Negative controls containing all reaction components except DPAT were used. Solution mixtures were pre-incubated at 37 °C for 30 minutes prior to initiating the reaction by the addition of DPAT. The enzymatic reaction was monitored as described above and performed in triplicate from a single enzyme preparation. The path lengths for each well were determined ratiometrically using the difference in absorbance between 900 and 998 nm.

4.7.4.10. Steady-state kinetics

Kinetic assays were performed as the substrate specificity profile assays but with the following modifications. The concentration of the substrate being analyzed was varied and approximately 2 mU of purified enzyme was added to each well to initiate the reaction. For all blanks, the aminotransferase was substituted for 100 mM CHES buffer, pH 9. The reactions were monitored by measuring the absorbance of NADH at 340 nm for 30 minutes in individual wells of 96-well plates (Greiner Bio-One) using an Infinite M1000 plate reader (Tecan). Nonlinear regression analysis of the initial rates as a function of substrate concentrations fit to the Michaelis-Menten equation was performed with Graphpad Prism software. For fitting of the kinetic data obtained using the (*S*)-4-phenyl-4-aminobutyrate substrates, a modified rate equation that takes into account substrate inhibition was used: $v_o = v_{max}\,[S] / (K_M + [S] + [S]^2 / K_i)$.

4.8. References

(1) Martínez-Rodríguez, S.; Martínez-Gómez, A. I.; Rodríguez-Vico, F.; Clemente-Jiménez, J. M.; Las Heras-Vázquez, F. J. *Chem. Biodivers.* **2010**, *7* (6), 1531–1548.

(2) Strömstedt, A. A.; Pasupuleti, M.; Schmidtchen, A.; Malmsten, M. *Antimicrob. Agents Chemother.* **2009**, *53* (2), 593–602.

(3) Miyao, K. *Bull. Agric. Chem. Soc. Japan* **1960**, *24* (1), 23–30.

(4) Coward, R.; Carson, C. *Ther. Clin. Risk Manag.* **2008**, *4* (6), 1315–1330.

(5) Kovacs, M. *Proc. Natl. Acad. Sci.* **2001**, *98* (4), 1829–1834.

(6) Koeller, K. M.; Wong, C. H. *Nature* **2001**, *409* (6817), 232–240.

(7) Hollmann, F.; Arends, I. W. C. E.; Holtmann, D. *Green Chem.* **2011**, *13* (9), 2285.

(8) France, S. P.; Hepworth, L. J.; Turner, N. J.; Flitsch, S. L. *ACS Catal.* **2017**, *7* (1), 710–724.

(9) Walton, C. J. W.; Parmeggiani, F.; Barber, J. E. B.; McCann, J. L.; Turner, N. J.; Chica, R. A. *ChemCatChem* **2017**, 10.1002/cctc.201701068.

(10) Sugio, S.; Petsko, G. a.; Manning, J. M.; Soda, K.; Ringe, D. *Biochemistry* **1995**, *34* (30), 9661–9669.

(11) Del Pozo, A. M.; Merola, M.; Ueno, H.; Manning, J. M.; Tanizawa, K.; Nishimura, K.; Soda, K.; Ringe, D. *J. Biol. Chem.* **1989**, *264* (30), 17784–17789.

(12) Wiyakrutta, S.; Meevootisom, V. *J. Biotechnol.* **1997**, *55* (3), 193–203.
(13) Khampha, W.; Yakovleva, J.; Isarangkul, D.; Wiyakrutta, S.; Meevootisom, V.; Emnéus, J. *Anal. Chim. Acta* **2004**, *518* (1–2), 127–135.
(14) Rojanarata, T.; Isarangkul, D.; Wiyakrutta, S.; Meevootisom, V.; Woodley, J. M. *Biocatal. Biotransformation* **2004**, *22* (3), 195–201.
(15) Kongsaeree, P.; Samanchart, C.; Laowanapiban, P.; Wiyakrutta, S.; Meevootisom, V. *Acta Crystallogr. Sect. D Biol. Crystallogr.* **2003**, *59* (5), 953–954.
(16) Nakai, T.; Okada, K.; Akutsu, S.; Miyahara, I.; Kawaguchi, S.; Kato, R.; Kuramitsu, S.; Hirotsu, K. *Biochemistry* **1999**, *38* (8), 2413–2424.
(17) Krissinel, E.; Henrick, K. *Acta Crystallogr. Sect. D Biol. Crystallogr.* **2004**, *60* (12), 2256–2268.
(18) Finn, R. D.; Coggill, P.; Eberhardt, R. Y.; Eddy, S. R.; Mistry, J.; Mitchell, A. L.; Potter, S. C.; Punta, M.; Qureshi, M.; Sangrador-Vegas, A.; Salazar, G. A.; Tate, J.; Bateman, A. *Nucleic Acids Res.* **2016**, *44* (D1), D279–D285.
(19) McPhalen, C. A.; Vincent, M. G.; Picot, D.; Jansonius, J. N.; Lesk, A. M.; Chothia, C. *J. Mol. Biol.* **1992**, *227* (1), 197–213.
(20) Liu, W.; Peterson, P. E.; Carter, R. J.; Zhou, X.; Langston, J. A.; Fisher, A. J.; Toney, M. D. *Biochemistry* **2004**, *43* (34), 10896–10905.
(21) Cha, H. J.; Jeong, J. H.; Rojviriya, C.; Kim, Y. G. *PLoS One* **2014**, *9* (11), 1–15.
(22) Steffen-Munsberg, F.; Vickers, C.; Kohls, H.; Land, H.; Mallin, H.; Nobili, A.; Skalden, L.; van den Bergh, T.; Joosten, H.-J.; Berglund, P.; Höhne, M.; Bornscheuer, U. T. *Biotechnol. Adv.* **2015**, *33* (5), 566–604.
(23) Stetefeld, J.; Jenny, M.; Burkhard, P. *Proc. Natl. Acad. Sci. U. S. A.* **2006**, *103* (37), 13688–13693.
(24) Wybenga, G. G.; Crismaru, C. G.; Janssen, D. B.; Dijkstra, B. W. *J. Biol. Chem.* **2012**, *287* (34), 28495–28502.
(25) Li, W.; Cowley, A.; Uludag, M.; Gur, T.; McWilliam, H.; Squizzato, S.; Park, Y. M.; Buso, N.; Lopez, R. *Nucleic Acids Res.* **2015**, *43* (W1), W580–W584.
(26) McWilliam, H.; Li, W.; Uludag, M.; Squizzato, S.; Park, Y. M.; Buso, N.; Cowley, A. P.; Lopez, R. *Nucleic Acids Res.* **2013**, *41* (W1), W597–W600.
(27) Sievers, F.; Wilm, A.; Dineen, D.; Gibson, T. J.; Karplus, K.; Li, W.; Lopez, R.; McWilliam, H.; Remmert, M.; Söding, J.; Thompson, J. D.; Higgins, D. G. *Mol. Syst. Biol.* **2011**, *7*, 539.
(28) Robert, X.; Gouet, P. *Nucleic Acids Res.* **2014**, *42* (W1), W320–W324.
(29) Eliot, A. C.; Kirsch, J. F. *Annu. Rev. Biochem.* **2004**, *73* (1), 383–415.
(30) Jomrit, J.; Summpunn, P.; Meevootisom, V.; Wiyakrutta, S. *Biochem. Biophys. Res. Commun.* **2011**, *405* (4), 626–631.
(31) Walton, C. J. W.; Chica, R. A. *Anal. Biochem.* **2013**, *441* (2), 190–198.
(32) Chantarasiri, A.; Meevootisom, V.; Isarangkul, D.; Wiyakrutta, S. *J. Mol. Microbiol. Biotechnol.* **2012**, *22* (3), 147–155.
(33) Crismaru, C. G.; Wybenga, G. G.; Szymanski, W.; Wijma, H. J.; Wu, B.; Bartsch, S.; de Wildeman, S.; Poelarends, G. J.; Feringa, B. L.; Dijkstra, B. W.; Janssen, D. B. *Appl. Environ. Microbiol.* **2013**, *79* (1), 185–195.
(34) Ho, S. N.; Hunt, H. D.; Horton, R. M.; Pullen, J. K.; Pease, L. R. *Gene* **1989**, *77* (1), 51–59.
(35) Ernst, O.; Zor, T. *J. Vis. Exp.* **2010**, No. 38, 1–6.

(36) Kabsch, W. *Acta Crystallogr. Sect. D Biol. Crystallogr.* **2010**, *66* (2), 125–132.
(37) Evans, P. R.; Murshudov, G. N. *Acta Crystallogr. Sect. D Biol. Crystallogr.* **2013**, *69* (7), 1204–1214.
(38) Zwart, P. H.; Afonine, P. V; Grosse-Kunstleve, R. W.; Hung, L.-W.; Ioerger, T. R.; McCoy, A. J.; McKee, E.; Moriarty, N. W.; Read, R. J.; Sacchettini, J. C.; others. In *Structural Proteomics*; Springer, 2008; pp 419–435.
(39) Adams, P. D.; Grosse-Kunstleve, R. W.; Hung, L.-W.; Ioerger, T. R.; McCoy, A. J.; Moriarty, N. W.; Read, R. J.; Sacchettini, J. C.; Sauter, N. K.; Terwilliger, T. C. *Acta Crystallogr. Sect. D Biol. Crystallogr.* **2002**, *58* (11), 1948–1954.
(40) Emsley, P.; Lohkamp, B.; Scott, W. G.; Cowtan, K. *Acta Crystallogr. Sect. D Biol. Crystallogr.* **2010**, *66* (4), 486–501.
(41) Williams, C. J.; Headd, J. J.; Moriarty, N. W.; Prisant, M. G.; Videau, L. L.; Deis, L. N.; Verma, V.; Keedy, D. A.; Hintze, B. J.; Chen, V. B.; others. *Protein Sci.* **2018**, *27* (1), 293–315.
(42) Sonke, T. **2008**, 320.

Chapter 5.
Conclusions & Perspectives

5. Conclusions & Perspectives

The research presented in previous chapters addressed the objectives established in Chapter 1. In this chapter, we will summarize the accomplishments and conclusions of the research chapters and discuss the perspectives of future work.

5.1. Objective 1: Develop a generally applicable method to screen aminotransferases in a high-throughput manner to identify ATs with a desired substrate specificity

5.1.1. Accomplishments and conclusions

The GDH assay we developed allows for the continuous high-throughput screening of mutant aminotransferase libraries of L- or D-amino acid specific ATs. The method of detection is based on a common substrate allowing for the screening of any α-kg-dependent AT. We demonstrated the potential of the assay by screening BCAT and DAAT libraries with model substrates and identified mutants with varying degrees of activity. The assay is sensitive as it enabled detection of a DAAT mutant with 632-fold lower catalytic efficiency than the wild type in a complex reaction mixture containing small quantities of enzyme. Finally, using this assay, we were able to identify a BCAT mutant, BCAT–F36W, which is approximately 60-fold more specific for L-leucine than L-phenylalanine compared with the wild type. Thus, demonstrating the assays potential for identifying ATs with desired substrate specificities and achieving objective 1.

5.1.2. Perspectives

The detection of enzymes with a desired substrate specificity is a vital step to develop a biocatalyst. But, as protein engineering and gene mining techniques have improved, the

number of potential variants and/or alternative genes requiring analysis has scaled non-linearly. Therefore, conventional analytic techniques such as mass spectrometry or high-performance liquid chromatography have become bottlenecks in the development pipeline. High-throughput screening techniques have been developed to alleviate those development bottlenecks and enabled researchers to find the few active variants among many. The high throughput screening techniques for ATs include enrichment cultivation,[1,2] common substrate-based assays,[3,4] and smart substrate based assays.[5,6] The targeting of common AT substrates, such as α-kg with the GDH assay, has inherent benefits as the screening strategy is generally applicable to wide variety of enzymes and substrates. Additionally, the continuous nature of the GDH assay provides quantitative information that qualitative methods, such as enrichment cultivation, fail to provide during an initial screening round.

In Chapter 2, we identified variants of two ATs with modified activities for L- and D-amino acids. We further demonstrated the assays applicability by using it to screen another AT for activity with β- and γ-amino acids in Chapter 4. Thus, with one assay we were able characterize three ATs and several variants with diverse substrate specificities. Yet, there exists a few endeavors future students can embark upon to improve the screening assay. The use of commercially available bovine GDH as the coupling enzyme was a fast and efficient method to develop the screening assay. However, the cost of commercial GDH for large-scale screening projects may be prohibitive. Ideally, an *E. coli* strain that incorporates a duel expression system could produce the AT of interest and the coupling enzyme. This would significantly reduce screening costs by eliminating an expensive reagent (bovine GDH) and the waste associate with purifying an enzyme that is added to cellular lysate. The use of recombinant GDH will provide a new set of problems that will

need to be addressed including whether an appropriate amount of GDH can be produced to assay the overexpressed AT. Alternatively, recombinant GDH could be produced separately and added to the reaction mixture.

Secondly, the screening assay enables the processing of more than 10^3 mutants per day, but combinatorial libraries with multiple mutations can require screening $>10^5$ mutants. Therefore, the screening assay can be further improved by adapting the assay to function as an ultra high-throughput screening (uHTS) assay or near-uHTS assay by increasing throughput and performing the screening in 384- or 1536-well plates. The reduced volumes will decrease reagent use, increase the number of mutants screened, and reduce the screening cost per mutant.

5.2. Objective 2: Engineer an AT with high catalytic activity for aromatic D-AAs with pharmaceutical relevance and incorporate the AT into a biocatalytic cascade to synthesis D-AAs

5.2.1. Accomplishments and conclusions

To engineer an AT with high catalytic activity for aromatic D-AAs we selected DAAT from *Bacillus sp.* YM-1 as our starting biocatalyst. We built a substrate specificity profile of the wild-type enzyme with a panel of D-amino acids. The wild-type displayed low to no activity for the aromatic D-amino acids including D-Phe. To increase the size of the binding pocket and accept bulky aromatic amino acids, we generated three single variants mutating the side-chain binding residues to the smaller glycine residue. These modifications to the binding pocket expanded the substrate specificity profiles for the three mutants which displayed high activity with a variety of aromatic D-amino acids.

Next, we characterized the wild-type and mutants to determine their kinetic parameters with D-Phe and five derivatives. The wild-type enzyme gave low catalytic efficiencies for D-Phe and its derivatives (≤10 M^{-1} s^{-1}). Whereas, the mutants displayed improved catalytic efficiencies for aromatic D-amino acids compared to the wild-type. DAAT-T242G displaying the highest catalytic efficiency for D-Phe (400 M^{-1} s^{-1}), which represents a 615-fold increase relative to the wild-type. The T242G mutant also displayed high catalytic efficiency for other aromatic D-amino acids including 3-methyl-D-Phe (703 M^{-1} s^{-1}). Therefore, we defined this variant as a near-native catalytic efficiency mutant for aromatic D-amino acids with broad specificity.

Finally, we verified our engineered AT was a suitable biocatalyst by producing a variety of pharmaceutically relevant D-amino acids. We started by performed transamination reactions with DAAT-T242G as a whole cell biocatalyst. The biotransformations of phenylpyruvate analogs resulted in D-Phe derivatives with high percent conversions (≥94%) and *ee* (≥98%) over a 12-hour period. Next, the DAAT-T242G mutant was incorporated into a biocatalytic cascade with LAAD from *Proteus mirabilis* that allowed the stereo-inversion of L-amino acids and deracemization of racemates producing D-phenylalanine derivatives with high *ee* (90% to >99%) in 4 hours. Finally, we performed a preparative scale synthesis of 4-fluoro-D-Phe which resulted in an optically pure product (99% *ee*) and 84% yield. Thus, we demonstrated our engineered AT has high catalytic efficiency with aromatic D-amino acids and can function in a biocatalytic cascade to produce optically pure aromatic D-amino acids which achieved objective 2.

5.2.2. Perspectives

The focus of this article was on the production of D-phenylalanine and its derivatives which are high-value pharmaceutical precursors. However, many other D-AAs are relevant for the pharmaceutical and fine chemical industries.[7] These include the aliphatic amino acids such as D-Val[8–10], D-norVal,[11] D-Leu,[12,13] D-Ile,[14] and D-Met.[15] The single DAAT mutants displayed moderate to high activity for aliphatic substrates such as D-Leu and D-Val (see Table S3.2). Therefore, an appropriate next step for this project is to characterize the single mutants with other desirable substrate and expand the biocatalytic cascade to produce those aliphatic D-AAs.

Secondly, a preliminary characterization of DAAT mutants that incorporated the double and triple glycine mutations was performed (see Appendix, Section A). Those results indicate the mutants have an expanded substrate scope and at least one may be suitable for the synthesis of D-Trp. The generation of a larger substrate specificity profile akin to the profile generated for the single mutants that incorporates D-Trp derivatives may provide evidence the double mutant can produce other non-canonical aromatic D-amino acids such as D-2-alkyltryptophans or D-halotryptophans.

Finally, a new biocatalytic cascade could be developed to produce D-Trp derivatives starting from L-Ser and indoles. This cascade would utilize L-Tryptophan synthase to produce L-Trp or its derivatives,[16] and the LAAD/DAAT pair to perform the tandem oxidation-reduction to produce the D-Trp derivatives.

5.3. Objective 3: Investigate a stereo-inverting AT with potential as a D-amino acid biocatalyst

5.3.1. Accomplishments and conclusions

To investigate the structure-function relationship of DPAT, we crystallized the apoenzyme and solved a partial crystal structure with a refined resolution of 1.82 Å. However, the structure was missing electron density surrounding the active site. Therefore, to gain a better understanding of the coordination in the active site, we identified homologous enzymes with solved crystal structures using PDBeFold. We used the structures and sequence alignment to develop a substrate binding hypothesis and identify active site residues. We determined the R34 & R407 residues are essential for the transamination reaction using the GDH assay with D-Phg as the amine donor, as no active mutants were found in the site-saturation libraries. Additionally, we identified several residues with reduced activity at positions 66, 213, and 301. The 66 and 213 positions are located in the O-pocket which indicates the pocket is amenable to substitution and it may be possible to engineer the substrate specificity for other D-amino acids.

Next, we built a substrate-specificity profile of the wild-type and Q301 mutants. The wild-type displayed high activity for several D-amino acids and two D-Phg analogs—(*S*)-3-phenyl-β-alanine and (*S*)-4-phenyl-4-aminobutyric acid. This is the first report of DPAT being an ω-AT and performing the transamination reaction with β- or γ-amino acids. As expected, the Q301 mutants displayed reduced specificity activity for D-amino acids as the mutation is located in the P-pocket. However, the specific activity for the three mutants with (*S*)-4-phenyl-4-aminobutyric acid was significantly decreased which contracted our binding hypothesis of Q301 being important for binding the shorter α-carboxylate of D-

Phg. To ascertain why the enzymes displayed low activity with (*S*)-4-phenyl-4-aminobutyric acid we kinetically characterized the wild-type and mutants with α-kg, D-Phg and the two analogs.

The kinetic results demonstrate the Q301 mutations increase the apparent K_M of D-Phg and do not significantly impact the K_M of α-kg or (*S*)-4-phenyl-4-aminobutyric acid compared to the wild-type. Thus, supporting our binding mode hypothesis that Q301 is important for the short α-carboxylate of D-Phg. The low specific activity observed during screening for the three mutants with (*S*)-4-phenyl-4-aminobutyric acid was due to substrate inhibition that often occurs in ATs at high substrate concentrations. Therefore, we achieved our objective by developing a binding hypothesis and identifying residues that are amenable to substitution which may lead to an engineered mutant with altered substrate specificity.

5.3.2. Perspectives

In Chapter 4, our main objectives were to elucidate the structure-function relationship of DPAT that enables the stereo-inversion and identify which residues form the binding pocket for D-AA side-chains. These objectives were set to learn how this novel enzyme functions and facilitate engineering the substrate specificity of DPAT towards other D-amino acids. Our comparison with other class III AT enzymes, the screening results, and kinetic results support our binding hypothesis of DPAT which should facilitate engineering the O-pocket substrate specificity towards other D-amino acids. We also determined the catalytic efficiency of DPAT with D-Phe and kinetically characterized the β-AT from *Variovorax paradoxus* (see Appendix, section B).

Therefore, the next step in this project is to characterize the O-pocket mutants for enhanced activity towards aromatic D-amino acids. This may lead to the identification of an engineered AT capable of producing D-amino acids from inexpensive L-Glu that can be incorporated into a biocatalytic cascade with LAAD. However, there are fundamental questions about the enzymes structure-function relationship that are particularly interesting and worth further investigation.

First, it is imperative a complete crystal structure of the holo form be solved with bound substrates. This will elucidate the binding modes that DPAT adopts when binding L-Glu and D-Phg. To achieve this objective, it is recommended that the soluble double mutant be used to solve the holo form. The use of this mutant may reduce or eliminate the solubility issues observed when co-crystallization experiments were performed with the native enzyme. However, the solubility mutant was engineered by identifying residues involved in protein crystal contacts.[17] This most likely will alter the conditions the enzyme will crystalize under and require new conditions to be identified. Alternatively, halophilic fusion peptides have recently been used to increase the solubility of DPAT to more than 70 mg mL^{-1} and may provide an alternative route to crystalizing the holo form.[18]

Secondly, the function of the latter half of the disordered loop (residues 146–178) in DPAT remains unknown. In GSAM, the loop undergoes a conformational change during catalysis and prevents the intermediate substrate (4,5-diaminovalerate) from being released which is paramount to the aminomutases functionality.[19] However, in DPAT it is not obvious why such a loop would be necessary for the transamination reaction to occur. It is possible this larger loop in DPAT relative to MesAT is vestigial or may function as part of the

coordinated hydrogen bond network in the P-pocket. The use of alanine scanning along the loop or the generation of loop chimeras using loops from GSAM and MesAT may assist in elucidating the loops function while crystallography experiments are ongoing.

5.4. References

(1) Yun, H.; Hwang, B. Y.; Lee, J. H.; Kim, B. G. *Appl. Environ. Microbiol.* **2005**, *71* (8), 4220–4224.
(2) Shin, J.-S.; Kim, B.-G. *Biosci. Biotechnol. Biochem.* **2001**, *65* (8), 1782–1788.
(3) Barber, J. E. B.; Damry, A. M.; Calderini, G. F.; Walton, C. J. W.; Chica, R. A. *Anal. Biochem.* **2014**, *463*, 23–30.
(4) Hwang, B.-Y.; Kim, B.-G. *Enzyme Microb. Technol.* **2004**, *34* (5), 429–436.
(5) Green, A. P.; Turner, N. J.; O'Reilly, E. *Angew. Chemie - Int. Ed.* **2014**, *53* (40), 10714–10717.
(6) Scheidt, T.; Land, H.; Anderson, M.; Chen, Y.; Berglund, P.; Yi, D.; Fessner, W.-D. *Adv. Synth. Catal.* **2015**, *357* (8), 1721–1731.
(7) Martínez-Rodríguez, S.; Martínez-Gómez, A. I.; Rodríguez-Vico, F.; Clemente-Jiménez, J. M.; Las Heras-Vázquez, F. J. *Chem. Biodivers.* **2010**, *7* (6), 1531–1548.
(8) Fitch, W. L.; Sjolander, A. C.; Miller, W. W. *J. Agric. Food Chem.* **1988**, *36* (4), 764–766.
(9) Abrão, R. A.; de Andrade, J. M.; Tiezzi, D. G.; Marana, H. R. C.; dos Reis, F. J. C.; Clagnan, W. S. *Gynecol. Oncol.* **2008**, *108* (1), 149–153.
(10) Liu, X.; Chen, H.; Patel, D. J. *J. Biomol. NMR* **1991**, *1* (4), 323–347.
(11) Brennan, T. M.; Hendrick, M. E. Branched amides of L-aspartyl-D-amino acid dipeptides. US 4411925 A, 1980.
(12) Kelly, D. R.; Roberts, S. M. *Pept. Sci.* **2006**, *84* (1), 74–89.
(13) Coccia, M. E.; Comparetto, C.; Bracco, G. L.; Scarselli, G. *Eur. J. Obstet. Gynecol. Reprod. Biol.* **2004**, *115*, S44–S56.
(14) Dooley, C.; Chung, N.; Wilkes, B.; Schiller, P.; Bidlack, J.; Pasternak, G.; Houghten, R. *Science (80-.).* **1994**, *266* (5193), 2019–2022.
(15) Sunkara, P. D-methionine formulation with improved biopharmaceutical properties. US20060058390A1, 2005.
(16) Corr, M. J.; Smith, D. R. M.; Goss, R. J. M. *Tetrahedron* **2016**, *72* (46), 7306–7310.
(17) Chantarasiri, A.; Meevootisom, V.; Isarangkul, D.; Wiyakrutta, S. *J. Mol. Microbiol. Biotechnol.* **2012**, *22* (3), 147–155.
(18) Javid, H.; Jomrit, J.; Chantarasiri, A.; Isarangkul, D.; Meevootisom, V.; Wiyakrutta, S. *J. Microbiol. Biotechnol.* **2014**, *24* (5), 597–604.
(19) Stetefeld, J.; Jenny, M.; Burkhard, P. *Proc. Natl. Acad. Sci. U. S. A.* **2006**, *103*, 13688–13693.

Appendix.

A. Additional results pertaining to DAAT

The combinatorial DAAT mutants that incorporate the glycine mutants at positions at V33, S240, and T242 were screened with a subset of the D-amino acid library. These mutants are referred to in Figure A1 as DAAT-VS (V33G & S240G), VT (V33G & T242G), ST (S240G & T242G), and VST (V33G, S240G, & T242G).

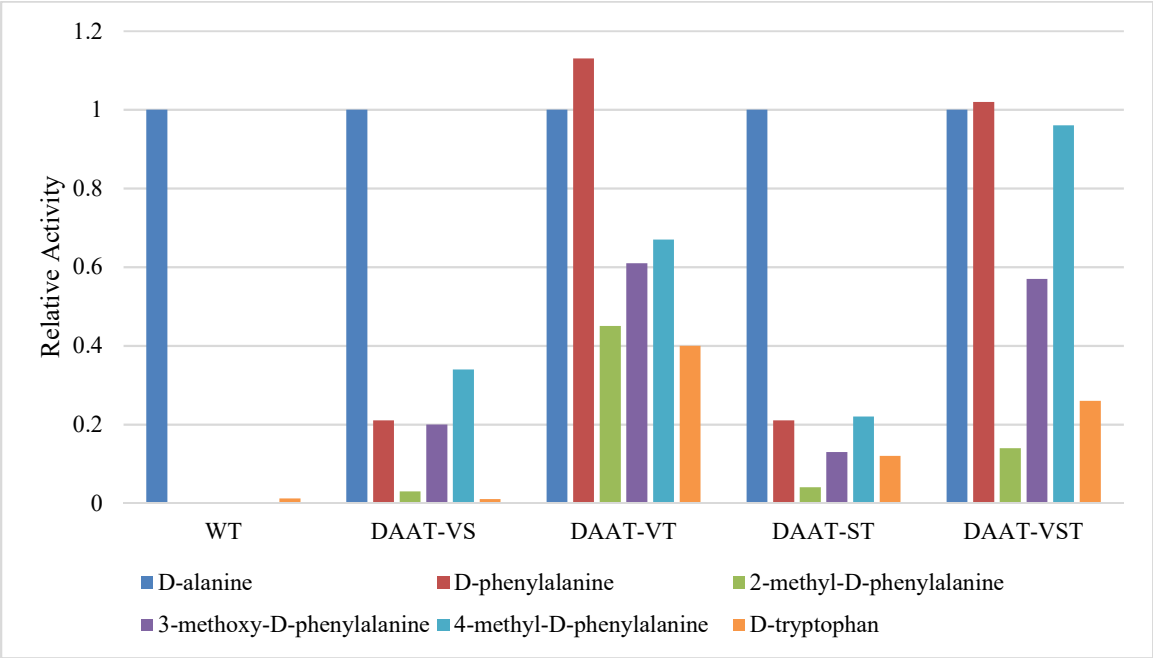

Figure A.1 Screening results of double and triple DAAT mutants with a subset of aromatic amino acids normalized to D-alanine activity.

Table A.1 Apparent kinetic parameters for the transamination of D-phenylalanine and D-tryptophan by DAAT double mutants.

Enzyme	D-amino acid	K_M (mM)	k_{cat} (s^{-1})	k_{cat}/K_M ($M^{-1}\ s^{-1}$)	Relative k_{cat}/K_M
Wild Type	Phenylalanine	-	-	0.65	1
	Tryptophan	10 ± 4	0.20 ± 0.06	20 ± 10	1
VT	Phenylalanine	4.5 ± 0.2	1.17 ± 0.02	260 ± 12	400
	Tryptophan	0.82 ± 0.05	0.57 ± 0.01	700 ± 44	35
ST	Phenylalanine	28 ± 2	5.3 ± 0.2	190 ± 15	292
	Tryptophan	1.8 ± 0.4	0.10 ± 0.01	56 ± 14	3

B. Additional results pertaining to DPAT

Table B.1 Apparent kinetic parameter for the transamination reaction of DPAT wild-type with D-phenylalanine.

Substrate[a]	Kinetic Parameter[b]	WT
D-phenylalanine	k_{cat} / K_M (M^{-1} s^{-1})	0.8

[a] acceptor substrate is 1 mM α-kg.
[b] K_M and k_{cat} could not be determined as substrate saturation was not possible within its solubility limit.

Table B.2 Specific activities of β-phenylalanine Aminotransferase from *Variovorax paradoxus* (VPAT) for various substrates.

Substrates	VPAT (mU mg^{-1})[a]
D-alanine	0
D-leucine	0
D-methionine	0
L-alanine	30 ± 7
D-serine	0
D-threonine	0
D-glutamine	0
L-glutamine	0
L-serine	0
L-aspartate	35 ± 3
D-arginine	0
D-lysine	0
aminomalonate	0
D-phenylglycine	20 ± 10
(*S*)-β-phenylalanine	2540 ± 80
(*S*)-4-phenyl-4-aminobutyric acid	3020 ± 40
D-histidine	0
D-tryptophan	0
D-phenylalanine	0
2-methyl-D-phenylalanine	0
3-nitro-D-phenylalanine	0
4-methyl-D-phenylalanine	0
4-nitro-D-phenylalanine	0
4-methoxy-D-phenylalanine	0

[a] 1 mU is defined as 1 nmol/min.

Table B.3 Apparent kinetic parameters for the transamination reaction of VPAT.

Substrate[a]	Kinetic parameters	VPAT
α-kg[b]	K_M (mM)	0.07 ± 0.01
	k_{cat} (s^{-1})	7.7 ± 0.7
	k_{cat} / K_M (M^{-1} s^{-1})	110,000
D-Phg	K_M (mM)	0.42 ± 0.07
	k_{cat} (s^{-1})	0.018 ± 0.001
	k_{cat} / K_M (M^{-1} s^{-1})	43
(*S*)-3-phenyl-β-alanine	K_M (mM)	0.15 ± 0.03
	k_{cat} (s^{-1})	6.6 ± 0.4
	k_{cat} / K_M (M^{-1} s^{-1})	44,000
(*S*)-4-phenyl-4-aminobutyric acid	K_M (mM)	0.99 ± 0.19
	k_{cat} (s^{-1})	0.96 ± 0.08
	k_{cat} / K_M (M^{-1} s^{-1})	974
D-Phe	k_{cat} / K_M (M^{-1} s^{-1})	0

[a] α-kg: α-ketoglutarate, D-Phg: D-phenylglycine, D-Phe: D-phenylalanine.
[b] donor substrate is 5 mM (*S*)-3-phenyl-β-alanine

List of Publications

Walton, C.J.W., Thiebaut, F., Brunzelle, J. S., Couture, J.F., Chica, R.A., Structural determinants of the stereo-inverting activity of Pseudomonas stutzeri D-phenylglycine aminotransferase. (Manuscript in preparation).

Walton, C.J.W., Parmeggiani, F., Barber, J.E.B., McCann, J.L., Turner, N.J. and Chica, R.A., Engineered Aminotransferase for the Production of D-Phenylalanine Derivatives Using Biocatalytic Cascades. *ChemCatChem*, **2018,** 10, 470-474. DOI:10.1002/cctc.201701068

Barber J.E.B., Damry, A.M., Calderini G.F., **Walton C.J.W.**, Chica R.A., Continuous colorimetric screening assay for detection of D-amino acid aminotransferase mutants displaying altered substrate specificity. *Analytical Biochemistry,* **2014**, 463, 23-30. DOI: 10.1016/j.ab.2014.06.006

Walton, C.J.W. and Chica R.A., A high-throughput assay for screening L- or D-amino acid specific aminotransferase mutant libraries. *Analytical Biochemistry,* **2013**, 441, 190-198. DOI: 10.1016/j.ab.2013.07.004